DESIGN IMPROVEMENT, QUALIFICATION TESTING, PURGE AND VENT INVESTIGATION, FABRICATION, AND DOCUMENTATION OF A GAC-9 INSULATION SYSTEM

GER-14915 S/9

Annual Summary Report

November 1971

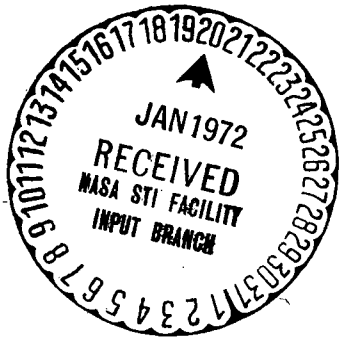

Contract No. NAS 8-26091
Control No. 1-0-50-09618 (1F)

Prepared for:

National Aeronautics and Space Administration
George C. Marshall Space Flight Center
Huntsville, Alabama

GOODYEAR AEROSPACE
CORPORATION

CODE IDENT NO. 25500

GOODYEAR AEROSPACE
CORPORATION

AKRON 15, OHIO

DESIGN IMPROVEMENT, QUALIFICATION TESTING, PURGE AND VENT INVESTIGATION, FABRICATION, AND DOCUMENTATION OF A GAC-9 INSULATION SYSTEM

Annual Summary Report

Contract No. NAS 8-26091

By

C.B. Shriver

J.N. Apisa

A.H. Kariotis

GER 14915 S/9
November 1971

For

George C. Marshall Space Flight Center
National Aeronautics and Space Administration

ABSTRACT

This summary report was prepared by Goodyear Aerospace Corporation (GAC) under Contract NAS 8-26091, "Design Improvement, Qualification Testing, Purge and Vent Investigation, Fabrication, and Documentation of a GAC-9 Insulation System", for the George C. Marshall Space Flight Center of National Aeronautics and Space Administration. The work was administered under the technical direction of the Astronautics Laboratory, Engineering Division of the George C. Marshall Space Flight Center, with Mr. Joseph M. Walters acting as project manager. This report summarizes the research, development, and testing that were accomplished during the 14-month effort. Most of the work was directed toward determining the purge and vent characteristics of the GAC-9 insulation system. This work included laboratory purge gas flow tests using a 30-cm (12-inch) diameter cylinder test apparatus, panel flow tests using a 94 x 122 cm (37 x 48 inch) test panel, and subscale tank testing using the 76-cm (30-inch) diameter double-guarded calorimeter for cryogenic tests to verify laboratory flow test results and demonstrate a purge system design. Other work included thermal conductivity testing using a 15-cm (6-inch) diameter flat-plate calorimeter, thermal conductivity tests of a simulated penetration on the 76-cm (30-inch) diameter calorimeter, and a feasibility study of techniques for mechanization of insulation panel drop thread installation.

TABLE OF CONTENTS

LIST OF ILLUSTRATIONS

LIST OF TABLES

SECTION I

INTRODUCTION

This report summarizes the research and development program conducted by GAC under Contract NAS 8-26091, "Design Improvement, Qualification Testing, Purge and Vent Investigation, Fabrication, and Documentation of a GAC-9 Insulation System," during the period from 28 May 1970 through 30 July 1971. The primary purpose of the program was to determine the purge and vent characteristics of the GAC-9 insulation system.

The work scope comprised a four-task effort:

(1) Literature survey

(2) Design improvement and installation effort

(3) Testing

(4) Evaluation of test results

The primary objectives to be realized from this effort are listed below:

(1) Define the purge gas flow characteristics of the GAC-9 insulation system through laboratory measurements.

(2) Demonstrate that the insulation is effective as a system for prelaunch purging and launch venting of the 76-cm (30-inch) diameter calorimeter, which is a subscale model simulating a realistic type of GAC-9 insulation application.

SECTION II

SUMMARY

The program consisted of design improvement studies, flat-plate calorimeter testing, purge and vent laboratory testing, and subscale tank testing of a GAC-9 insulation purge system.

Design improvement studies involved investigation of perforated aluminized Mylar radiation shields, methods of drop thread mechanization, and laboratory tests to obtain purge gas flow characteristics parallel to and across the layers of GAC-9 insulation.

To improve broadside venting of internal gases in GAC-9 insulation, a concept incorporating aluminized Mylar radiation shields perforated to 2.38 percent open area was evaluated for thermal performance and purge gas flow. The broadside gas flow was increased from virtually no measurable flow to 0.0013 m^3/s (0.04 std ft^3/min) at atmospheric pressure and 13.3 N/m^2 (0.10 torr) pressure differential. The use of perforations increased the emittance value of the radiation shields and consequently increased the radiation heat transfer. A thermal conductivity test was conducted on the 15-cm (six-inch) diameter flat-plate calorimeter at specimen compression pressures of 68.9 to 6.89 N/m^2 (0.01 to 0.001 $lbf/in.^2$). At 6.89 N/m^2 (0.001 $lbf/in.^2$) the insulation K value measured 3.9×10^{-5} J/m-s-^oK (2.26×10^{-5} Btu/ft-hr-^oF). This value is approximately 52 percent higher than the measured thermal conductivity of GAC-9 insulation containing unperforated Mylar radiation shields.

A study was conducted to determine the feasibility of mechanizing the installation of drop threads in the GAC-9 insulation composite. Sewing machines were generally not adaptable for this application. A Model LT 280 mattress tufting machine, manufactured by the United Mattress Machine Company, has demonstrated a capability of installing drop threads in GAC-9 insulation. The demonstration drop threads were somewhat heavier than desired; however, the machine may be altered to handle lightweight thread material. The tufting machine is designed to handle items of mattress size and may be readily modified to accommodate insulation panels of larger size.

Laboratory tests were conducted on 30-cm (12-inch) diameter cylinder and disc specimens to obtain basic engineering data on purge gas flow through GAC-9 insulation. These data were required to design and demonstrate a purge system for the GAC-9 insulation on the 76-cm (30-inch) diameter calorimeter. Flow coefficient measurements were obtained as a function of pressure differential on purge gas flow parallel to and perpendicular to the layers

of insulation. Measurements were made at various absolute pressures in the continuum flow and the free molecular flow regimes. These values compared favorably with flow coefficients obtained theoretically.

Additional laboratory testing was conducted on a 94 x 122 cm (37 x 48 inch) GAC-9 insulation panel assembly comprising two panels butt-joined together. The tests were performed to obtain purge gas flow coefficients, pressure-flow profiles, and the effect of panel joints on gas flow through typical GAC-9 insulation panels. Test results of steady-state and transient pressure tests were in good agreement with flow model values computed from test data obtained from small laboratory flow test specimens. Interstitial gas helium purity was measured as a function of time. Purging was accomplished with an inlet flow rate of 0.000472 m^3/s (1.00 ft^3/min); a 99 percent helium purity level was achieved in approximately 1.08×10^3 seconds (18 minutes).

Subscale tank LH_2 boil-off tests were conducted on the 76-cm (30-inch) diameter double-guarded cylindrical calorimeter insulated with GAC-9 insulation panels. The insulation system included a helium purge system designed within the parameters of the laboratory purge and vent test data obtained in earlier phases of the program. Four boil-off tests were conducted to verify the feasibility and reliability of the GAC-9 insulation system to be purged and vented under cryogenic conditions. The boil-off tests are described below.

Test No. 1 - Initial space environment test without purge jacket

Test No. 2 - Ground-hold, ascent pressure decay, and limited space test with purge jacket

Test No. 3 - Ground-hold and ascent pressure decay test without purge jacket

Test No. 4 - Ground-hold, ascent pressure decay, and limited space test with purge jacket

The initial space test was conducted without the purge jacket to determine the effect of pressure-sensing instrumentation and the purge system components on the thermal performance of the GAC-9 insulation. The average sidewall equilibrium heat leak for 5.08-cm (2-inch) thick GAC-9 insulation was 0.280 W/m^2 (0.089 $Btu/hr\text{-}ft^2$). This value is compared to 0.0277 W/m^2 (0.088 $Btu/hr\text{-}ft^2$) obtained on the same insulation system prior to the addition of the purge system and pressure-sensing instrumentation. The degradation in thermal performance is small because certain extraneous heat sources and sinks were eliminated with the installation of the purge system, thus offsetting the heat leaks introduced by the pressure-sensing instrumentation.

The ground-hold and ascent portion of test No. 2 was conducted to evaluate the helium purge system. After 7200 seconds (2 hours) of flow-through gaseous helium purge at a rate of 0.000472 m^3/s (1.0 ft^3/min), essentially 100 percent helium purity was measured at the insulation helium outlet. Approximately 10 changes in the insulation and purge jacket gas volume were made during purging. The purge jacket failed to open during ascent pressure decay, and the test was stopped due to excessive time required to reach space test conditions.

Test No. 3 (ground-hold and ascent) was run without the purge jacket to determine the ground-hold and ascent thermal performance of the GAC-9 insulation system under ideal purge and vent conditions. Purging was accomplished by vacuum chamber evacuation and gaseous helium backfill. During the ground-hold portion of the test, the GAC-9 insulation bulk temperature and LH_2 boil-off reached equilibrium in approximately 7.2×10^3 seconds (2 hours) which is the same length of time measured on a previous ground-hold test conducted under Contract NAS 8-30140. This performance was also the same as measured on the ground-hold portion of test No. 2 with a purge jacket and flow-through helium purge. The ascent pressure decay boil-off performance was essentially the same as test No. 2.

The ground-hold portion of test No. 4 was conducted to measure ground-hold and ascent pressure decay performance with a purge jacket. Prior to this test, the operation of the purge jacket zipper opening device was satisfactorily demonstrated under a simulated ascent pressure decay condition. During ground-hold, the flow-through helium purge performance was satisfactory (the same as measured in test No. 2). The ascent pressure decay was comparable to the ascent performance of the ground-hold portion of test No. 3, which was run without a purge jacket; therefore, the purge gas venting was not impeded by the purge jacket vent opening. The insulation thermal performance during both the ascent pressure decay and the early period of space performance was normal; therefore, the test was concluded before reaching equilibrium boil-off in the space test condition. Based on the venting performance of the 76-cm (30-inch) calorimeter purge system, a purge jacket vent opening in excess of 2 percent of the insulation surface area is adequate for venting a GAC-9 insulation and purge system with similar proportions.

It was concluded from the results of the purge and vent subscale tank tests that the GAC-9 insulation system could be adequately purged with gaseous helium during ground-hold conditions and that the insulation with a comparable ratio of surface area to panel joint length will vent this purge gas during ascent conditions if the purge jacket or envelope has adequate clearance from the insulation and a vent opening in excess of 2 percent of the outside surface area of a 5.0-cm (2-inch) thickness of insulation. In the 76-cm (30-inch) diameter calorimeter

configuration, the GAC-9 insulation under these venting conditions will reach space performance in a period of approximately 9 x 10^3 seconds (2.5 hours); however, during the last 90 percent of that period, the average thermal performance is about one-half the space performance or 800 times better than ground-hold performance.

A subscale tank LH_2 boil-off test was performed on the 76-cm (30-inch) diameter calorimeter to study the effect of a protrusion insulation on the GAC-9 insulation thermal performance. A 5.0-cm (2-inch) diameter x 25.4-cm (10-inch) long penetration was added to the calorimeter wall in the measuring vessel area. A 2.54-cm (1-inch) thick GAC-9 insulation flanged sleeve surrounded the penetration. The ground-hold and ascent phase performance was unaffected by the penetration insulation. The space performance heat leak was 651 W (6.07 Btu/hr) compared to the heat leak of 332.75 W (3.15 Btu/hr) from test No. 1 on the insulated calorimeter without the penetration. It was concluded from this test that 73 percent of penetration heat leak occurred across the fiberglass wool opacifying material placed between the calorimeter surfaces and the flange of the penetration GAC-9 insulation sleeve. Reducing the area of the fiberglass wool insert should significantly reduce the heat leak attributed to the penetration.

SECTION III

DESIGN IMPROVEMENT, LABORATORY TESTING, AND INSTALLATION EFFORT

A. GENERAL

The GAC-9 insulation system developed under Contract NAS 8-30140 (ref. 1) has been demonstrated as a multilayer composite that is suitable for vehicle-tank application on space missions exceeding 60 days. The feasibility of applying the insulation as prefabricated panels on small-scale cryogen-filled calorimeter test tanks has been demonstrated. These tanks have been subjected to the environments of ground-hold, rapid evacuation, and space. The composite defined as GAC-9 consists of alternate layers of thinly sliced polyurethane foam and doubly aluminized Mylar (DAM) film radiation shields.

The effective thermal conductivity of the GAC-9 insulation system is 0.187 J/m-s-^{o}K (3.0×10^{-5} Btu/ft-hr-^{o}F) when the gas pressure within the insulation is 0.013 N/m^2 (10^{-4}torr) or lower (space condition). This effective thermal conductivity will increase by a factor of 1000 (in proportion to the pressure) in the 13.3 to 0.013 N/m^2 (10^{-1} to 10^{-4} torr) range; thus the performance of the insulation is critically affected by the pressure of the interstitial gases. It is important that the condensing or trapping of these gases be prevented prior to reaching the operational phase of a mission. Therefore, the major emphasis of the current program under Contract NAS 8-26091 was placed on determining and improving the purge and vent characteristics of the GAC-9 insulation system. This effort included a materials investigation and flat-plate calorimeter tests of improved materials.

Also of importance is the degree to which the GAC-9 insulation system can lend itself to a practical method of fabrication and installation on cryogenic tanks. Reliability of fabrication techniques to repeatably produce insulation panels of acceptable quality is of importance. The fabrication operation for installation of drop threads has a potential for introduction of variations in insulation panels. As a part of the continuing program to optimize fabrication and assembly techniques, an investigation was conducted to determine the feasibility of installing drop threads in panelized GAC-9 insulation by mechanical methods.

B. LITERATURE SURVEY

The literature survey included a review of documents concerning investigations of interstitial gas flow characteristics of multilayer insulation systems. The applicable reports are listed in references 2 through 5. These reports were used to compare analytical results and as a guide in selecting pressure-measuring techniques. The literature survey also

included a review of documents describing machinery applicable to mechanization of drop threads in multilayer insulation systems. These documents are general descriptive brochures on sewing machines and mattress tufting machines. The brochures are not identified by document numbers for reference; however, the instruction manuals for the mattress tufting machinery of interest are listed in references 6 and 7.

C. PURGE AND VENT LABORATORY INVESTIGATION

1. General

The GAC-9 insulation purge and vent study was initiated under Contract NAS 8-30140 (ref. 1) to define the gas flow characteristics through a multilayer type of insulation. The primary objectives of this continuing investigation are to demonstrate by laboratory test methods the feasibility and reliability of purging and venting the GAC-9 insulation and to establish engineering data for the design of purge systems.

Laboratory testing included purge gas flow tests (both axial and normal flow) using a 30-cm (12-inch) diameter cylinder test apparatus, panel flow tests using a 94 x 122 cm (37 x 48 inch) test panel, and a series of tests to evaluate the purge and vent pressure-sensing instrumentation. Analyses were performed to demonstrate correlation of equations with laboratory test data. Results of the laboratory tests were verified by cryogenic tests on the 76-cm (30-inch) diameter cylindrical calorimeter insulated with the GAC-9 insulation system.

2. Determination of Pressure-Gas Flow Relationships

a. General. The design of a purge system requires that certain flow coefficients be known. First, the inlets must be located and the inlet pressure (P_i) and helium flow rate $(\dot{m}_{He})_i$ must be calculated. Then the time required to adequately purge the system is determined where the flow at some extreme point ($\dot{m}_o$) has acceptable amounts of air ($\dot{m}_{air}$) and helium ($\dot{m}_{He}$). These calculations require a set of engineering equations containing variables or flow characteristics that must be known. Since the material is not homogeneous, its flow characteristics are different for the various flow directions.

An example of purge gas flow through insulation on a tank is illustrated in Figure 1. A typical cross section of the insulation is also shown. In this cross section the different flow paths are designated by the arrows and the flow coefficients are designated as K. The purge gas must flow down through the insulation parallel to the layers that have a flow coefficient $K_=$. At the same time, the purge gas can flow out of the panel in the normal direction, in which case the flow coefficient is $K_\perp$. A unique flow path for the purge gas is through a joint between panels, resulting in a flow coefficient of K_J. Since the insulation consists of more than one

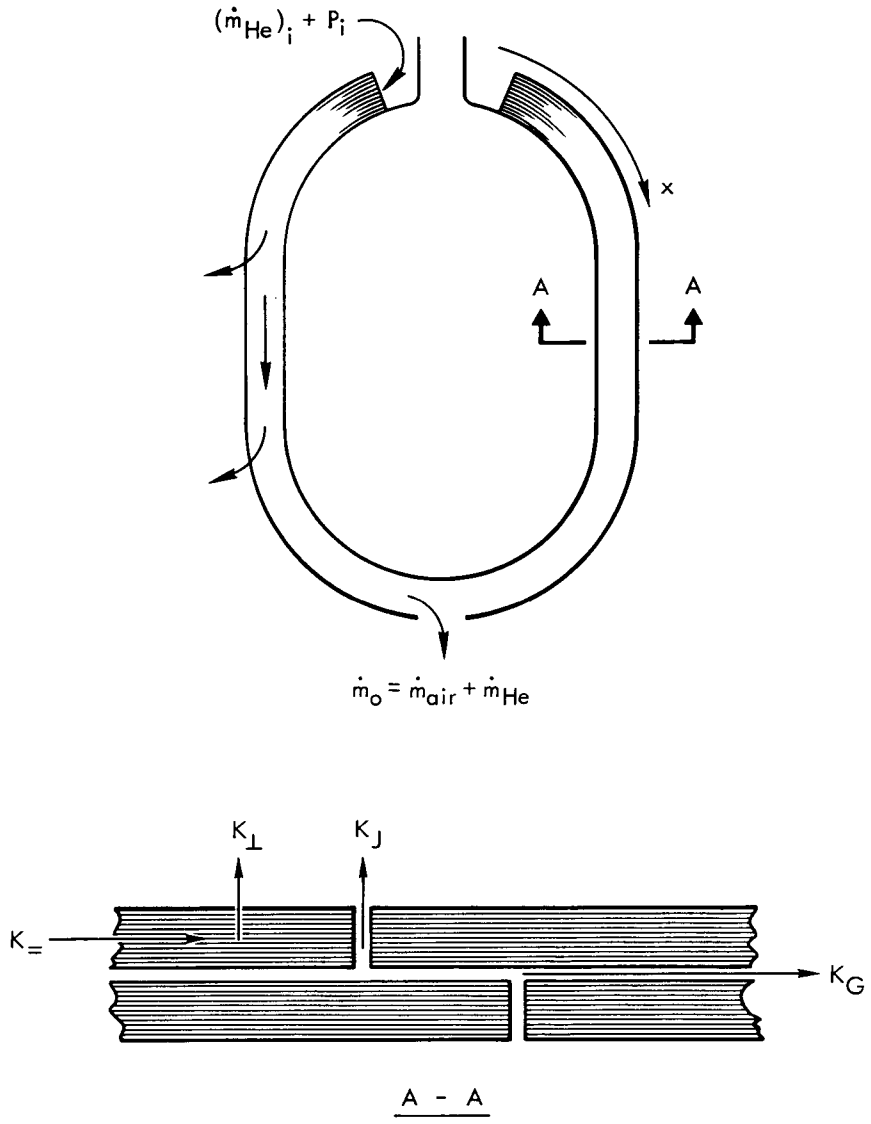

Figure 1. - Purge gas flow through typical tank insulation.

panel, the purge gas from the bottom panel can flow between the panels, parallel to the layers. This interface between panels has a flow coefficient of K_G. This example shows that there are at least four coefficients that must be obtained for the GAC-9 panel design before a purge system can be analyzed to the extent required in conceiving a workable design. A summary of the flow analysis equations and how they are used is described in detail in the following paragraphs.

b. Test Data Evaluation and Correlation (Steady-State). Two flow regimes of significance are encountered during the launch and ascent of a space vehicle. The first regime, called a "continuum" regime, exists during purge and ground-hold conditions. As the absolute pressure within an insulation blanket drops during the ascent of a space vehicle, the flow changes from continuum flow to "free molecular flow." Free molecular flow is characterized by gas flows that are independent of both viscosity and absolute pressure.

Under steady-state, isothermal, incompressible flow conditions, which exist during purge and ground-hold, a single testing procedure can be used to generate flow coefficients for the full range of gas flows. The coefficients are defined by the relation

$$\dot{m} = C_M(\partial P/\partial x)$$

where $\dot{m}$ = the rate of mass flow per unit area
C_M = the characteristic flow coefficient
$\partial P/\partial x$ = the pressure gradient

Since the tests have been designed as parallel flows (i.e., only one velocity component is different than zero), the pressure gradient remains constant across the specimen and $\partial P/\partial x$ is equal to $\Delta P/L$. This result has been verified by preliminary tests at ambient pressure.* The parameter C_M will be used; C_M is the mass flow per unit time per flow area per unit pressure gradient. This coefficient will vary over the different flow regimes and can be computed by the following equation:

$$C_M = \frac{\dot{m}L}{\Delta P} \text{ or } \frac{\rho Q L}{A \Delta P}$$

where ρ = the fluid density
Q = the flow rate
L = the length
A = the area
ΔP = the pressure drop

The value C_M can be determined by testing over various ranges of pressures, lengths, and flow rates.

* These tests are reported in a previous progress report, GER-14915S/5 (Figure 20, page 41).

A theoretical analysis has been made to determine the flow coefficient for all flow regimes. The flow coefficient (C_M) can be calculated (ref. 2) as follows:

$$C_M = \frac{\rho h^2}{3\mu} + \frac{4h\sqrt{\frac{8\bar{R}T}{\pi}}}{3\bar{R}T}$$

where C_M = the flow coefficient

ρ = the density of helium gas

h = the flow channel height

μ = the viscosity of helium gas

T = the gas temperature

$\bar{R}$ = the helium-gas constant

The flow channel height (h) for the GAC-9 insulation system installed in the axial flow test chamber is calculated from

$$h = \frac{\frac{1}{n} - t}{2} = \frac{\frac{2.54}{41} - 38 \times 10^{-3}}{2} = 0.119 \text{ mm } (4.7 \text{ mils})$$

where h = the flow channel height

n = the number of foam spacers

t = the thickness of a foam spacer

The flow channel height is modeled in Figure 2, where the Mylar shield is shown halfway between the foam spacers. Its thickness is negligible. The actual height is somewhat less and can be anywhere from h to 2h, with 2h occurring when the Mylar is pushed against the foam spacer.

The calculated flow coefficient is based on the assumption that there is no flow through the foam spacers. If we assume that there is no flow through the foam, then the actual flow area is the cross-sectional area of the specimen minus the area of the foam layers.

In the theoretical equation for C_M, the height h used in computing the flow coefficient becomes rather critical. It appears as a squared parameter in the continuum-flow term and as a single parameter in the free-molecular-flow term. A slight variation in the value used for the height can give large deviation when predicting flow rates.

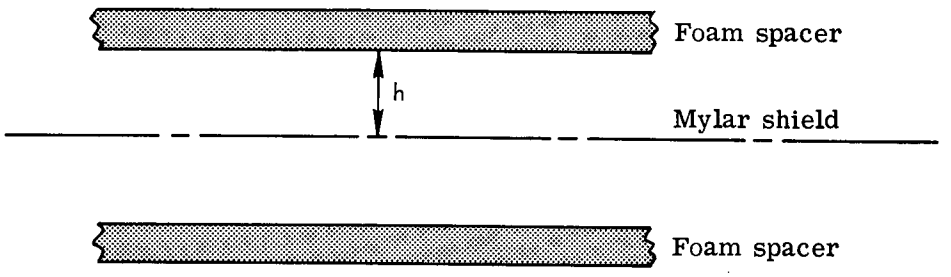

Figure 2. - Flow channel model.

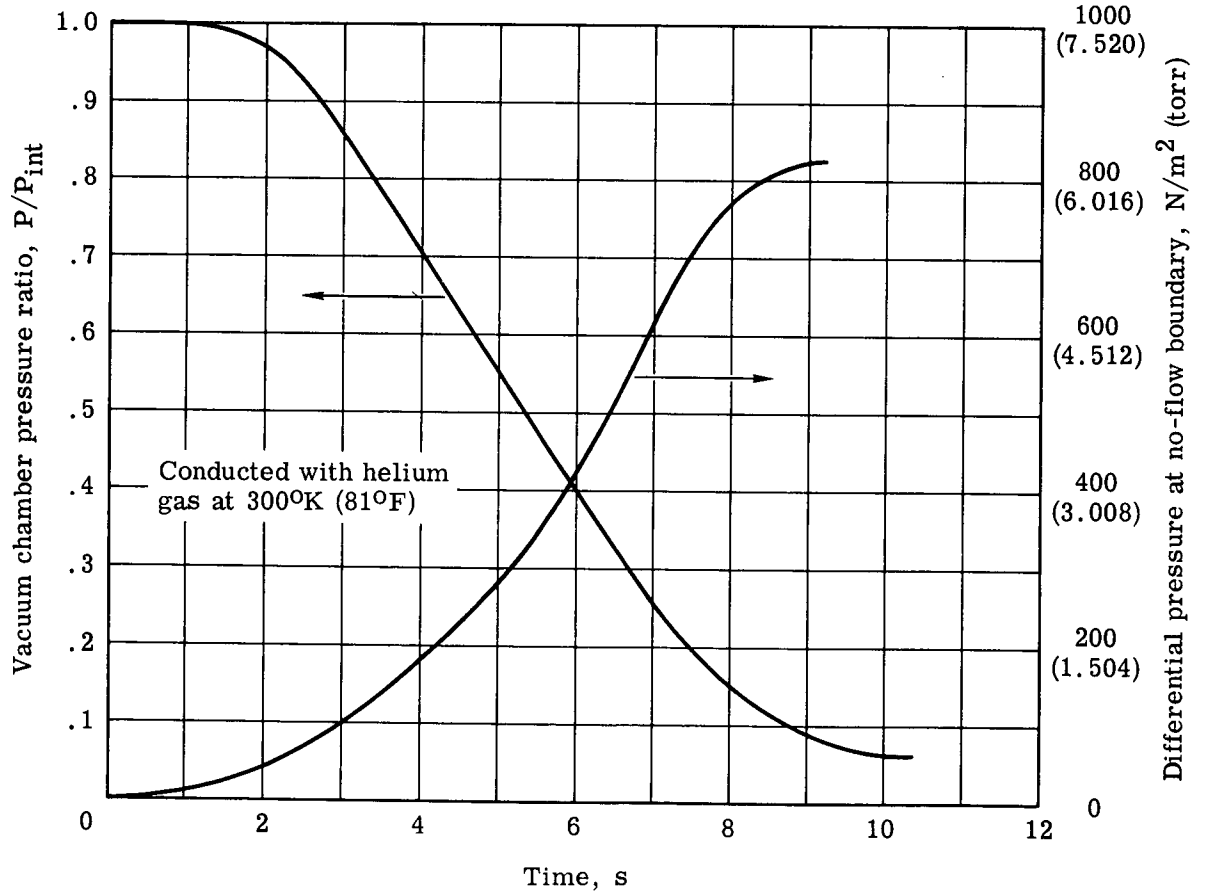

Figure 3. - Predicted pressure differential across a 61-cm (24-in.) axial flow test specimen during rapid chamber evacuation.

c. Transient Analysis. The flow coefficients generated in the evaluation of steady-state test data are used in predicting insulation pressures during the transient of launch and ascent. Although the gas temperature will vary and the flow will be multi-dimensional within an actual propellant tank insulation blanket, a useful first step is to analyze the system by assuming an isothermal and one-dimensional flow.

A one-dimensional, isothermal, transient analysis was programmed on the IBM 360 digital computer. The computer program utilizes a finite difference solution to the equations of flow through porous media and has been checked against similar analyses documented in references 2 and 3. Good agreement was obtained.

A channel height of 0.119 mm (4.7 mils) was assumed in a preliminary analysis of the evacuation characteristics of GAC-9 insulation. The pressure differential at the no-flow boundary is illustrated in Figure 3 for a chamber evacuation profile approximately 10 times more severe than the nominal Saturn 5 profile.

The axial flow and normal flow models used in the computer analysis are shown in Figure 4. The flow equations were combined, simplified, and modified to produce the following final equation:

$$P_i' = P_i \left[1 - \frac{2\bar{R}T\, C_M\, \Delta t}{(\Delta x)^2} \right] + \frac{\bar{R}T\, C_M\, \Delta t}{(\Delta x)^2} \left[P_{(i+1)} + P_{(i-1)} \right]$$

$$+ \frac{h\, h^2\, \Delta t}{12 \mu\, (\Delta x)^2} \left[P_{(i+1)} - P_{(i-1)} \right]^2$$

where $\Delta t \leq \dfrac{0.5\,(\Delta x)^2}{\bar{R}T\, C_M}$ for stability purposes and the terms used in the equation are:

P = the pressure
μ = the viscosity of gas
$\bar{R}$ = the helium gas constant
T = the temperature
C_M = the flow coefficient
Δt = the time increment
Δx = the length increment
h = the flow channel height

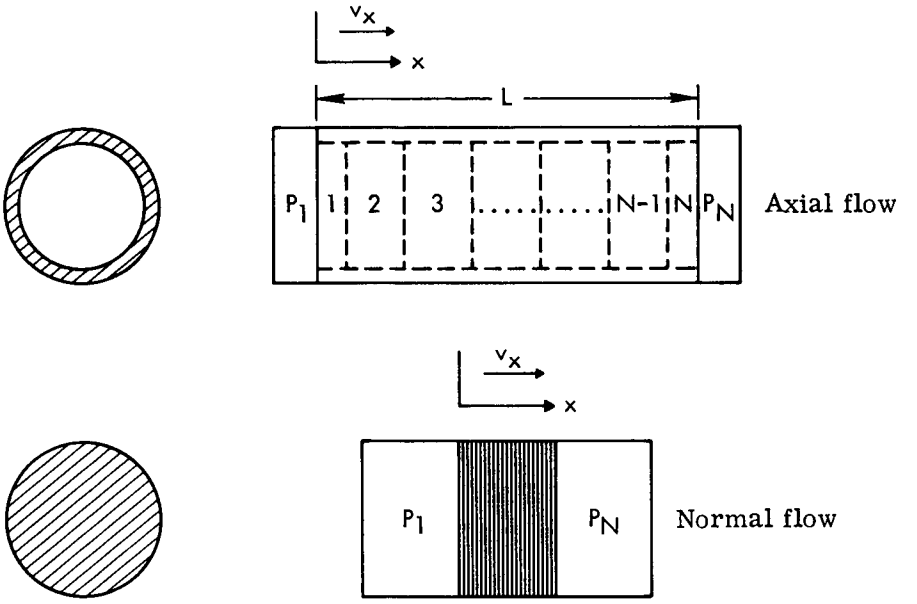

Figure 4. - Axial flow and normal flow models.

3. Axial and Normal Flow Tests

a. Test Plan. The logic used in establishing the test plan for obtaining the necessary purge gas flow coefficients is described in the following paragraphs.

To obtain the flow coefficient $K_{\perp}$, a GAC-9 insulation specimen in the shape of a disc is installed in a circular duct test fixture. The flow of helium gas through the specimen is measured as a function of pressure differential. As part of the specimen installation checkout, a sealing membrane is installed on the upstream side of the specimen and the specimen installation fixtures leak checked. The membrane is then removed and the test continued.

A disc type of GAC-9 insulation test specimen is used to obtain the flow coefficient of a typical joint, K_J. This specimen consists of two halves joined together to form a joint across the diameter.

The flow coefficient parallel to the layers ($K_{=}$) is measured in the same test fixture. However, the GAC-9 insulation is wrapped around a mandrel and inserted into the circular duct. Again, pressure flow measurements are made. To obtain the interface flow coefficient, K_G, the GAC-9 insulation parallel flow test specimen is constructed with two plies of fiberglass outer grid layers sandwiched between the multilayer insulation material. Flow measurements of these four types of test specimens are made at ambient temperature and pressure

with helium gas to provide flow coefficients that apply to a purge system design. Additional testing is performed at a lower pressure to obtain coefficients to be used in determining the venting capability of the material.

The test plan, which is outlined in Table I, involves purge and vent flow tests conducted in both the continuum and free molecular regimes, using the laboratory test apparatus, test procedures, and test specimens described in the following paragraphs.

TABLE I. - TEST PLAN FOR LABORATORY PURGE AND VENT INVESTIGATION - AXIAL AND NORMAL FLOW TESTS

Specimen No.	Specimen description	Test objective
	Normal Flow Tests	
1N	GAC-9 with drop threads. 40 layers per 2.54 cm (1.0 in.) radiation shield density.	Obtain flow coefficients across the insulation and show the effect of drop threads.
2N	GAC-9 with joint and drop threads. 40 layers per 2.54 cm (1.0 in.) radiation shield density.	Obtain flow coefficients across the insulation and show the effect of joint.
3N	GAC-9 with radiation shields perforated 10 holes per 2.54 cm^2 (1.0 $in.^2$), 2.38% open area. 40 layers per 2.54 cm (1.0 in.) radiation shield density.	Obtain flow coefficients across the insulation and show the effect of perforations.
4N	Same as specimen 3N except 1.27 cm (0.5 in.) thickness, 20 radiation shields.	Show the effect of perforations and insulation thickness.
5N	Same as specimen 3N except 30 layers per 2.54 cm (1.0 in.) radiation shield density.	Show the effect of perforations and insulation density.
	Axial Flow Tests	
1A	GAC-9 insulation. 40 layers per 2.54 cm (1.0 in.) radiation shield density. 61 cm (24 in.) long x 31.5 cm (12.39 in.) OD x 26.4 cm (10.39 in.) ID.	Obtain flow coefficients and obtain gas flow characteristics and engineering data on continuum and molecular flow.
2A	Same as specimen 1A except double layer of fiberglass grids inserted at approximately layer No. 20.	Obtain gas flow characteristics of interface between two insulation panels.

b. Test Apparatus. The existing purge and vent apparatus was redesigned to accommodate axial and normal flow testing in accordance with the test plan. The following design modifications were made:

(1) Pressure taps were installed on the test chamber so that gas pressure measurements can be made within the insulation.

(2) An electronic pressure meter was installed for recording total pressure measurements in the range from 0.067 to 133 x 10^3 N/m^2 (10^{-4} to 1000 mm Hg) during steady-state and transient tests.

(3) A helium gas analyzer was installed for determining the time required to completely purge the specimen.

(4) A 12-valve manifold was installed to facilitate rapid pressure measurements.

(5) High vacuum type quick-disconnect couplings were installed at all pressure tap and valve manifold connections to facilitate rapid installation and removal of the specimen from the test chamber.

(6) Precision metering valves were installed at the inlet and outlet connections of the test chamber to permit accurate control of gas flow rates and absolute chamber pressures.

(7) A support frame was fabricated for retaining the position of the normal flow specimens in the test chamber.

(8) A hollow aluminum mandrel and supports were fabricated to facilitate fabrication and testing of axial flow specimens.

Figure 5 shows the complete test setup including the test chamber, vacuum pumping system, and associated instrumentation. This setup was designed for determining the gas flow characteristics of multilayer insulation in the continuum, transition, and free molecular flow regimes within the following flow and pressure ranges:

(1) Flow Rate: 0.0167 x 10^{-4} to 1.0 liter/second

(2) Pressure: 0.067 to 133 x 10^3 N/m^2 (10^{-4} to 1000 mm Hg)

Absolute or differential pressure measurement tests with the purge gas flow parallel to the insulation were conducted using the axial flow setup shown schematically in Figure 6. This setup permits measuring the pressure gradient within the insulation at 10 different locations and the total pressure drop across the insulation specimen. The holes for the pressure

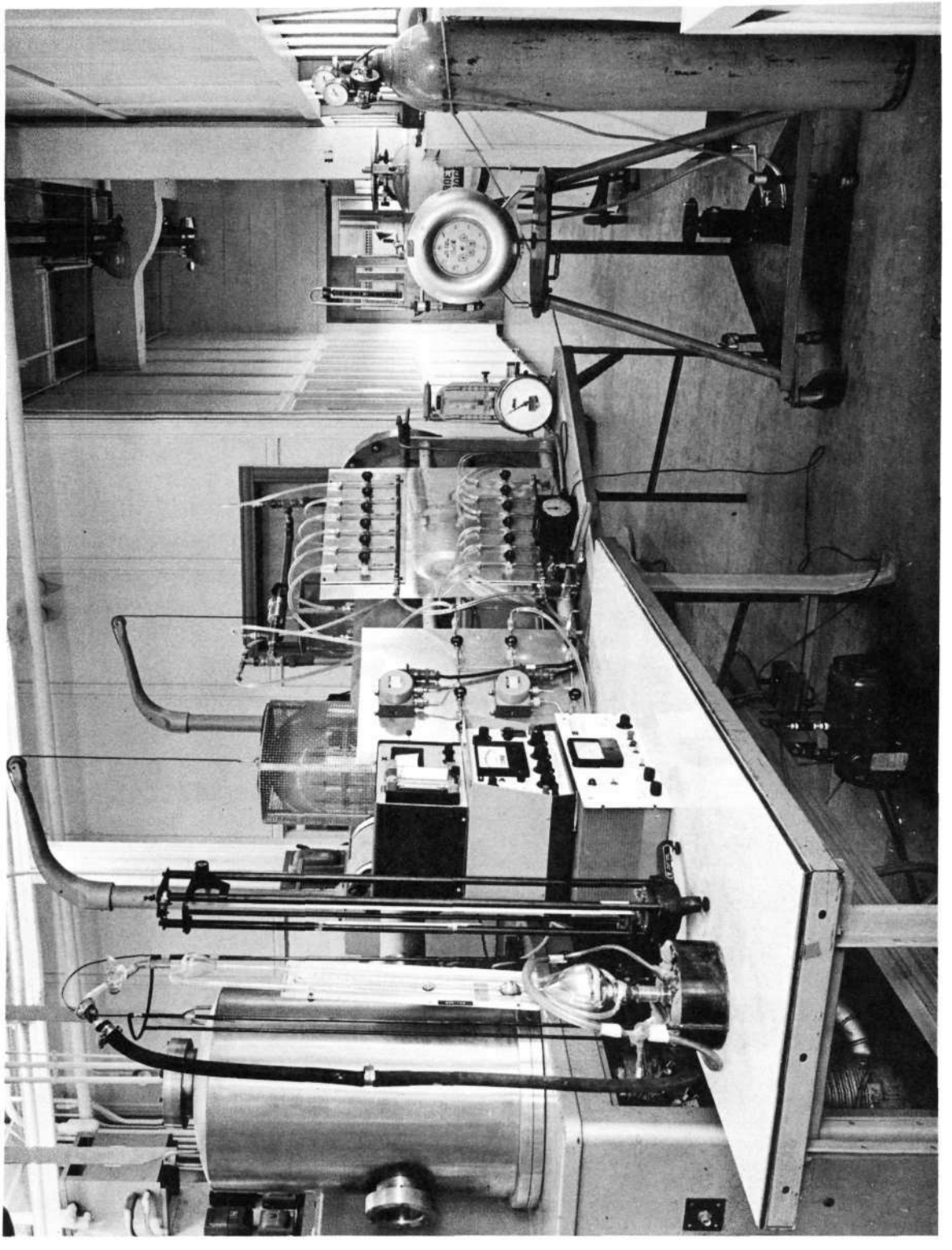

Figure 5. - Laboratory purge and vent test apparatus.

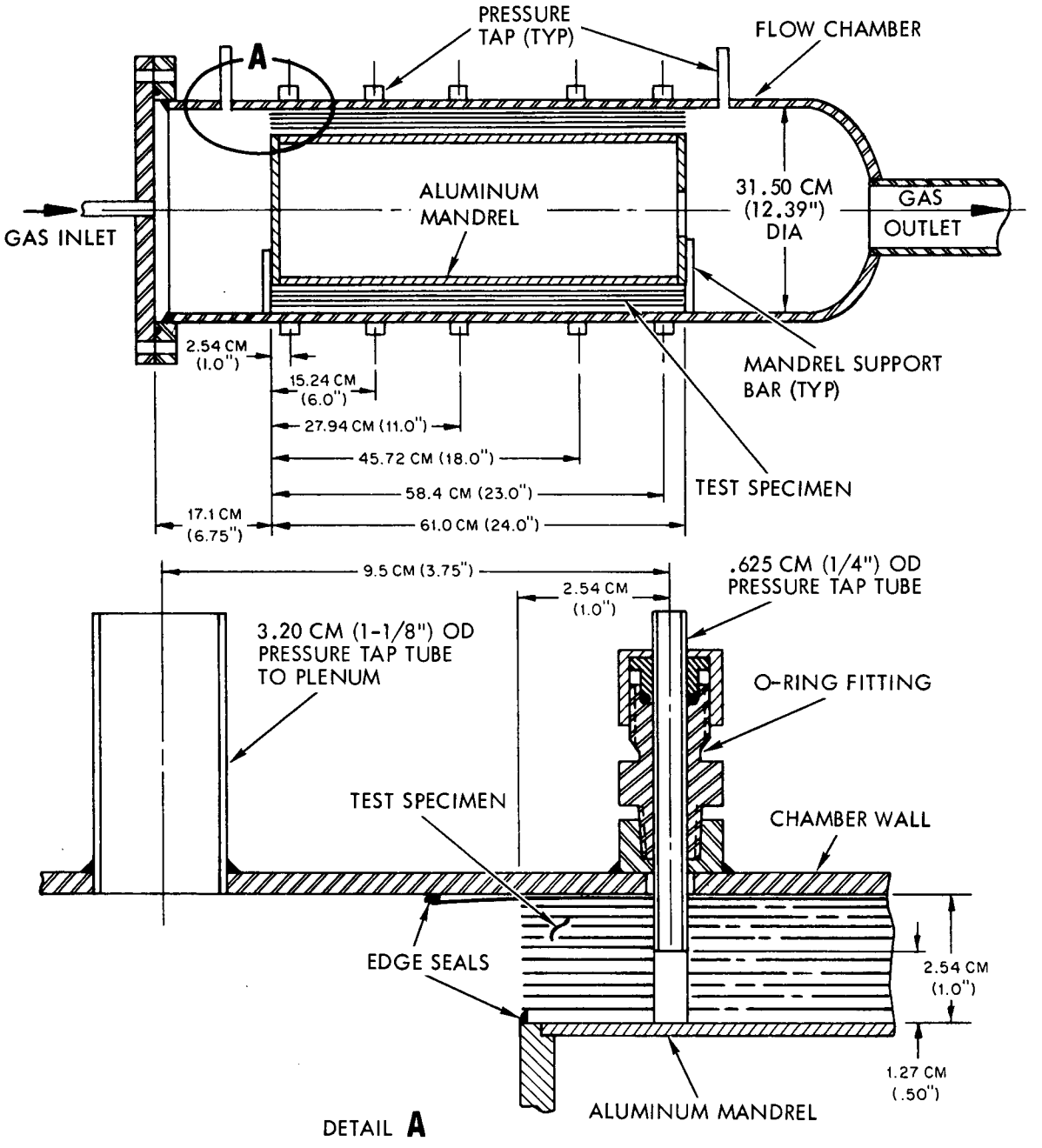

Figure 6. - Axial flow test setup.

taps within the insulation are drilled after the specimen is installed in the test chamber to ensure proper alignment of the holes with respect to the pressure taps. A diagram of the instrumentation used in conjunction with this test is shown in Figure 7.

Tests with the gas flow perpendicular to the insulation were conducted using the normal flow setup shown schematically in Figure 8. In this setup, the pressure drop across the specimen is measured using the instrumentation shown in Figure 7 connected to the appropriate chamber pressure taps.

c. Test Procedures. The purge and vent test was conducted on axial flow specimen 1A to accomplish the following:

(1) Verify predicted flow coefficients and instrumentation repeatability.

(2) Investigate high flow rate and compressibility effects.

(3) Establish effective flow test procedures.

The tests on this specimen were conducted in the sequence shown in Table II. Test runs No. 1 through 29 consisted of measuring absolute chamber pressure, the differential pressure across the specimen, and helium gas flow rates.

At the conclusion of test run No. 26, the specimen was conditioned for 8.64×10^4 seconds (24 hours) in a vacuum of 133×10^{-5} N/m^2 (1×10^{-5} torr). Test runs No. 27, 28, and 29 were then conducted.

Analysis of the test results on specimen 1A indicated that tests on the remaining normal and axial flow specimens should be conducted in accordance with the following revised test procedures:

(1) Install the test specimen in the flow chamber and apply a room-temperature-curing, two-component, silicone, edge seal adhesive.

(2) Allow edge seal adhesive to cure for a minimum of 4.32×10^4 seconds (12 hours) at room temperature before starting test.

(3) For normal flow specimens, conduct edge seal leak test at ambient pressure by applying a differential pressure of 13.3 N/m^2 (0.10 torr) across the specimen and measuring the helium gas flow rate through the specimen.

(4) Verify that the edge seal leak is less than 1 percent of the predicted helium gas flow rate through the specimen at ambient pressure and then remove the upstream membrane seal.

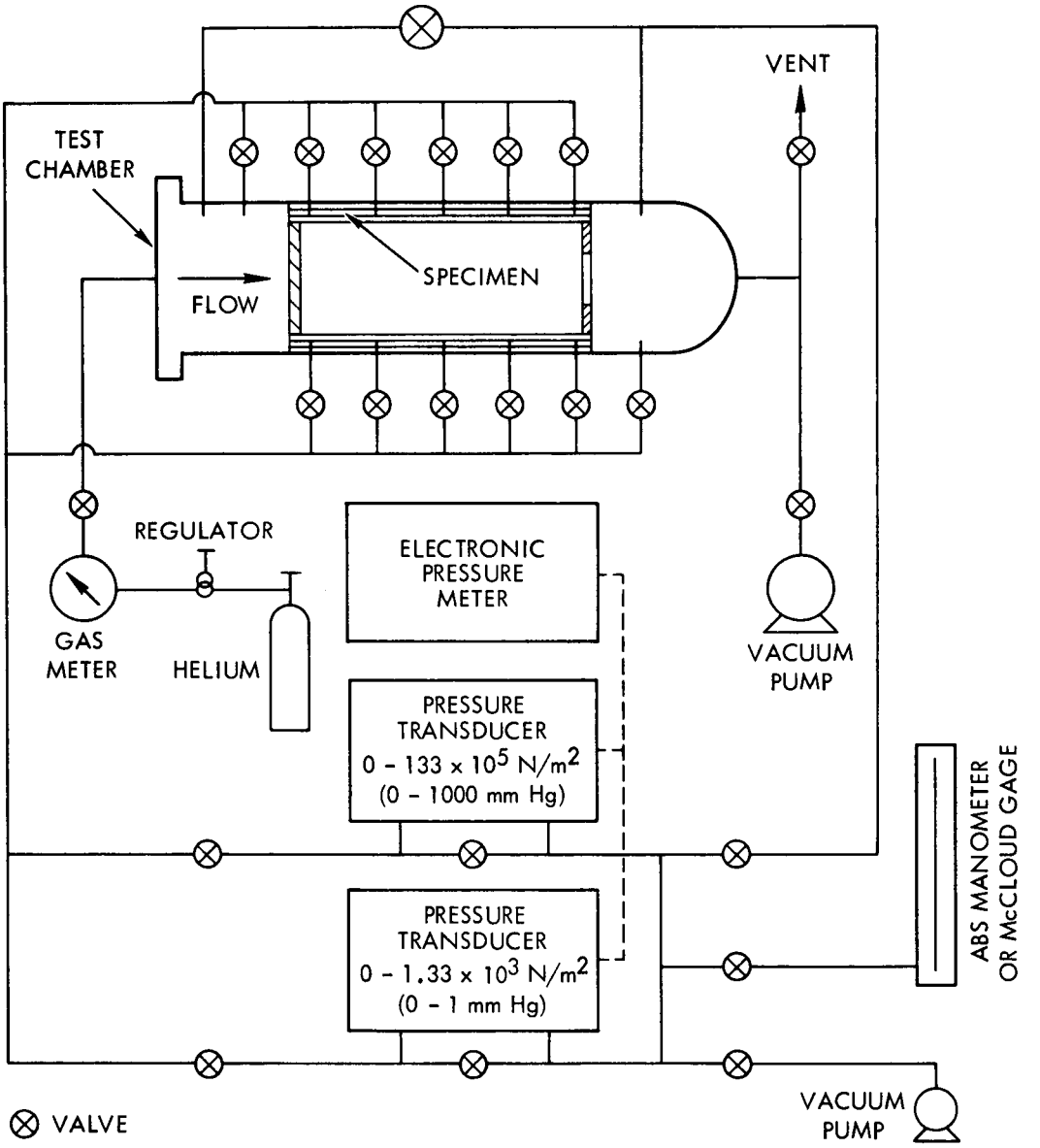

Figure 7. - Axial flow test instrumentation diagram.

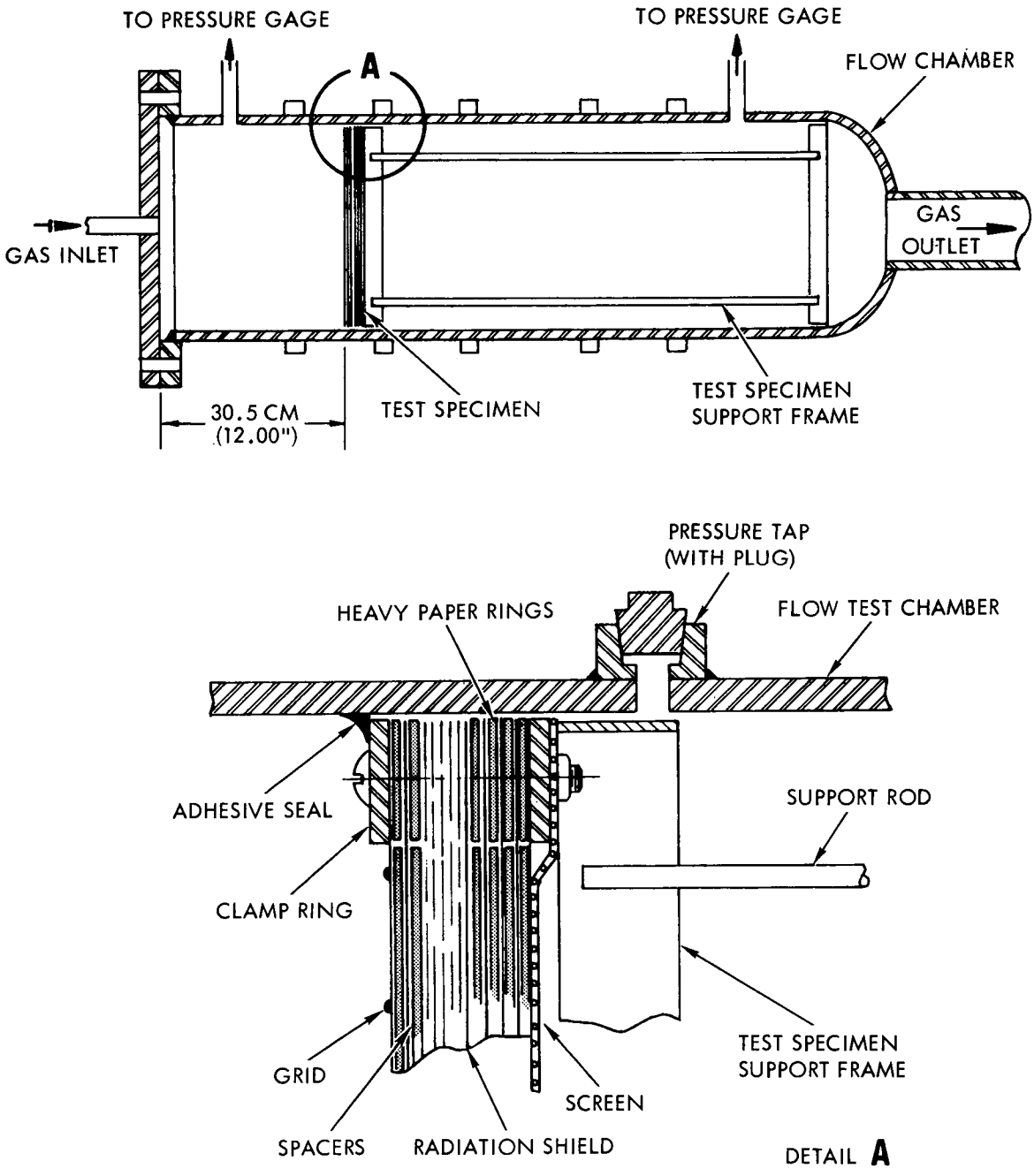

Figure 8. - Normal flow test setup.

TABLE II. - PURGE AND VENT TEST SEQUENCE FOR AXIAL FLOW SPECIMEN 1A

Run No.	Absolute chamber pressure, N/m^2 (torr)	Differential pressure across specimen, N/m^2 (torr)
1	981×10^2 (736)	72.4 (0.543)
2	988×10^2 (741)	249.3 (1.87)
3	1007×10^2 (755)	424.0 (3.18)
4	981×10^2 (736)	66.0 (0.495)[a]
5	991×10^2 (743)	132.0 (0.990)[a]
6	1007×10^2 (755)	198.6 (1.49)[a]
7	668×10^2 (501)	140.8 (1.056)
8	340×10^2 (255)	68.3 (0.512)
9	39.1×10^2 (29.3)	69.3 (0.520)
10	59.3×10^2 (44.5)	125.9 (0.944)
11	59.9×10^2 (44.9)	125.3 (0.940)
12	57.6×10^2 (43.2)	188.5 (1.414)
13	62.0×10^2 (46.5)	586.6 (4.40)
14	64.8×10^2 (48.8)	839.9 (6.30)
15	67.7×10^2 (50.8)	725.3 (5.44)
16	67.7×10^2 (50.8)	589.3 (4.42)
17	55.9×10^2 (41.9)	602.6 (4.52)
18	984×10^2 (738)	200.0 (1.50)
19	989×10^2 (742)	417.3 (3.13)
20	987×10^2 (740)	297.3 (2.23)
21	992×10^2 (744)	566.6 (4.25)
22	984×10^2 (738)	298.6 (2.24)
23	984×10^2 (738)	498.6 (3.74)
24	984×10^2 (738)	124.7 (0.935)
25	992×10^2 (744)	666.6 (5.00)
26	992×10^2 (744)	933.3 (7.00)
27	3.60 (0.027)	5.3 (0.0395)
28	10.00 (0.075)	4.6 (0.0341)
29	213.00 (1.60)	4.3 (0.032)

[a] Differential pressure data at 10 taps in specimen measured during run.

(5) Conduct normal or axial specimen flow tests at the pressures specified in Table III.

Laboratory purge and vent tests on normal flow specimens 1N, 2N, 3N, 4N, and 5N and axial flow specimen 2A were performed in accordance with the above test procedures. Test results and analysis are present in paragraph 3-e of this subsection.

TABLE III. - PURGE AND VENT TEST PRESSURES FOR AXIAL AND NORMAL FLOW TEST SPECIMENS

Absolute chamber pressure, N/m^2 (torr)[a]	Differential pressure across specimen, N/m^2 (torr)[a]
98.6×10^3 (740)	≤ 13.33 (≤ 0.10)
9.86×10^3 (74)	≤ 13.33 (≤ 0.10)
0.986×10^3 (7.4)	≤ 13.33 (≤ 0.10)
≤ 0.0133 ($\leq 10^{-4}$)	0.00 (0.00)[b]
0.933 (0.007)	≤ 2.66 (≤ 0.02)
9.331 (0.07)	≤ 6.66 (≤ 0.05)
98.6 (0.74)	≤ 6.66 (≤ 0.05)

[a] The pressures given are approximate and may vary depending on the flow characteristics of the specific test specimen.

[b] Condition specimen for 8.64×10^4 seconds (24 hours) to remove water vapor and other volatile materials.

d. Test Specimens. Cylindrical axial flow specimen 1A is 61.0 cm (24 inches) long with a 2.54-cm (1.0-inch) wall consisting of 42 layers of 0.0038-mm (0.15-mil) doubly aluminized Mylar (DAM) and 41 layers of 0.043-cm (0.017-inch) NC (non-combustible) foam applied alternately in concentric layers around the aluminum mandrel (fig. 9). Due to the inherent tightening effect of concentric wrapping of the insulation layers, specimen 1A thickness was less than 2.54 cm (1.0 inch) with 40 layers of DAM and 39 layers of foam. A specimen thickness of 2.54 cm (1.0 inch) is critical to the proper operation of the axial flow test fixture. Therefore, two extra layers of DAM and foam were added to increase the specimen thickness to 2.54 cm (1.0 inch). It was estimated that the additional layers would have a negligible effect on flow characteristics. For pressure measurements within the specimen, five pairs of 0.635-cm (0.25-inch) diameter holes are drilled full depth into the specimen at diametrically opposite locations as shown in Figure 6.

Axial flow specimen 2A was designed and constructed to obtain flow characteristics of the interface between two insulation panels. This specimen, identical with specimen 1A in size, contains 40 layers of 0.0038-mm (0.15-mil) DAM alternated with 39 layers of 0.038-cm (0.015-inch) NC foam. At Mylar layer No. 20, two layers of fiberglass roving grids are included in the specimen. One grid with fiberglass edge bands was wrapped around the specimen

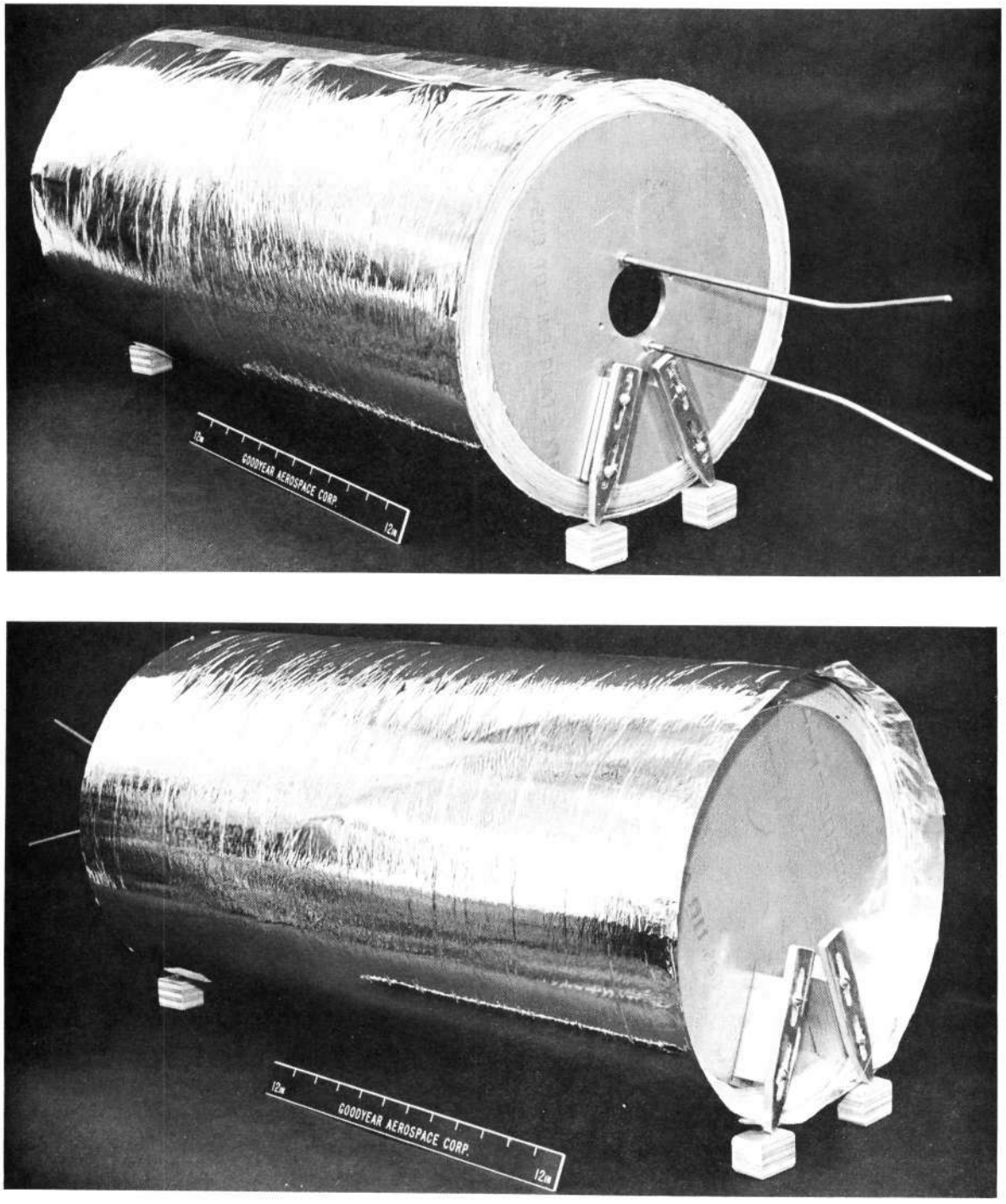

Figure 9. - Views of axial flow specimen 1A.

and laced together in the same manner as a typical GAC-9 insulation panel-to-panel joint. The joint was aligned with the axis of the cylindrical specimen. The second grid layer, without edge band, was wrapped over the first grid to simulate a panel-to-panel interface.

Normal flow specimen 1N, shown in Figure 8, was designed to eliminate the perimeter sealing deficiency encountered in previous flow test runs under Contract NAS 8-30140 (ref. 1). The specimen is 2.54-cm (1.0-inch) thick GAC-9 insulation consisting of 40 layers of 0.0038-mm (0.15-mil) DAM and 39 layers of 0.043-cm (0.017-inch) NC foam alternately applied between two grid face sheets. The perimeter of each foam layer is surrounded by a washer-like ring of heavy paper the same thickness as the foam. The perimeter area of each layer of Mylar was clamped between the paper rings when the specimen was assembled with metal clamping rings and bolts. The tightly clamped paper rings form a rigid edge band that will prevent edge leak of purge gas and will not compress during flow tests, thus precluding peeling failure of the adhesive bead seal between the specimen and the inner wall of the flow test chamber. This seal and the specimen installed in the test chamber are shown in Figure 10. A layer of 0.0063-mm (0.25-mil) DAM was installed over the grid on the upstream face of the test specimen to prevent flow through the specimen during checkout of the adhesive bead seal. This seal membrane was removed after a leak check of the adhesive bead seal.

Normal flow specimen 2N was designed to incorporate a typical butt joint between the GAC-9 insulation panels. This specimen is 2.54-cm (1.0-inch) thick GAC-9 insulation consisting of 40 layers of 0.0038-mm (0.15-mil) DAM and 39 layers of 0.043-cm (0.017-inch) foam applied between grid face sheets with edge bands positioned along a butt joint at the center axis as shown in Figure 11. The perimeter of this test specimen incorporates the tightly clamped paper ring edge band described for normal flow specimen 1N.

Normal flow specimen 3N was constructed with 40 radiation shields of 0.0038-mm (0.15-mil) DAM perforated to pattern 9810 and 39 layers of 0.043-cm (0.017-inch) NC foam. The design of this specimen deleted the washer-like rings of heavy paper used on specimens 1N and 2N. It was observed that the small gap between the perimeter of each of the foam spacers and the mating paper rings would contribute to serious local leak on the perforated shield specimen. To avoid this problem, the foam spacers were extended to the outside diameter of the specimen and the edge area clamped tightly between the metal clamping rings as shown in Figure 12.

The clamped edge of the specimen was very firm and will not compress during flow tests, thus precluding failure of the adhesive bead seal between the test specimen and the wall of the flow test chamber.

Figure 10. - Normal flow specimen 1N in flow test chamber.

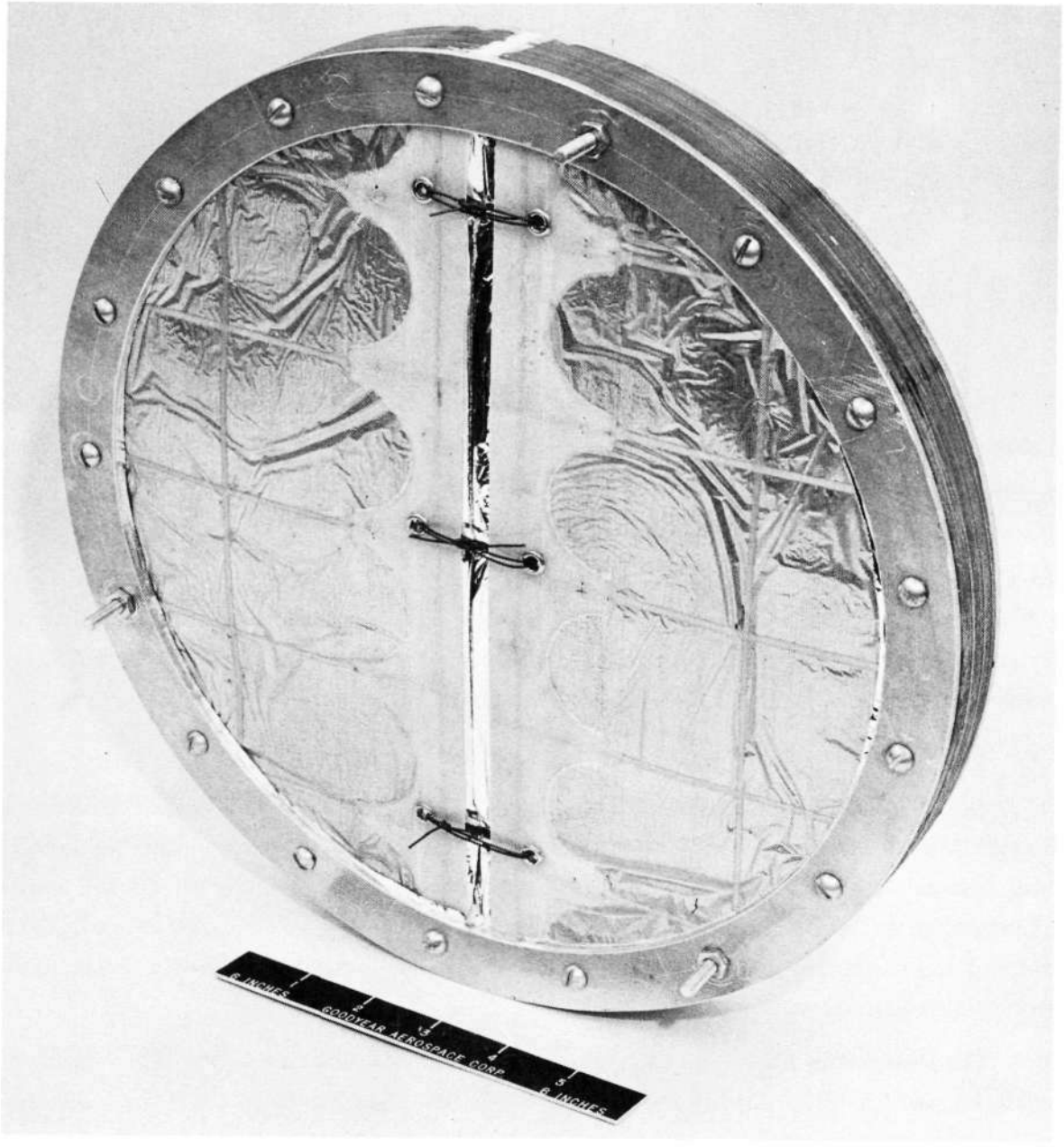

Figure 11. - Normal flow specimen 2N with butt joint.

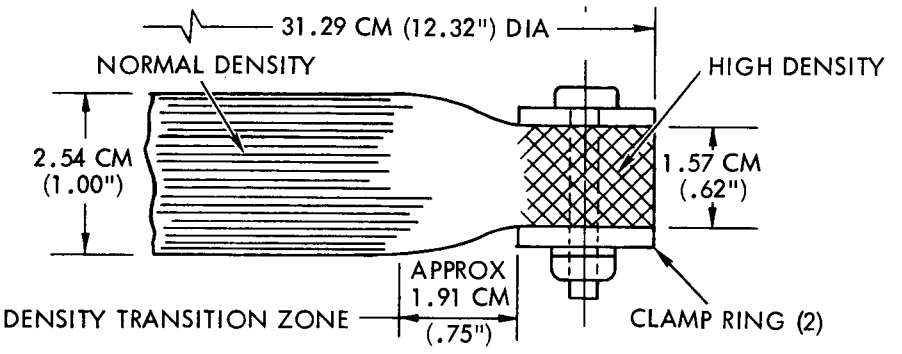

Figure 12. - Edge details of normal flow specimen 3N.

Normal flow specimen 4N was fabricated by removing 20 layers each of Mylar radiation shields and foam spacers from specimen 3N to create a 1.27-cm (0.5-inch) thick specimen containing 20 Mylar shields and 19 foam spacers.

Normal flow specimen 5N was fabricated with 30 radiation shields of 0.0038-mm (0.15-mil) DAM perforated to pattern 9810 and 29 layers of 0.043-cm (0.017-inch) NC foam. The design of this specimen is similar to normal flow specimen 3N, but a washer-like ring of heavy paper was installed at the perimeter of every third layer of foam to provide sufficient edge thickness for a 2.54-cm (1.0-inch) thick specimen.

e. Prediction and Evaluation of Test Results

(1) General. The purpose of conducting one-dimensional, steady-state flow tests on both axial flow and normal flow test specimens in the laboratory was to generate basic engineering data sufficient for predicting the purge and vent characteristics of the GAC-9 multilayer insulation system. Later in the program, this information was utilized to predict and correlate the test results for applications both to large panels and to the 76-cm (30-inch) diameter calorimeter insulation panels.

The flow theory used to predict flow coefficients both for flows parallel to the layers of insulation and for flows through the joints between panels is represented by the following equation from reference 2.

$$C_M = \frac{h^2\rho}{3\mu} + \frac{4h\sqrt{\frac{8\bar{R}T}{\pi}}}{3\bar{R}T}$$

where C_M = the specific mass flow coefficient
h = the flow channel height
ρ = the helium gas density
μ = the helium gas viscosity
$\bar{R}$ = the helium gas constant
T = the helium gas temperature

The specific mass flow coefficient can be determined from pressure-flow test data in the laboratory and then correlated with the flow coefficient predicted from theory. The specific mass flow coefficient is determined from test data by the following relation:

$$C_M = \frac{\dot{m}L}{\Delta P} = \frac{Q\rho L}{A_F \Delta P}$$

where Q = the gas flow
ρ = the gas density
L = the specimen length
$\dot{m}$ = the rate of mass flow per unit area
A_F = the flow area
ΔP = the pressure differential

(2) Axial Flow Tests. The mass flow coefficient C_p for flow parallel to the layers of insulation has been based on the cross-sectional area of the panel rather than the actual flow area (cross-sectional area minus the foam thickness). The relation between C_M and C_p is

$$C_p = \frac{A_F}{A} C_M$$

where A_F = the actual flow area
A = the cross-sectional area

The mass flow coefficient is used to predict gas flows in the multilayer insulation blanket by the relation

$$Q = C_p A \frac{\Delta P}{\rho L}$$

where ΔP = the pressure differential
L = the blanket length

Axial flow specimen 1A was tested to investigate the flow parallel to the layers of insulation. At low flows and pressure differentials, the test results for axial flow specimen 1A

closely agreed with the theoretical prediction. The mass flow coefficient is shown in Figure 13 as a function of absolute chamber pressure (P) for helium gas at 300°K (540°R). The theoretical prediction is based on the analysis described above for a channel height h calculated from

$$h = \frac{1/N - t_f}{2} = 0.094 \text{ mm } (0.0037 \text{ in.})$$

where h = the height of the flow channel

N = the number of layers per insulation thickness

t_f = the thickness of an average foam spacer

The predicted flow coefficient is based on the assumptions that the gas flows through the space between adjacent foam layers and that the presence of the Mylar shields has a negligible effect on the flow.

As predicted from theory, the specific mass flow coefficient is essentially a linear function of the absolute pressure in the continuum regime and constant in the free molecular regime.

Since larger flows and pressure differentials might be experienced in either purge or vent applications, the pressure-flow relations were thoroughly investigated on test specimen 1A at pressure differentials up to 934 N/m^2 (7 torr) and at absolute pressures of 0.987×10^5 N/m^2 (740 torr) and 0.6×10^4 N/m^2 (45 torr). The results of this investigation are plotted in Figures 14 and 15, which show the mass flow rate as a function of pressure differential for the two absolute pressures. At each absolute pressure, the flow rate is shown to increase nonlinearly with increasing pressure differential. This is contrary to normal viscous flow phenomena in that the mass flow is generally a linear function of the pressure gradient in cases where the absolute pressure and temperature have been held constant.

In order to verify the linearity of the test apparatus and to assure the significance of the test results, the pressure gradient was measured at five locations along the length of test specimen 1A, at taps located both above and below the specimen. The results given in Figure 16 show that the pressure gradient was linear across the length of the test specimen for both high and low rates of flow.

The only explanation for the nonlinear increase of mass flow with increasing pressure differential is that the specimen was effectively "opening" at higher rates of flow. Apparently, the higher rates of flow were sufficient to widen the flow paths through the layers of insulation.

Sym	Spec	Material	Layers
○	1A	.043-cm (.017-in.) foam	41
		.0038-mm (.15-mil) DAM	42
□	2A	.038-cm (.015-in.) foam	19
		.0038-mm (.15-mil) DAM	20
		Fiberglass grids	2
		.038-cm (.015-in.) foam	20
		.0038-mm (.15-mil) DAM	20

Nominal helium gas temp = 300°K (540°R)

Specimen length = 0.610 m (24 in.)

Specimen area = 0.228×10^{-1} m^2 (35.4 $in.^2$)

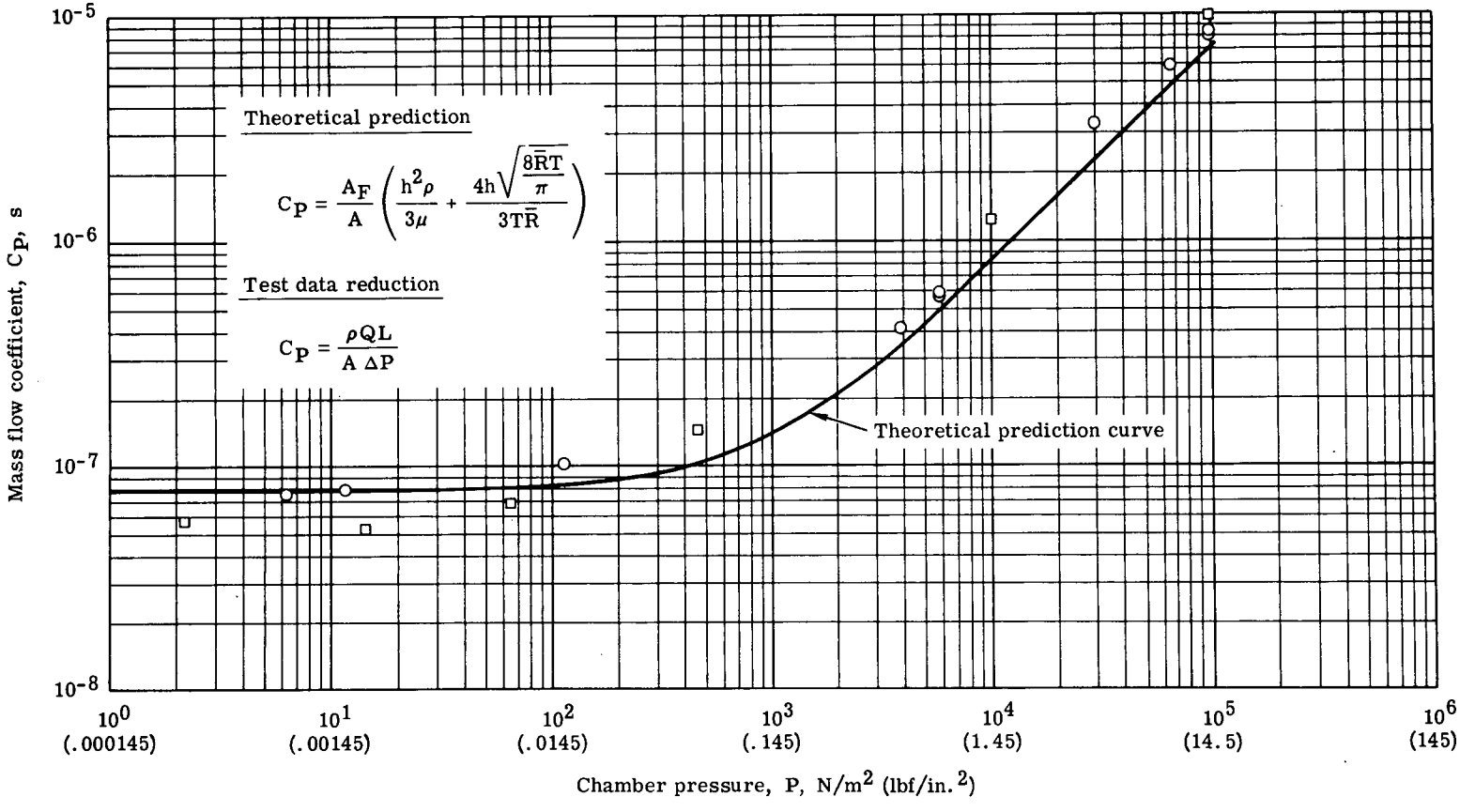

Figure 13. - Helium gas flow characteristics - axial flow specimens 1A and 2A.

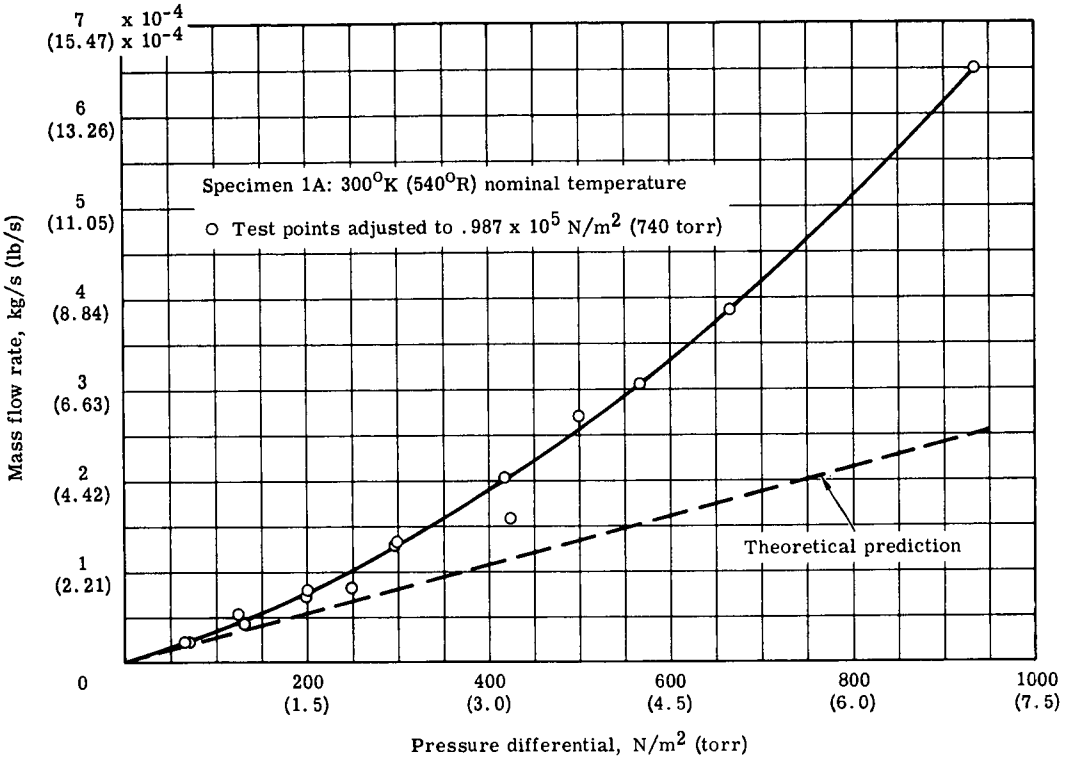

Figure 14. - Mass flow versus pressure differential at 0.987 x 10^5 N/m^2 (740 torr) downstream pressure - axial flow specimen 1A.

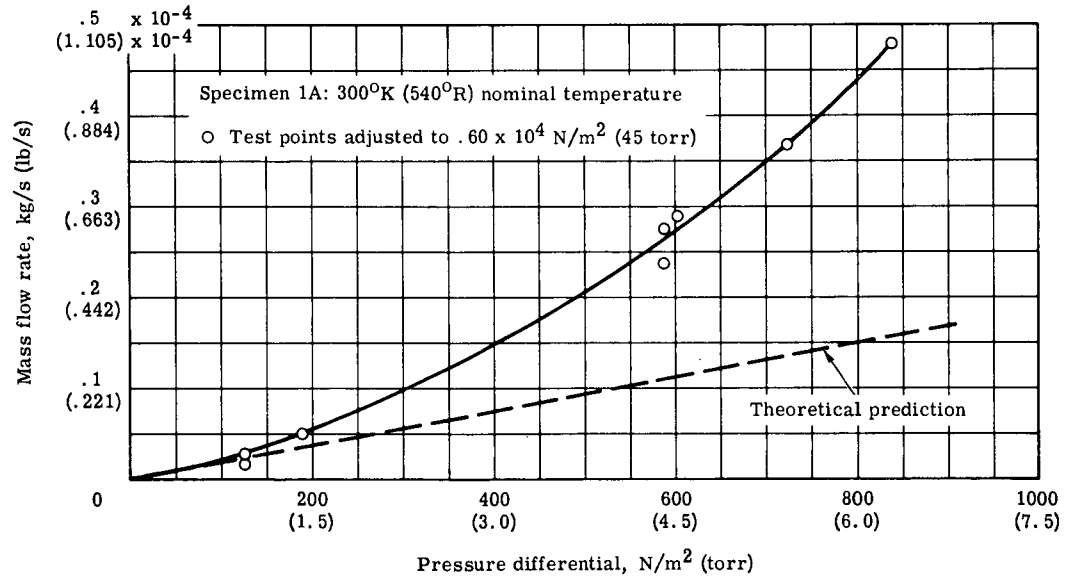

Figure 15. - Mass flow versus pressure differential at 0.6 x 10^4 N/m^2 (45 torr) downstream pressure - axial flow specimen 1A.

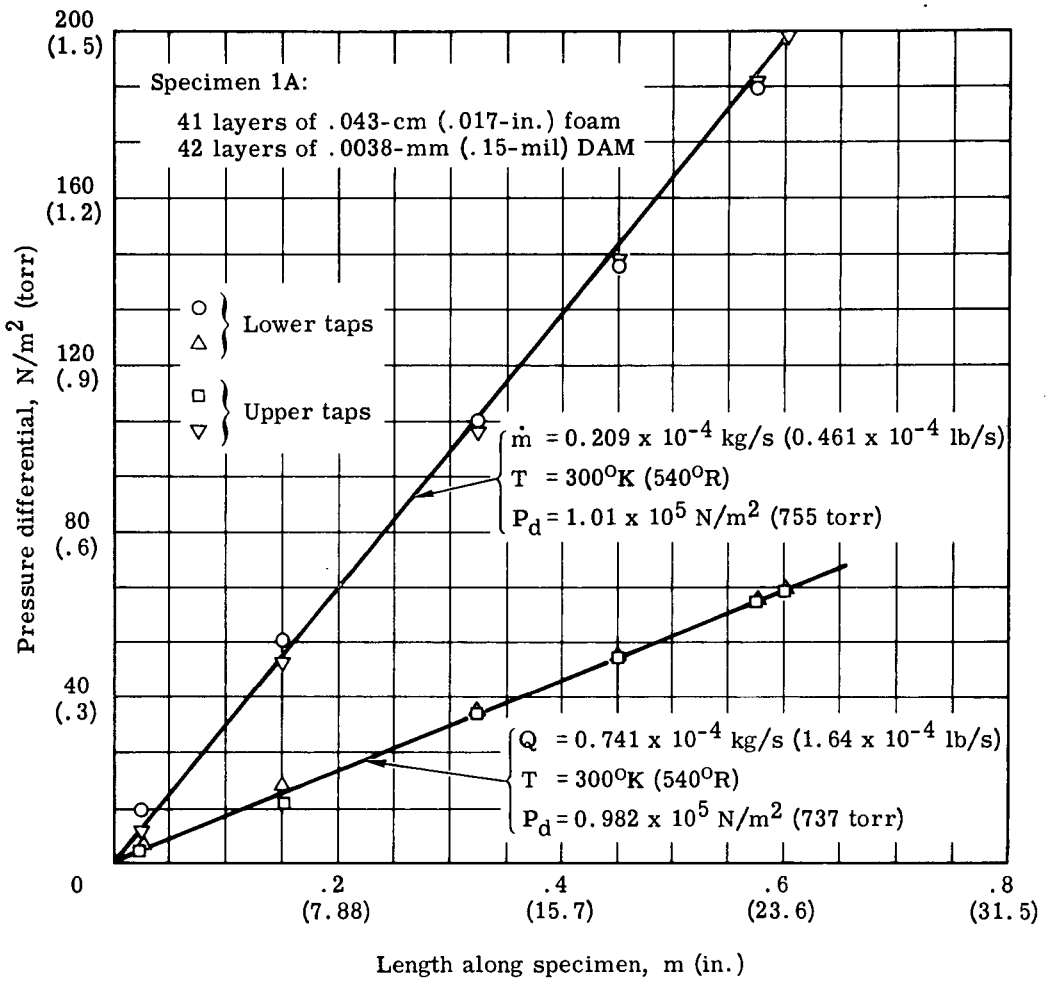

Figure 16. - Pressure gradient along axial flow specimen 1A.

Figures 13, 14, and 15 show that test data and theoretical predictions are in close agreement at low rates of flow and small pressure differentials. Since higher rates of flow will open the insulation material and therefore increase either the rate of purging or the rate of venting above what might have been expected, the use of the reported flow coefficients will generally be a conservative approach in the design and analysis of actual applications.

Axial test specimen 2A was designed and tested to determine the effect of joint grid-lacing on the axial flow coefficient. Since the space between the laced grid face sheets of panel joints constitutes a potential flow path, it was felt that the flow coefficient for specimen 2A might be higher than the coefficient previously determined for specimen 1A.

The flow coefficients measured for specimen 2A are shown as a function of mean chamber pressure in Figure 13. The flow coefficient for specimen 2A is higher at pressures above 133 N/m^2 (1 torr) and lower at pressures below 133 N/m^2 (1 torr) than the coefficients measured for specimen 1A. The inclusion of the grid facings and lacing strip in specimen 2A should have increased the flow coefficient if everything else were held constant. The increase was verified above 133 N/m^2 (torr). Below 133 N/m^2 (1 torr), the flow coefficient for specimen 2A was of smaller magnitude than the coefficient for specimen 1A. The only explanation is that because specimen 2A was an entirely new specimen, the hypothetical flow coefficient for specimen 2A without the lacing strip would have been different from the coefficient measured for specimen 1A. This can be expected since there will be unavoidable variations in the fabrication of the two specimens.

Because the variation in flow coefficients for specimens 1A and 2A is small relative to variations that might be expected as a result of differences in fabrication, we can conclude that the lacing strip has a negligible effect on the axial flow coefficient.

(3) Normal Flow Tests (Specimen 1N). The first specimen was tested to determine the flow coefficient normal to the layers, primarily through the drop thread holes. No measurable flow could be detected; therefore, this coefficient is assumed to be zero.

(4) Normal Flow Tests (Specimen 2N). A mass flow coefficient C_J for flow between joints in the multilayer insulation blanket was predicted from theory and correlated with test data. The mass flow coefficient is used to predict gas flows in the multilayer blanket by the relation

$$Q = C_J \frac{\ell \Delta P}{t \rho}$$

where Q = the gas flow

C_J = the mass flow coefficient

ℓ = the joint length

t = the blanket thickness

ΔP = the pressure differential

ρ = the gas density

The test results and theoretical predictions for specimen 2N were in reasonable agreement, as illustrated in Figure 17. The predicted flow coefficient was calculated as described earlier (see general discussion) using an assumed joint width of 0.26 mm (0.0105 inch).

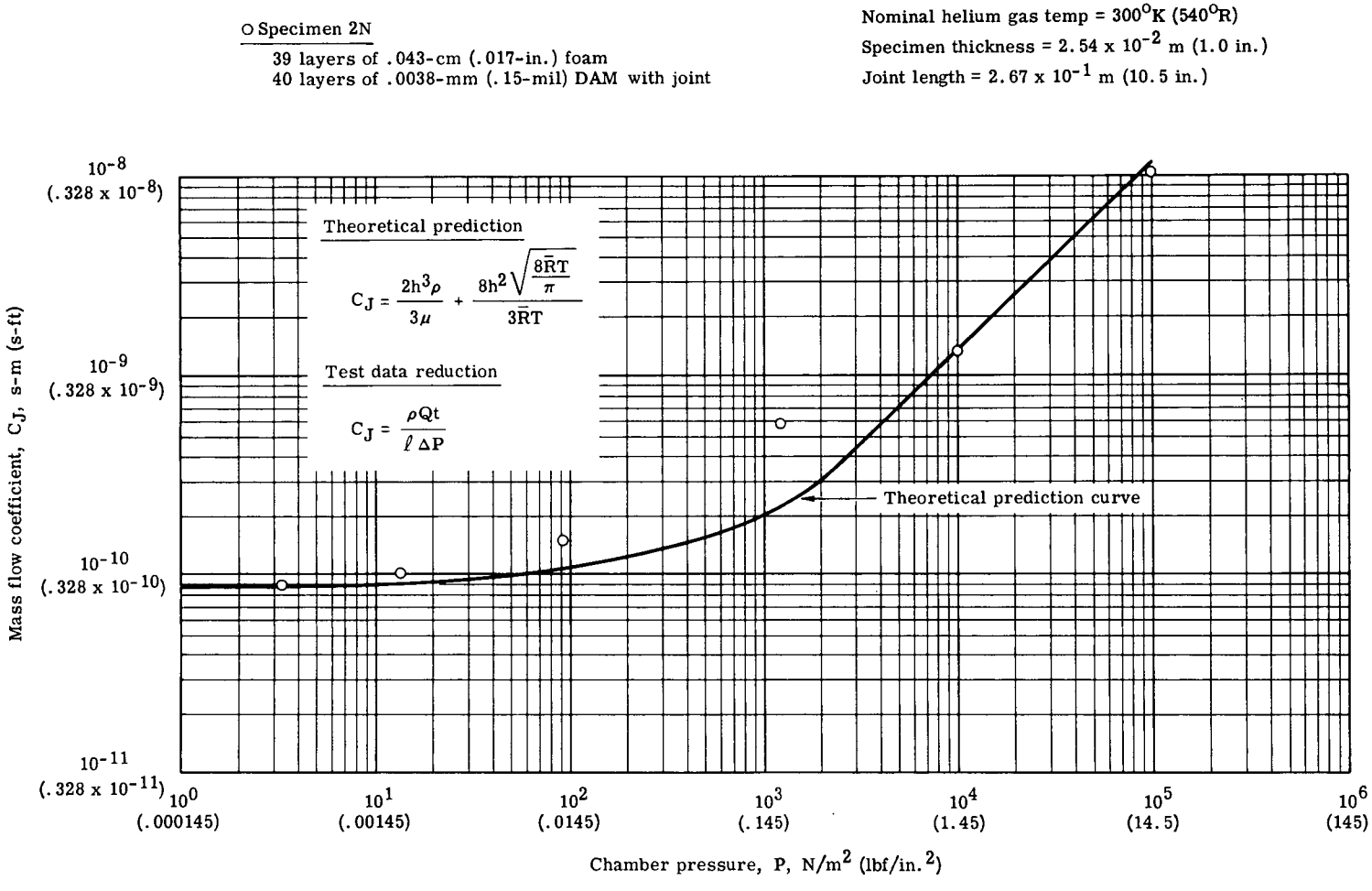

Figure 17. - Helium gas flow characteristics - normal flow specimen 2N.

(5) Normal Flow Tests (Specimens 3N, 4N, and 5N). Theoretical predictions for flow coefficients that characterize the pressure-flow relationship for flows normal to insulation blankets composed of perforated DAM radiation shields have not been developed. However, mass flow coefficients (C_N) have been determined from test data and are plotted in Figure 18 for specimens 3N, 4N, and 5N.

The mass flow coefficient C_N is used to predict flows normal to the layers in multilayer insulation blankets composed of perforated DAM radiation shields. The relation used to characterize such flows is

$$Q = \frac{C_N A_S \Delta P}{t\rho}$$

where Q = the gas flow

C_N = the volumetric flow coefficient

A_S = the insulation blanket surface area

ΔP = the pressure differential

t = the insulation blanket thickness

ρ = the gas density

Each normal flow specimen had a broadside (flow) area of 0.0558 square meter (86.5 square inches). Specimens 3N and 5N were 2.54-cm (1.0-inch) thick; specimen 4A was 1.27-cm (0.5-inch) thick. Specimen 3N consisted of 40 layers of insulation per 2.54 cm (1.0 inch). Specimen 4N consisted of 20 layers of insulation per 1.27 cm (0.5 inch). Specimen 5N consisted of 30 layers of insulation per 2.54 cm (1.0 inch).

In an attempt to explain the variation in the coefficients for specimens 3N and 5N, the model illustrated in Figure 19 was devised. The model assumes that the flow may be of two types; one is normal flow through the layers of foam and perforated DAM, and the other is parallel flow through the space between layers. The total flow resistance may then be defined by two resistances, R_N and R_L, for flow normal and flow lateral to the layers, respectively.

The total resistance in the continuum regime is equivalent to the sum of the resistances R_N and R_L. Reducing the number of layers from 40 to 30 will decrease resistance R_N by 25 percent. Therefore, at least 75 percent of the change in total resistance is attributable to resistance R_L. Resistance R_L, however, changes inversely as the square of the gap between sheets. If the foam thickness is subtracted from the distance between Mylar sheets to obtain the "gap" between layers, resistance R_L decreases by 79.0 percent. Therefore, if R_N

Sym	Spec	Thickness	Material	Layers
○	3N	2.54 cm (1.0 in.)	.043-cm (.017-in.) foam .0038-mm (.15-mil) DAM (perforated)	39 40
△	4N	1.27 cm (.5 in.)	.043-cm (.017-in.) foam .0038-mm (.15-mil) DAM (perforated)	19 20
□	5N	2.54 cm (1.0 in.)	.043-cm (.017-in.) foam .0038-mm (.15-mil) DAM (perforated)	29 30

Nominal helium gas temp = $300^{o}K$ ($540^{o}R$)

Normal flow area = 0.558×10^{-1} m^2 (86.5 $in.^2$)

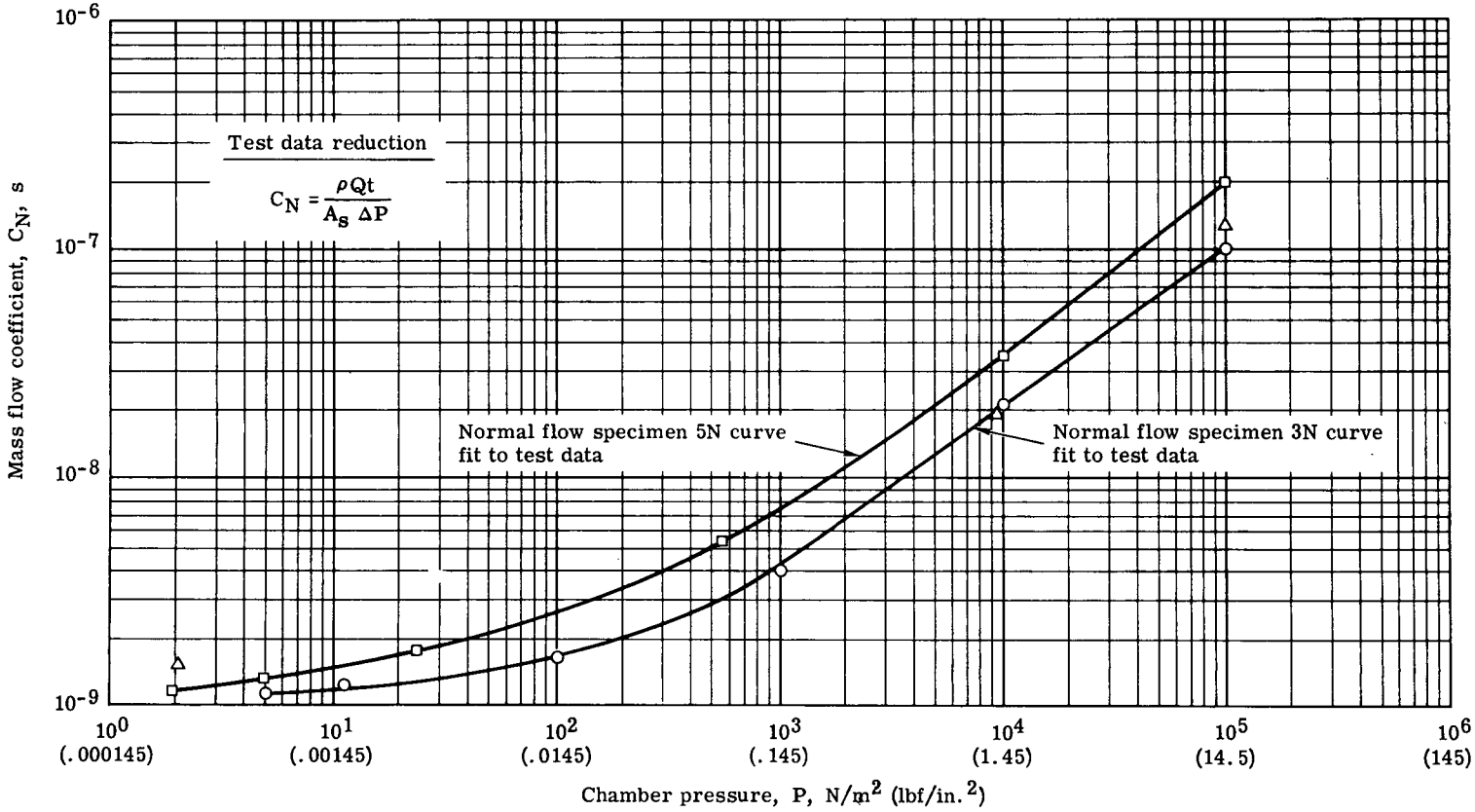

Figure 18. - Helium gas flow characteristics - normal flow specimens 3N, 4N, and 5N.

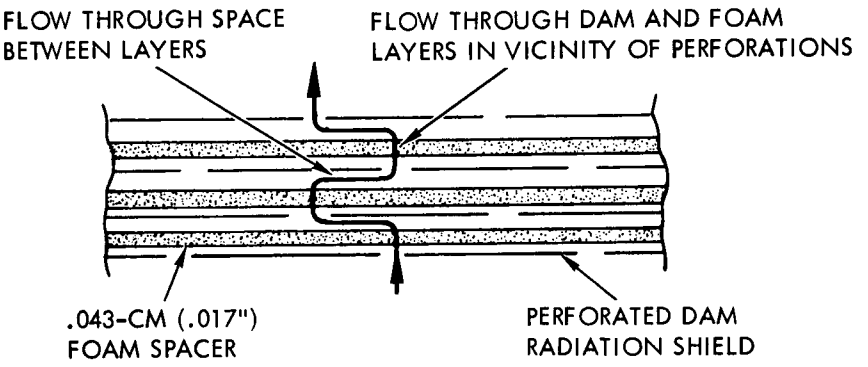

Figure 19. - Normal flow model.

and R_L are numerically equivalent for specimen 3N (a hypothesis that should be verified in future programs), the flow resistance of specimen 5N should be approximately 50 percent the resistance of specimen 3N.

As shown in Figure 18, the coefficients of specimens 3N and 5N tend to coalesce at 1.33 N/m^2 (10^{-2} torr), but at 987 x 10^5 N/m^2 (740 torr) the coefficient of specimen 5N is twice that of specimen 3N.

Normal flow specimen 4N was used to investigate the effect of the specimen thickness (or number of layers) on the flow coefficient. As expected, the flow coefficient of specimen 4N conforms closely to that measured for specimen 3N. This is explained by the fact that each was composed of the same number of insulation layers per 2.54 cm (1.0 inch).

4. Panel Flow Tests

a. Test Plan. The test plan for the laboratory purge and vent investigation was expanded to include flow tests on a typical GAC-9 insulation panel. The insulation panel specimen is a logical extension of the test program to define the ability to analytically predict the purge and venting performance of GAC-9 insulation on a cryogenic storage tank. The GAC 76-cm (30-inch) diameter double-guarded cylindrical calorimeter with GAC-9 insulation and the associated pressure-sensing instrumentation is a complex configuration to model and test. The one-dimensional flow tests on axial and normal flow test specimens have generated engineering numbers for the basic flow coefficients $K_=$, $K_\perp$, K_J, and K_G, which define the insulation flow characteristics. It is necessary to show good prediction/performance agreement to verify that all one-dimensional flow coefficients can be used successfully in a three-dimensional analytical model. This must be done with a simple three-dimensional panel flow test specimen that

introduces the minimum possibility of erroneous flow behavior. This specimen consists of two rectangular GAC-9 insulation panels joined together to form a single curvature panel assembly having a joint aligned with the longitudinal axis. The panel flow test plan is given in Table IV.

TABLE IV. - TEST PLAN FOR LABORATORY PURGE AND VENT INVESTIGATION - PANEL FLOW TESTS

Specimen No.	Specimen description	Test objectives
1P	GAC-9 insulation panels 20.3 x 122 cm (8 x 48 in.) and 73.7 x 122 cm (29 x 48 in.) laced together to form a 94 x 122 cm (37 x 48 in.) panel assembly with the joint aligned with the major axis. Single curve contour along minor axis.	Obtain flow coefficients across the insulation panel and show the effect of a joint. Determine panel and panel joint venting characteristics.

b. Test Specimens and Flow Test Fixture. The panel and test fixtures were designed to permit testing under steady-state pressure conditions of purge gas flow introduced parallel to the plies of multilayer insulation and transient pressure conditions of gas flow out of the multilayer insulation during launch pressure decay. The test objectives are listed below.

(1) Obtain purge gas flow characteristics of a flight-size GAC-9 insulation panel including a panel-to-panel joint.

(2) Provide information for the design of a purge system for the GAC-9 insulation now installed on the 76-cm (30-inch) diameter double-guarded calorimeter.

(3) Verify installation techniques and performance of pressure-sensing probes in the GAC-9 insulation panel.

The flow test panel and test fixture details are shown in GAC drawing 70QS1709 (Fig. 20). The panel assembled in the text fixture is shown in Figure 21. Salient features are listed below.

(1) The test panel consists of two GAC-9 insulation panels secured together by a typical panel-to-panel joint. One panel is approximately 73.7 x 122 cm (29 x 48 inches), and the second panel is approximately 20.3 x 122 cm (8 x 48 inches). Together the two panels form a flow test panel area of slightly over 1.115 square meters (12 square feet). The joint between panels is aligned with the panel major axis.

(2) For future test considerations, a grid edge band is provided in the larger test panel to permit this panel to be cut to approximately 61 x 122 cm (24 x 48 inches). A second panel (same size) may be joined to it to form a flow test panel comprising two panels of equal width. The objective would be to determine the effect of panel width on purge gas flow characteristics.

(3) When assembled on the flow test fixture, the test panel is in single curve contour, with the curve along the minor axis. A 133.4-cm (52.5-inch) radius, simulating a 2.66-meter (105-inch) diameter tank section, was selected for the test panel. The straight edges of the panel are sealed to prevent edge leakage of the purge gas, and the curved edges are capable of flowing purge gas.

(4) Pressure taps are built into the test panel to sense purge gas pressure in 12 areas of the middle layer of the assembled test panel. In the same areas, pressure taps are also provided in the surface of the test fixture to monitor purge gas pressure at the inner surface of the panel.

(5) The curved aluminum test fixture, which simulates a 2.66-meter (105-inch) diameter tank section, is shown in Figure 22. Plenums are provided on either end of the fixture for supplying and venting of purge gas in and out of the test panel. Aluminum zees attached to each side of the fixture are provided with holes for lacing the test panel to the fixture. Pressure taps, consisting of 0.381-cm (0.18-inch) bore aluminum tubes, are mounted flush with the curved surface of the fixture to permit pressure measurements at 15 points.

(6) Provisions are made in the test fixture for the addition of five pressure-sensing probes in the form of small bore tubes running the full length of the test panel in the middle insulation layer. These tubes may be moved during testing to sense pressures along the length of the test panel.

(7) An aluminum angle frame above the test panel supports the pressure-sensing tubing and prevents deformation of the insulation in the area of the pressure taps.

(8) The test fixture and associated plumbing are designed to be used in the laboratory for ambient pressure tests and also to be mounted in the LH_2 test facility vacuum chamber for transient pressure and free molecular regime steady-state tests.

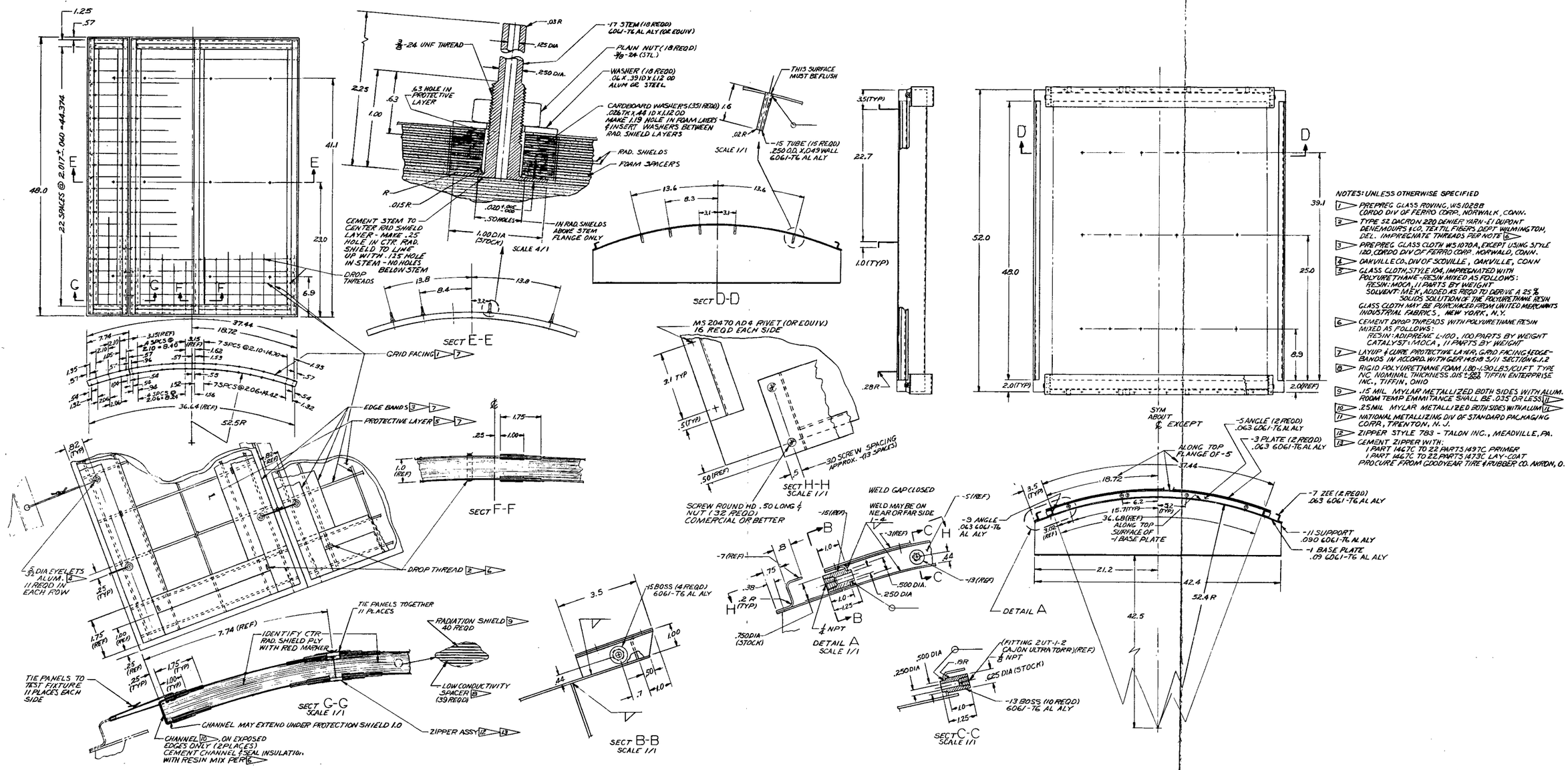

NOTES: UNLESS OTHERWISE SPECIFIED

1. PREPREG GLASS ROVING, WS 1028B CORDO DIV OF FERRO CORP., NORWALK, CONN.
2. TYPE 52 DACRON 220 DENIER YARN-51 DUPONT DENEMOURS & CO. TEXTIL FIBERS DEPT WILMINGTON, DEL. IMPREGNATE THREADS PER NOTE 6
3. PREPREG GLASS CLOTH WS 1070A, EXCEPT USING STYLE 120, CORDO DIV OF FERRO CORP. NORWALD, CONN.
4. OAKVILLE CO., DIV OF SCOVILLE, OAKVILLE, CONN
5. GLASS CLOTH, STYLE 104, IMPREGNATED WITH POLYURETHANE-RESIN MIXED AS FOLLOWS:
   RESIN: MOCA, 11 PARTS BY WEIGHT
   SOLVENT: MEK, ADDED AS REQD TO DERIVE A 25% SOLIDS SOLUTION OF THE POLYURETHANE RESIN
   GLASS CLOTH MAY BE PURCHASED FROM UNITED MERCHANTS INDUSTRIAL FABRICS, NEW YORK, N.Y.
6. CEMENT DROP THREADS WITH POLYURETHANE RESIN MIXED AS FOLLOWS:
   RESIN: ADIPRENE L-100, 100 PARTS BY WEIGHT
   CATALYST: MOCA, 11 PARTS BY WEIGHT
7. LAYUP & CURE PROTECTIVE LAYER, GRID FACING & EDGE-BANDS IN ACCORD. WITH GER MS 18 S/11 SECTION 6.1.2
8. RIGID POLYURETHANE FOAM 1.80-1.90 LBS/CU FT TYPE NC, NOMINAL THICKNESS .015 ± .003, TIFFIN ENTERPRISE INC., TIFFIN, OHIO
9. .15 MIL MYLAR METALLIZED BOTH SIDES WITH ALUM. FROM TEMP EMMITANCE SHALL BE .035 OR LESS 11
10. .25 MIL MYLAR METALLIZED BOTH SIDES WITH ALUM 11
11. NATIONAL METALLIZING DIV OF STANDARD PACKAGING CORP., TRENTON, N. J.
12. ZIPPER STYLE 783 - TALON INC., MEADVILLE, PA.
13. CEMENT ZIPPER WITH:
    1 PART 1462C TO 22 PARTS 1497C PRIMER
    1 PART 1462C TO 22 PARTS 1473C LAY-COAT
    PROCURE FROM GOODYEAR TIRE & RUBBER CO. AKRON, O.

Figure 20. - Flow test panel and test fixture.

FOLDOUT FRAME - 1

FOLDOUT FRAME - 2

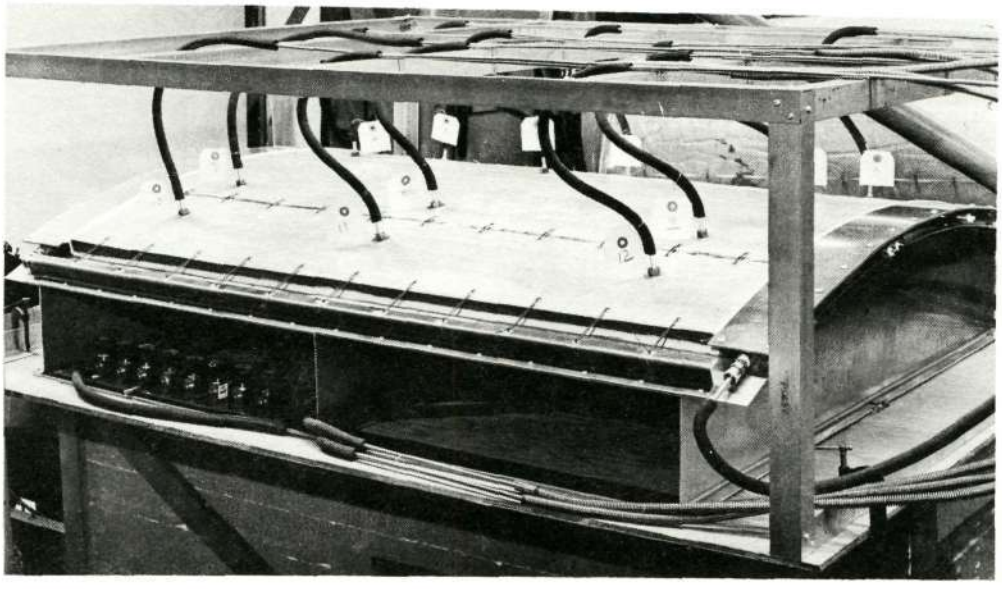

Figure 21. - Flow test panel assembled in test fixture.

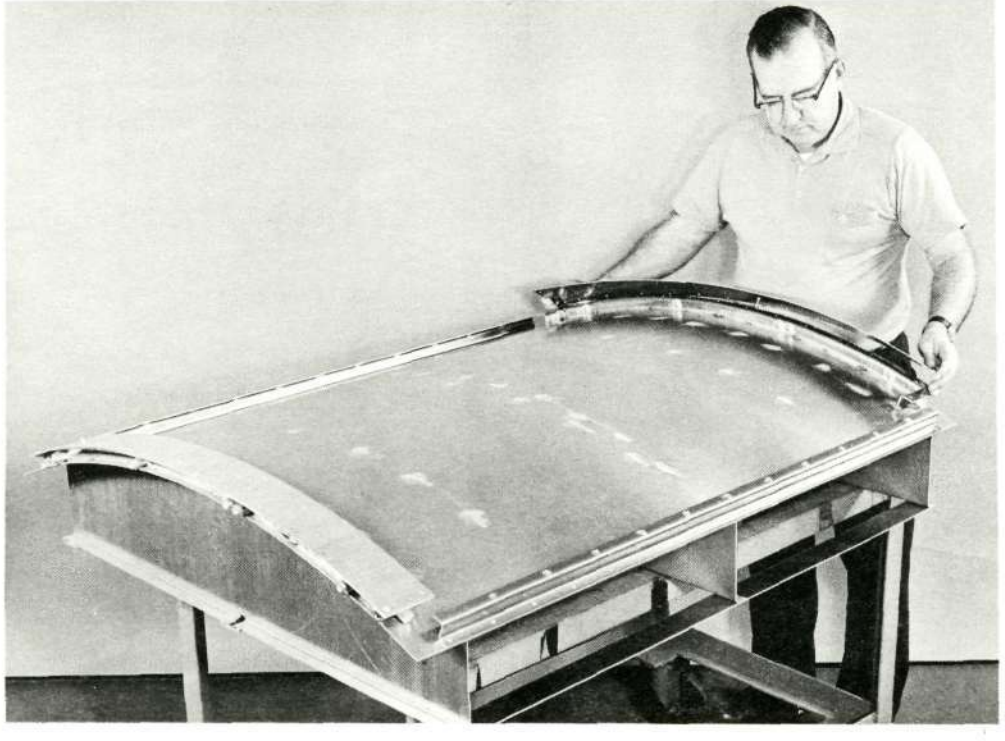

Figure 22. - Panel flow test fixture.

The 20.3 x 122 cm (8 x 48 inch) and the 73.7 x 122 cm (29 x 48 inch) GAC-9 insulation flow test panels were fabricated without difficulty, using established GAC-9 insulation fabrication procedures. Installation of pressure taps during fabrication of the panel involved cementing the taps to Mylar radiation shield No. 20 and cutting clearance holes for tap stems in Mylar layers 21 through 40 and foam layers 20 through 39. At each pressure tap, the cutouts in foam layers were sufficiently oversize to receive an equivalent thickness cardboard washer, which provides a high density spacer to resist the clamping load of the pressure tap seal nut. Construction of a pressure tap is shown in Figure 23. A typical Mylar radiation shield layer is shown in Figure 24. A typical foam layer with cardboard washer inserts is shown in Figure 25. The completed panel assembly is shown in Figures 26 and 27. The cords protruding from the ends of the panel were to facilitate installation of the movable small diameter pressure-sensing tubes; however, these tubes were not used.

The panel flow test fixture is shown in Figure 22 with the cover of one plenum chamber removed to reveal the chamber outline and pressure-sensing tube ports.

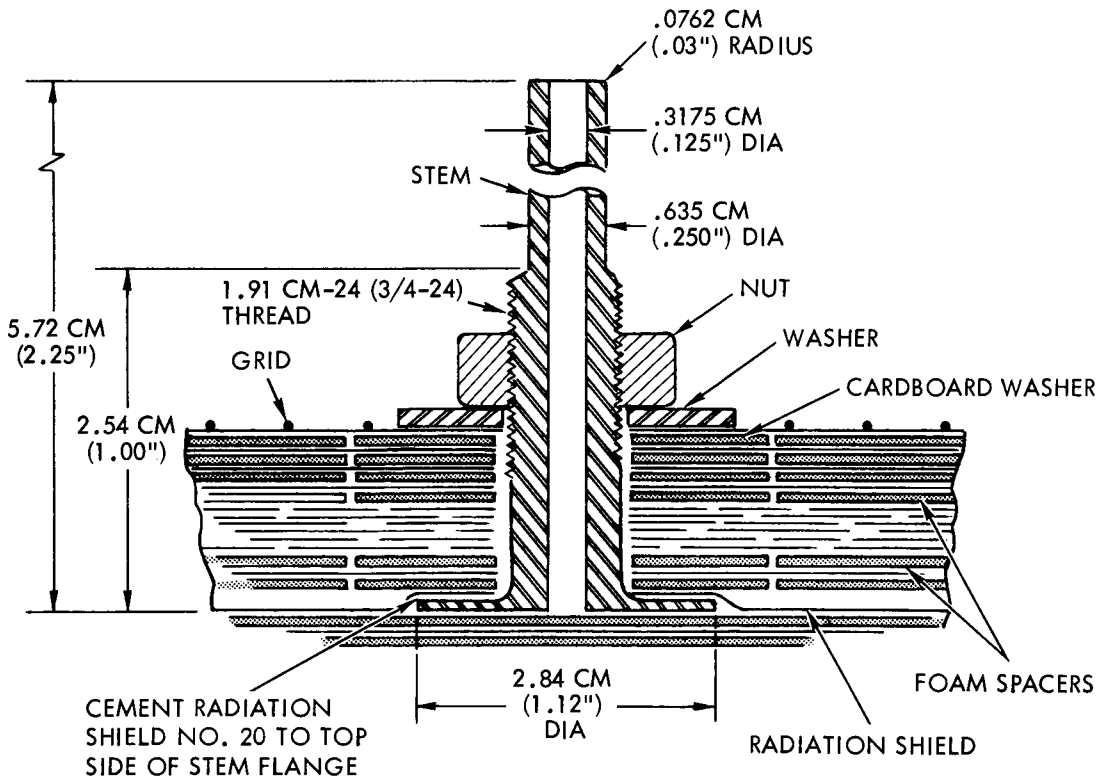

Figure 23. - Pressure tap details.

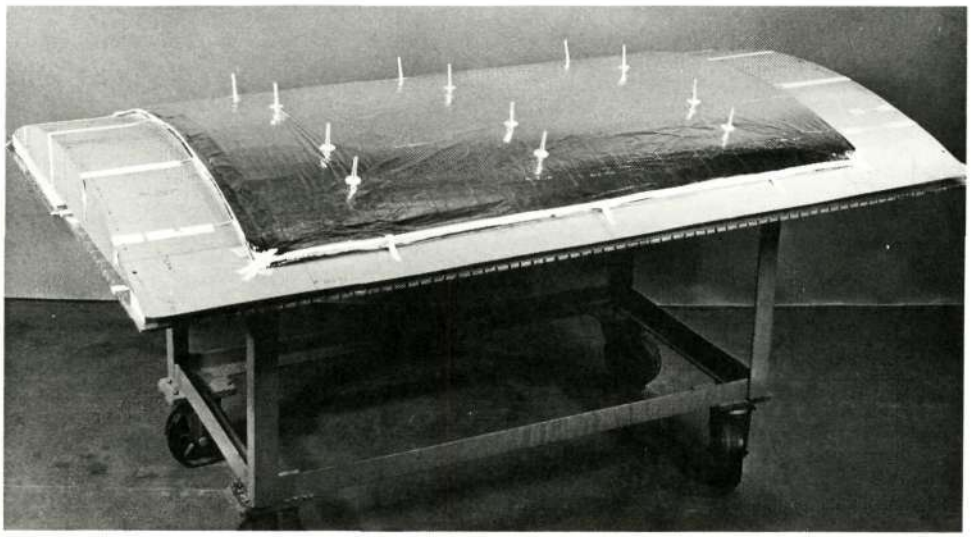

Figure 24. - Flow test panel fabrication showing radiation shield layer with cardboard washers installed at pressure taps.

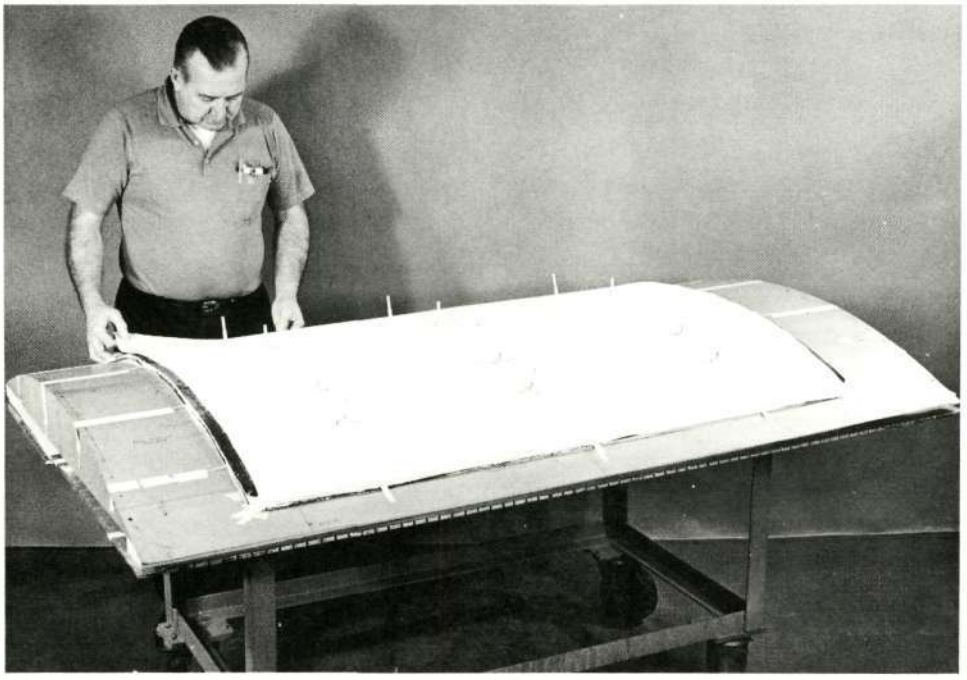

Figure 25. - Flow test panel fabrication showing typical foam spacer layer with cardboard washers in place at pressure taps.

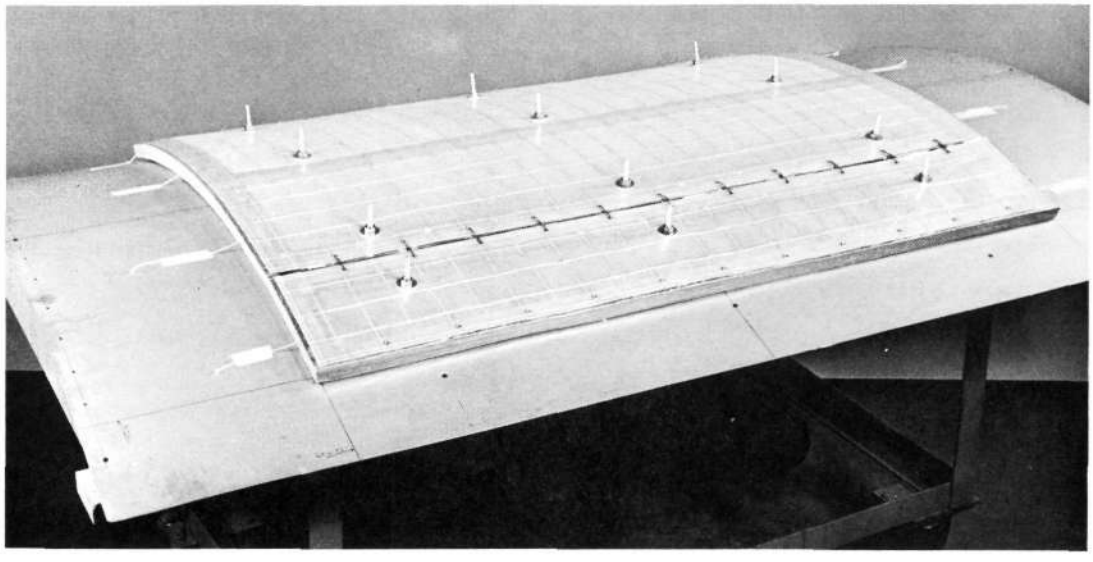

Figure 26. - Side view of flow test panel assembly 1P.

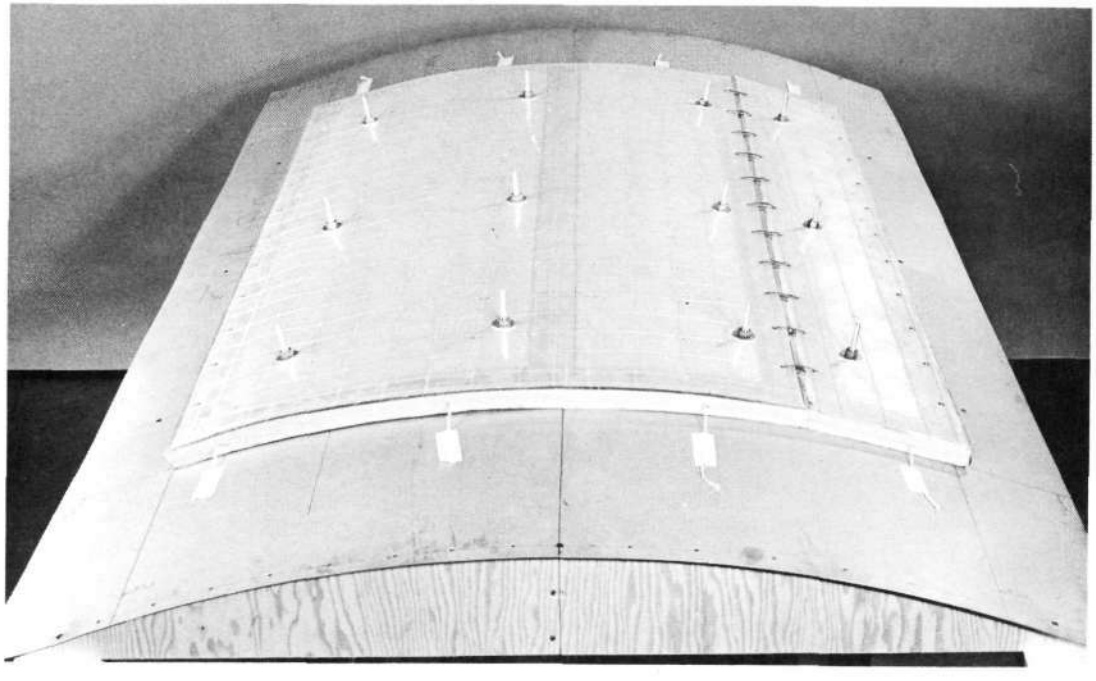

Figure 27. - End view of flow test panel assembly 1P.

The flow test panel outer grid edge band was laced to the test fixture as shown in Figure 28. The lacing simulates panel-to-panel attachment and provides hoop strength in the panel outer grid to resist panel swelling during purge gas flow tests.

The pressure-measuring instrumentation employed in the panel flow tests was designed for use both on the panel test fixture and in the GAC 1.83-meter (6-foot) diameter vacuum chamber. The system was basically designed for the panel flow tests; however, very little modification was required for use in the 76-cm (30-inch) diameter calorimeter purge and vent tests. Figure 29 shows the pressure-measuring instrumentation for panel testing in the vacuum chamber. Additional discussion of the flow test pressure-sensing instrumentation development is presented in paragraph 5 of this subsection.

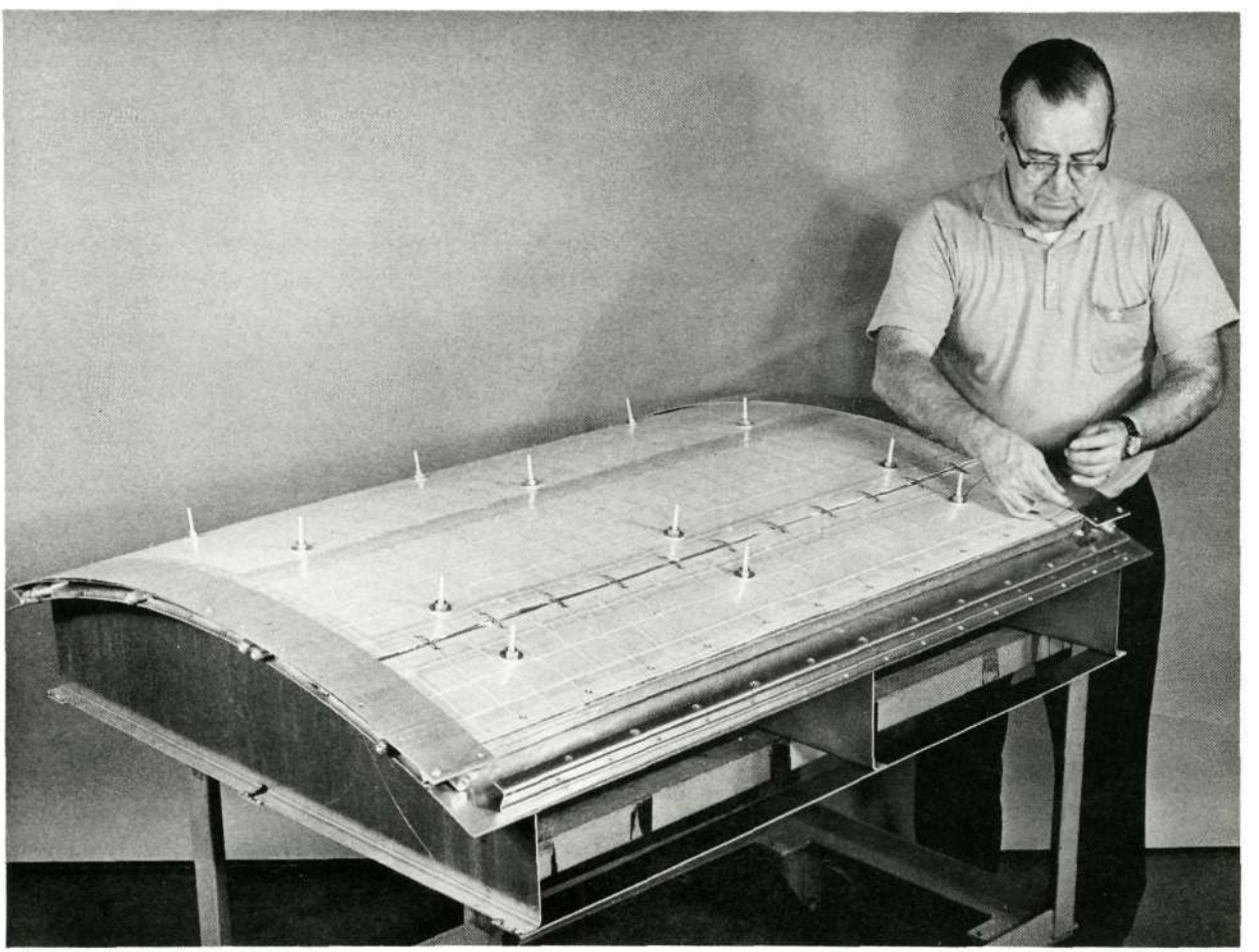

Figure 28. - Application of edge band lacing during installation of flow test panel in test fixture.

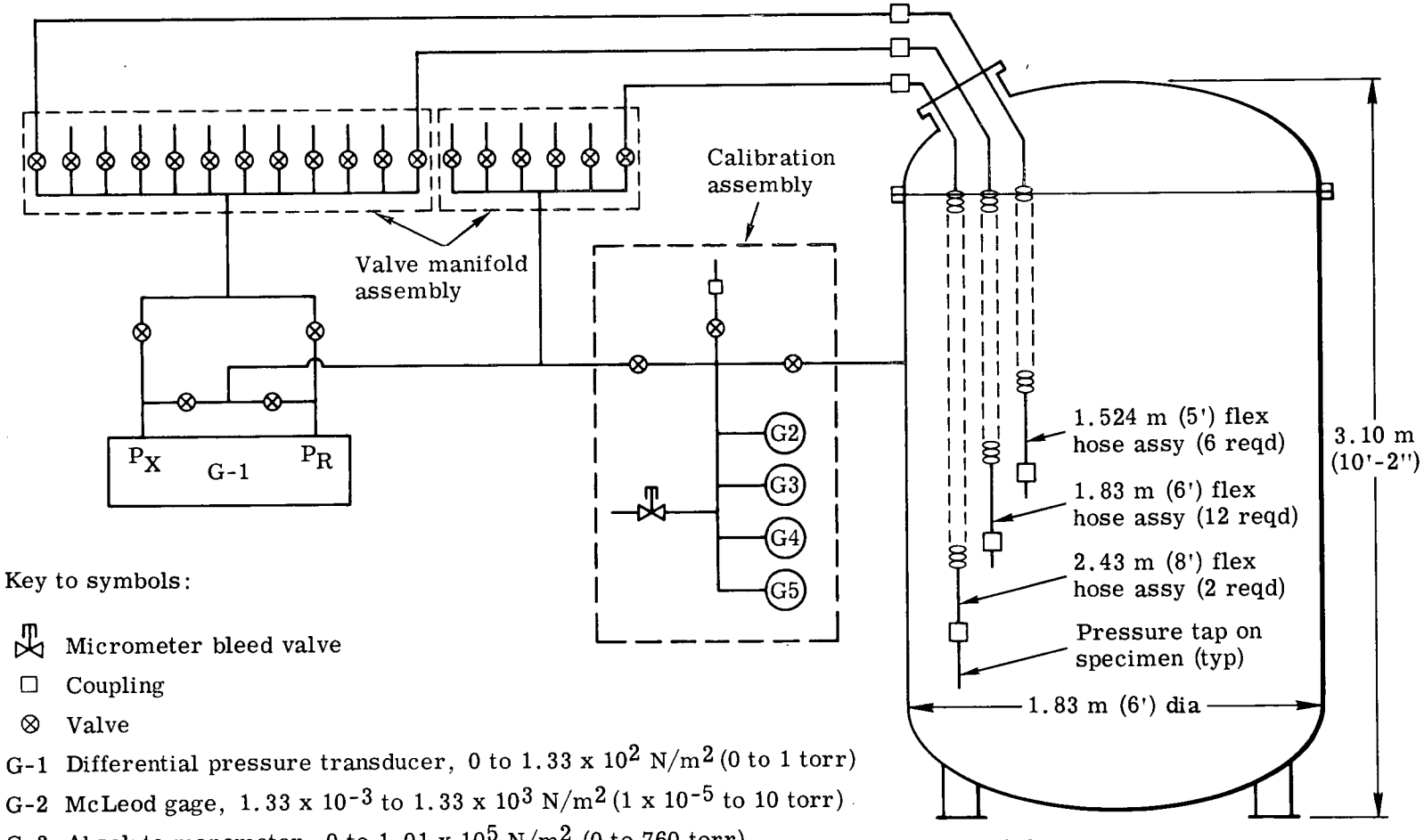

Key to symbols:

- Micrometer bleed valve
- □ Coupling
- ⊗ Valve

G-1 Differential pressure transducer, 0 to 1.33×10^2 N/m^2 (0 to 1 torr)

G-2 McLeod gage, 1.33×10^{-3} to 1.33×10^3 N/m^2 (1×10^{-5} to 10 torr)

G-3 Absolute manometer, 0 to 1.01×10^5 N/m^2 (0 to 760 torr)

G-4 Pressure transducer, 0 to 1.01×10^5 N/m^2 (0 to 760 torr)

G-5 Ionization gage, 1.33×10^{-5} to 1.33×10^{-1} N/m^2 (1×10^{-7} to 1×10^{-3} torr)

Figure 29. - Pressure-measuring instrumentation for panel vent tests.

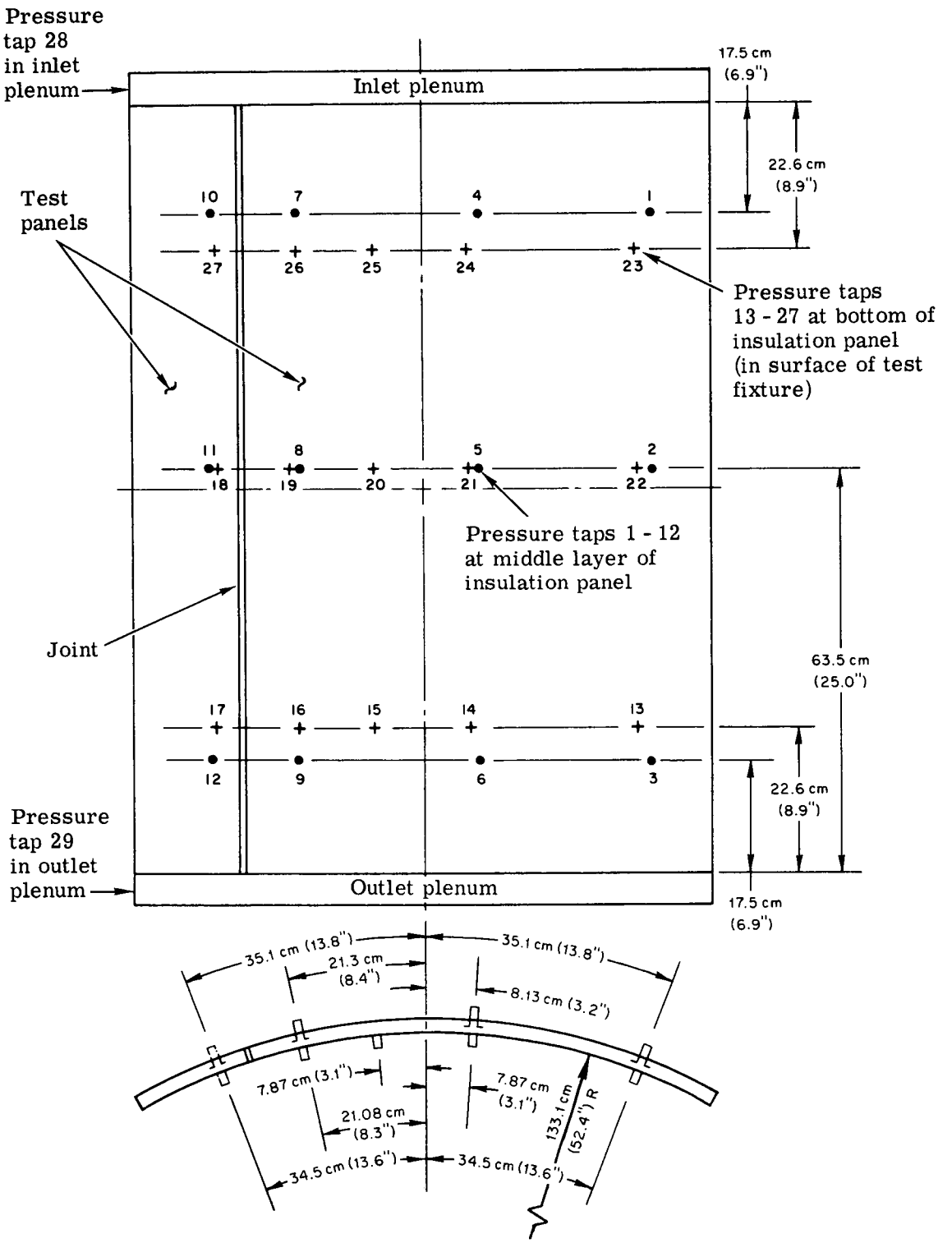

Figure 30. - Pressure tap locations on flow test panel 1P.

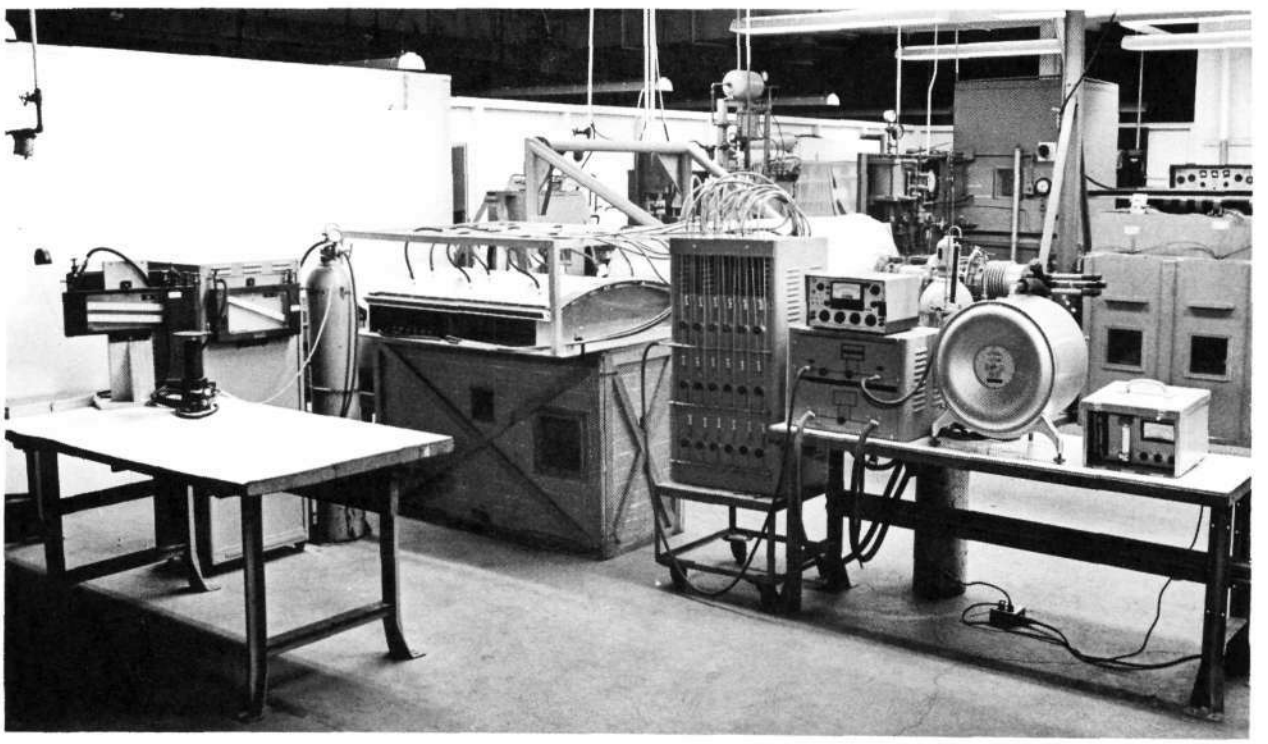

Figure 31. - Panel flow test laboratory setup.

c. Test Procedures. The steady-state purge tests consisted of (1) measuring the pressures at the 29 tap locations shown in Figure 30 while metering the flow of nitrogen or helium gas to the inlet plenum; (2) measuring the helium gas purity at the outlet plenum and at pressure taps 1, 5, 9, 3, and 13; and (3) measuring gas flow rates at the outlet plenum. The complete laboratory test setup is shown in Figure 31. The tests were conducted at ambient temperature and pressure in the sequence listed in Table V.

Transient pressure tests for determining the venting characteristics of flow test panel 1P were conducted in the 1.83-meter (6-foot) diameter vacuum chamber using the instrumentation described in Figure 29. For transient pressure tests, the inlet and outlet plenum chambers on the test fixture were filled with aluminum strips to minimize the void gas volumes. The test fixture and the flow test panel were attached to the chamber lid as shown in

TABLE V. - PANEL PURGE TEST SEQUENCE

Run No.[a]	Purge gas		Test procedure
	Type	Inlet Flow, m^3/s (ft^3/min)	
1	N_2	4.72×10^{-4} (1.0)	Equipment checkout; measure pressures at 29 taps and gas flow at outlet plenum.
2	N_2		Repeat run No. 1 after tightening lacing at panel joint.
3	He		Measure gas purity at outlet plenum.
4	He		Repeat run No. 3.
5	He		Repeat run No. 3, and measure pressure at all taps.
6	He		Measure gas purity at tap No. 1.
7	He		Measure gas purity at tap No. 5.
8	He		Measure gas purity at tap No. 9.
9	He		Measure gas purity at tap No. 3.
10	He		Measure gas purity at tap No. 13.

[a]After each run using helium, the panel was purged with a minimum of 1.132 m^3 (40 ft^3) of N_2 flowing at approximately 4.72×10^{-4} m^3/s (1 ft^3/min).

Figures 32 and 33. The tests consisted of measuring the pressures at panel taps 1, 2, 4, 5, 7, 8, 11, and 21 (fig. 30) during chamber evacuation from ambient to 1.33×10^{-3} N/m^2 (10^{-5} torr). Testing was conducted in the sequence listed in Table VI.

Test runs 6 and 12 were conducted to check the pressure differential across the pair of reference tubes to the vacuum chamber. Run 6 was made using nitrogen, and run 12 was conducted using helium. Run 10 was made to check the repeatability of the pressure measurements made during run 1 at panel tap 5.

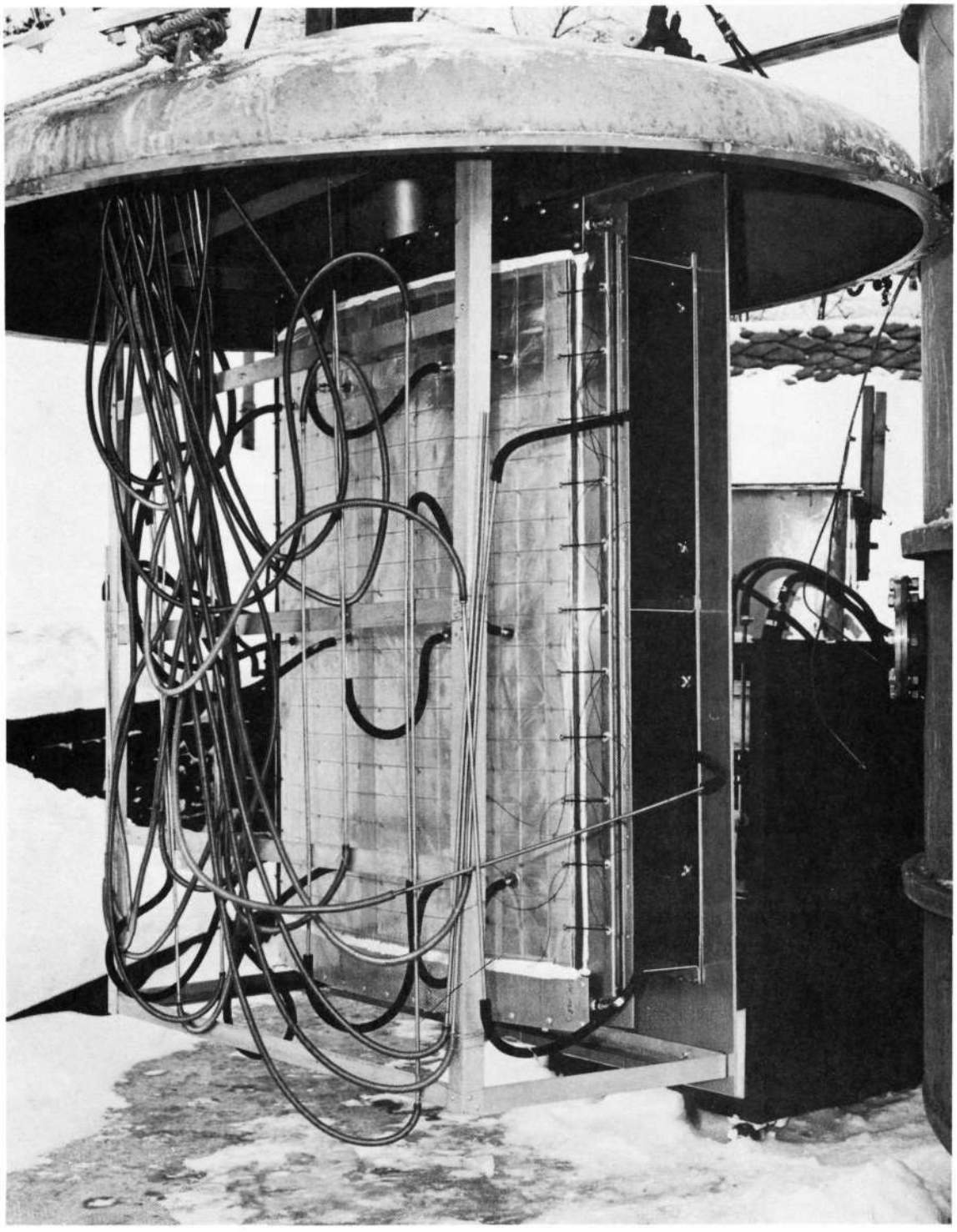

Figure 32. - Flow test panel 1P and holding fixture mounted on vacuum chamber lid.

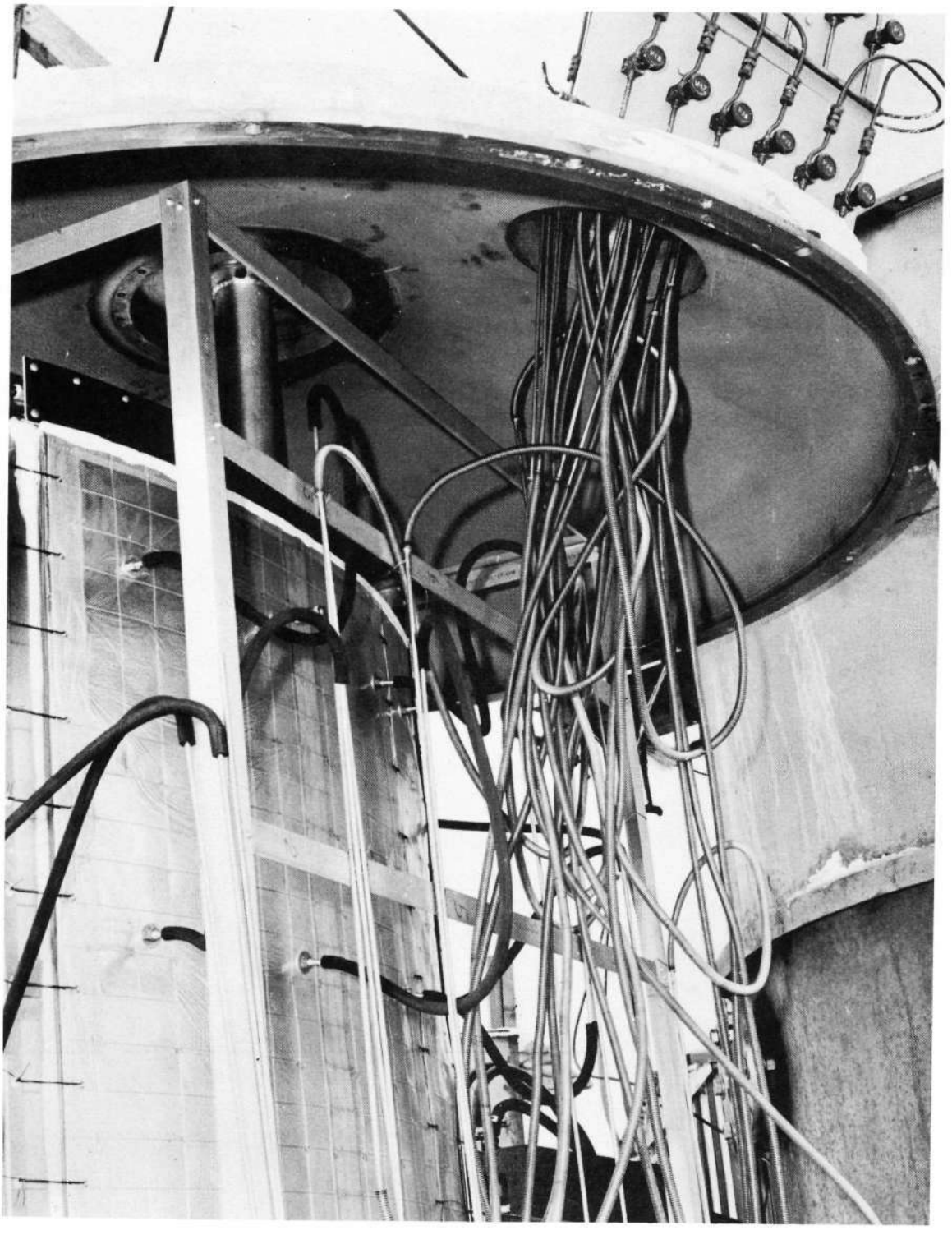

Figure 33. - Flow test panel 1P pressure-sensing lines feed through to selector valve panel mounted on lid of vacuum chamber.

TABLE VI. - PANEL VENT TEST SEQUENCE

Run no.	Purge gas	Pressure test tap	Run no.	Purge gas	Pressure test tap
1[a]	N_2	5	7	N_2	4
2	N_2	1	8	N_2	7
3	N_2	2	9	N_2	21
4	N_2	8	10[a]	N_2	5
5	N_2	11	11	He	5
6	N_2	Tube check	12	He	Tube check

[a] Panel conditioned 5.76×10^4 seconds (16 hours) in vacuum of 1.33×10^{-3} N/m^2 (10^{-5} torr) before test run.

d. Panel Flow Tests and Analysis of Test Results

(1) Steady-State Pressure Tests. Two purge gas flow tests were conducted on flow test panel 1P. These tests consisted of pressure measurements at various locations in the panel and measurements of the flow rates in the panel inlet plenum chamber. The pressure tap locations are shown in Figure 30. In actual practice, helium will be used as the flow medium, since it is the gas used for system purging. The use of helium for all panel flow tests is both expensive and unnecessary; therefore, one test was conducted with dry nitrogen gas to establish flow trends and patterns prior to the final run with helium gas. The measured test data was used to verify the ability to predict panel purging performance using the one-dimensional flow coefficients obtained in the laboratory flow tests on axial flow and normal flow specimens. The analytical predictions are based on a three-dimensional flow model programmed for the IBM 360 computer.

(a) Test No. 1. Dry nitrogen gas was used as the test medium for test No. 1. The inlet and outlet flow rates were 4.72×10^{-4} and 0.944×10^{-4} m^3/s (1.00 and 0.20 ft^3/min), respectively. The results of panel flow test No. 1 are shown in Figures 34 and 35, where the isobars - lines of constant pressure (solid lines) - and flow directions (dotted lines) are drawn. Figure 34 shows the pressures from the pressure taps sensing in the middle layer of the panel. Figure 35 shows the pressures along the bottom of the panel as sensed by the pressure taps

Notes: 1. Data from test run No. 2.

2. Circled numbers are pressures in N/m^2 at pressure tap locations. Parenthetical values are in in. H_2O.

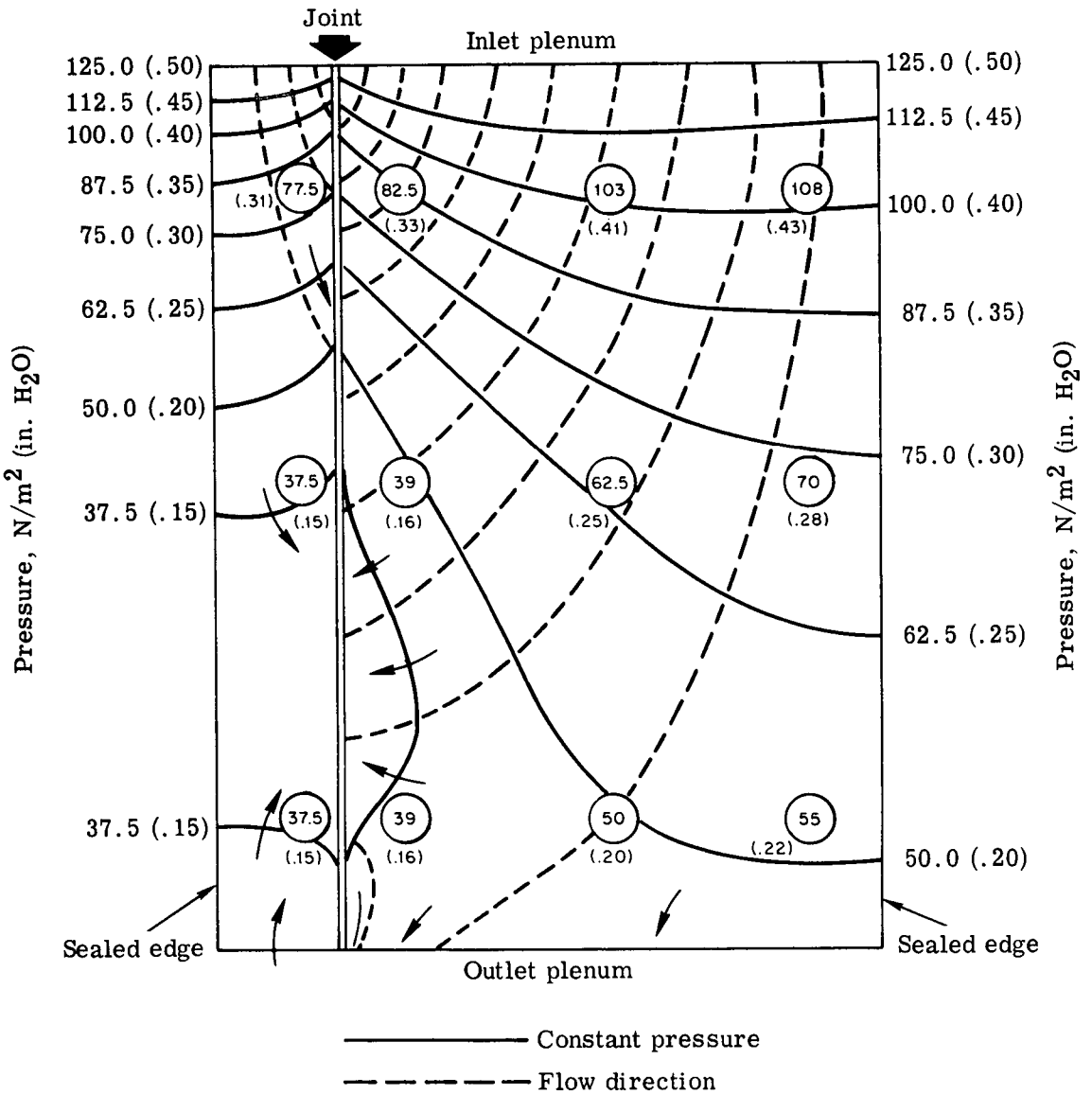

Figure 34. - Pressure-flow contours at middle layer of flow test panel 1P - nitrogen purge.

Notes: 1. Data from test run No. 2.

2. Circled numbers are pressures in N/m^2 at pressure tap locations. Parenthetical values are in in. H_2O.

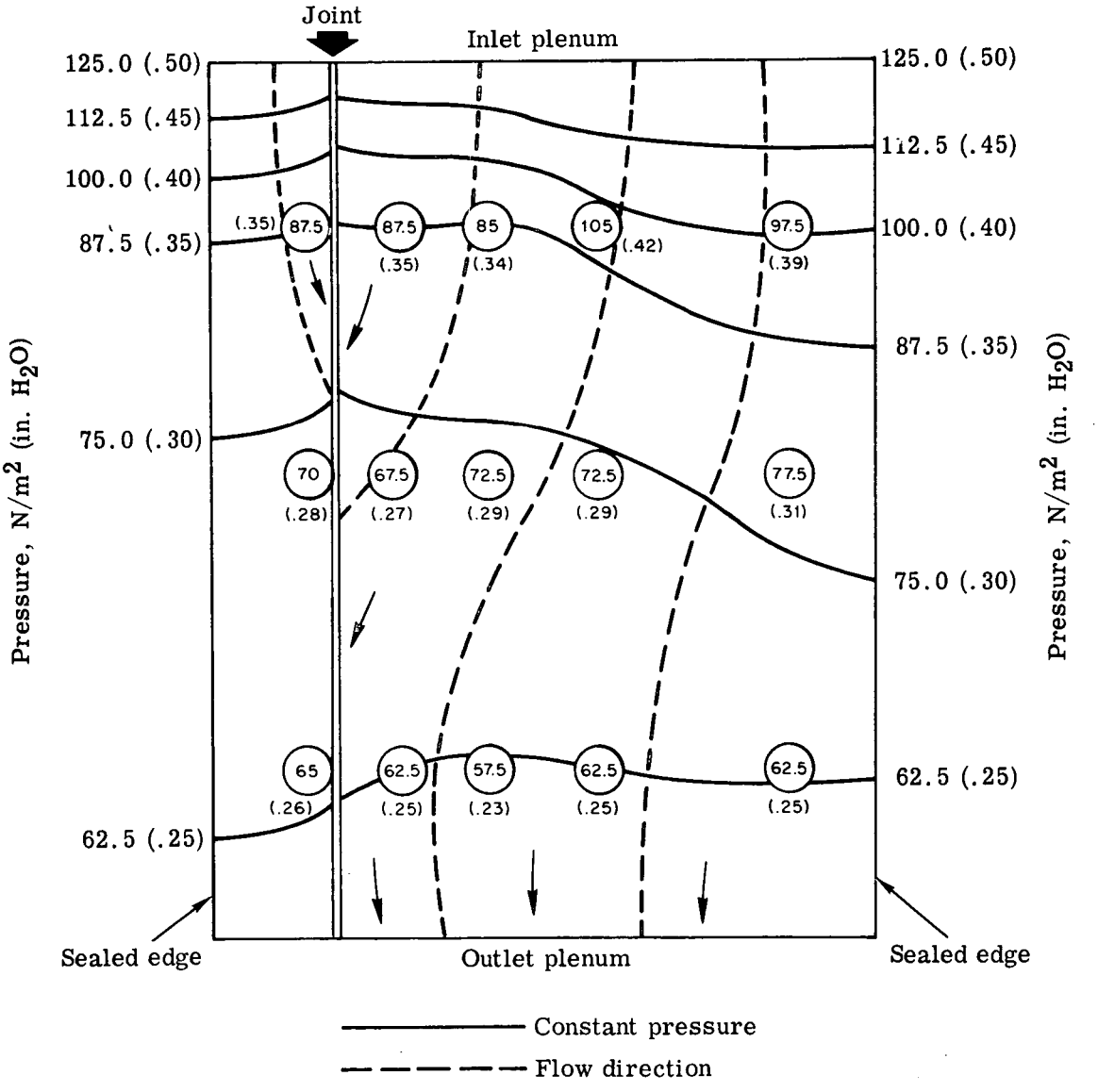

Figure 35. - Pressure-flow contours at bottom of flow test panel 1P - nitrogen purge.

located at the test fixture surface. The flow lines in Figure 34 show that the gas flow is toward the joint between panels and leaks out the joint to the atmosphere. At the extreme right side of the large panel, the entering gas will not reach the joint but will exit at some point midway between the sides, producing a general sweep toward the joint. The pressures in the large panel are nearly equal in an area adjacent to the panel joint in the downstream half of the panel. This area tends to stagnate since most of the gas has escaped from the joint near the inlet plenum chamber and little of the gas from the right side has reached this area. The purge gas pressures along the bottom of the panel are shown in Figure 35. The flow lines are nearly parallel to the inlet flow and indicate that the seam has less effect on the flow and that most of the gas will exit at the outlet plenum chamber.

(b) Test No. 2. Helium gas was used as the test medium for test No. 2. The inlet and outlet flow rates were 4.72×10^{-4} and 0.944 m^3/s (1.00 and 0.20 ft^3/min), respectively. As shown in Figures 36 and 37, the helium gas flow trend is nearly the same as the nitrogen gas flow shown in Figures 34 and 35. The flow lines in Figure 36 show the helium gas flow in the middle layer of insulation to be predominantly toward the joint between panels. In Figure 37 it is shown that the gas flow at the bottom of the panel is less affected by the joint and that most of the gas exits the panel at the outlet plenum chamber.

(2) Helium Purity Tests. Helium purity tests were conducted on flow test panel 1P. Helium gas at a flow rate of approximately 4.72×10^{-4} m^3/s (1.0 ft^3/min) was forced through the insulation at an inlet pressure of 124.5 N/m^2 (0.5 inch of H_2O). The first two tests consisted of measuring the purity of the outlet plenum chamber, where all the gas leaving the panel will accumulate. Figure 38 shows the time required to reach an average purity level in the outlet plenum. Both tests were in good agreement where approximately 1080 seconds (18 minutes) are required to obtain a 99 percent purity level of helium and 1 percent air.

Another series of tests was conducted to determine the helium purity level gradient as a function of panel length and time. Data from the middle layer of insulation is given in Figures 39 and 40. These plots show that times in excess of 1200 seconds (20 minutes) are required to approach the 99 percent helium purity level. Figure 41, data from the bottom of the panel, shows that the 99 percent helium purity level is reached in approximately 300 seconds (5 minutes). This occurs since most of the helium entering the exit manifold comes from the bottom layers of insulation. The gas in the insulation middle layers will more readily leak out the joint and therefore requires more time to reach the desired purity level.

Notes: 1. Data from test run No. 5.

2. Circled numbers are pressures in N/m^2 at pressure tap locations. Parenthetical values are in in. H_2O.

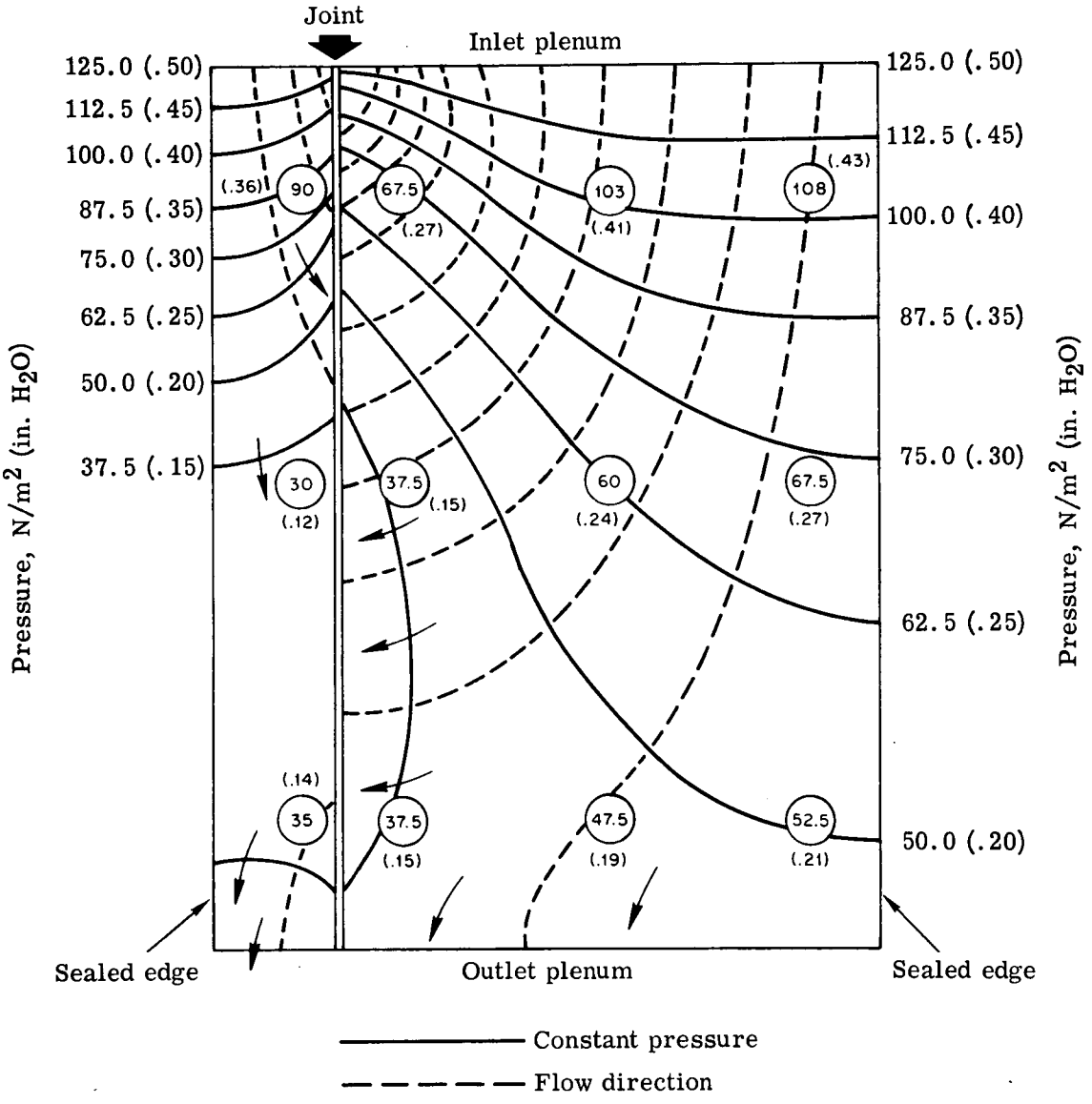

Figure 36. - Pressure-flow contours at middle layer of flow test panel 1P - helium purge.

Notes: 1. Data from test run No. 5.

2. Circled numbers are pressures in N/m^2 at pressure tap locations. Parenthetical values are in in. H_2O.

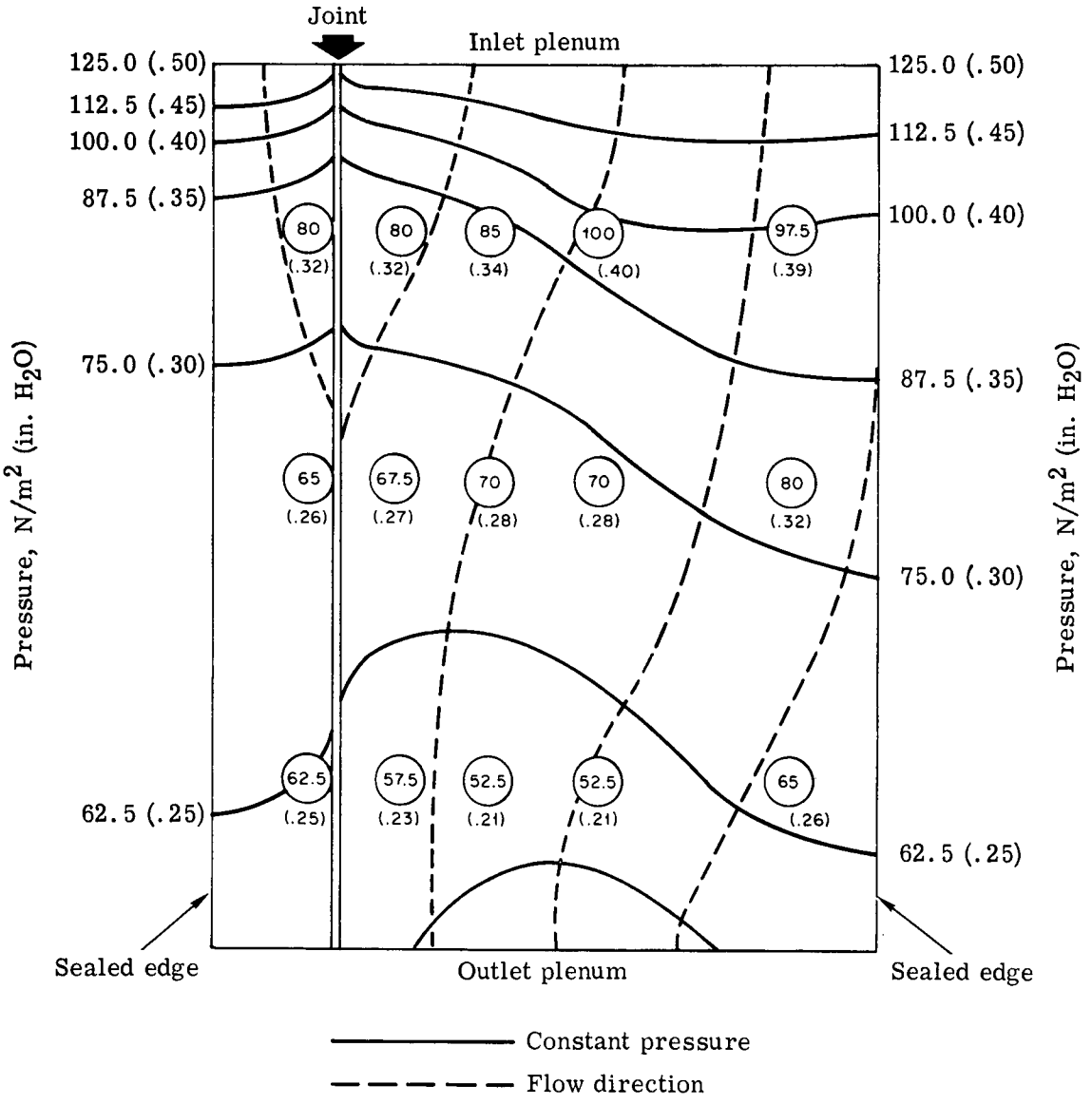

Figure 37. - Pressure-flow contours at bottom of flow test panel 1P - helium purge.

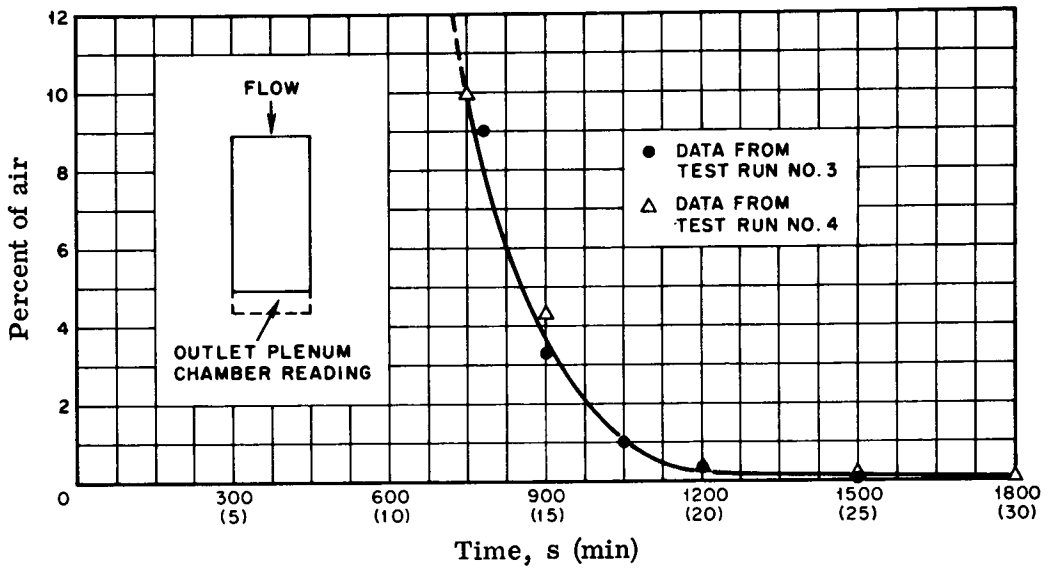

Figure 38. - Helium purity at outlet plenum on flow test panel 1P.

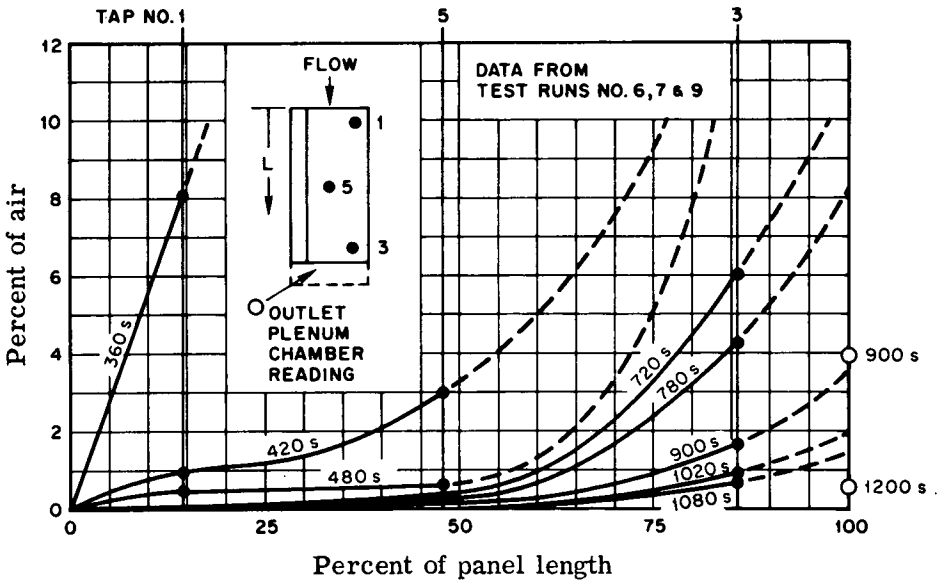

Figure 39. - Helium purity at pressure taps 1, 3, and 5 in middle of flow test panel 1P.

F

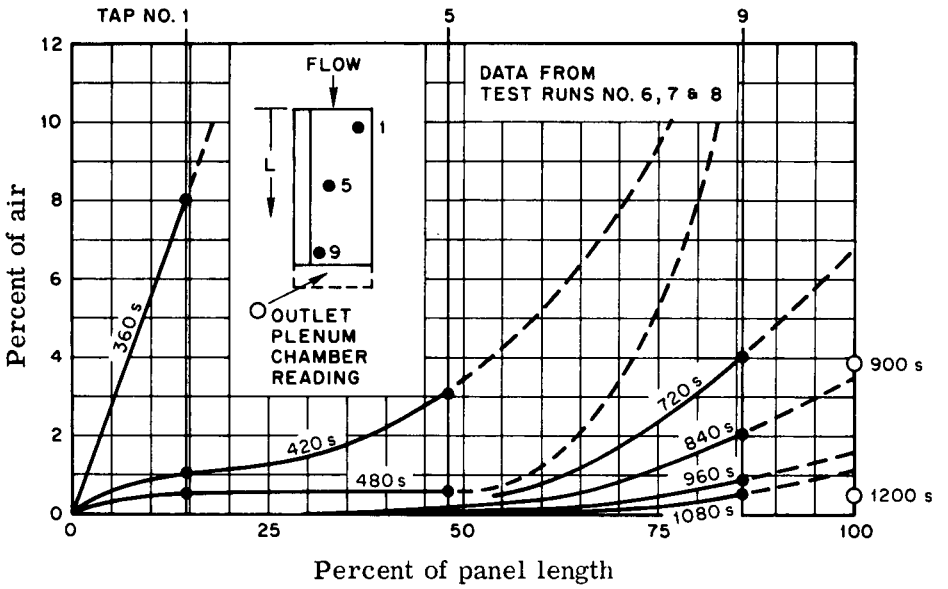

Figure 40. - Helium purity at pressure taps 1, 5, and 9 in middle of flow test panel 1P.

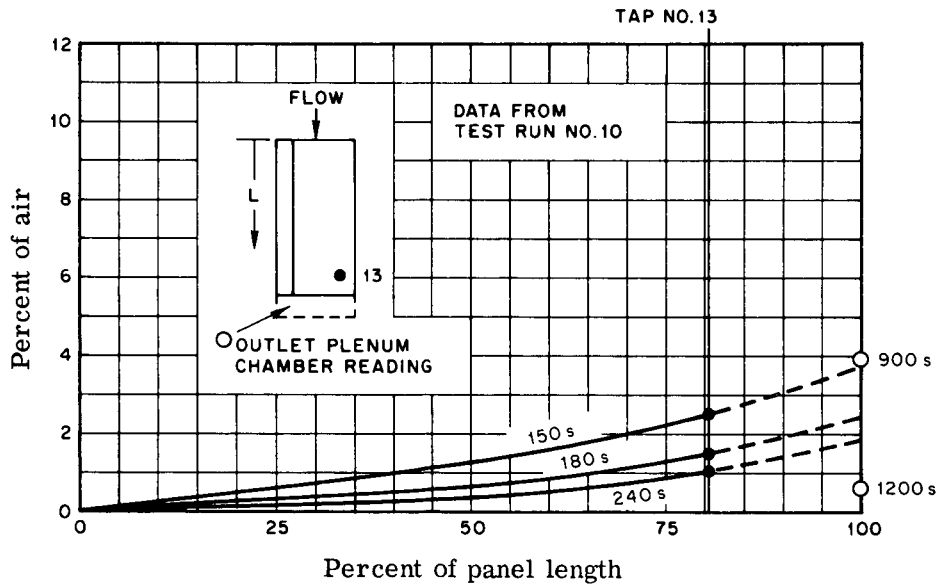

Figure 41. - Helium purity at pressure tap 13 at bottom of flow test panel 1P.

(3) Transient Pressure Tests. The chamber pressure history that was used in all panel testing is shown in Figure 42. Flow test panel 1P was tested in the 1.83-meter (6-foot) diameter vacuum chamber under transient pressure conditions. Using matched 0.475-cm

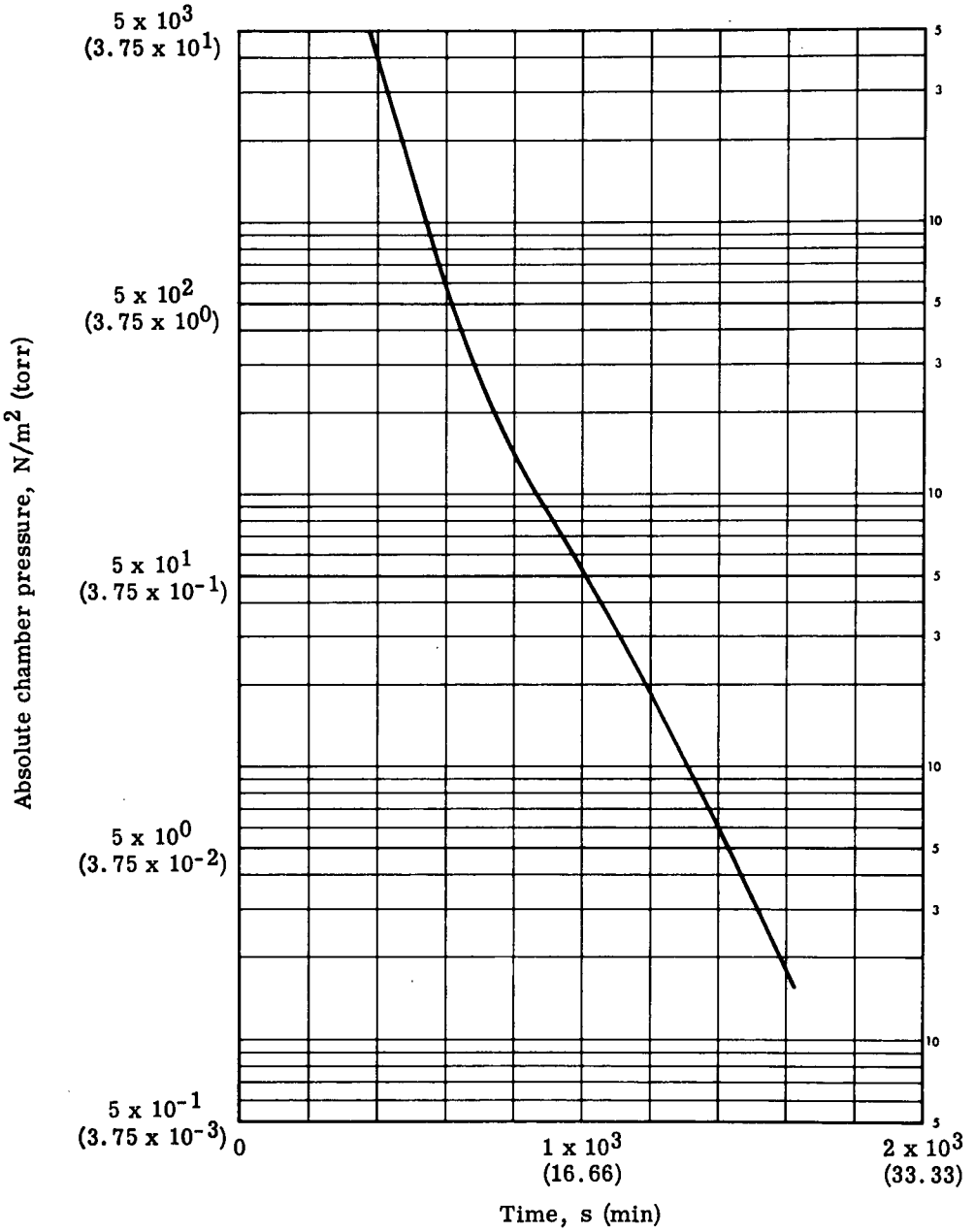

Figure 42. - Vacuum chamber pressure history for flow test panel 1P tests.

(0.189-inch) bore tubing, differential pressures were measured between selected taps and the chamber pressure as a function of time. A typical transient pressure response curve for the matched tubing only (not connected to the panel pressure taps) is shown in Figure 43. The pressure lag was considered negligible compared to the predicted insulation pressures to be measured during transient tests. The taps at which differential pressures were measured under transient panel testing include numbers 2, 5, 8, 1, 4, 7, 11, and 21, as identified in Figure 30.

Since there is essentially no flow normal to the layers of insulation, gas flows from the panel interior toward the panel joint, and the flow is one-dimensional until reaching the

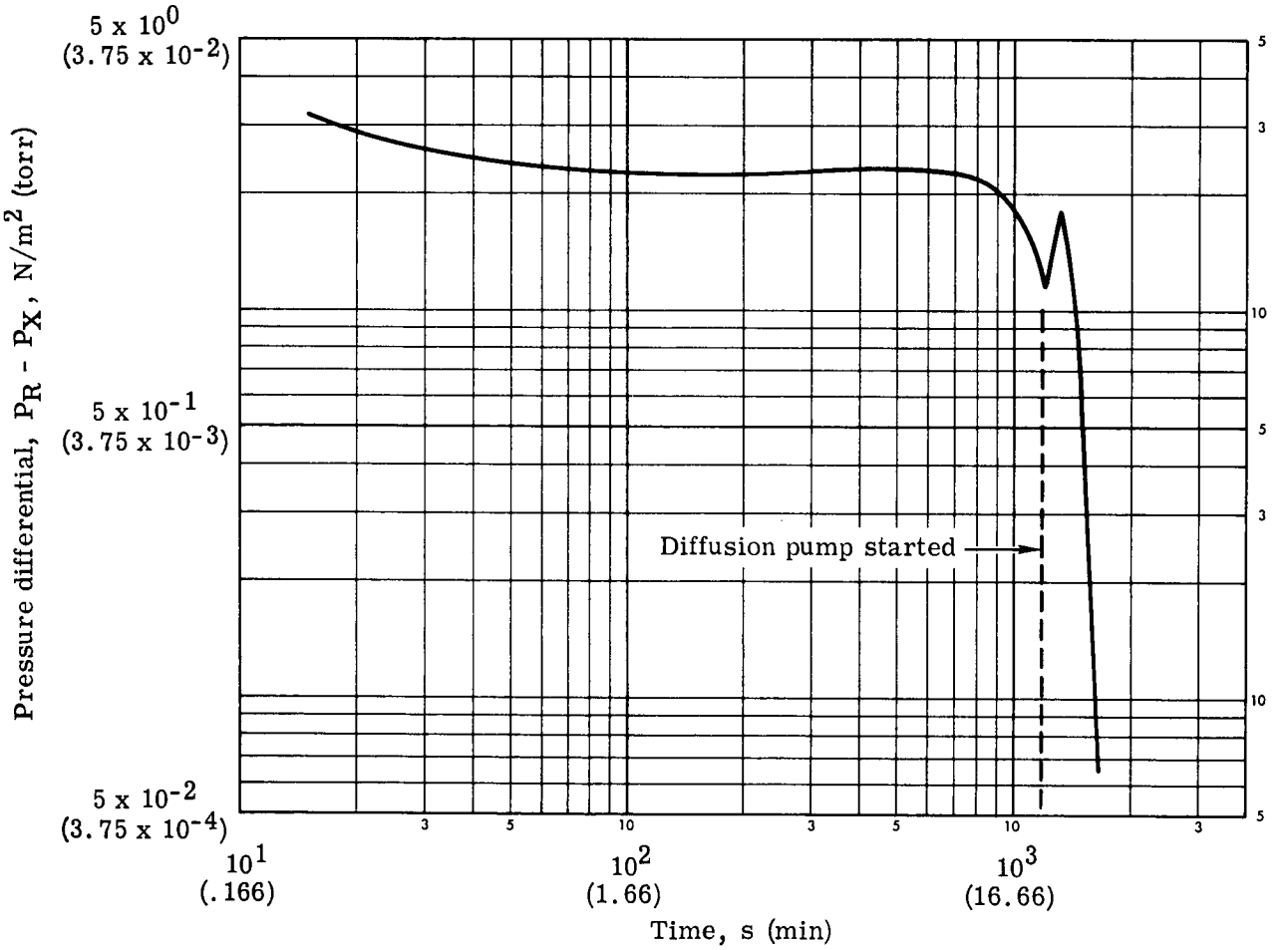

Figure 43. Transient pressure response curve for matched 0.457-cm (0.187-in.) tubing used in flow test panel 1P tests (nitrogen gas).

joint. Assuming that the resistance to flow may be uniform along the length of the joint, gas would flow along lines normal to the joint as indicated in Figure 44. In Figure 44 the differential pressure at tap 5 is shown as a function of time for helium gas at 269°K (25°F). As indicated in Table VI, most of the panel testing was done using nitrogen gas; therefore, the remaining panel test data are presented for nitrogen gas at a nominal temperature of 269°K (25°F).

Time-pressure curves were also plotted for taps 2, 8, 1, 4, 7, 11, and 21. All of the curves had the same general shape as the curve for tap 5 (fig. 44). Taps 1, 4, and 7 had the same trend as taps 2, 5, 8, and 11, where pressure differentials of 2.66 to 5.32 N/m^2

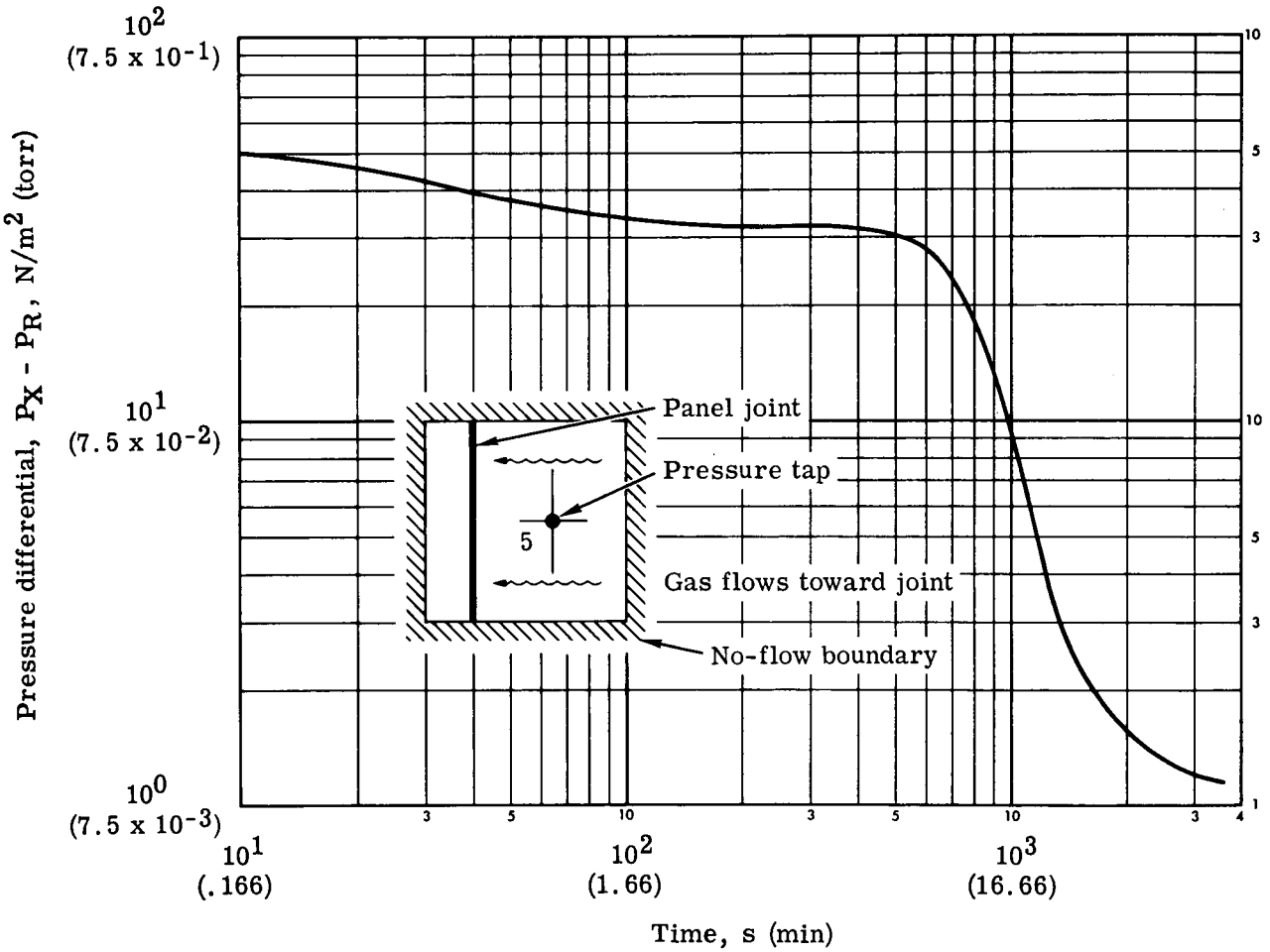

Figure 44. - Results of transient panel tests at tap 5 for nitrogen gas at 269°K (25°F).

(0.02 to 0.04 torr) were obtained at 1.2×10^3 seconds (20 minutes). For the same time period, however, the pressure differential at tap 11 was smaller: 0.80 N/m^2 (0.006 torr). The smaller differential is to be expected since tap 11 is very close to the panel joint and thus has a shorter path to the chamber environment.

e. Flow Model and Analytical Predictions

(1) General. A computer program was used to predict the flow, rate, pressures, and leakage rates of a helium purge gas in a typical multilayer insulation panel. This program is a modification of an existing GAC program that calculates flows and pressures of a three-dimensional model. The program basically divides a typical panel into a specific number of individual nodes and by iterative methods obtains a flow balance on each node until all pressures, flows, and leak rates approach equilibrium with the specified boundary conditions. In solving the equations, the method of simultaneous displacement is used instead of solving a large number of simultaneous equations.

The results obtained from the analytical model can be compared to the three-dimensional steady-state test data obtained from the laboratory flow tests. In order to make a comparison between the test data and the analytical model, the flow coefficients for axial flow and joint flow were modified until the flow rates in the inlet and outlet plenum chambers agreed with the test data. At this condition, the internal pressures of the analytical model were compared with the test data.

(2) Method of Analysis. The analytical model for the 94 x 122 cm (37 x 48 inch) GAC-9 flow test panel is shown in Figure 45. The model is divided into a number of individual

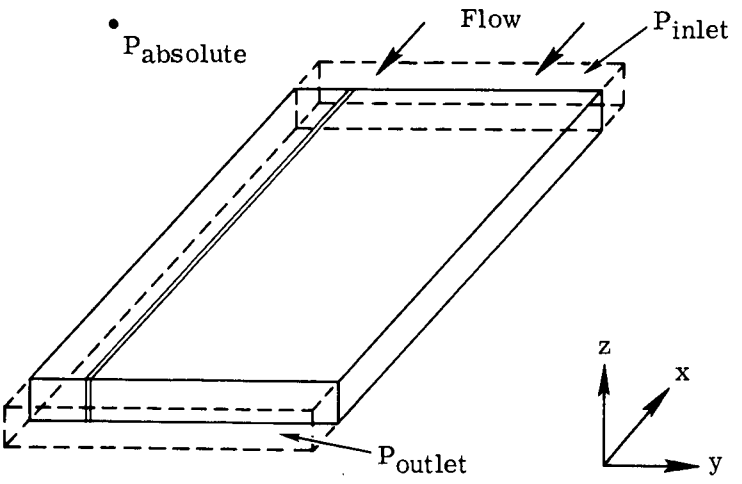

Figure 45. - Flow panel analytical model.

nodes, and a flow balance is conducted on each node. A typical node (i, j, k) will have six flow inputs, one from each adjacent face as shown in Figure 46.

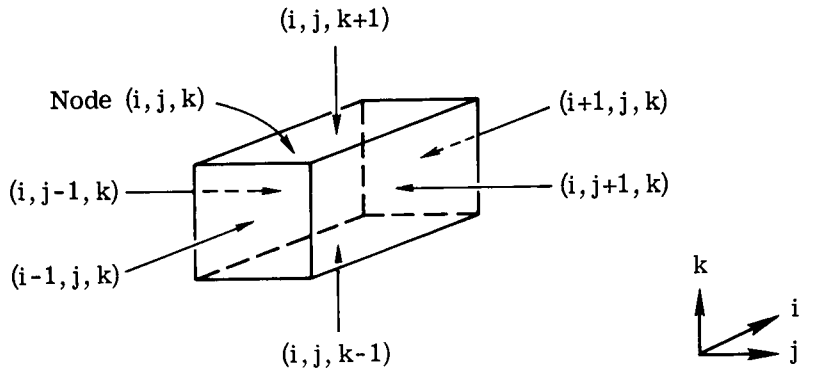

Figure 46. - Typical flow model node.

The flow summation must be equal to zero since the flow is assumed to be at steady-state conditions. The equation is

$$\sum_{n=1}^{n=6} Q_n = 0 \tag{1}$$

where Q_n = flow through surface n

Equation 2 shows the flow into or from an adjacent node as a function of the pressure difference between the nodes.

$$Q_{(i,j)} = \frac{C_{(i,j)}\ A_{(i,j)}}{X_{(i,j)}} \left(P_{(i)} - P_{(j)}\right) \tag{2}$$

where $Q_{(i,j)}$ = flow between nodes
$C_{(i,j)}$ = flow coefficients
$A_{(i,j)}$ = flow area
$X_{(i,j)}$ = flow distance
$P_{(i)}$ = pressure of node i
$P_{(j)}$ = pressure of node j

By combining equations 1 and 2 and letting

$$\frac{C_{(i,j)}\ A_{(i,j)}}{X_{(i,j)}} = K_{(i,j)} \tag{3}$$

we can obtain the expression for $P_{(i,j,k)}$ in three-dimensional coordinates:

$$P_{(i,j,k)} = \Big[K_{(i-1,j,k)}\ P_{(i-1,j,k)} + K_{(i+1,j,k)}\ P_{(i+1,j,k)} + K_{(i,j-1,k)}\ P_{(i,j-1,k)} + K_{(i,j+1,k)}\ P_{(i,j+1,k)} + K_{(i,j,k-1)}\ P_{(i,j,k-1)} + K_{(i,j,k+1)}\ P_{(i,j,k+1)}\Big] \Big/ \Big[K_{(i-1,j,k)} + K_{(i+1,j,k)} + K_{(i,j-1,k)} + K_{(i,j+1,k)} + K_{(i,j,k-1)} + K_{(i,j,k+1)}\Big] \tag{4}$$

The program is written where boundary conditions are fixed for each of the six faces of the test panel. For the two ends, the inlet and outlet manifold pressures are used. Ambient pressure is assumed for the top surface and zero pressure assumed for the bottom and two sides since these surfaces are sealed. These pressures will remain constant throughout the calculations as they are the boundary conditions imposed on the test panel.

A linear pressure gradient is assumed through the panel for the initial pressure distribution. The method of simultaneous displacement is now used where the new pressure for each node is computed from equation 4 by using old pressures of the adjacent nodes. After new pressures have been computed for all nodes, the new values replace the old pressures and a new pressure is computed for each node. This iteration process is continued until the pressure differential between the old and new calculations approaches some limit that is less than 4.78 N/m^2 (0.10 lbf/ft^2).

The flows in and out are computed by summation of the pressure differences between the manifold and adjacent nodes times their respective flow coefficients. The difference between these values will give the leakage rate through the joint area.

(3) Results. The flow test panel was divided into 450 nodes for this analysis; the width consisted of 9 nodes, the length 10 nodes, and the thickness 5 nodes. A comparison of the pressure taps and node locations is shown in Figure 47. Helium gas was used as a purging fluid, and pressures of 124.5 and 24.9 N/m^2 (0.50 and 0.10 in. H_2O) were used for the inlet and outlet manifolds, respectively.

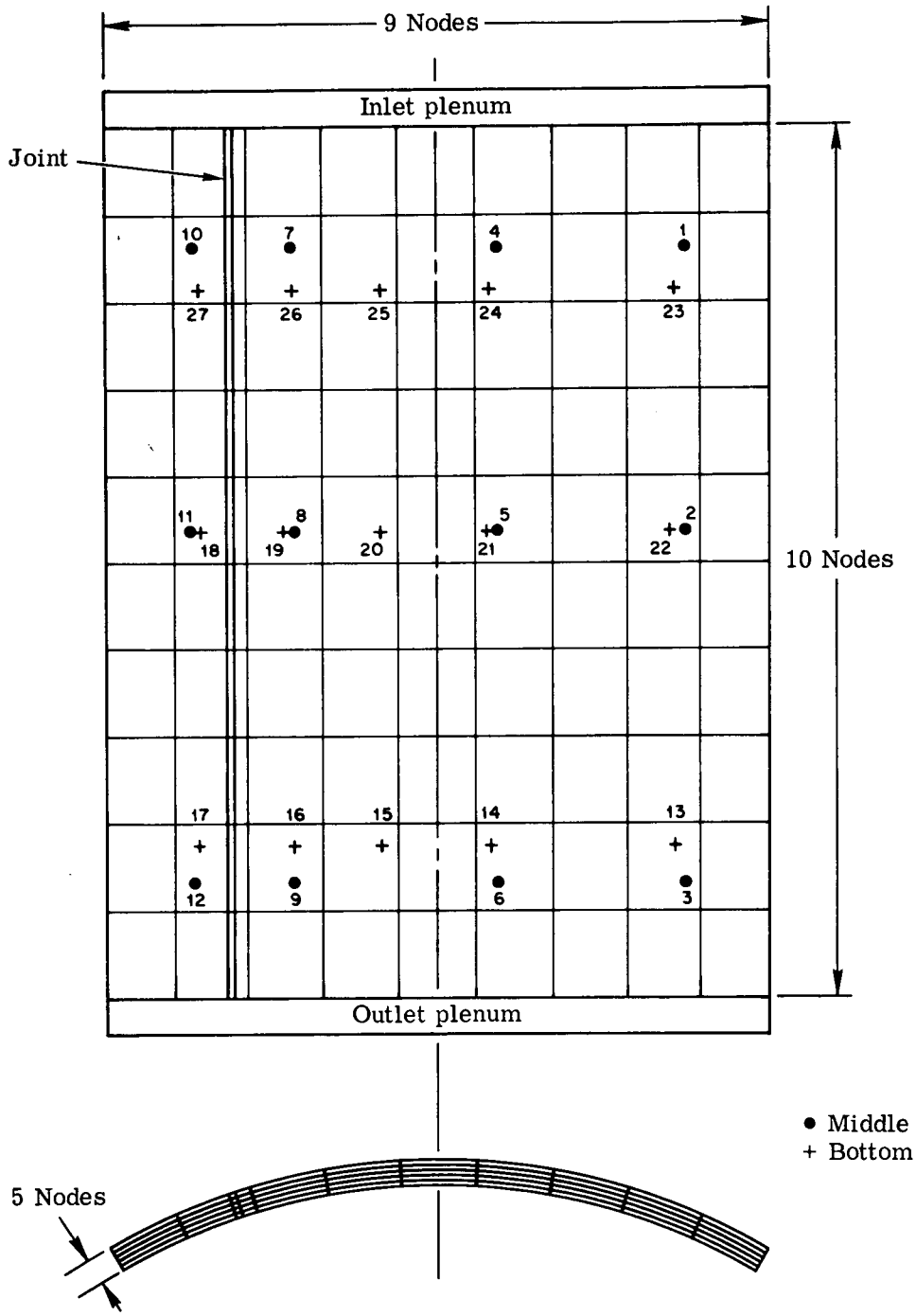

Figure 47. - Comparison of test panel pressure taps and computer model node locations.

Figure 48 shows the pressure-flow contours obtained from laboratory testing of the flow test panel. Figure 49 shows the values calculated for the computer model panel. The tabulated data are given in Table VII. Comparison of Figures 48 and 49 shows that good agreement was obtained along the right side of the panel and near the top inlet plenum. At the joint, the pressures are lower for the test panel and all the flow lines tend to bend more rapidly toward the joint. The calculated pressures on the bottom surface are also higher than the test values. This difference in pressure may be due to the construction of the seam or joint. For the theoretical or calculated values a uniform joint is assumed, but in the actual fabrication of the panel this joint can vary. From the test results it appears that the joint was wider at the outlet plenum end. Indications are that the bottom of the panel has less flow resistance, which could be due to clearance created by the insulation panel grid face between the panel and the test fixture. No attempt was made to give each joint node a different flow coefficient to allow for this variation since this would increase the complexity of determining the flow results. In actual practice, this joint will vary from location to location and an average value of the flow coefficient must be obtained.

The flow coefficients obtained theoretically and verified by the one-dimensional flow tests are given below.

$$C_{axial} = 5.7365 \frac{m^4}{kg\text{-}s} \left(0.233 \times 10^4 \frac{ft^3/min - in.}{ft^2 - lbf/in.}\right)$$

$$C_{joint} = 0.1086 \frac{m^5}{kg\text{-}s} \left(0.1344 \times 10^2 \frac{ft^3/min - in.}{ft - lbf/in.}\right)$$

To obtain agreement in the flow rates, these values were modified in the computer program as follows:

$$C_{axial} = 16.003 \frac{m^4}{kg\text{-}s} \left(0.650 \times 10^4 \frac{ft^3/min - in.}{ft^2 - lbf/in.}\right)$$

$$C_{joint} = 0.2044 \frac{m^5}{kg\text{-}s} \left(0.253 \times 10^2 \frac{ft^3/min - in.}{ft - lbf/in.}\right)$$

These values do not differ by an order of magnitude but do show a large variation from the measured values. The one-dimensional flow coefficients used to verify the theory were obtained from a small flow test specimen, whereas the computer analysis flow model is a much larger specimen where the edge effects are imposed on the model. The edge effects plus the

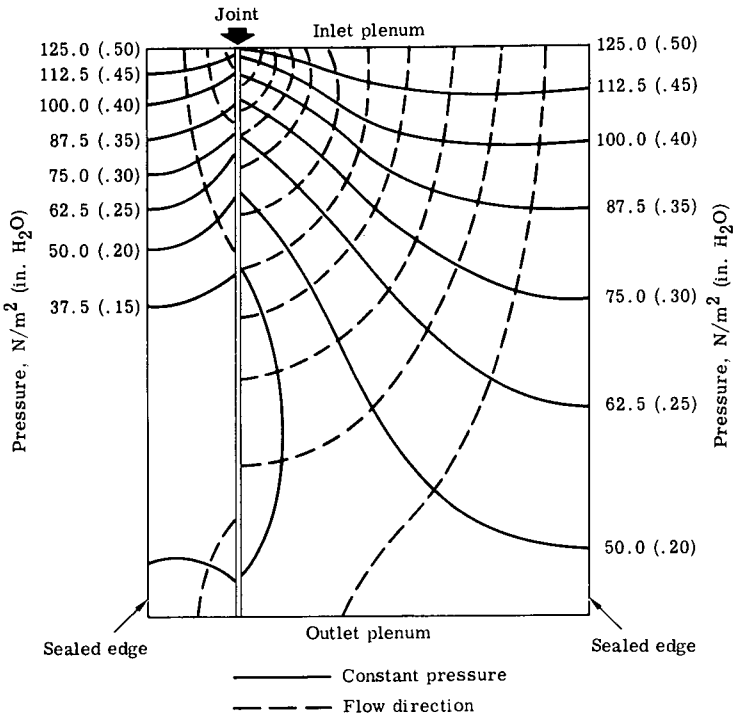

Figure 48. - Pressure-flow contours at middle layer of flow test panel - helium purge.

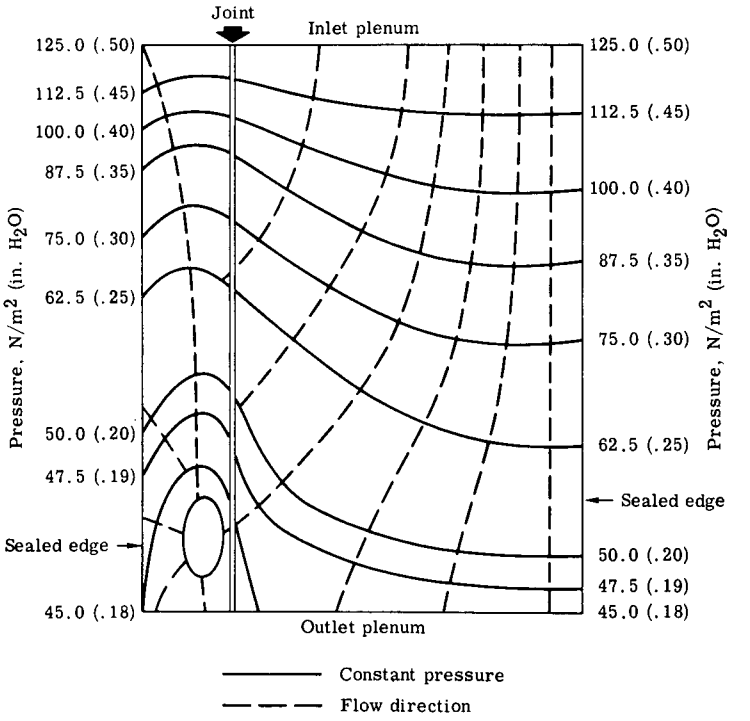

Figure 49. - Pressure-flow contours at middle layer of computer model panel - helium purge.

TABLE VII. - COMPARISON OF TEST DATA AND CALCULATED DATA FOR HELIUM PURGE TEST PANEL

Tap No.	Pressure, N/m^2 (in. H_2O)	
	Calculated[a]	Test[b]
1	108.7 (0.437)	107.7 (0.433)
2	80.4 (0.323)	66.7 (0.268)
3	53.0 (0.213)	51.0 (0.205)
4	107.0 (0.430)	100.8 (0.405)
5	77.1 (0.310)	59.5 (0.239)
6	51.8 (0.208)	46.0 (0.185)
7	98.5 (0.396)	65.2 (0.262)
8	65.4 (0.263)	38.1 (0.153)
9	46.3 (0.186)	37.3 (0.150)
10	92.1 (0.370)	65.2 (0.262)
11	59.0 (0.237)	28.9 (0.116)
12	43.0 (0.173)	34.3 (0.138)
13	54.8 (0.220)	63.2 (0.254)
14	54.2 (0.218)	52.3 (0.210)
15	52.5 (0.211)	52.0 (0.209)
16	51.3 (0.206)	56.2 (0.226)
17	49.8 (0.200)	61.0 (0.245)
18	72.4 (0.291)	64.9 (0.261)
19	76.1 (0.306)	65.9 (0.265)
20	78.9 (0.317)	69.4 (0.279)
21	82.4 (0.331)	70.2 (0.282)
22	84.1 (0.338)	78.4 (0.315)
23	110.7 (0.445)	96.8 (0.389)
24	109.5 (0.440)	99.5 (0.400)
25	107.7 (0.433)	84.3 (0.339)
26	106.3 (0.427)	79.1 (0.318)
27	103.8 (0.417)	78.4 (0.315)

[a]Calculated flow values:

Flow in = 5.04×10^{-4} m^3/s (1.068 ft^3/min)

Flow out = 1.46×10^{-6} m^3/s (0.003 ft^3/min)

Leakage = 5.027×10^{-4} m^3/s (1.065 ft^3/min)

[b]Test flow values:

Flow in = 4.812×10^{-4} m^3/s (1.020 ft^3/min)

Flow out = 7.552×10^{-6} m^3/s (0.016 ft^3/min)

Leakage = 4.73×10^{-4} m^3/s (1.004 ft^3/min)

variations in fabrication will cause a difference in the test results and the calculated values. However, the pressure distribution and flow patterns do show reasonable agreement. Therefore, the computer program will be used to predict the flow rates for determining the insulation purging requirements for the 76-cm (30-inch) diameter calorimeter.

5. Development of Pressure-Sensing Instrumentation

a. General. The primary objective of the 76-cm (30-inch) diameter calorimeter liquid hydrogen boil-off tests conducted during this program is to obtain purge gas flow characteristics in GAC-9 insulation panels under cryogenic tanking conditions. Essential to the attainment of this objective is the use of pressure sensing-tubes, installed in the insulation, with acceptable minimum time of pressure response. The purge and vent pressure-sensing instrumentation tubing was evaluated to determine which tube size would result in the best compromise of least local pressure influence and the most rapid pressure response. Three flow areas of interest in regard to instrumentation tubing are listed below with the corresponding pressure ranges.

(1) Purging: 1.013×10^5 N/m^2 (760 mm Hg or torr)

(2) Evacuation (or initial venting): 1.013×10^5 to 1.33×10^2 N/m^2 (760 to 1 torr)

(3) Venting (or final evacuation): below 1.33 N/m^2 (10^{-2} torr)

The following three candidate tube sizes were selected for evaluation based on handling and installation considerations:

Tube	Outside diameter cm, (inch)	Inside diameter or bore cm, (inch)
1	0.158 (0.062)	0.106 (0.042)
2	0.318 (0.125)	0.175 (0.069)
3	0.635 (0.250)	0.475 (0.187)

The two smaller sizes represent diameters considered practical for use within GAC-9 insulation wherein the tubes are emplaced parallel to the insulation layers. The larger size tube is for use external to the insulation or within the insulation when the tube is inserted perpendicular to the layers of insulation.

The range of tube lengths is from 53.4 cm (21.0 inches) to 213.0 cm (84.0 inches). This range is representative of the shortest to the longest pressure-sensing tube lengths anticipated for use in the purge and vent tests of the GAC-9 insulation on the 76-cm (30-inch) diameter calorimeter.

Evaluation of the three tube sizes was accomplished in two test phases: (1) single tube tests and (2) matched (in pairs) tubing tests. Acceptable pressure response limits were established as follows: (1) for initial venting, approximately 10 percent of the initial gas load, or 100 N/m^2 (0.75 torr), was set as an acceptable upper limit. (2) For final evacuation, it was assumed that 0.1 N/m^2 (10^{-3} torr), or one order of magnitude, would be sufficiently accurate. This limit was established because of the difficulty in obtaining the low pressure measurements used to determine how fast the insulation reaches the high-performance regime, which spans two to three orders of magnitude.

b. Single Tube Tests. These tests were conducted primarily to determine the usefulness of the candidate tube sizes for measuring interstitial gas pressures within the GAC-9 multilayer insulation during purge and vent studies. The tests consisted of a series of steady-state and transient pressure measurements to determine the tubing pressure response or difference in pressure from a known source. The test setup is shown in Figure 50. Essentially, the test procedure consisted of measuring the differential pressure across the test tube and the absolute pressure inside the vacuum chamber. The lines connected across the test tube were matched in length to null out pressure differences in the lines. The chamber pressure (P_R) was controlled manually to simulate the Saturn ascent pressure profile.

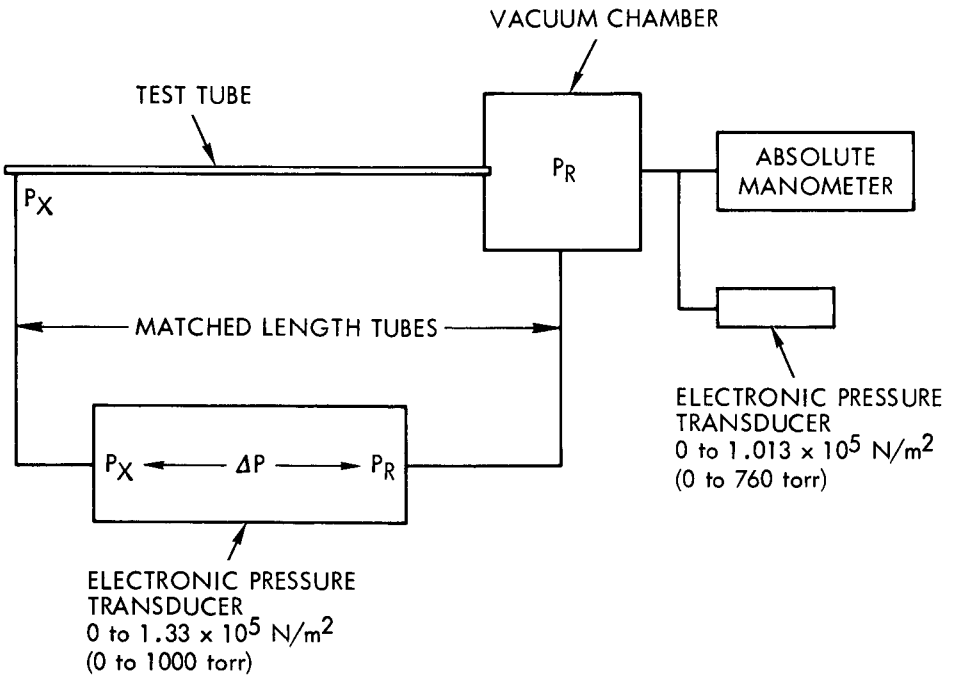

Figure 50. - Transient pressure response test setup for small-diameter tubing.

In order to successfully measure steady-state and transient pressures in the GAC-9 insulation, large enough tubing must be used to prevent a large pressure variation between the test area of interest and the pressure-sensing instrument. From the pressure response curves shown in Figure 51, it can be seen that the use of improper tube sizes will cause a serious pressure response lag. It was concluded from these tests that the 0.106-cm (0.042-inch) bore tubing is unacceptable because after 120 seconds (2 minutes) the pressure response lagged 300 N/m^2 (2.25 torr) in the evacuation (or initial venting) regime (where internal gases are rapidly leaving the insulation, imposing maximum pressure differentials and loads on the insulation).

In the venting (or final evacuation) regime, where the objective is to determine how fast the insulation reaches high performance, the range of internal gas pressure in the area of interest is from 1.33×10^{-1} to 1.33×10^{-2} N/m^2 (10^{-3} to 10^{-4} torr). The 0.175-cm (0.069-inch) bore tubing did not look promising because these tubes lagged about 2 N/m^2 (0.015 torr), which is two orders of magnitude above the region of interest.

Steady-state tests were run concurrently with the transient pressure response tests. The results indicate that the 0.475-cm (0.187-inch) bore tubing facilitated quick and accurate steady-state testing at differential pressures of 1.33×10 N/m^2 (0.10 torr). On the basis of steady-state and transient pressure test results, the 0.475-cm (0.187-inch) bore tubing was selected for use in the two-dimensional purge and vent flow testing of the 94 x 122 cm (37 x 48 inch) GAC-9 insulation panel. This tubing was installed in the 0.635-cm (0.250-inch) bore pressure taps described earlier in this subsection.

Flow test panel 1P was used to evaluate the effects of large line volumes. The volume of the 0.475-cm (0.187-inch) bore pressure-sensing tubing affects the pressure in the vicinity of the pressure taps under transient conditions. The results of an analysis of this effect are shown in Figure 52. Using a one-dimensional transient flow model, predictions of the pressure within the insulation were made using flow coefficients determined both in the one-dimensional steady-state testing and in the two-dimensional steady-state panel testing. As shown in Figure 52, the analysis using the two-dimensional flow coefficients closely predicts the pressures that were measured on flow test panel 1P. When the effect of the pressure-sensing tubing volumes is removed from the analytical model, then curve E is obtained. Thus the analysis shows that the volume of the pressure- sensing tubing increases the pressure differential at the sensing tap by an order of one magnitude.

c. Matched Tubing Tests. During the 94 x 122 cm (37 x 48 inch) flow panel purge and vent testing, a literature survey (ref. 4) resulted in the approach of using matched pairs of tubing to circumvent the pressure response problem. In the matched tubing concept of pressure

Curve No.	Tube dimensions, cm (in.)		
	Outside diameter	Inside diameter	Length
1	.159 (.062)	.106 (.042)	213.0 (84)
2	.159 (.062)	.106 (.042)	86.4 (34)
3	.159 (.062)	.106 (.042)	43.1 (17)
4	.318 (.125)	.175 (.069)	213.0 (84)
5	.318 (.125)	.175 (.069)	106.7 (42)
6	.318 (.125)	.175 (.069)	53.4 (21)
7	.635 (.250)	.475 (.187)	213.0 (84)

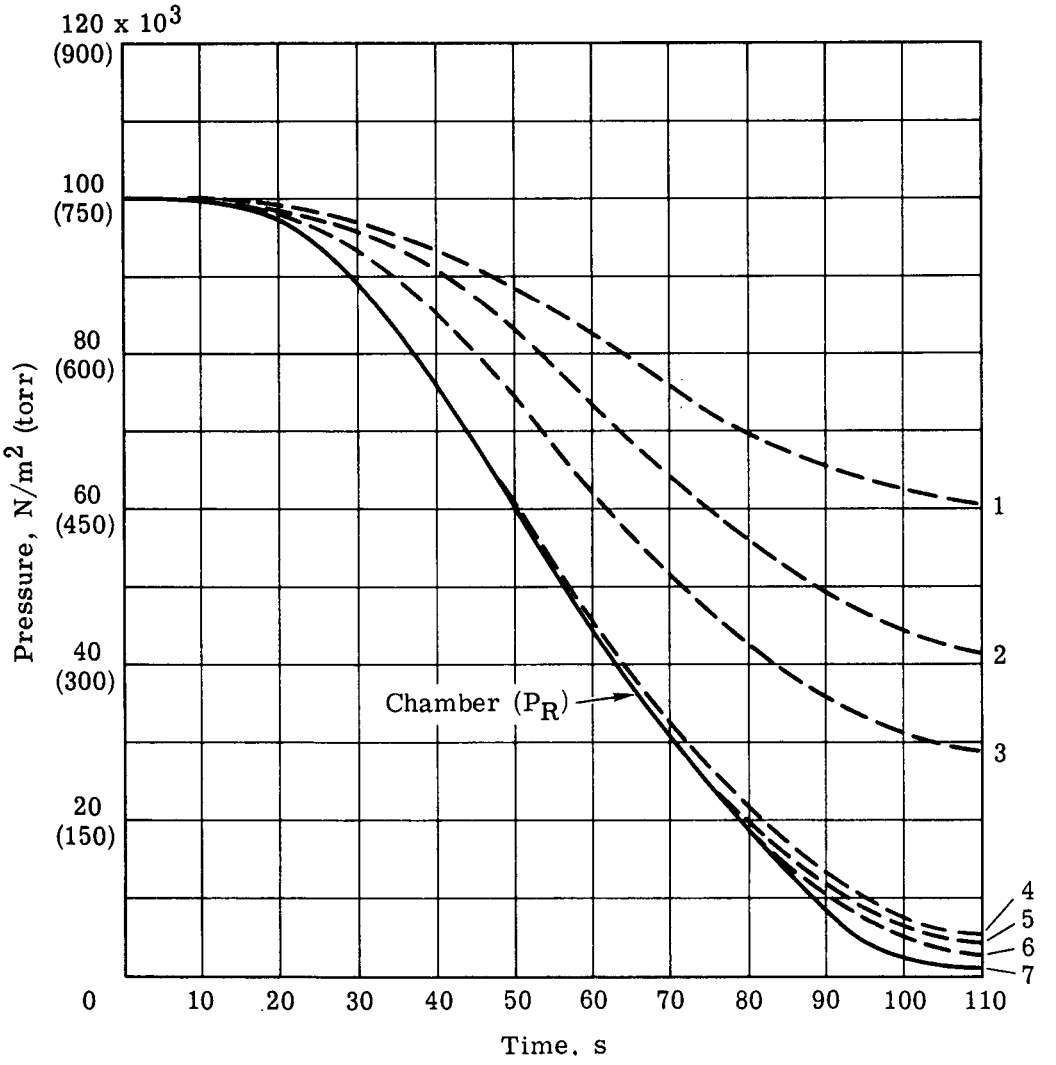

Figure 51. - Pressure response curves.

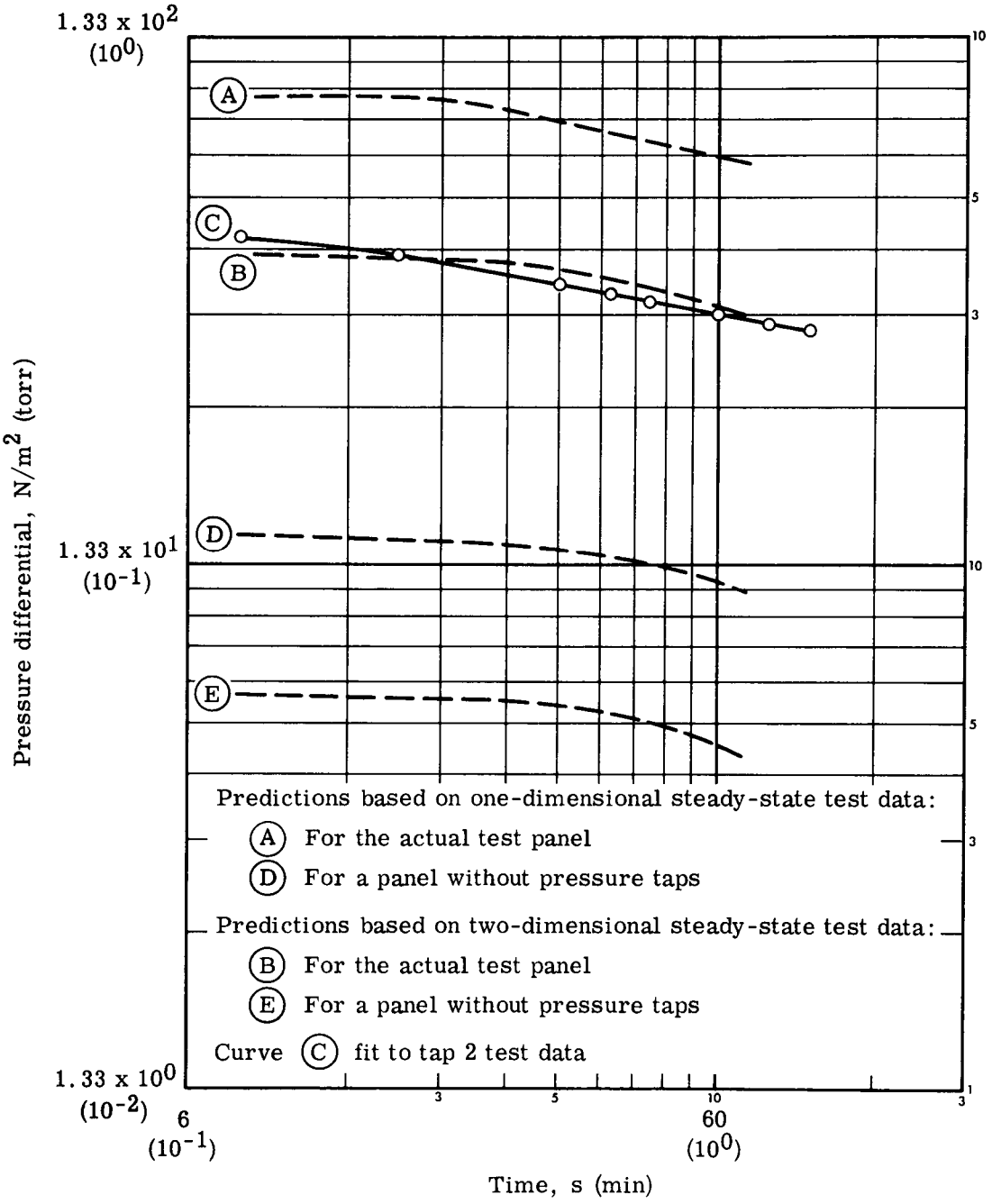

Figure 52. - Predicted and measured pressure differentials as a function of time at tap 2 for nitrogen at 269°K (25°F).

measurements, the pressure gradients between the insulation and the vacuum chamber are measured with an electronic differential pressure meter by referencing one side of the meter to the chamber vacuum through a tube of size, shape, and length identical with the tube from the insulation to the other side of the meter. Therefore, the pressure lag in the tubing should be approximately the same for both sides and should not introduce a significant error.

Further investigations were made to explore the feasibility of using matches pairs of the 0.175-cm (0.069-inch) and 475-cm (0.187-inch) bore tubing in the 76-cm (30-inch) diameter calorimeter insulation. Transient pressure response tests were conducted on matched pairs of pressure-sensing tubing to determine the difference in pressure between the sensor head and the sensing end of the tubes without the impedence of the insulation panel at the sensing end. This test was made to determine whether or not the pressure difference in unimpeded pressure-sensing tubing is small relative to the pressure differential that exists in a system having the sensing end impeded by its location in the insulation panel. If the differential is small, then the matched tubing concept is acceptable.

Seven pairs of tubing were fabricated to the exact lengths and shapes (bends representing the maximum and minimum lengths of pressure-sensing tubing planned for the 76-cm (30-inch) diameter calorimeter GAC-9 insulation. The pressure response tests, performed using the test setup shown schematically in Figure 53, consisted of measuring the differential pressure across matched length tube assemblies during the chamber evacuation.

The test results, presented graphically in Figure 54, are summarized below.

(1) Tube assembly 1, representing long 0.175-cm (0.069-inch) ID and long 0.475-cm (0.187-inch) ID tubing, reached a pressure differential of 399 N/m^2 (3 torr) after 600 seconds (10 minutes).

(2) Tube assemblies 2, 3, and 4, representing short 0.175-cm (0.069-inch) ID and long 0.475-cm (0.187-inch) ID tubing, reached a pressure differential of 67 N/m^2 (0.5 torr) after 600 seconds (10 minutes). Tube assembly 2 was run for 1800 seconds (30 minutes). This assembly reached 46.5 N/M^2 (0.35 torr) at 900 seconds (15 minutes) and was unchanged at 1800 seconds (30 minutes). None of these tube assemblies are considered acceptable.

(3) Tube assembly 5, representing full-lenth 0.175-cm (0.069-inch) ID tubing, reached a pressure differential of 13 N/m^2 (10^{-1} torr) in 480 seconds (8 minutes) and remained unchanged. This tube assembly is not considered acceptable.

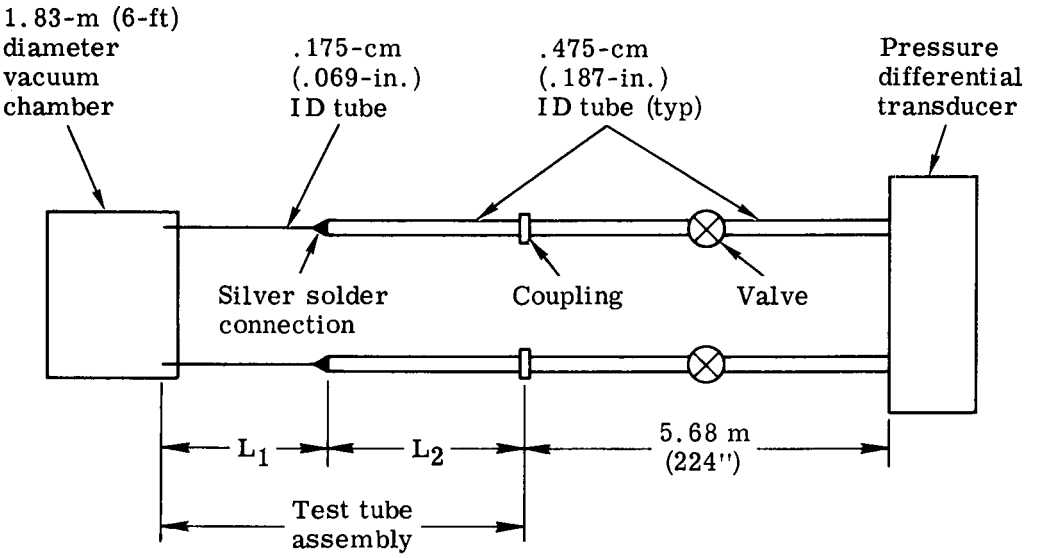

Tube assembly No.	Length, m (in.)	
	L_1	L_2
1	1.93 (76)	4.06 (160)
2	.76 (30)	4.06 (160)
3	.76 (30)	4.06 (160)
4	.76 (30)	4.06 (160)
5	5.00 (197)	--
6	--	3.43 (135)
7	--	4.64 (183)

Figure 53. - Transient pressure response test setup for matched tube assemblies.

(4) Tube assemblies 6 and 7, representing full-length 0.475-cm (0.187-inch) ID tubing, reached a pressure differential of 1.3 N/m^2 (10^{-2} torr). Tube assembly 7, the longest tubing tested, was run for 1800 seconds (30 minutes), at which time the matching differential was in the range of 0.66 N/m^2 (10^{-3} torr). The full-length 0.475-cm (0.187-inch) ID tube assemblies had the most rapid pressure response and the least pressure differential; therefore, these assemblies were selected as the acceptable pressure-sensing system for the 76-cm (30-inch) diameter calorimeter.

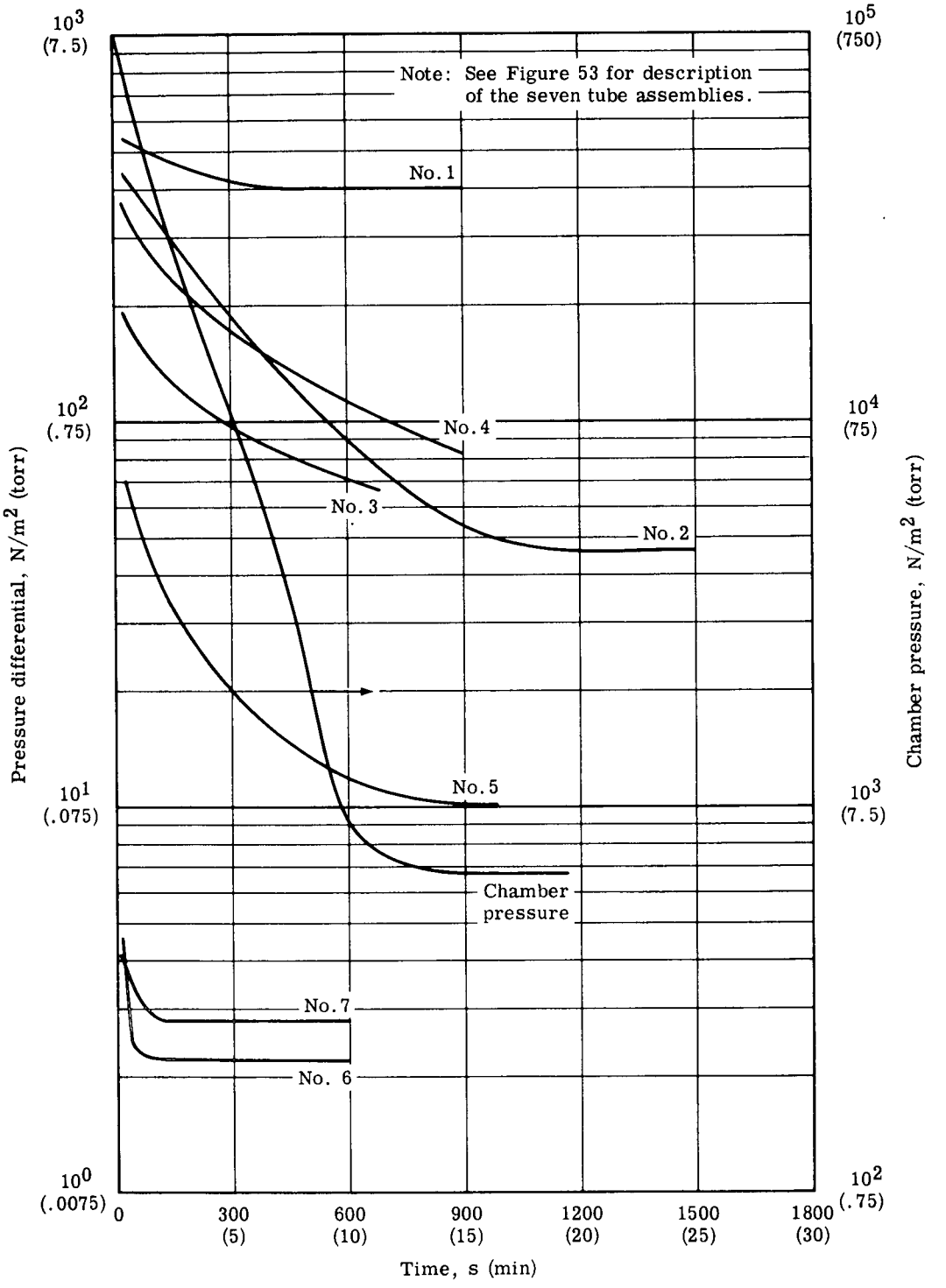

Figure 54. - Transient pressure test data for matched tube assemblies.

d. Conclusions and Recommendations. All candidate tubing sizes are acceptable for steady-state measurements in the higher pressure regime: 1.01×10^5 N/m^2 (760 mm Hg or torr). At lower pressure regimes, transient pressure response governs the tubing size. From 1.01×10^5 to 1.33×10^3 N/m^2 (760 to 10 torr), transient pressure measurements can be made with the 0.175-cm (0.069-inch) and 0.475-cm (0.187-inch) bore tubing. At low pressures, around 1.33×10^{-1} N/m^2 (10^{-3} torr) after 1800 seconds (30 minutes) of venting, the slow pressure response of the 0.175-cm (0.069-inch) bore tubing gives pressure differential of readings that are two to three orders of magnitude high. The 0.475-cm (0.187-inch) bore tubing has acceptable pressure response; however, the tubing gas volume raises the local pressure at the insulation when sensing pressures at a single layer of insulation. The 0.475-cm (0.187-inch) bore tubing gas volume has less effect on local pressures when sensing the average pressure across the full thickness of insulation. Therefore, the 0.475-cm (0.187-inch) bore tubing was recommended for the 76-cm (30-inch) diameter calorimeter pressure-sensing instrumentation.

D. MATERIALS INVESTIGATION

In purge and vent laboratory flow tests, the GAC-9 insulation system, which consists of alternate layers of thin sliced foam spacers and aluminized Mylar radiation shields, has shown negligible broadside or normal flow of helium purge gas through drop thread holes in the insulation composite. The effect of this characteristic will depend on the mission of the vehicle using the insulation. The use of perforations in the radiation shields may increase the performance of the GAC-9 insulation over a short period during launch to some orbital position; however, the perforations may degrade the insulation performance over the entire time of space operation. The degradation occurs in increasing the overall emittance value of the radiation shields. To evaluate the perforation of radiation shields, a survey was made of perforation patterns used on Mylar films. The patterns in past and current use are described in Table VIII. An experimental quantity of pattern 9810, available in 0.0038-mm (0.15 mil) DAM, was obtained for purge and vent normal flow tests, flat-plate calorimeter tests, and micrometeoroid impact tests.

The laboratory purge and vent tests are discussed in subsection C of this section and the flat-plate calorimeter tests in subsection E. Micrometeoroid test specimens of GAC-9 insulation with perforated Mylar shields were fabricated as shown in Figure 55. These specimens were delivered to NASA-MSFC for testing at the Materials Laboratory Hypervelocity Range facility. The test results are given in the appendix.

TABLE VIII. - MYLAR RADIATION SHIELD PERFORATION DATA

Pattern No.	Hole diameter, cm (in.)	Percent open area	Hole spacing (center to center), cm (in.)
9804	0.139 (0.055)	0.712	1.574 (0.62)
S603	0.119 (0.047)	0.70	1.371 (0.59)
9803	0.139 (0.055)	1.06	1.092 (0.43)
S605	0.119 (0.047)	1.82	0.711 (0.28)
9810	0.139 (0.055)	2.38	0.787 (0.31)
9802	0.139 (0.055)	5.0	0.558 (0.22)
--	0.236 (0.093)	1.8	1.796 (0.707)

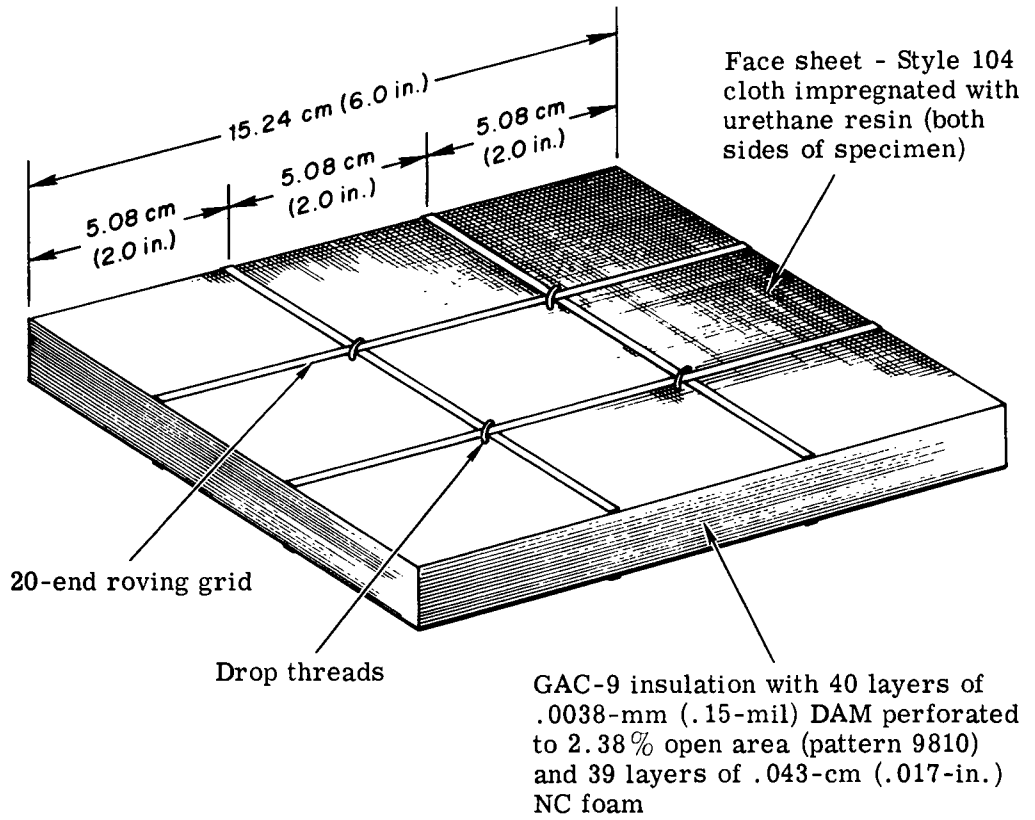

Figure 55. - GAC-9 insulation micrometeoroid test specimen.

At the beginning of the program, it was planned to investigate ECN (Engineered Cellular Nylon) foam as an alternate spacing material. Prior to initiating the evaluation of this foam, DuPont was contacted regarding availability of additional samples of ECN foam. The Explosives Department of DuPont has discontinued the development of ECN foam. Development and marketing of ECN foam have not been undertaken by other departments at DuPont. Work on the evaluation of ECN foam was deferred to divert funds to critical program areas such as procurement of liquid hydrogen for 76-cm (30-inch) diameter calorimeter testing of GAC-9 insulation purge system.

E. FLAT-PLATE CALORIMETER TEST PROGRAM

1. General

An important task in improving the purge and vent characteristics of the GAC-9 insulation system was the determination of thermal performance of GAC-9 insulation modified by addition of perforations to the Mylar radiation shields. A thermal performance screening test of the modified GAC-9 insulation system was conducted using the GAC 15-cm (6-inch) diameter flat-plate calorimeter with liquid hydrogen. The calorimeter setup shown schematically in Figures 56 and 57 is the same apparatus employed on previous contracts (NAS 8-30140 and NAS 8-24884).

Multilayer insulation efficiency is sensitive to compressive loads; therefore, the test sample was tested at zero load condition and two compressive load levels: 68.9 N/m^2 (0.001 $lbf/in.^2$) and 6.89 N/m^2 (0.001 $lbf/in.^2$). It is recognized that these low pressures cannot be reliably attained with the flat-plate calorimeter dead-weight apparatus; therefore, the specimen was tested for thermal performance as a function of insulation thickness. A duplicate test specimen was checked in an Instron machine to establish a stress-strain curve for relating thermal performance to specimen loading and/or thickness. The distance between the calorimeter hot and cold plate surfaces (specimen thickness when less than free height) was measured optically with a cathetometer.

2. Test Specimens

The flat-plate calorimeter specimen of GAC-9 insulation modified with perforated Mylar was identified as VL-99. This specimen was fabricated in a layup sequence of 11 foam spacers alternated with 10 DAM (doubly aluminized Mylar) radiation shields. The radiation shields were cut from 0.0038-mm (0.15-mil) Mylar aluminized both sides and perforated with a pattern of 0.0139-cm (0.055-inch) diameter holes to 2.38 percent open area.

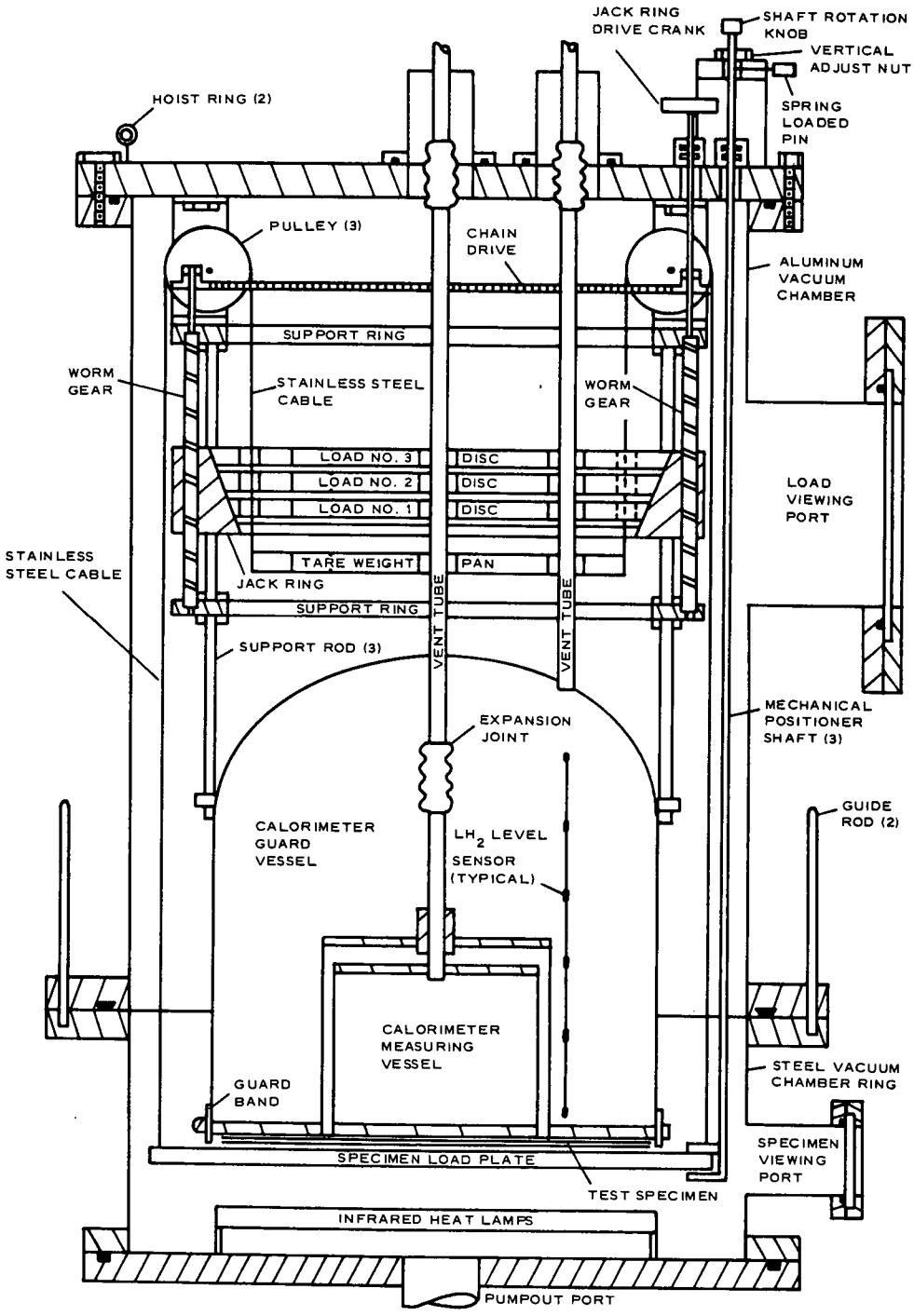

Figure 56. - GAC 15-cm (6-in.) diameter flat-plate calorimeter.

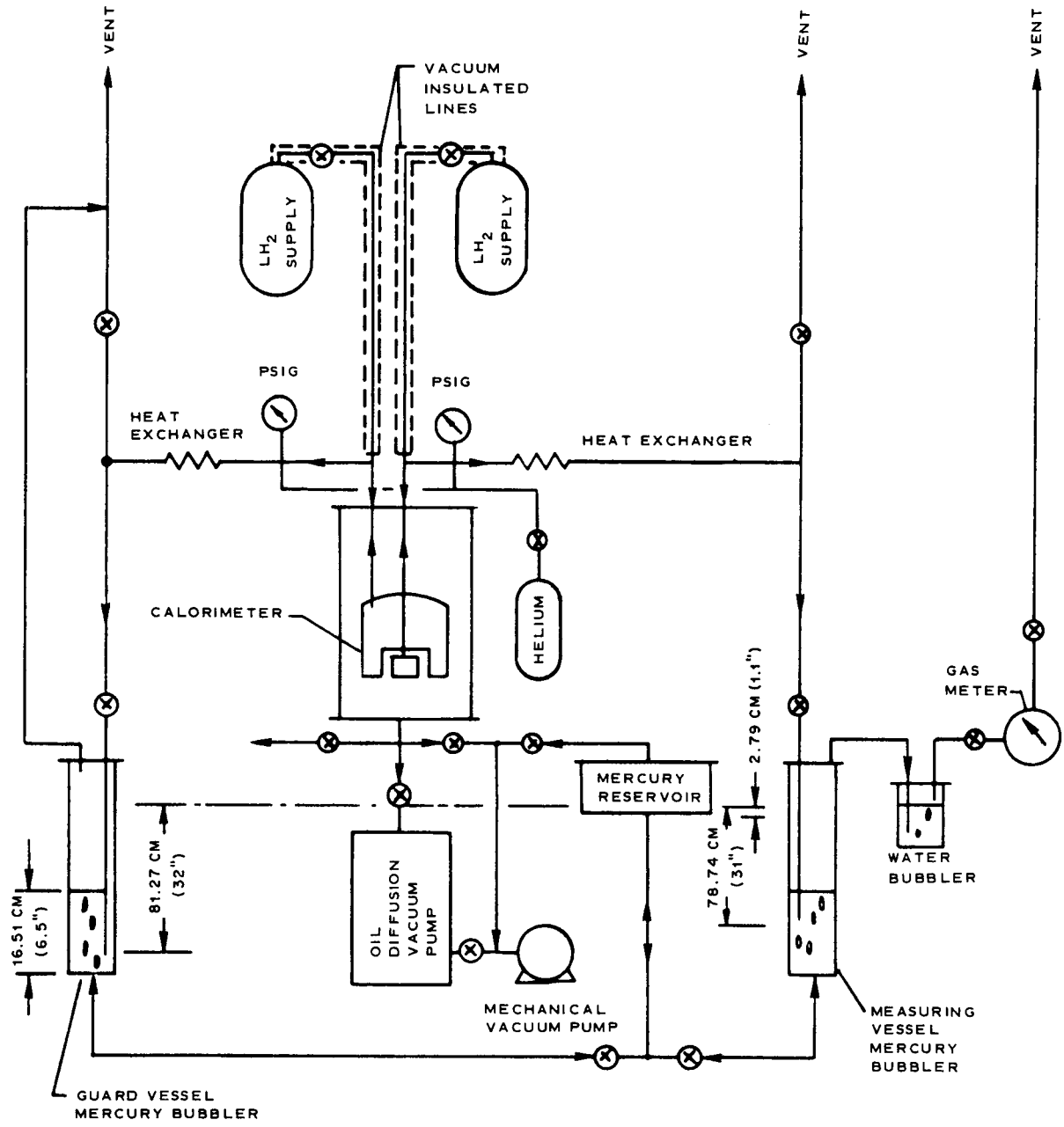

Figure 57. - Flat plate calorimeter gas flow diagram.

Two specimens were fabricated, measured for free height by cathetometer technique, and weighed before testing. One specimen was used for Instron stress-strain curve evaluation and the other for flat-plate calorimeter testing. Both specimens were nearly identical in weight (15.1 and 15.3 grams) and in free height: 0.76 cm (0.300 inch) and 0.77 cm (0.304 inch).

3. Test Procedure.

Operating procedures for the calorimeter were essentially the same as those employed on previous programs. These procedures are given below.

(1) Mount the specimen in the apparatus and set the distance between the bottom of the calorimeter and the top of the load plate to a predetermined dimension to simulate a mechanical compression of 68.9 N/m^2 (0.01 $lbf/in.^2$). Dimensional settings will be determined from Instron stress-strain tests.

(2) Purge the calorimeter and lines with dry helium gas.

(3) Fill the calorimeter with LH_2 to provide a cold surface temperature of 20^oK (-423^oF).

(4) Control the hot surface at 297^oK (75^oF).

(5) Keep the measuring vessel vent tube thermally shorted to LH_2 in the guard vessel.

(6) Maintain the ullage pressure in the guard vessel 2.54 cm (1.0 inch) of mercury higher than in the measuring vessel to prevent recondensation of vent gas from the measuring vessel.

(7) Maintain the ullage pressure in the measuring vessel at 78.7 cm (31.00 inches) of mercury absolute, using pressure-damping apparatus to minimize boil-off gas rate fluctuations resulting from barometric pressure changes.

(8) Measure the rate of boil-off gas from the measuring vessel.

(9) Repeat steps 4 through 8 at various dimensional settings between the bottom of the calorimeter and top of the load plate to obtain gas boil-off rates at 6.89 N/m^2 (0.001 $lbf/in.^2$) and at least two zero load conditions.

Initially, the following data were recorded on the calorimeter data sheet shown in Figure 58.

(1) Specimen number
(2) Test number

No.	Temperatures °F Location	CLOCK TIME								
1	Guard Band									
2	Load Plate									
3	Outside Ambient									
4										
5										
6										
7										
8										
9										
10										
11										
12										
Guard LH_2 Level (in.)										
Pressure	Chamber (mm Hg)									
	Hg Reservoir (μ)									
	Fore Pump (μ)									
	Barometric (in. Hg)									
	Temp (°C)									
Gas Meter	Press. (mm H_2O)									
	Reading (liters)									
	Boil-Off Rate (l/hr)									

Average specimen thickness:_____inches at _____lb load

Average specimen thickness:_____inches at_____lb load

Distance between calorimeter and load plate:_____inches at zero load

Specimen Dia:_____inches Test No. _____

Specimen Wt:_____grams Specimen No. _____

Sheet No. _____of _____

Tested by:_____ Date_____

Figure 58. - Flat-plate calorimeter test data sheet.

(3) Nominal free height thickness of the specimen

(4) Compressive load on the specimen

(5) Thickness of specimen under load

(6) Date

(7) Name of test operators

Then the following data were recorded on the calorimeter data sheet at 1800-second (30-minute) intervals after the gas began to flow through the gas meter.

(1) Guard band temperature

(2) Load plate temperature

(3) Outside ambient temperature

(4) Barometric pressure at the test site

(5) Vacuum chamber pressure

(6) Mercury bubbler reservoir pressure

(7) Gas meter reading

(8) Gas boil-off rate

(9) Gas meter pressure

(10) Gas temperature in meter

(11) Guard vessel LH_2 level

The data were recorded every 1800 seconds (30 minutes) until equilibrium boil-off conditions were obtained for each compressive load condition. Equilibrium was defined as the condition at which the measured boil-off leveled out and fluctuated at less than 3 percent of the indicated flow rate over a period of 7200 seconds (2 hours).

4. Test Results and Analysis

a. Stress-Strain Instron Tests. Instron stress-strain data obtained for the VL-99 flat-plate calorimeter test specimen construction are shown in Figure 59. The stress-strain curve is presented in the load range of 0 to 70 N/m^2 (0 to 0.012 $lbf/in.^2$) for the purpose of showing specimen heights or thicknesses for selected specimen loadings during flat-plate calorimeter tests.

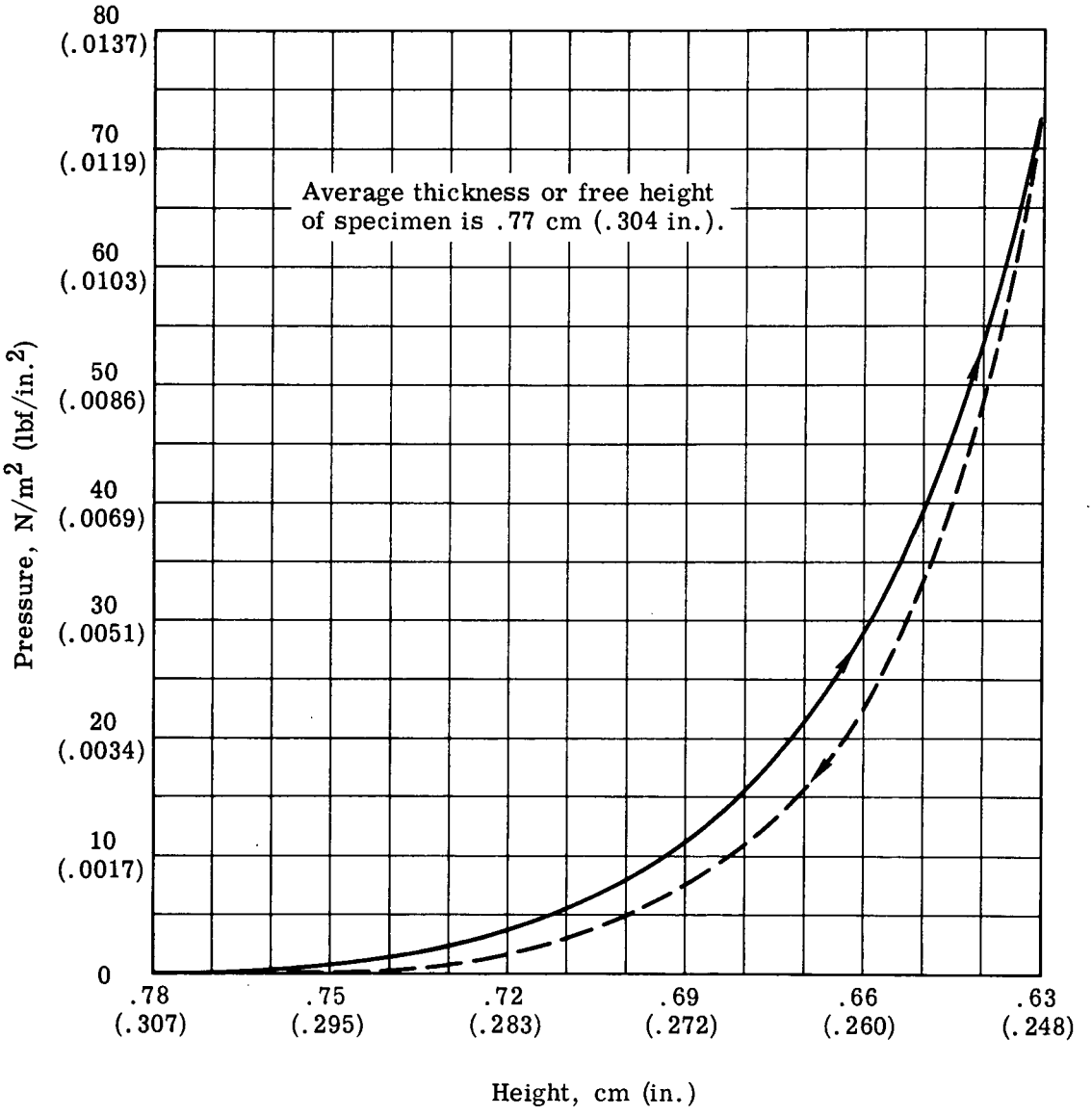

Figure 59. - Stress-strain curve - flat-plate calorimeter test specimen VL-99.

b. Calorimeter Data Reduction - Method of Analysis. The method of analysis used to determine the thermal conductivity of the flat-plate calorimeter specimen is discussed in the following paragraphs.

(1) Heat Flux Through Insulation. In order to determine the thermal conductivity of the insulation, the heat energy that penetrates the insulation must be known and is calculated by the following equation:

$$Q = \Delta h_c \, (\dot{W})$$

where Q is the heat energy

Δh_c is the change in cryogen enthalpy

$\dot{W}$ is the boil-off rate (one dimensional, through insulation only), which is calculated as

$$\dot{W} = \dot{W}_{corr} \pm \Delta\dot{W}_0 \pm \Delta\dot{W}_{edge} \pm \Delta\dot{W}_{storage}$$

where $\Delta\dot{W}_0$ is the zero heat leak, or calorimeter heat leaks

$\Delta\dot{W}_{edge}$ is the edge of the specimen heat leak, or two-dimensional effects

$\Delta\dot{W}_{storage}$ is the change in heat capacity of liquid cryogen due to variation in ullage pressure

The change in cryogen enthalpy (Δh_c) is merely the heat of vaporization of the particular fluid being used. This value of heat vaporization is determined at the pressure of the test measuring container, which is slightly higher than the ambient pressure. The sensible heating of the gas from vaporization temperature is not charged to the insulation, as this gas is heated externally by a liquid heat exchanger to raise the temperature to near ambient conditions.

(2) Corrected Boil-Off. The amount of the cryogen boiled off or evaporated is a direct measurement taken by a wet gas meter instrument. This instrument gives a reading in a volume per unit time and must be corrected for temperature and pressure. The corrections are as follows:

$$\dot{W}_{corr} = \dot{W}_{measured} \times \frac{T_{standard}}{T_{reading}} \times \frac{(P_{test} + \text{bubbler head})}{P_{standard}}$$

where the temperature readings are in absolute units. The value of P_{test} is set at the test site and is usually 78.74 cm (31.00 inches) of Hg, and the bubbler head is approximately 5.08 cm (2 inches) of water.

(3) Calorimeter Heat Leaks. The vent line is shorted by the guard vessel to minimize radiation and conduction heat transfer from ambient into the measuring vessel. The measuring vessel is separated from the guard vessel by an evacuated gap. In addition, the guard is held at a slightly higher pressure than the measuring vessel so that the measuring vessel boil-off gas will not recondense and also any heat transfer between vessels, although small, will result in an excess boil-off charged against the material being tested.

(4) Edge Heat Leak. One important aspect is the edge heat penetration or losses that must be added or subtracted to the boil-off heat rate. These losses or penetrations are minimized by reducing the diameter of the aluminized Mylar radiation shields. This reduction in diameter allows the exposed area to consist only of the insulating spacer (buffer zone), which is normally a low conducting material. A cold band is also used around the exposed area to reduce the external heat penetration. Various testing procedures were conducted previously and comparisons made where a cold band was used or not used, where radiation shields had a smaller diameter, etc. It was found that the reduced diameter and cold band down was the most efficient method of testing. For high ratios of lateral to normal thermal conductivity and excessive specimen thickness, an edge heat leak correction factor would have to be made using a steady-state, two-dimensional heat transfer computer program. These two factors must be considered together. The lateral to normal thermal conductivity ratio is in the range of 10 percent or less for the test specimens evaluated on this program. The uncertainty for input data needed to evaluate a correction factor could be greater than this.

(5) Heat Storage Capacity. Another consideration is the barometric pressure variations that can alter the boil-off rate. A variation in the heat energy should be accounted for due to sensible heating of the liquid or increased boil-off due to changes in the boiling point caused by this pressure variation. This condition has been minimized by using the mercury bubbler or damper and letting the system reach an equilibrium condition before any data is taken.

(6) Thermal Conductivity. The thermal conductivity is then calculated by the equation:

$$K = \frac{Qx}{A\,(\Delta T)}$$

where K is the thermal conductivity

Q/A is the heat flux per unit area

x is the thickness of insulation

ΔT is the temperature difference (temperature of hot surface - cryogen boiling point)

c. Test Results. The results of the flat-plate calorimeter test are plotted in Figure 60 for test specimen VL-99. The performance curve for GAC-9 test specimen VL-87 is included for comparison. The test was conducted primarily to determine the insulation thickness where minimum boil-off or heat leakage rate occurred. Various gaps between the hot and cold plates of the calorimeter were used for test points, and these are plotted as a function of heat leakage rate in Figure 60. A U-shaped curve was obtained, which is to be expected when plotted in this form. With a large gap, the heat leakage rate is high because of radiation energy penetration from the sidewalls. As the gap is decreased, the boil-off decreases to a minimum where all radiation from external sources is eliminated and all the heat energy transferred must pass through the insulation, neglecting side effects. The point where no radiation energy is present and the mechanical pressure on the insulation is negligible or practically zero should be the point of minimum heat leakage. As the pressure is increased, the heat leakage rate increases due to the increase in the contact pressure between the foam spacers and radiation shields. Previous work and tests have shown that the mechanical pressure on a multilayer type of insulation has considerable effect on the insulation performance. The values of mechanical loading on the insulation are also shown in Figure 60. The minimum thermal conductivity for specimen VL-99 was 3.90×10^{-5} J/m-s-^{o}K (2.27×10^{-5} Btu/hr-ft-^{o}F) at 0.71 cm (0.28 inch) of thickness.

d. Conclusions. A comparison of the performance between the perforated (VL-99) and unperforated (VL-87) specimens can be made from the results plotted in Figure 60. Approximately, a 50 percent degradation was noted for specimen VL-99. Minimum thermal conductivity also occurs at a smaller thickness. The test results are as expected where the thermal conductivity was increased as the effective emissivity of the radiation shields increased and in turn increased the heat losses. During fabrication of the test specimen, layup of the perforated Mylar produced a smoother (wrinkle-free) surface than previously experienced with unperforated Mylar radiation shields. Therefore, a decrease in specimen thickness occurred as expected due to the higher density ratio obtained with perforated Mylar film.

F. FEASIBILITY OF DROP THREAD MECHANIZATION

To implement a continuing improvement of fabrication and assembly techniques, an investigation was conducted to determine the feasibility of installing GAC-9 insulation drop threads by mechanical methods.

The primary function of drop threads in the GAC-9 panelized multilayer insulation is to hold the layers of the panel together during panel trimming and handling operations. When panels are installed on a tank, the panel grid facings, joined by panel-to-panel lacing, become

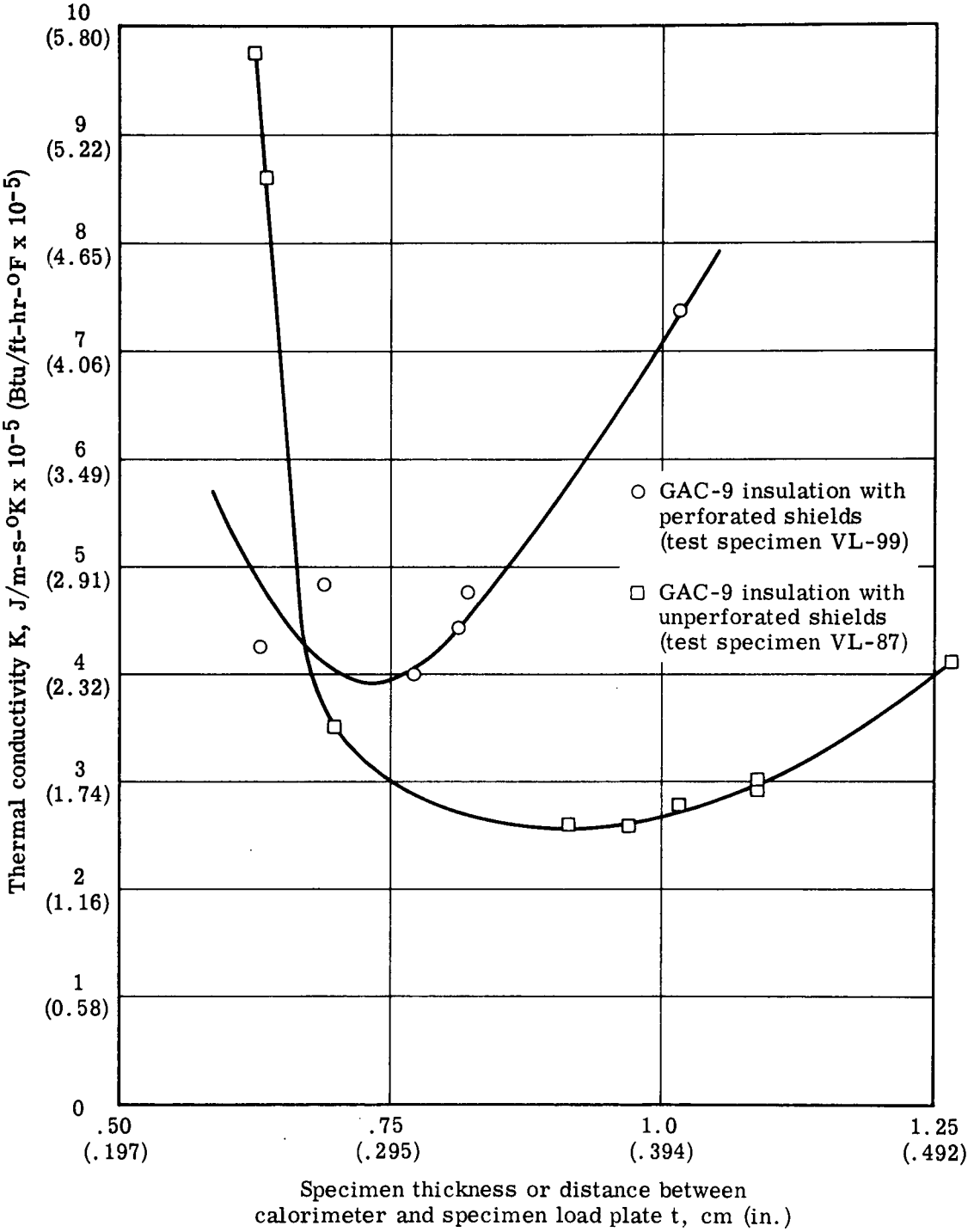

Figure 60. - Thermal conductivity versus thickness - flat-plate calorimeter test specimen VL-99.

the lightweight structure holding the panels together, and the role of drop threads is of lesser structural importance to resist interlaminar movement of the shields and spacers.

The present drop thread design, which consists of a loop of light Dacron thread circling the grid strands on opposite faces of the panel, has been installed by hand-sewing methods on small to medium size GAC-9 insulation panels such as the existing 76-cm (30-inch) diameter calorimeter and 2.66-meter (105-inch) diameter tank panels. For large-scale panels adaptable to tanks up to 100 meters (33 feet) in diameter, it is recognized that mechanization of the drop thread installation or portions of the installation may be advantageous in terms of labor savings and quality control.

It is known that bearing pressures on the insulation degrade the insulation performance. Therefore, an important factor in the selection of the mechanical installation method is assurance that the bearing pressure in the vicinity of the drop threads will not exceed the 6.89 to 20.6 N/m^2 (0.001 to 0.003 $lbf/in.^2$) range after drop thread installation. Pressure on the insulation may be higher during drop thread installation provided that crushing or permanent deformation does not occur.

Other factors to be considered are listed below.

(1) The capability of the machine to install drop threads at intervals ranging from 3.8 to 20.3 cm (1.5 to 8 inches) and at drop thread strand spacing of 0.63 to 1.9 cm (0.25 to 0.75 inch).

(2) Ability to use lightweight Dacron strands or thread.

(3) Ability to tie off loops of drop thread.

(4) Insulation panel maximum and minimum size.

During this study, the devices investigated for mechanically sewing drop threads were commercial sewing machines and mattress manufacturing machinery.

The Singer Company Industrial Machine Division technical representatives studied the drop thread installation problem and concluded that drop thread installation in the GAC-9 insulation composite is not feasible with conventional sewing machines. The following reasons are cited:

(1) The interval of thread installation is too great.

(2) The low bearing pressure requirement is incompatible with the sewing machine technique, which depends upon thread tension to accomplish the sewing operation.

The Singer Model 12 W Jump Baister sewing machine was the only recommendation for the drop thread application. This type of sewing machine can program wide interval thread spacing by manual or automatic indexing the sewing operation. Undesirable features of the drop thread installation would be the task of tying the thread at each interval; therefore, the thread would span the insulation surface between drop thread intervals. Without tying, the drop thread tension becomes difficult to control to the desired low compressive load on the insulation. The Singer Company technical representatives felt that control of the drop thread tension would require an extensive investigation beyond the scope of this study and concurred that machinery used in the mattress industry may be more applicable to the drop thread installation.

Akron Mattress Company was consulted to discuss the feasibility of mechanically installing drop threads in GAC-9 insulation with the equipment used in installation of mattress tufting. It was concluded that the Mattress Lace Tufter Machine, manufactured by United Mattress Machine Company, Quincy, Massachusetts, offered the best possibility of installing drop threads in the GAC-9 insulation. The machine may be indexed to nearly any desired pattern or spacing of drop thread and is capable of sewing a loop of thread through 2.54-cm (1.0-inch) thick material and tying the loop on one side of the panel. Akron Mattress Company did not have this machine; however, one was located at Ideal Bedding Company in Cleveland, Ohio. During a visit to the latter company, several attempts were made to install tufting braid in a small sample of GAC-9 insulation to observe the action of the lace tufter machine on the 2.54-cm (1.0-inch) thick Mylar and foam insulation composite. The Model LT 280 United Lace Tufting Machine shown in Figure 61 and described in reference 6 was used for the demonstration. Because of the time involved, no attempt was made to change the machine setting for a loop height of 2.54 cm (1.0 inch). Consequently, the loop was large, as shown in Figure 62. Observations from this experiment are summarized below.

(1) At head setting No. 5, the compression foot to throat plate clearance was 2.54 cm (1.0 inch) and the braid was installed without crushing the composite. At setting No. 5-1/2, the composite was compressed approximately 0.318 cm (0.125 inch) but returned to its original thickness without crushing or permanent set. At lower head settings, some crushing damage occurred.

(2) The machine had no difficulty in penetrating the composite and tying the cord even though the loop height exceeded the thickness of the material.

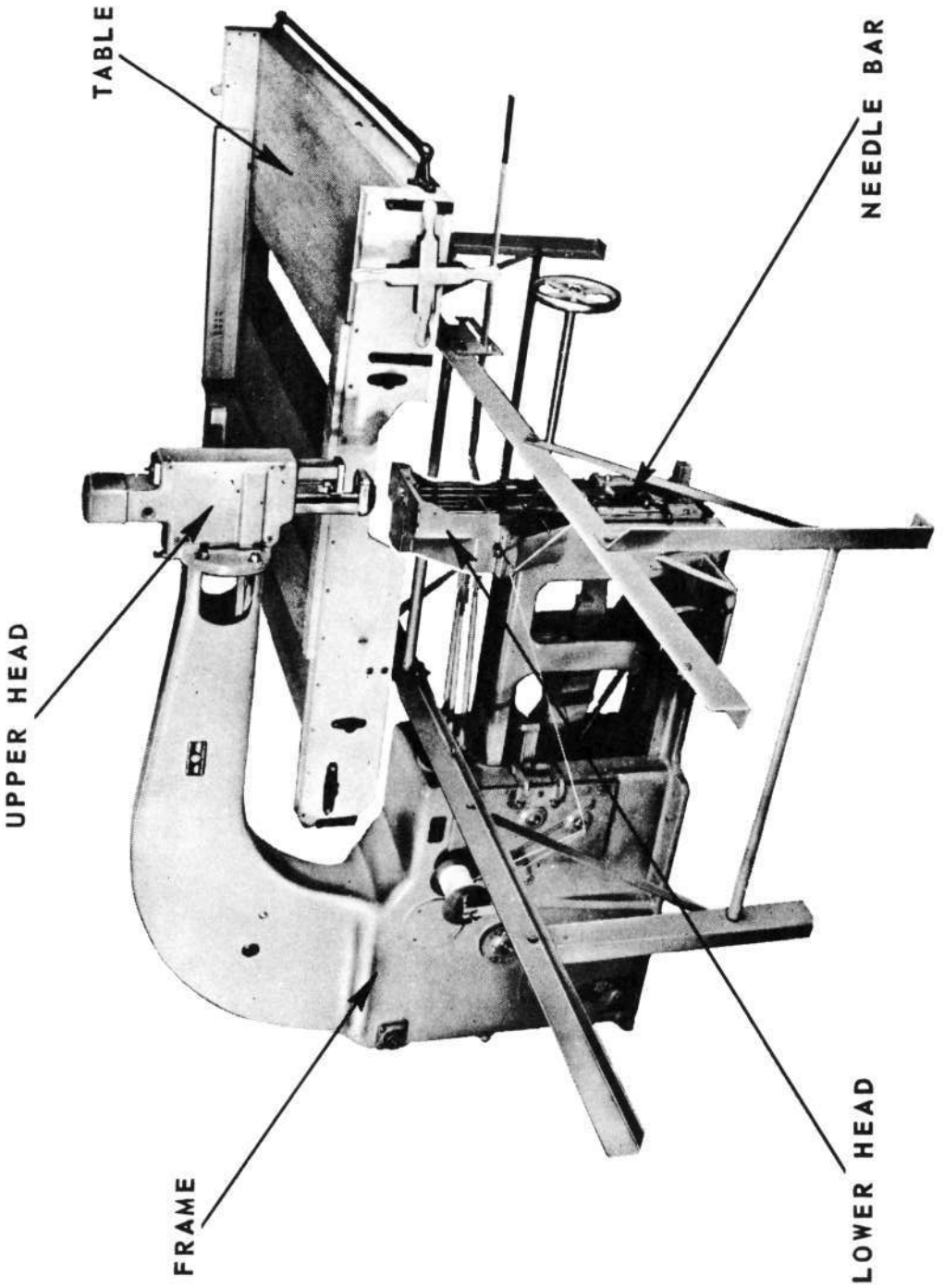

Figure 61. - United Lace Tufting Machine, Model LT 280.

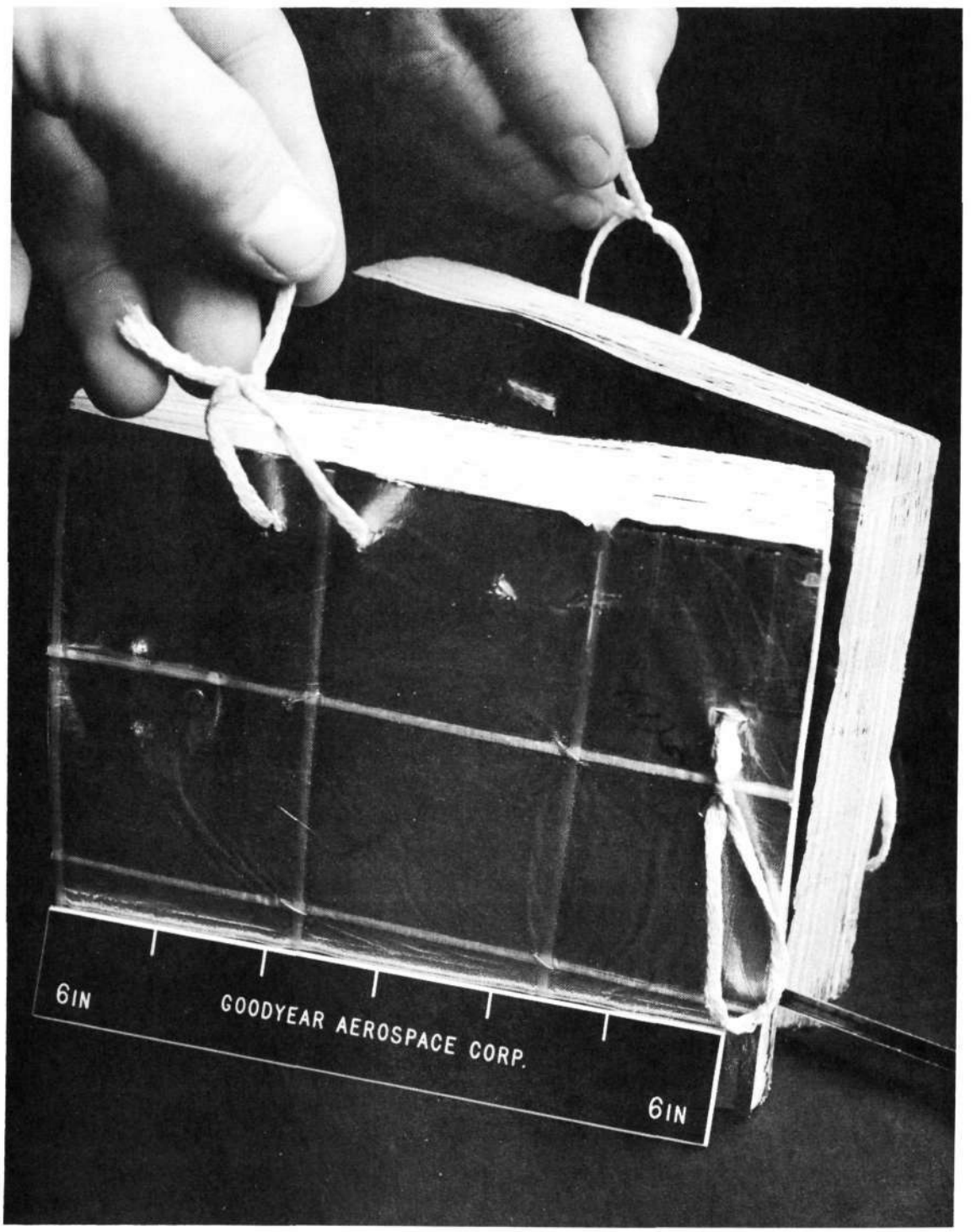

Figure 62. - GAC-9 insulation sample with loops of tufting braid installed during demonstration of Model LT 280 Tufting Machine.

(3) The needle holes in the insulation and the lacing braid were much heavier than desired; however, this was acceptable considering the preliminary nature of the experiment.

Based on the observations of the LT 280 machine, several changes would be necessary to adapt the machine for installation of satisfactory drop threads in the GAC-9 insulation composite. These changes are listed below in order of priority.

(1) Lighter cord should be used, preferably of Type 55 Dacron, 220 denier yarn or closest possible size compatible with machine. The lightest possible cord is necessary to reduce heat transfer across the insulation.

(2) The cord should be installed in a loop height equal to insulation thickness with the knots on one surface of the insulation. It is desirable that the knots be visible for inspection and cementing. The purpose of the cement is two-fold: to prevent the knot from loosening and to prevent the cord or thread from chafing on the hole.

(3) The needle holes in the insulation should be smaller. The present 0.475-cm (0.187-inch) diameter needles leave a pair of holes larger than desired in the insulation. If needles could be reduced to 0.238-cm (0.093-inch) diameter or smaller, the attendant smaller needle holes would be more acceptable. The large needle holes degrade the insulation performance by providing paths for radiation heat leak; therefore, smallest possible holes are desired.

(4) Closer spacing of needles would be desirable. The loop strands of current drop threads are installed 0.635 to 1.27 cm (0.250 to 0.50 inch) apart. It should be noted that the present drop threads straddle the 0.318-cm (0.125-inch) wide fiberglass grid strands on the insulation face sheets. The drop threads should be placed as close as practical to the edges of the strands.

Samples of GAC-9 insulation were sent to United Mattress Machine Company for experimental use to determine if the Lace Tufting Machine can be adapted to accommodate the above noted changes for installation of the lightweight drop threads currently in use.

After examination of the GAC-9 insulation samples and the modifications required to adapt the LT 280 machine as noted above, the United Mattress Machine development engineers suggested that the Cotton Tufter Machine is better adapted to handle the lightweight Dacron strands desired for the insulation drop threads. This machine, shown in Figure 63 and described in reference 7, ties a drop thread loop having two strands on one leg and one strand on

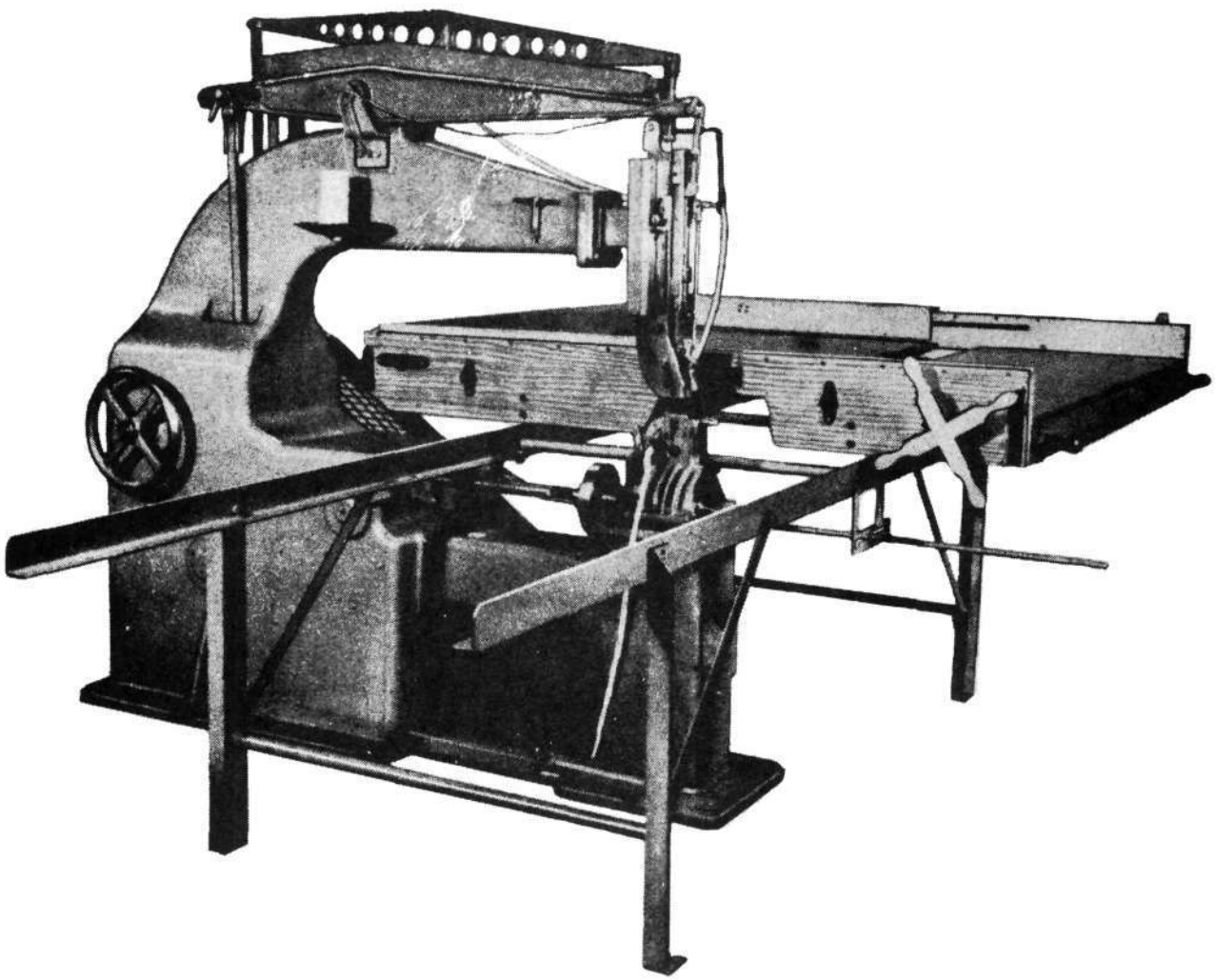

Figure 63. - United Mattress Machinery Company Cotton Tufter Machine.

the other leg. The extra strand on one leg is not objectionable if the machine can handle strands significantly smaller than the minimum size tufting braid installed with the Lace Tufter Machine.

A meeting was held at the United Mattress Machinery Company to further discuss the drop thread installation problems and to demonstrate the action of the Cotton Tufter Machine on the GAC-9 insulation samples. This machine utilized a cotton cord that is heavy compared to the GAC-9 insulation drop threads; however, the cord is lighter than the tufting braid previously demonstrated with the LT 280 machine.

Observations from this demonstration are summarized below.

(1) The machine head settings are very similar to the LT 280 machine.

(2) The machine had no difficulty in penetrating the insulation and tying the cord, as shown in Figure 64. The machine makes a weaver's knot, which depends upon cord tension to tie the knot. The cord tension produced an undesirable compression of the insulation.

(3) The machine has a single needle that must index and penetrate the insulation two times before tying the knot. As the knot is tied, the cord tension draws the loop tight and distorts the insulation inside the loop. By contrast, the Model LT 280 Lace Tufter Machine has two needles that penetrate the insulation and hold the loop at the needle spacing as the knot is made without distorting the insulation.

(4) The needle holes in the insulation were much larger than desired, and the holes were further elongated by the cord tension to cause a severe light leak through the thickness of the insulation sample. Considering the nature of the demonstration, the large needle holes would be acceptable, but the extra elongation of the holes caused by cord tension is not acceptable.

(5) An attempt was made to hold the loop at the needle spacing by placing metal strips on both sides of the insulation and tying the loop over these strips. The strips are then removed. The experiment was fairly successful because the loop did not elongate the needle holes and the insulation distortion was reduced. Also, the cord tension was relieved due to the extra length gained by the thickness of the metal strips. It was apparent from this experiment that the machine would require the addition of a device to simulate the action of the metal strips.

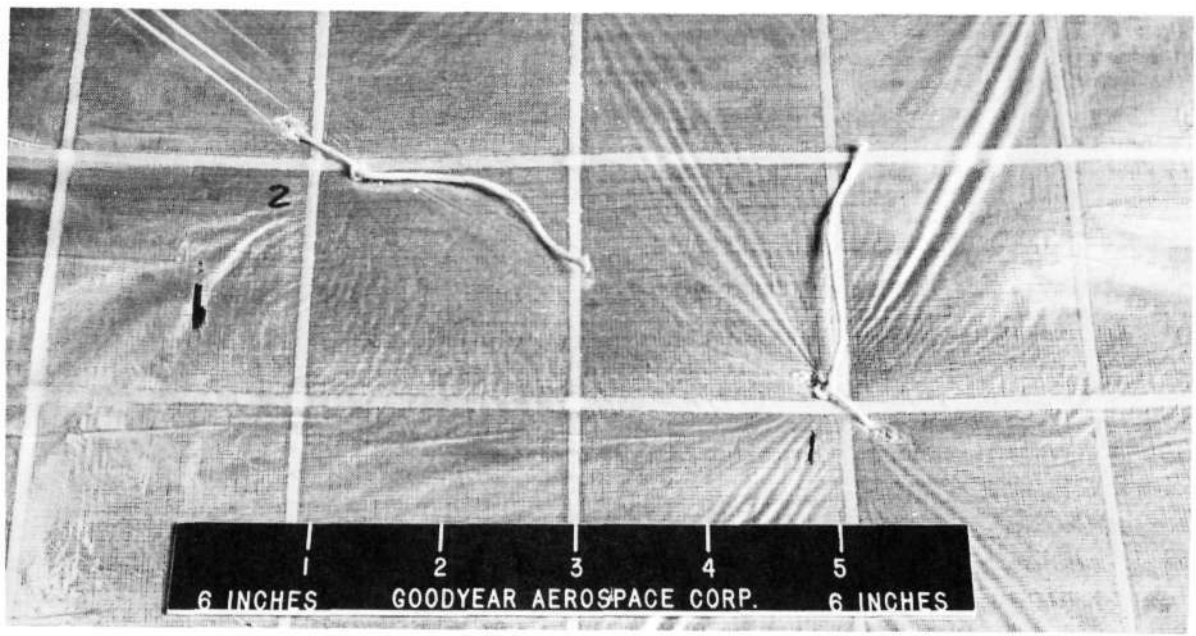

A. Top side of panel showing knot on loop

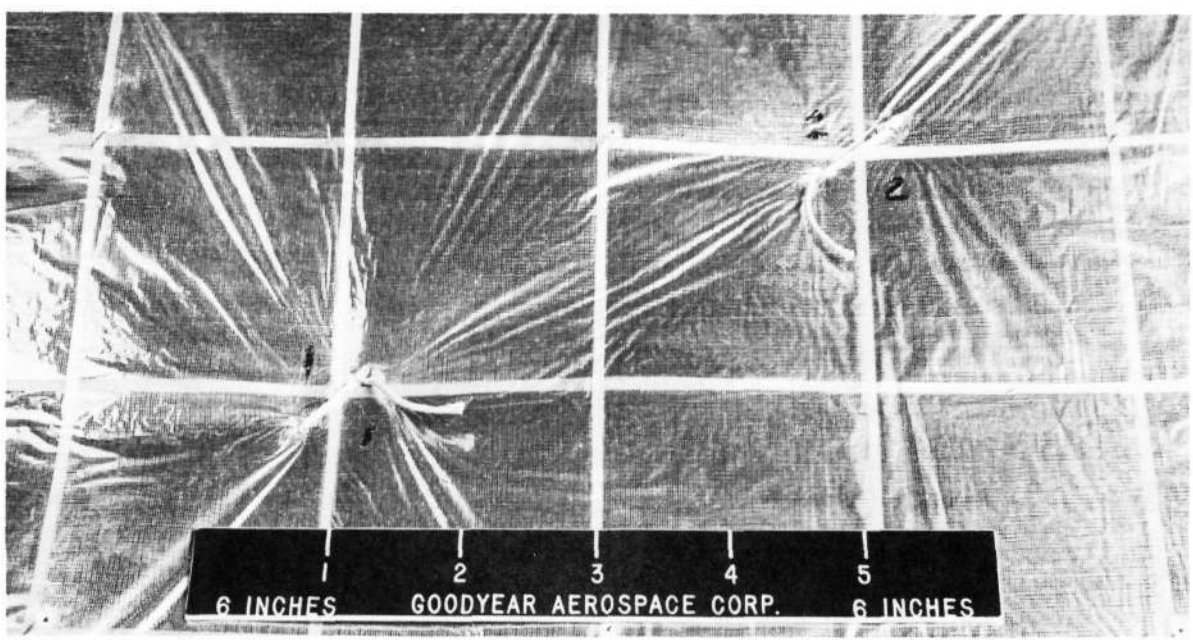

B. Bottom side of panel showing second strand of loop extending from insulation

Figure 64. - GAC-9 insulation sample with loops of cord installed during demonstration of Cotton Tufter Machine.

From the demonstrations of the Cotton Tufter Machine and the Lace Tufter Machine it was concluded that the Lace Tufter Machine would be the best choice for the drop thread installation because the basic principle of this machine will avoid compressing the insulation by tying a bowline knot without tensioning the drop thread loop.

The United Mattress Machine Company development engineers were confident that the Model LT 280 type of machine could be constructed to mechanically drop thread tie GAC-9 or like insulation material.

Although the principle of tying a mattress and GAC-9 insulation are alike, the machine parts will have to be reduced in size by nearly 50 percent. Also, the adjustment for controlling the compression and length of tie will need refining to meet the compression requirement. A complete new design expressly for laminated insulation tying is recommended. The design would incorporate the following changes:

(1) The needle size would be reduced from 0.475-cm (0.187-inch) to 0.24-cm (0.093-inch) diameter to reduce the hole size in the insulation. The smaller needle size was hand-demonstrated and produced an acceptable hole in the GAC-9 insulation. The hole, although large for the drop thread, was small enough to contract to a very small size after needle withdrawal.

(2) The distance between needles would be reduced to a maximum of 1.27 cm (0.50 inch).

(3) The loop mechanism would be redesigned as required to handle the 220-denier Dacron thread currently in use on GAC-9 insulation. Similar threads of other materials could also be used.

(4) The length of needle stroke would be limited to 1.27 to 5.08 cm (0.50 to 2.00 inches). This may be greater if decided before the machine design is started.

An indexing table can be supplied that will position the drop threads in any desired pattern on GAC-9 insulation panels. The panels may be flat, single curved, or compound curved. The indexing may be accomplished manually or automatically.

It is estimated that the machine and indexing table could work at a rate of twenty ties per minute. A device known as a "tie detector" may be incorporated that shuts off the machine if a tie fails to form properly.

A rough estimate of the cost to design and manufacture a prototype drop thread tying machine and indexing table, for flat work only, would be in the $50,000 to $100,000 range.

SECTION IV

SUBSCALE TANK TESTS OF GAC-9 INSULATION PURGE AND VENT SYSTEM

A. GENERAL

One dimensional and two dimensional purge gas flow characteristics of GAC-9 insulation have been measured on small scale laboratory test specimens as discussed in Section III of this report. The engineering numbers determined by these tests are to be used in design/analysis of a GAC-9 insulation system. To verify the application and usefulness of these numbers, a purge system was designed for the existing GAC-9 insulation on the 76-cm (30-inch) diameter cylindrical calorimeter. The purge system performance was evaluated under simulated ground-hold and ascent pressure decay test conditions. Purge performance was measured in terms of purge gas flow, volume and time required to reach a high level of helium purity at the purge system outlet. The venting capability was determined from thermal performance of the GAC-9 insulation measured as a function of liquid hydrogen boil-off.

The cylindrical calorimeter (see Figure 65) consists of three separate chambers: upper guard vessel, center measuring vessel, and lower guard vessel. All components are fabricated from Type 304L stainless steel. The three chambers are separated by a gap of approximately 0.38 inch. The fill and vent tubes of the calorimeter are of a double-wall construction and are vacuum-jacketed to minimize heat transfer between any of the liquid-filled chambers and boil-off gas from the lower chambers.

B. DESIGN AND FABRICATION OF PURGE SYSTEM AND PRESSURE SENSING INSTRUMENTATION ON 76-CM (30-INCH) DIAMETER CYLINDRICAL CALORIMETER

1. Purge System

Considering the period of performance of this program, it was important that the purge system be designed for direct application to an existing GAC-9 insulation system on the 76-cm (30-inch) diameter cylindrical calorimeter. For this reason GAC has selected the GAC-9 insulation panel arrangement shown on Figure 66 for evaluation of the purge system. The insulation consists of two layers of 2.54-cm (one-inch) thick GAC-9 insulation panels with each layer configured in two half-shell panels butt-joined along an axial split line. To minimize heat leaks at the joints, the outer panel joints are rotated 1.57 radians (90 degrees) from the inner panel joints.

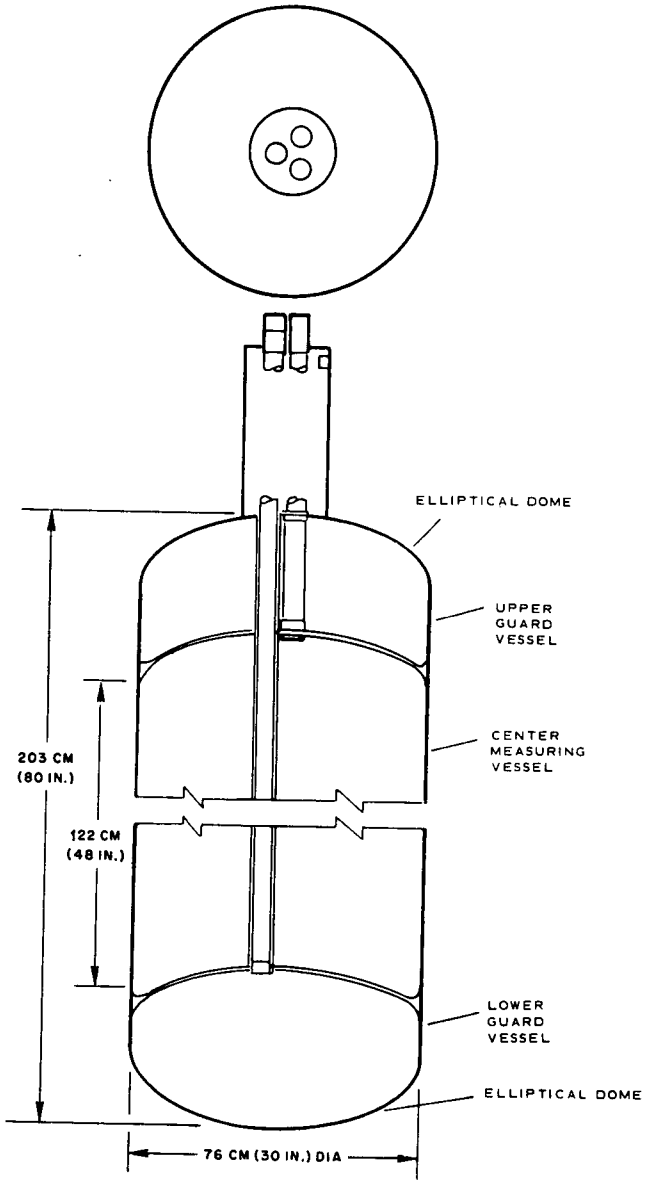

Figure 65. - 76-cm (30-in.) diameter cylindrical calorimeter.

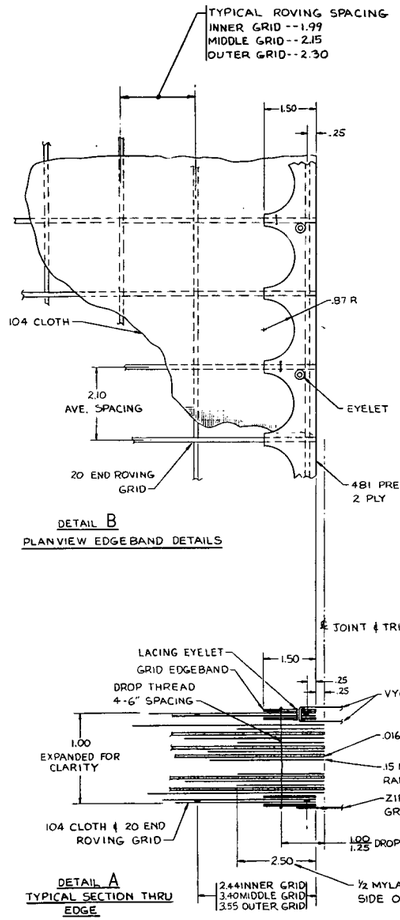

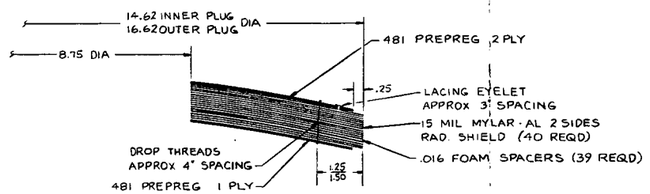

DETAIL G
MULTILAYER INSULATION PLUG
SECTION SCHEMATIC

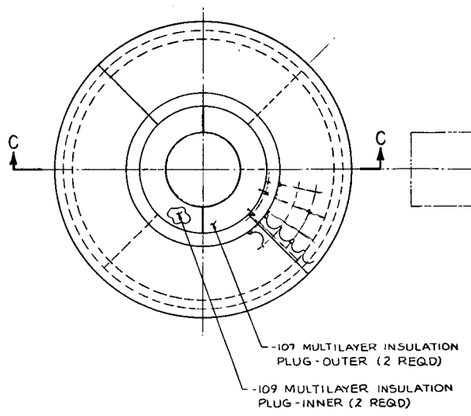

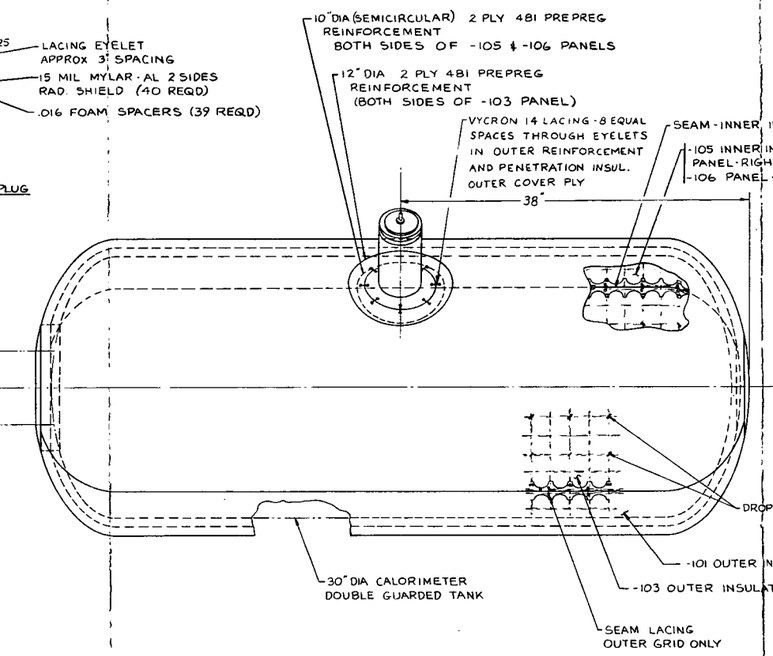

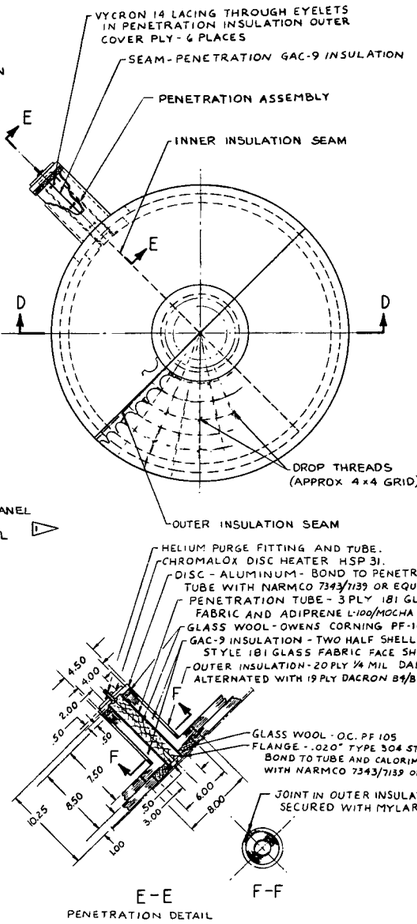

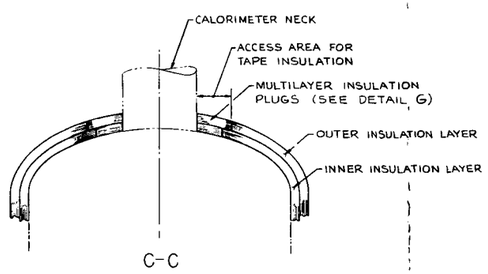

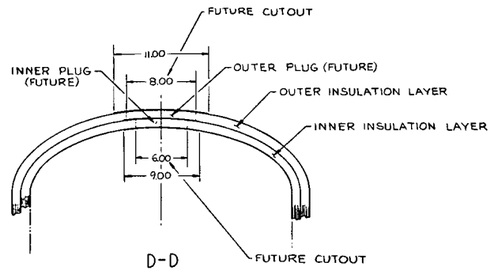

NOTE:
1 ASSEMBLE PANELS PER GAC PROCESS SPEC. GER 13308.

Figure 66. - 76-cm (30-in.) diameter cylindrical calorimeter insulation.

FOLDOUT FRAME - 1

FOLDOUT FRAME - 2

At the top or neck end, the insulation panels terminate at an annular gap around the calorimeter neck. The gap provides access to panel joint zipper fasteners and is also a convenient area for purge system helium inlet.

The bottom dome area of the insulation panels have provisions for cutouts as shown in Section D-D of Figure 66. These provisions include a grid edgeband configured for a circular cutout and the joint zipper fasteners terminating short of the cutout diameter to prevent damage to the zipper when cutouts are made. The cutout diameters were selected to approximately simulate manhole-to-tank diameters ratio for existing NASA test tanks. The cutout provisions are utilized in this program to provide a purge system helium outlet plenum.

The measuring vessel area of the insulation panels have included accommodations for addition of a simulated tank penetration configured as a tube extending radially from the tank wall as shown in Section E-E of Figure 66. The fiberglass grids on the inner and outer insulation panels include the proper edge band configuration for future penetration cutouts. The penetration and related insulation is discussed in subsection 3 of this portion of the report.

The purge system for the GAC-9 insulation panels on the cylindrical calorimeter is a flow-through type which is designed to flow helium through the insulation to purge out the air and maintain a helium environment under a slight positive pressure while tanking with liquid hydrogen. The helium purge system shown in GAC drawing 70QS1727 (Figure 67), is comprised of (1) a flexible helium purge jacket surrounding the calorimeter, (2) an inlet plenum chamber directing the helium purge gas into the top edge of the insulation panels at the base of the neck on the calorimeter, (3) a purge gas outlet plenum at the bottom dome of the insulation and (4) purge gas outlet lines from the outlet plenum and the purge jacket.

A nominal purging time of two hours was selected for the cylindrical calorimeter purge and vent tests. From the three-dimensional computer analysis and purging tests conducted on the 94 cm x 122 cm (3 ft x 4 ft) GAC-9 insulation test panel, calculations show that ten volumetric changes will insure sufficient gas purging to obtain an excess of 95% helium in the insulation residual gases. The purge volume of the insulation and purge jacket is approximately 0.344 m^3 (120 ft^3). To provide the 10 volume changes over a two hour period the flow rate is computed by the following equation:

$$q = \frac{10\ V}{t}$$

where q = flow rate - m^3/s

V = volume - m^3

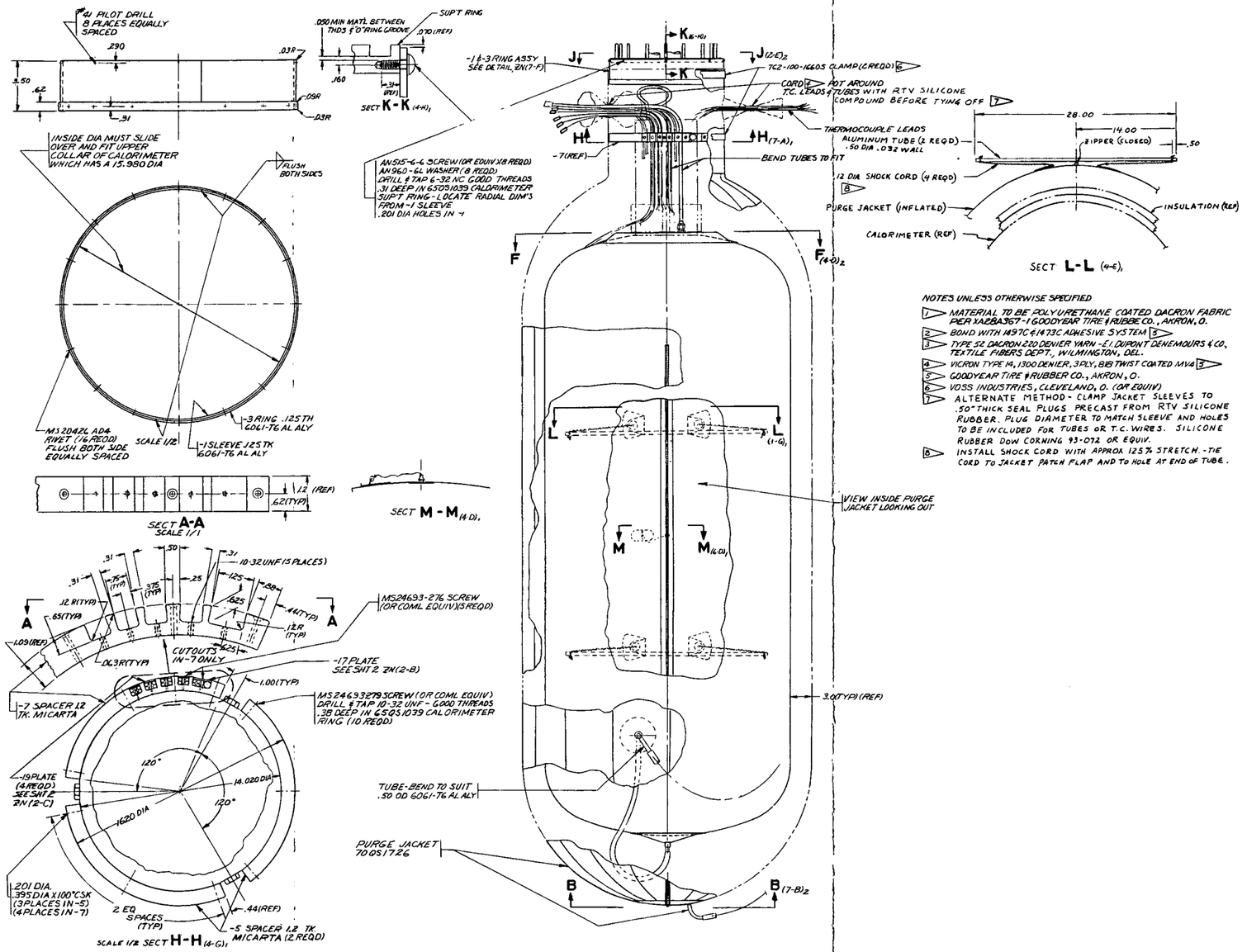

NOTES UNLESS OTHERWISE SPECIFIED

1. MATERIAL TO BE POLYURETHANE COATED DACRON FABRIC PER XA2BA367-1 GOODYEAR TIRE & RUBBER CO., AKRON, O.
2. BOND WITH H97C & H73C ADHESIVE SYSTEM 3
3. TYPE 52 DACRON 220 DENIER YARN - E.I. DUPONT DENEMOURS & CO. TEXTILE FIBERS DEPT., WILMINGTON, DEL.
4. VICRON TYPE 14, 1300 DENIER, 3 PLY, B/B TWIST COATED MV4 3
5. GOODYEAR TIRE & RUBBER CO., AKRON, O.
6. VOSS INDUSTRIES, CLEVELAND, O. (OR EQUIV)
7. ALTERNATE METHOD - CLAMP JACKET SLEEVES TO .50" THICK SEAL PLUGS PRECAST FROM RTV SILICONE RUBBER. PLUG DIAMETER TO MATCH SLEEVE AND HOLES TO BE INCLUDED FOR TUBES OR T.C. WIRES. SILICONE RUBBER DOW CORNING 93-072 OR EQUIV.
8. INSTALL SHOCK CORD WITH APPROX 125% STRETCH. - TIE CORD TO JACKET PATCH FLAP AND TO HOLE AT END OF TUBE.

Figure 67. - Purge jacket installation on the cylindrical calorimeter, GAC-9 insulation. (Sheet 1 of 2)

FOLDOUT FRAME -1

FOLDOUT FRAME -2

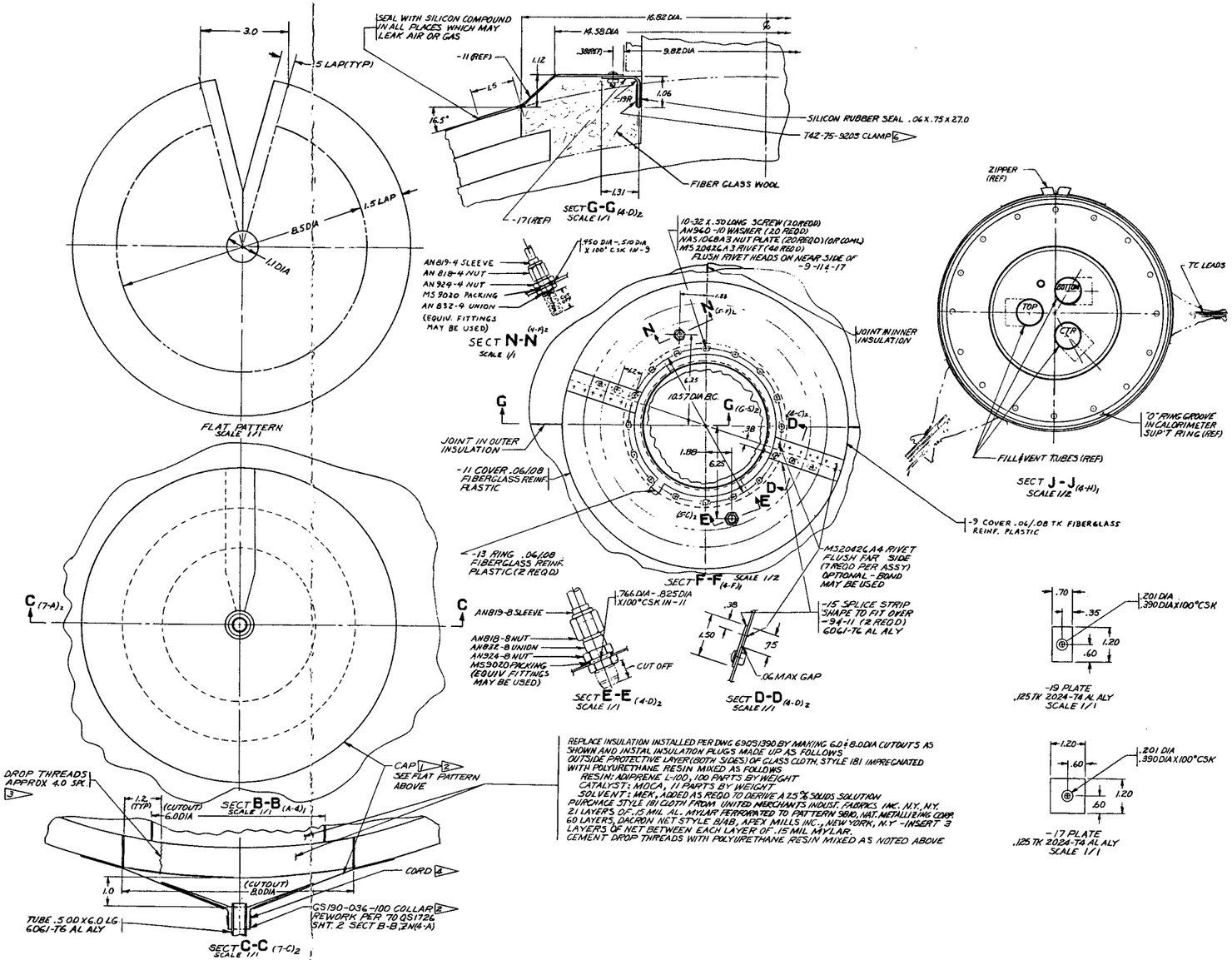

Figure 67. - Purge jacket installation on the cylindrical calorimeter, GAC-9 insulation. (Sheet 2 of 2)

FOLDOUT FRAME -1

FOLDOUT FRAME-2

t = time - s

or $q = \frac{10 \times 0.344}{7.2 \times 10^3}$

$q = 4.77 \times 10^{-4}$ m^3/s (1.0 ft^3/min)

The pressure drop requirements to insure this flow rate can be determined by the following equations:

$$p = \frac{q\,L}{C_H A_c}$$

where p = pressure drop - N/m^2

q = flow rate - m^3/s

L = length - m

C_H = flow coefficient = $\frac{m^5}{s\text{-}m}$

A_c = crossectional area - m^2

or $p = \frac{4.77 \times 10^{-4} \times 1.778}{1.58 \times 10^{-4} \times 0.0765}$

p = 70.2 N/m^2 (0.28 inches H_2O)

It is desirable to keep the purge gas inlet flow rate and pressure at a low level to prevent internal pressure loading that would separate the inlet plenum from the insulation.

The inlet plenum is designed to distribute the purge gas to the exposed edges of the GAC-9 insulation panels. The plenum cover, detailed on section F-F of Figure 67, is a two-piece construction to permit installation around the calorimeter neck. The inboard edge of the cover is bolted to a curved angle which is clamped and sealed to the calorimeter neck. The outboard edge of the cover rests on the top insulation panel and is sealed to the panel with Dow Corning 93-072 RTV silicone rubber. The plenum cover and curved angle are fiberglass laminates to reduce the heat transfer between the outer insulation panel and the calorimeter neck. The plenum cover with helium inlet and pressure measurement lines attached to the cover are shown in Figures 68 and 69. The calorimeter neck, with a measured temperature of 66°K (-340°F), is a heat sink for the adjacent insulation panels. To alleviate the neck heat sink problem, the annular space between the edges of the insulation panels and the calorimeter

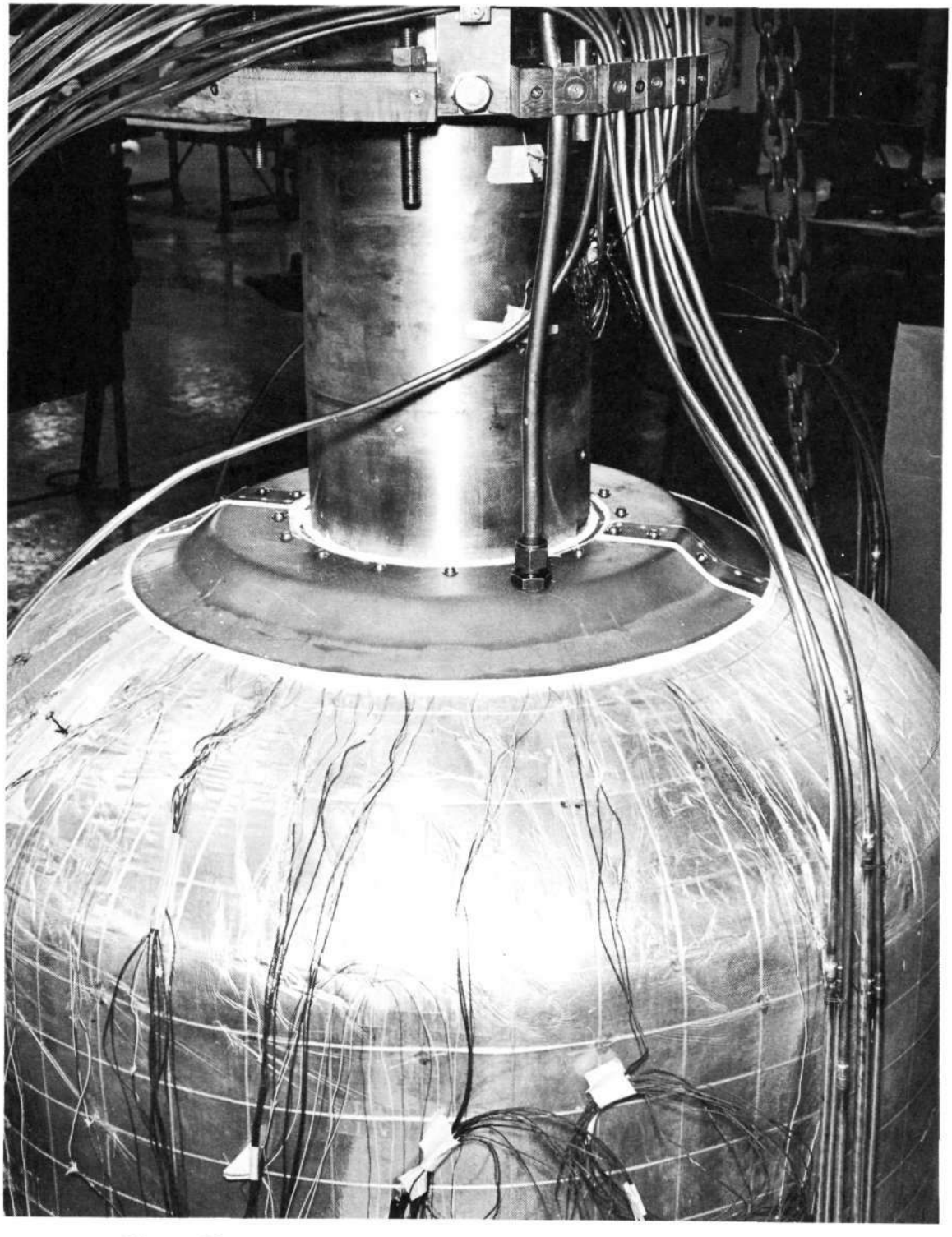

Figure 68. - Cylindrical calorimeter GAC-9 insulation purge gas inlet plenum chamber showing purge gas supply line.

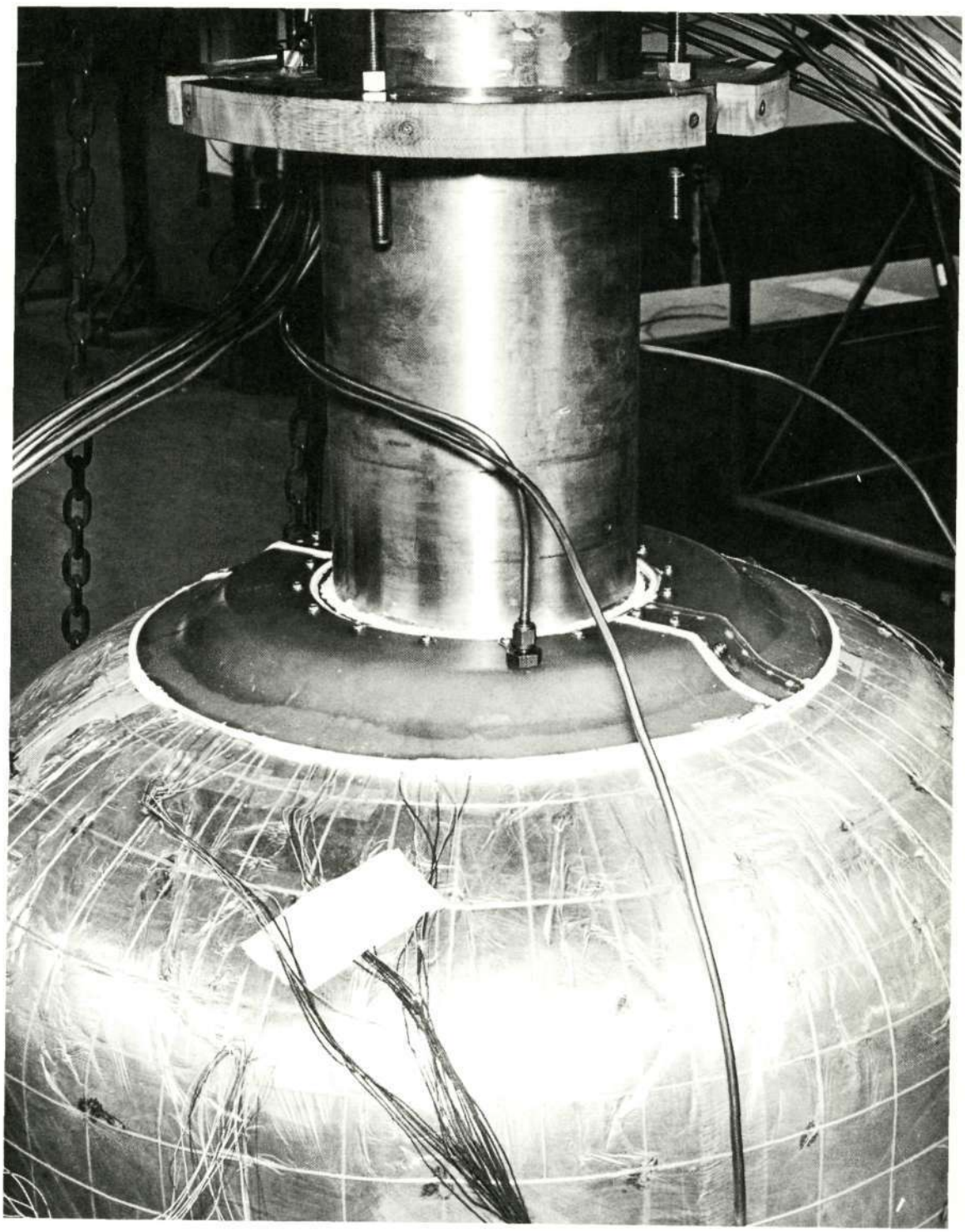

Figure 69. - Cylindrical calorimeter GAC-9 insulation purge gas inlet plenum chamber showing plenum pressure tap.

neck is filled with Owens-Corning PF105-500 fiberglass wool to provide an opacifying media having low impedence to purge gas flow.

To provide a purge gas outlet, the bottom polar cap region of the calorimeter insulation panels are modified by cutouts in the GAC-9 insulation and addition of 15.2-cm (6-inch) and 20.3-cm (8-inch) diameter polar cap plugs as shown in section B-B of Figure 67, and Figure 70. The plugs, designed for easy broadside venting of the purge gas into an outlet plenum, are each sized to have an area at least 1.5 times the perimeter area of the cutout in calorimeter insulation and are constructed of perforated aluminized Mylar radiation shields and Dacron net spacers. The outlet plenum, fitted over the polar cap plugs, as shown in Figure 71, is constructed from urethane coated Dacron fabric. The plenum outlet tube is connected to a helium gas purity meter to monitor the percent helium in the gas emerging from the polar cap plugs during the purging operation. The purge gas escaping from the calorimeter insulation joints is collected in the purge jacket and exhausted through the purge gas vent line.

Results of the 94 x 122 cm (37 x 48 inch) panel flow tests reported in section III show that substantial purge gas leakage could be expected from the calorimeter insulation panel joints in the top dome region near the inlet plenum. To improve the purge system effectiveness, the insulation panel joints in the top dome region were covered with Mylar tape to prevent gas losses before diffusing into the cylinder section of the insulation.

The purge jacket design is shown in GAC drawing 70AS1726 (Figure 72). The jacket design is based on previous purge jackets designed and/or fabricated for the NASA/MSFC 1.77 m (70-in.) diameter tank, the strut-supported 2.66 m (105-in.) diameter tank, and the cone-supported 2.66 m (105-in.) diameter tank. Pertinent design features are as follows:

(1) The jacket has a minimum of three-inch radial clearance with the GAC-9 insulation on the 76-cm (30-in.) diameter calorimeter.

(2) To permit easy installation and removal of the purge jacket from the insulated calorimeter, the jacket is split along a meridional seam the full length along one side and extending approximately 75% the length of the opposite side to form two halves joined by a single leak-tight zipper fastener. Each half is comprised of eight gore segments made up of urethane elastomer coated Dacron fabric having warp and fill fibers aligned with principal stresses.

(3) The jacket material is The Goodyear Tire & Rubber Co. Code V328A100 urethane-coated dacron fabric having a low helium gas permeability rate of

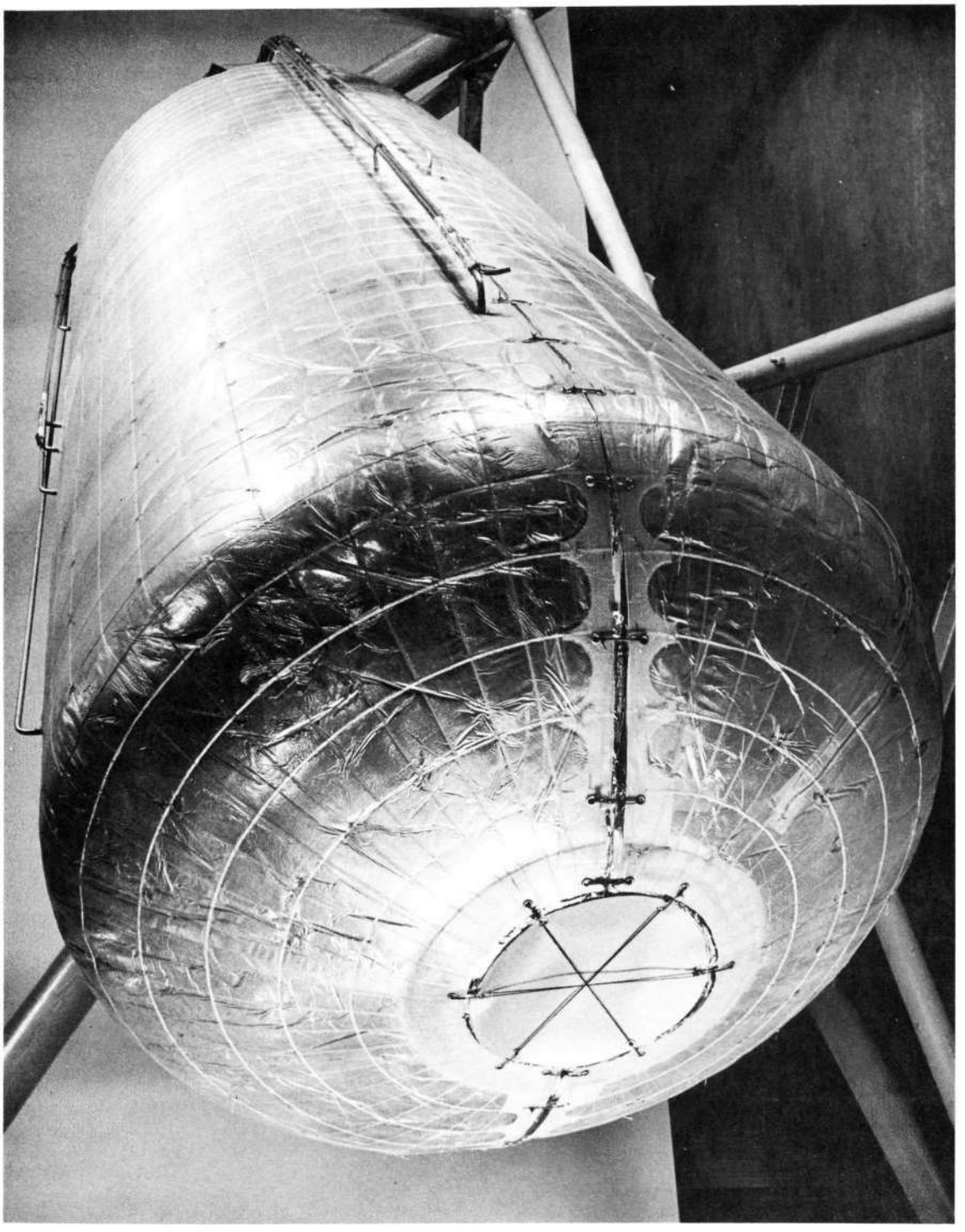

Figure 70. - Cylindrical calorimeter with GAC-9 insulation outer panels viewed from bottom dome showing polar cap plugs, pressure taps, and tubing.

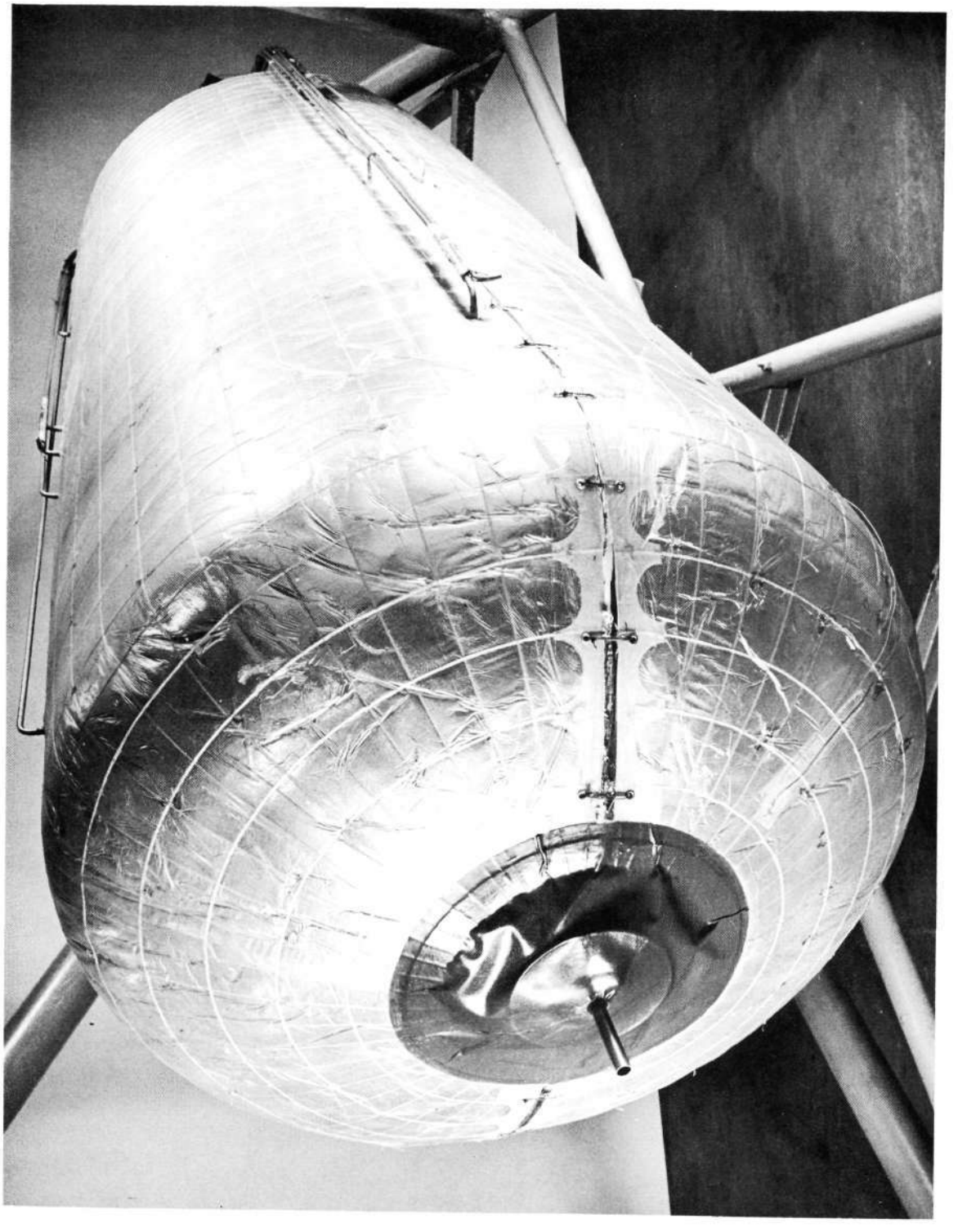

Figure 71. - Cylindrical calorimeter with GAC-9 insulation outer panels showing purge gas outlet plenum in bottom polar cap region.

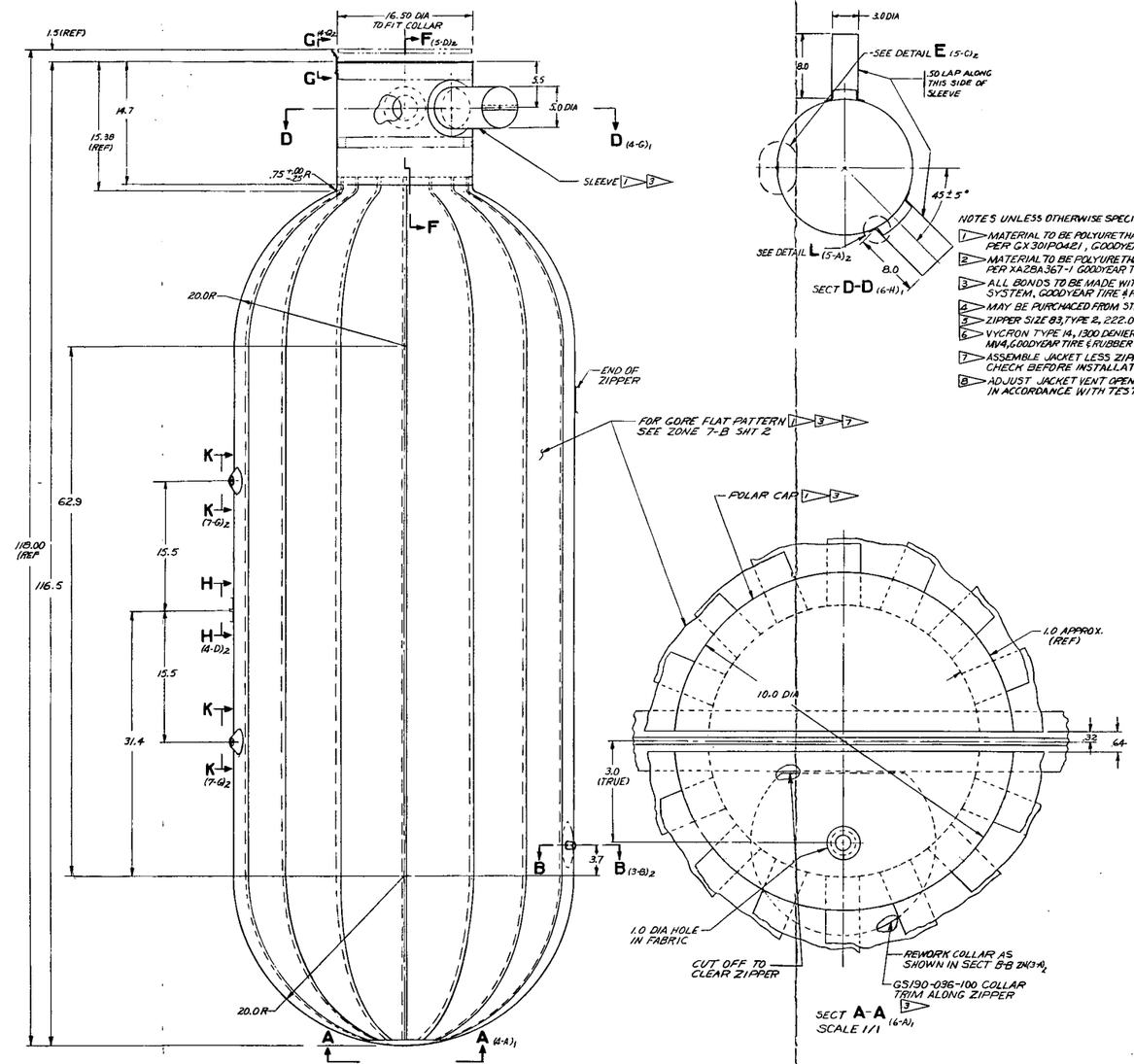

NOTES UNLESS OTHERWISE SPECIFIED

1. MATERIAL TO BE POLYURETHANE COATED DACRON FABRIC PER GX301P0421, GOODYEAR AEROSPACE CORP, AKRON, O.
2. MATERIAL TO BE POLYURETHANE COATED DACRON FABRIC PER XA28A367-1 GOODYEAR TIRE & RUBBER CO., AKRON, O.
3. ALL BONDS TO BE MADE WITH H97C & 1473C ADHESIVE SYSTEM, GOODYEAR TIRE & RUBBER CO., AKRON, O.
4. MAY BE PURCHACED FROM STIMPSON CO. INC., BROOKLYN, N.Y.
5. ZIPPER SIZE 83, TYPE 2, 222.0 LONG, TALON INC., MEADVILLE, PA.
6. VYCRON TYPE 14, 1300 DENIER, 3PLY, 8/8 TWIST COATED WITH MV4, GOODYEAR TIRE & RUBBER CO. (TEXTILE & RESERCH) AKRON, O.
7. ASSEMBLE JACKET LESS ZIPPER, INFLATE AND DIMENSION CHECK BEFORE INSTALLATION OF ZIPPER
8. ADJUST JACKET VENT OPENING PRESSURE TO .5 ± .05 PSI IN ACCORDANCE WITH TEST PLAN

Figure 72. - Purge jacket for the cylindrical calorimeter - GAC-9 insulation. (Sheet 1 of 2)

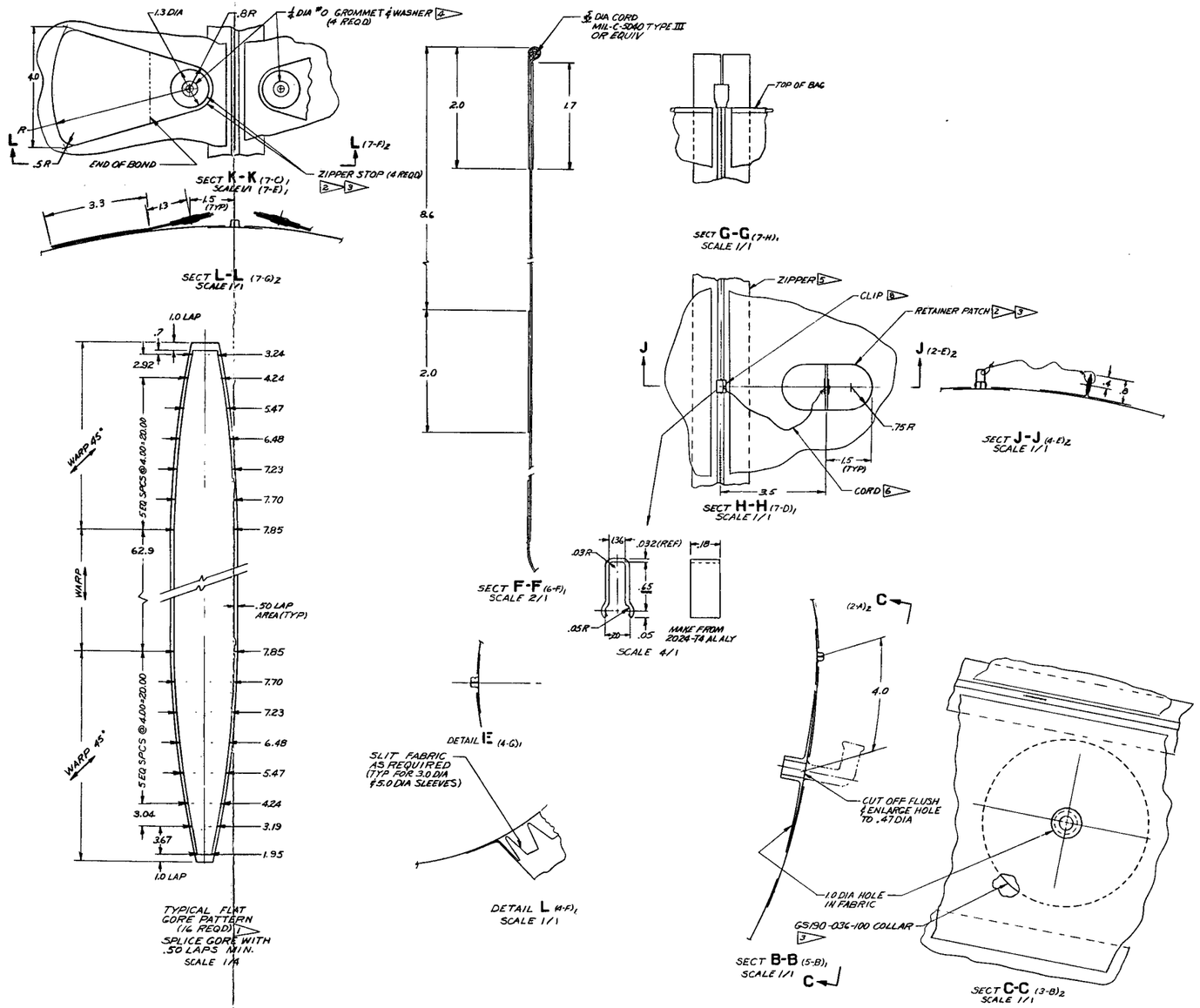

Figure 72. - Purge jacket for the cylindrical calorimeter - GAC-9 insulation. (Sheet 2 of 2)

less than 1 liter/square meter/24 hours at 3 cm H_2O pressure. The fabric weighs 0.16 kg/m^2 (4.7 oz/yd^2) and has a strength of 7.9 N/cm (45 pounds/in.) in the warp and 9.6 N/cm (55 pounds/in.) in the fill direction. At the maximum pressure loading, a 3.5 margin of safety is predicted for this jacket material.

(4) A Talon OEM leak-tight zipper assembly is provided along the meridional seam. The leak tightness is rated at 0.019 gram of water vapor/.3 meter of fastener/7.6 x 10^4 seconds (0.019 gram of water vapor/foot of fastener/24 hours).

(5) Sleeves are provided in the neck of the jacket for egress of thermocouple wires and pressure-sensing tubing assemblies.

(6) The jacket incorporates a provision for automatically opening to vent the purge gas at an internal pressure of 3.1 to 3.8 x 10^3 N/m^2 (o.45 to 0.55 lbf/in.^{2}). A simple and reliable pressure-relief device is a retainer clip snapped over the zipper fastener where teeth have been removed from the zipper. In this area, the jacket pressure loads across the zipper are carried by the retainer clip, shown in Figure 73, which is designed to yield and snap off at the strain level imposed by 3.4x10^3 N/m^2 (0.5 lbf/in.^{2}) internal pressure in the jacket. As the clip is released, the zipper will open to provide a vent for the purge gas.

The zipper opening is designed to be held open by elastic cords attached to tension tie patches located in the area of the zipper vent opening device. The elastic cords are anchored to small aluminum spreader rods which suspend across the closed zipper as shown in Figure 74. The elastic cord action to hold the zipper open is shown in Figure 75.

Four opening cycle tests were performed at room temperature conditions to verify the operation of the zipper release device. Pressure within the jacket was monitored by means of a water manometer attached to the purge gas outlet. The desired internal pressure of the jacket at zipper release is 3.1 to 3.8 x 10^3 N/m^2 (0.45 to 0.55 lbf/in.^{2}). The test zipper release pressures are given in Table IX.

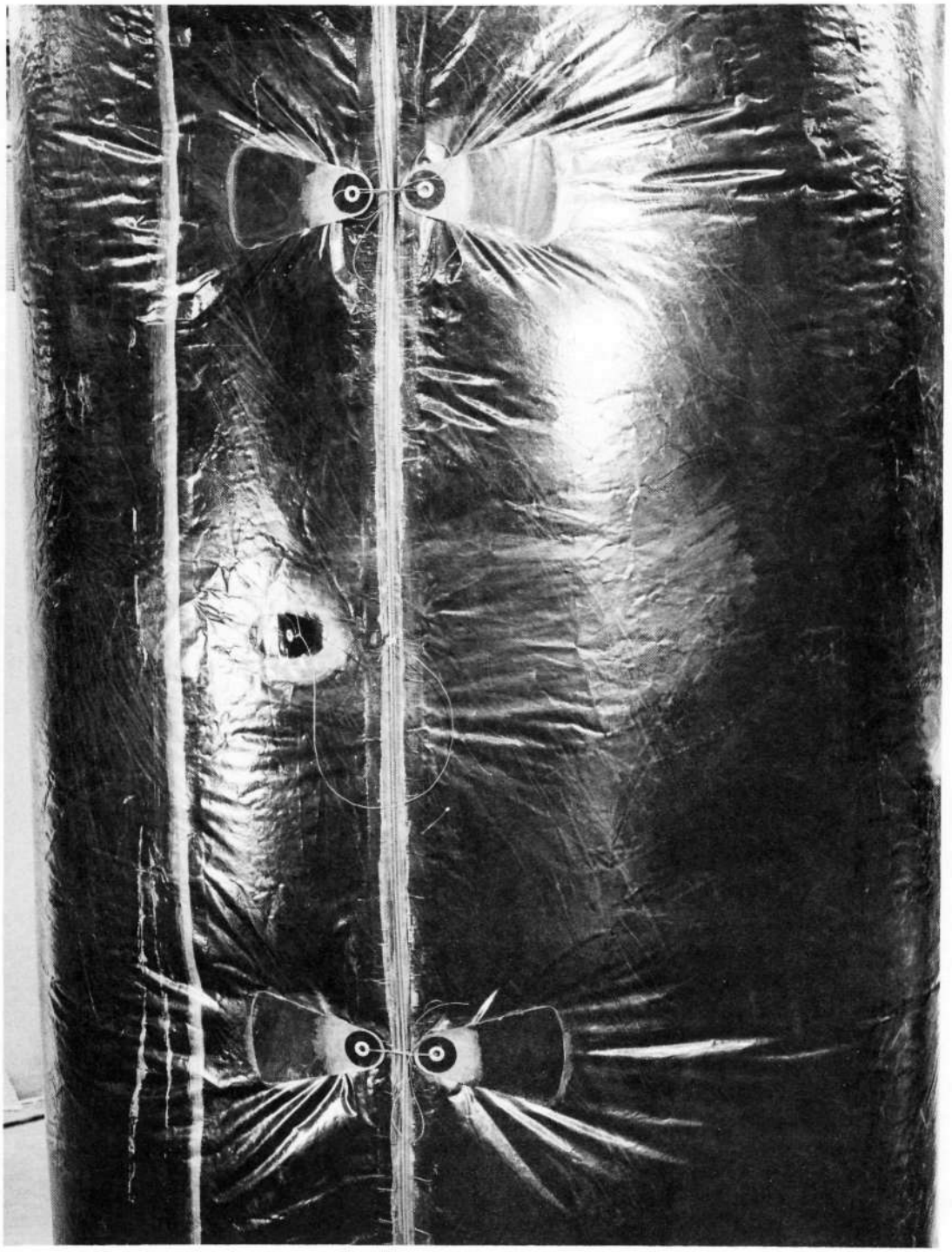

Figure 73. - Cylindrical calorimeter purge jacket showing release clip and tension tie patches.

Figure 74. - Purge jacket vent opening spreader rods with jacket zipper in closed position.

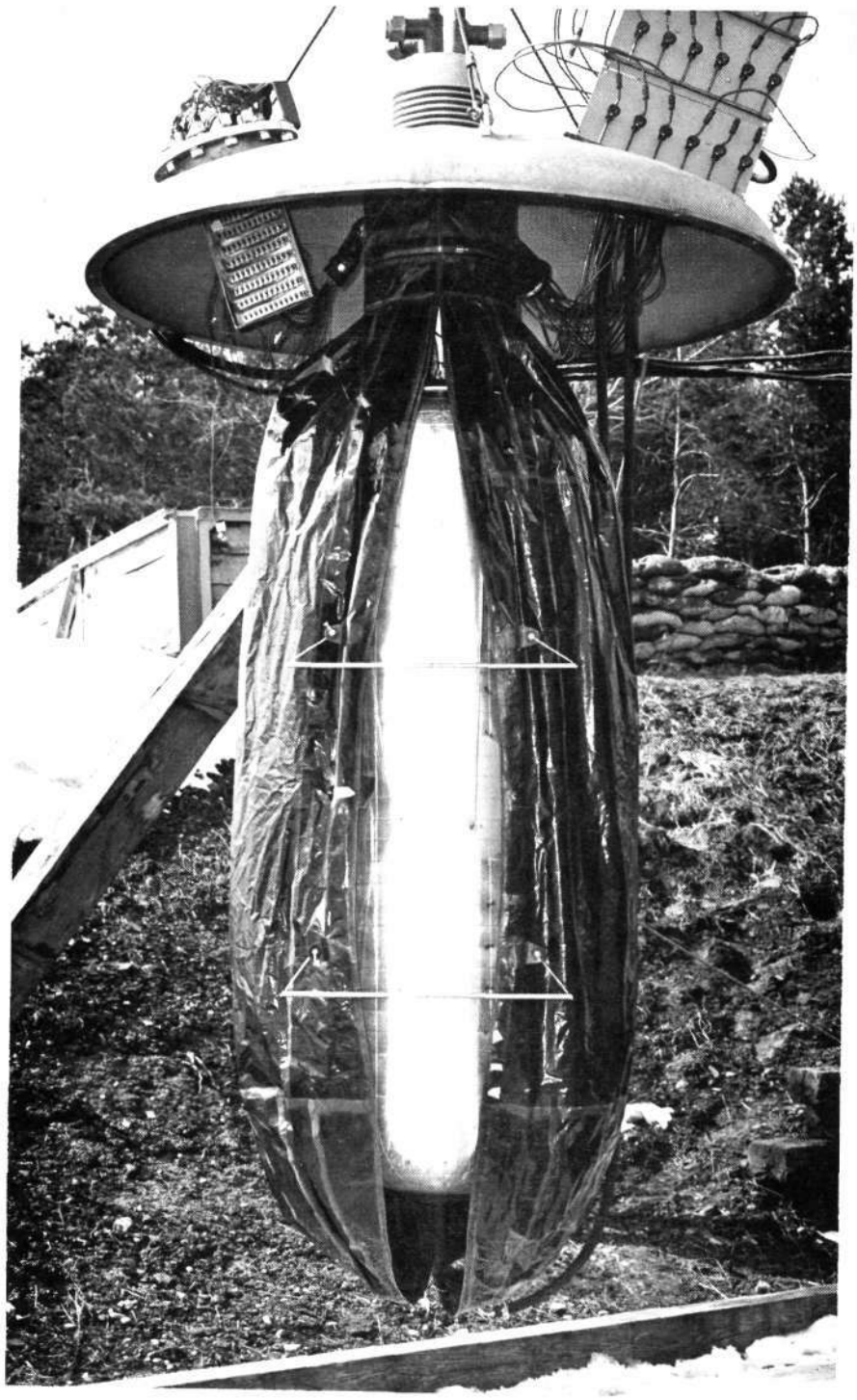

Figure 75. - Purge jacket opening spreader rods holding jacket zipper open.

TABLE IX. - ZIPPER RELEASE TEST PRESSURE

Pressure Test No.	Zipper teeth removed	Opening pressure N/m^2 ($lbf/in.^2$)
1	4	3.67×10^3 (0.533)
2	4	3.47×10^3 (0.504)
3	4	3.42×10^3 (0.496)
4	5	2.97×10^3 (0.432)

During pressure tests 1, 2 and 3 the zipper opened in the desired pressure range, however, prior to test 4 the fifth zipper tooth was removed to insure zipper clip release and zipper opening below 3.4×10^3 N/m^2 (0.50 $lbf/in.^2$) at room temperature. During the 76-cm (30-in.) calorimeter LH_2 tests the jacket will be colder than room temperature and less pliable, therefore removal of the fifth tooth is beneficial to maintaining the desired pressure range of jacket opening under the calorimeter ground-hold test conditions.

2. Pressure Sensing Instrumentation Installation

Based on matched tube test results, the 76-cm (30-in.) diameter calorimeter pressure sensing tubes were designed to be .475-cm (0.187-inch) bore tubes entering the insulation panels normal to the panel surface at the pressure sensing points. To reduce heat leaks into the insulation the tubes or pressure taps in the insulation panels are fabricated of fiberglass reinforced plastic. Figure 76 shows the plastic pressure tap configurations designed for the cylindrical calorimeter panels. The taps extend full depth of the insulation thickness and are slotted to obtain the purge gas average pressure across the thickness of the panel. A typical outer panel pressure tap is shown in Figure 77. Location of the pressure taps on the inner and outer insulation panels of the calorimeter are shown in Figure 78. As shown in Figure 76, the plastic pressure taps extend beyond the surface of the outer insulation panels and are joined to 0.475-cm (0.187-inch) bore stainless steel tubes which extend along the outside of the insulation, as shown in Figure 79, to the base of the top dome. At this point the stainless steel tubing is joined to 0.475-cm (0.187-inch) bore copper tubing which is routed through the calorimeter neck region, as shown in Figures 79 and 80, to the purge jacket egress sleeve, as shown in Figure 81. To facilitate sealing the jacket sleeves to the pressure sensing tubing and the thermocouple wires, the tubing and wires were enclosed in silicone rubber feed through plugs, as shown in Figure 81.

The pressure sensing tubes exiting from the purge jacket sleeve are routed through the vacuum chamber lid feed-throughs and secured to the selector valve panel mounted on the

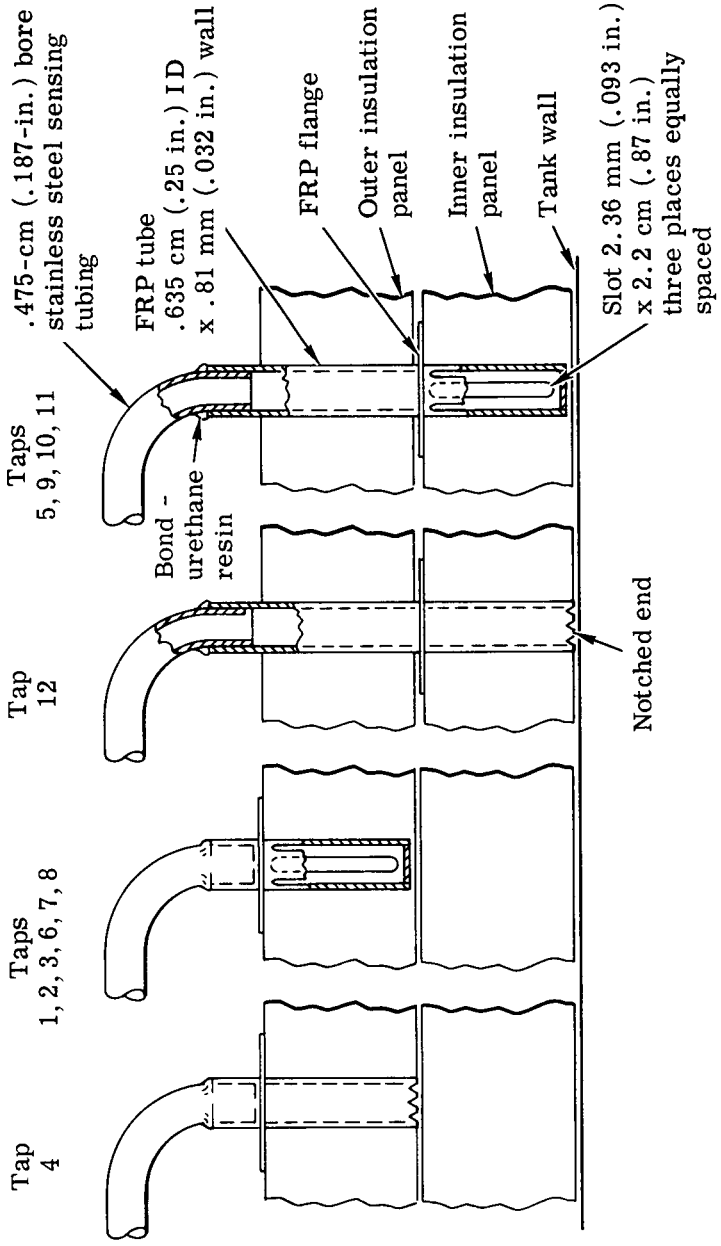

Figure 76. - Plastic pressure tap configurations - cylindrical calorimeter insulation.

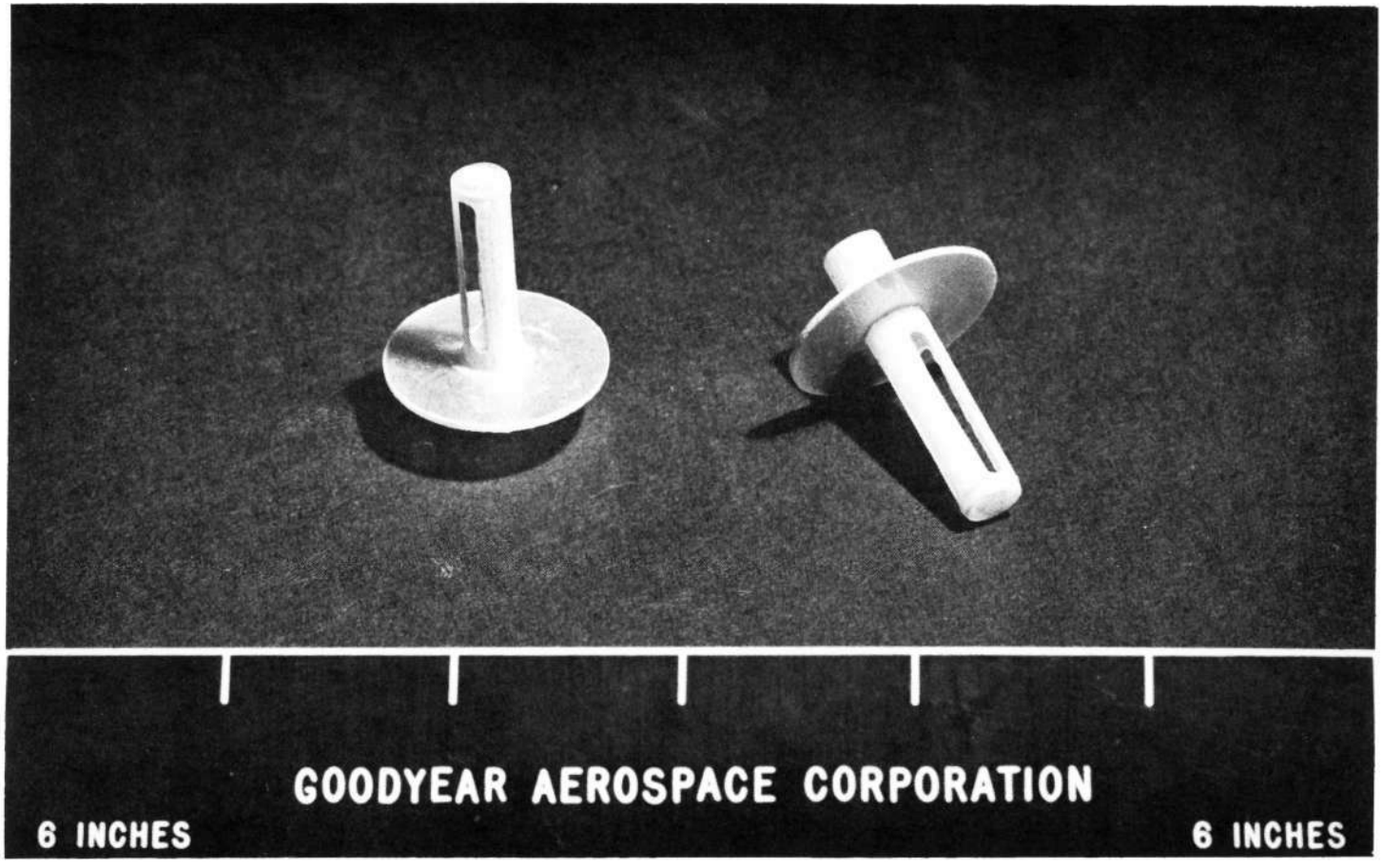

Figure 77. - Typical outer panel pressure sensing tap.

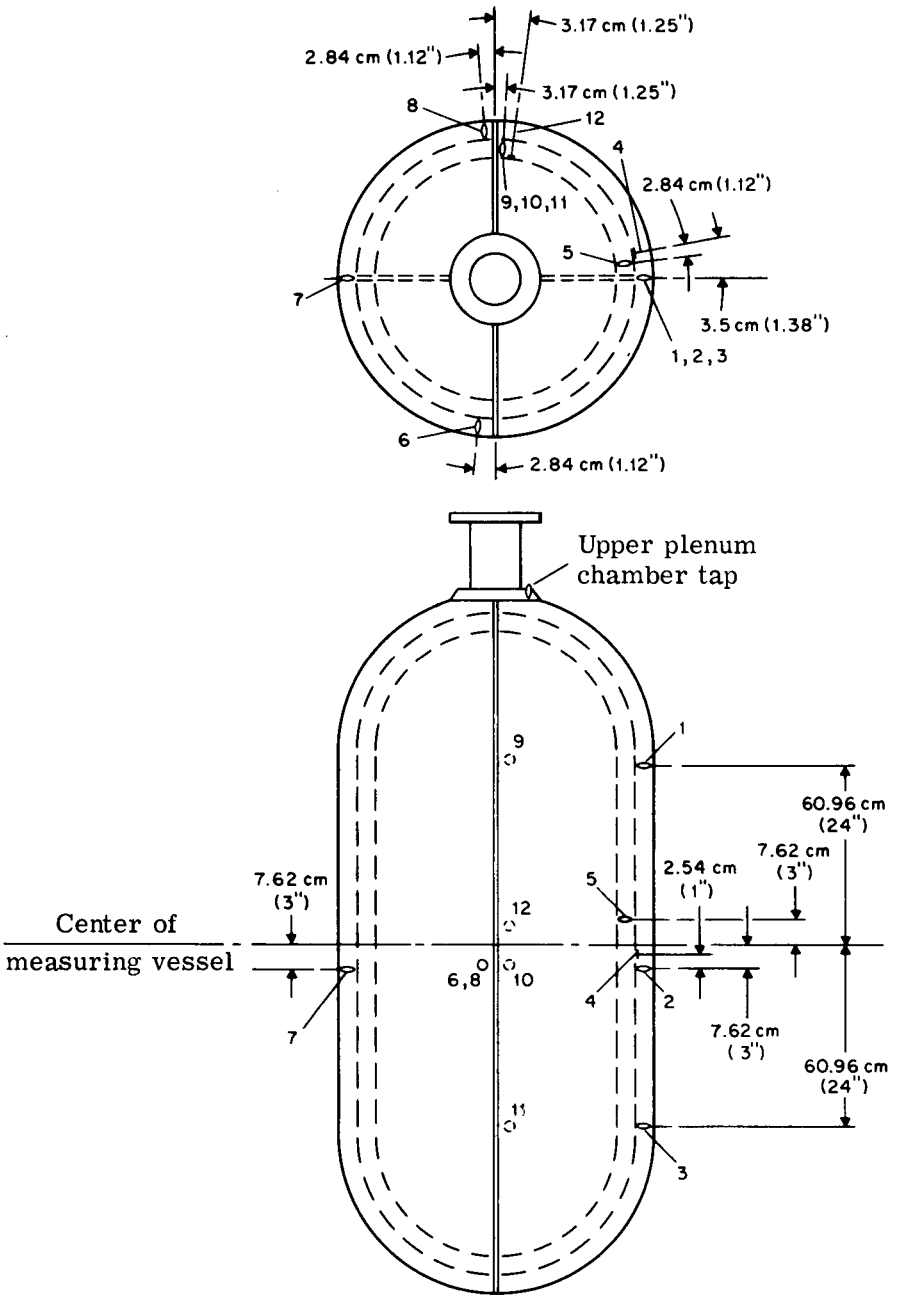

Note: All dimensions are on outer surface of insulation.
For tap details see Fig. 76.

Figure 78. - Pressure tap locations in GAC-9 insulation panels on cylindrical calorimeter

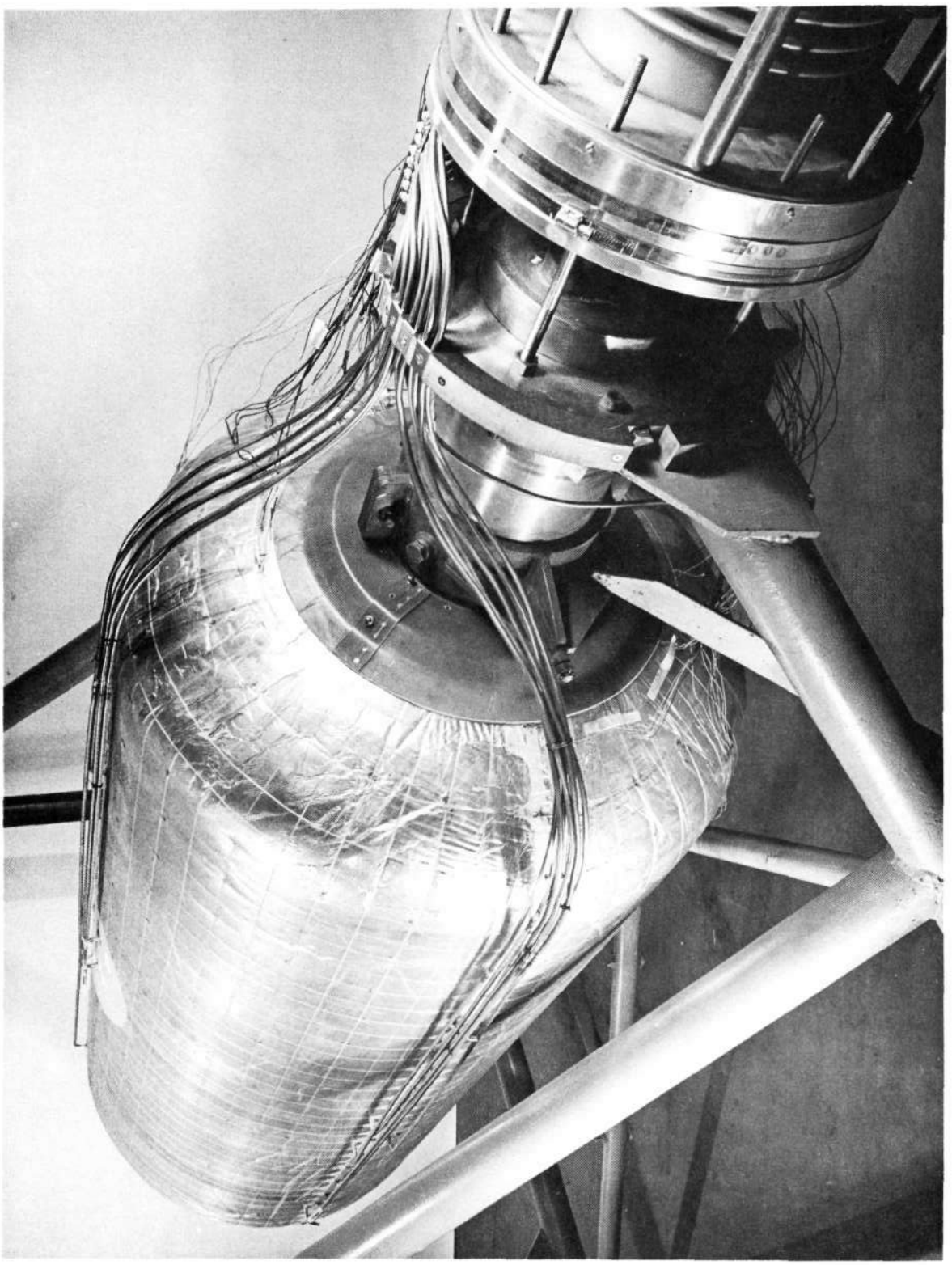

Figure 79. - Cylindrical calorimeter with GAC-9 insulation outer panels showing pressure sensing tubing routed along sidewall and neck region.

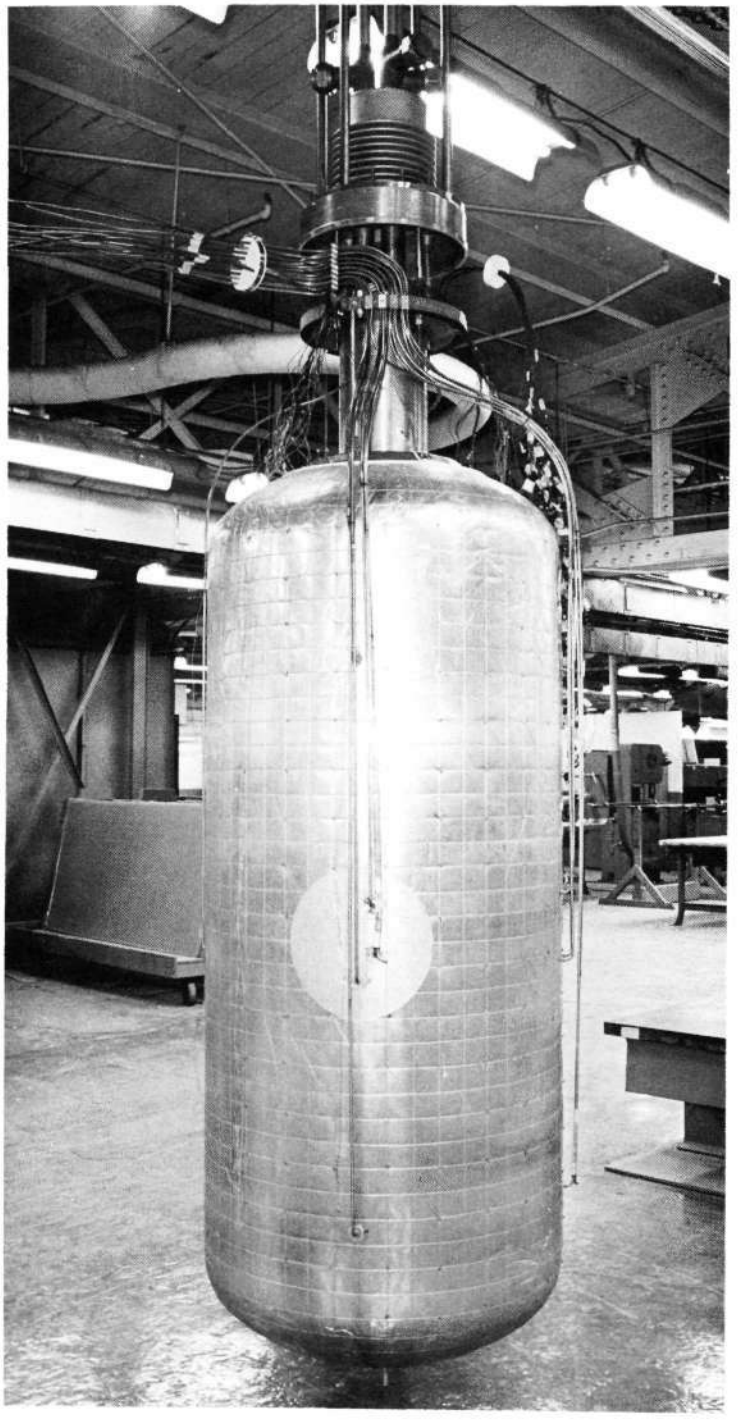

Figure 80. - Cylindrical calorimeter with GAC-9 insulation prior to installation of purge jacket.

Figure 81. - Cylindrical calorimeter with purge jacket.

outside of the chamber lid. From this point the pressure sensing instrumentation is the same as used on the 94-cm x 122-cm (3 ft x 4 ft) test panel described in section III of this report.

3. Penetration Insulation

a. General. A simulated penetration and associated insulation was added to the cylindrical calorimeter for the purpose of evaluating the performance of the penetration GAC-9 insulation. In a previous program, the GAC-9 insulation panels on the calorimeter were designed and fabricated with provisions for incorporating the penetration. Details of the penetration are shown on GAC drawing 69QS1390 (Figure 66). The evaluation consisted of liquid hydrogen boil-off tests under ground hold, ascent and space conditions. The test results were compared with test data from test No. 1 to determine the effect of the penetration and its insulation.

b. Design and Fabrication of Insulated Penetration. At the request of the NASA COR, the insulated penetration was designed to limit the heat leak to approximately 50 percent of average heat leak into the GAC-9 insulated 76-cm (30-in.) diameter calorimeter. This would be approximately 0.58 W (2.0 Btu/hr). The penetration is designed as a fiberglass reinforced plastic tube 5 cm (2.0 inches) diameter x .76 mm (.030 inch) wall thickness x 25.4 cm (10 inches) long.

A stainless steel flange is incorporated on one end of the plastic tube to facilitate bonding the tube to the calorimeter wall. The opposite end of the plastic tube is fitted with an aluminum disc heat sink and heater element to control the tube outer end temperature within $\pm 1.67^{\circ}K$ ($\pm 3^{\circ}F$). A small tube is incorporated in the aluminum disc to direct helium purge gas into the Owens Corning type PF105-500 glass wool opacifying media in the core of the plastic penetration tube. Purge gas venting is provided by holes drilled in the penetration tube wall near the aluminum disc. Detail parts of the penetration tube, heat sink and insulation are shown in Figure 82.

The penetration insulation is designed to isolate the penetration tube from the outside environment. The insulation is a flanged sleeve of one-inch thick GAC-9 insulation constructed of 40 alternate layers of DAM radiation shields and 39 layers of thin urethane foam sheet spacers.

Each radiation shield layer is comprised of two parts, a washer-like flange and a single ply wrap on the cylinder section. The hole in the flange is notched to form tabs which are bent upward and overlap the cylinder section. A typical radiation shield layer is shown in Figure 83. Each foam spacer layer is also in two pieces, however the center hole in the flange is fitted to the outside diameter of the cylinder section so that the cylinder section foam layer

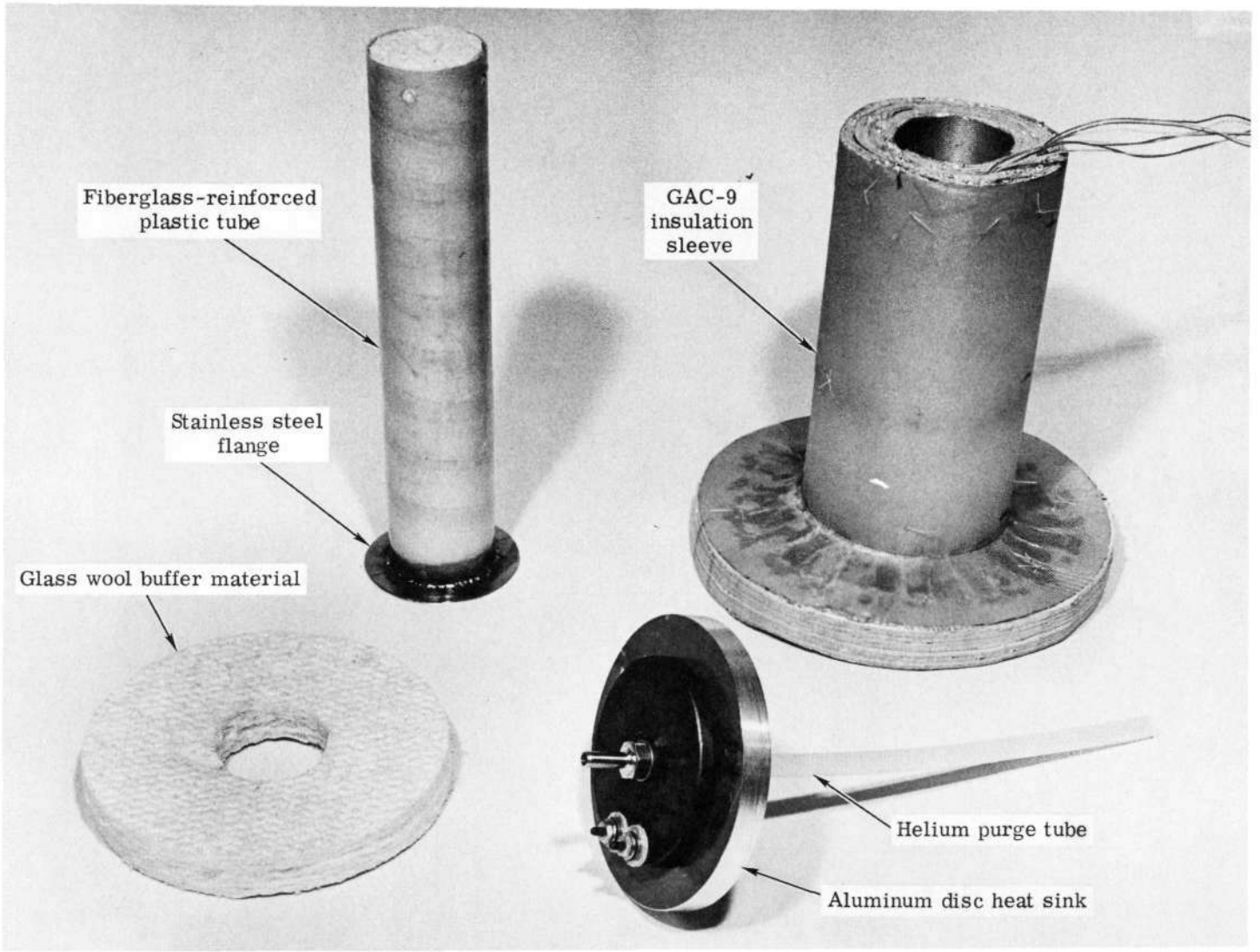

Figure 82. - Detail parts of penetration tube and insulation for cylindrical calorimeter.

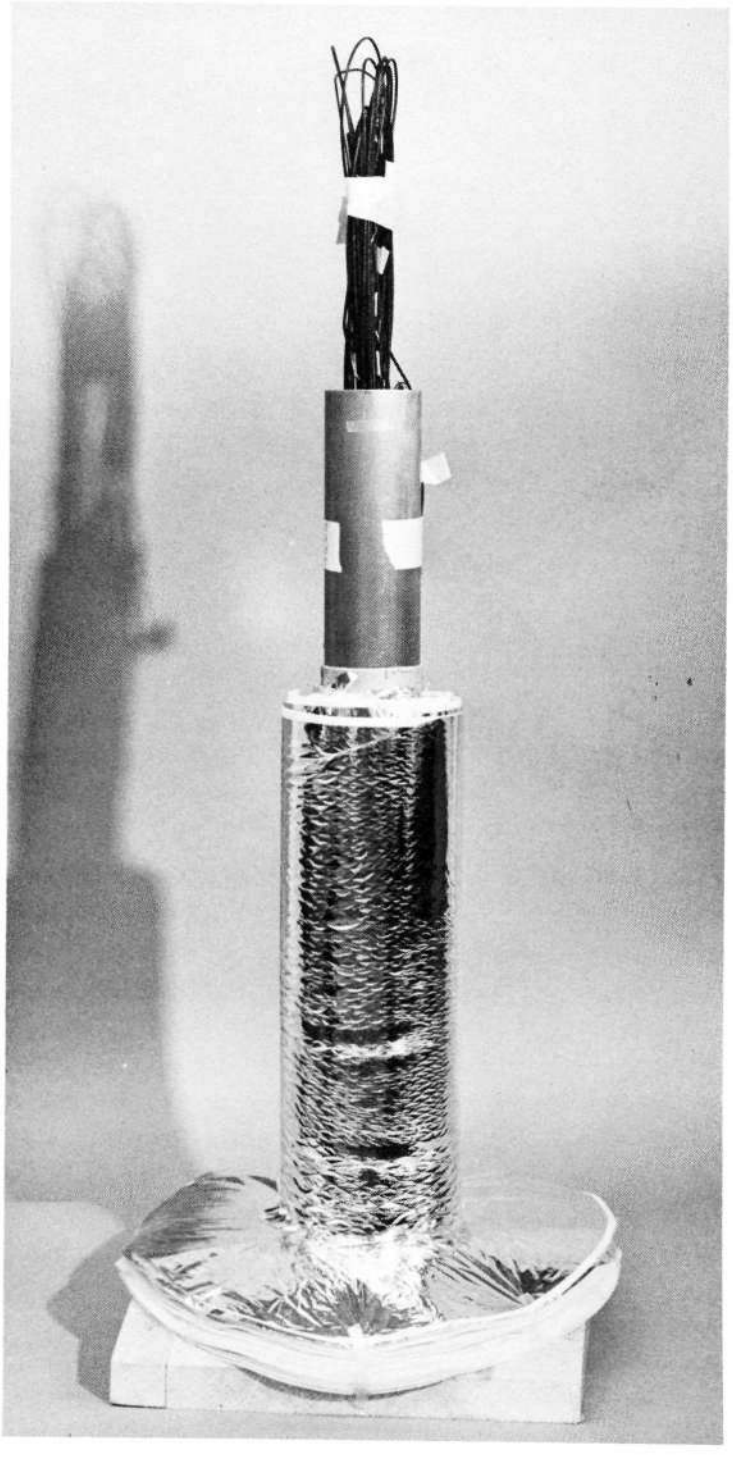

Figure 83. - Typical radiation shield layer during layup of penetration insulation sleeve.

is butt joined to the flange as shown in Figure 84. A typical foam spacer layer is shown in Figure 85. Due to the small size of the penetration, it is impractical to use fiberglass roving grids that are customary on the faces of GAC-9 insulation, therefore the inner and outer surface layers of the penetration insulation sleeve are designed to be fabricated from a single ply of style 181 glass cloth impregnated with a polyurethane resin. The insulation drop threads and lacing eyelets are secured to the cloth layers. Trimming was accomplished with a knife-edge bandsaw. The insulation sleeve is split into two half shells to simulate a typical penetration insulation which is installed by placing around the penetration rather than sliding it on from the end. To reduce heat leaks through the joints in the cylindrical portion of the insulation, a second layer of multilayer insulation is applied over cylinder section only. The second layer is comprised of 20 each, alternate layers of double aluminized Mylar shields and Dacron net spacers. One longitudinal joint in the second insulation layer is located between joints in the penetration GAC-9 insulation.

From previous studies conducted on GAC-4 insulation under Contract NAS 8-11747, the heat transfer along the multilayer insulation can be relatively high because the thermal conductivity in this direction is approximately five magnitudes greater than the conductivity across the insulation. At the penetration clearance cutout in the calorimeter inner insulation panel, the edge of the insulation is protected from this effect by the addition of a one-inch thick layer of Owens-Corning type PF 105-500 glass wool placed in the annular space between the base of the penetration tube and the multilayer insulation. The heat energy being transferred along the penetration GAC-9 insulation will tend to be distributed along the outer layer of insulation on the calorimeter to minimize the external heat leak into the calorimeter measuring vessel.

c. Installation of Penetration and Insulation. At the penetration location, the GAC-9 insulation panels on the calorimeter were concentrically cutout to 15.2-cm (6.00-inch) diameter on the inner panel and 20.3-cm (8.00-inch) diameter on the outer panel. Knife edged circular cutters were used by hand rotation to make the cutouts. Lacing eyelets were installed in the fiberglass laminate edgeband surrounding the cutout in the outer insulation panel.

The metal flange end of the plastic penetration tube was bonded to the calorimeter surface using a urethane resin suitable for cryogenic service. Thermocouple wires were added to the exterior of the plastic tube prior to installation of the penetration insulation. The thermocouple arrangement for the penetration installation is shown on Figure 86.

A disk of glass wool type PF 105-500 (Owens-Corning Corp.) was placed in the annular space between the penetration tube and the cutout in the inner insulation panel as shown in

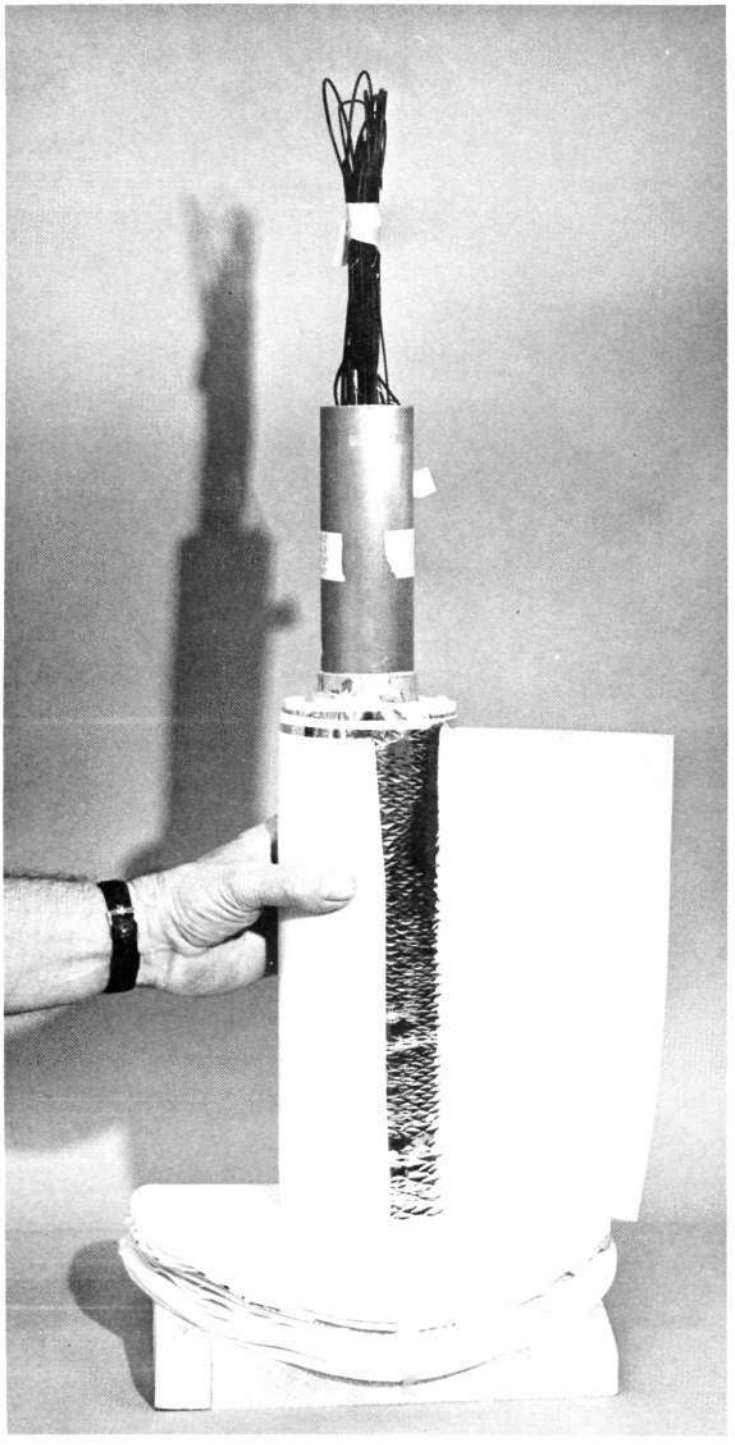

Figure 84. - Installation of foam layer cylinder sheet during layup of penetration insulation sleeve.

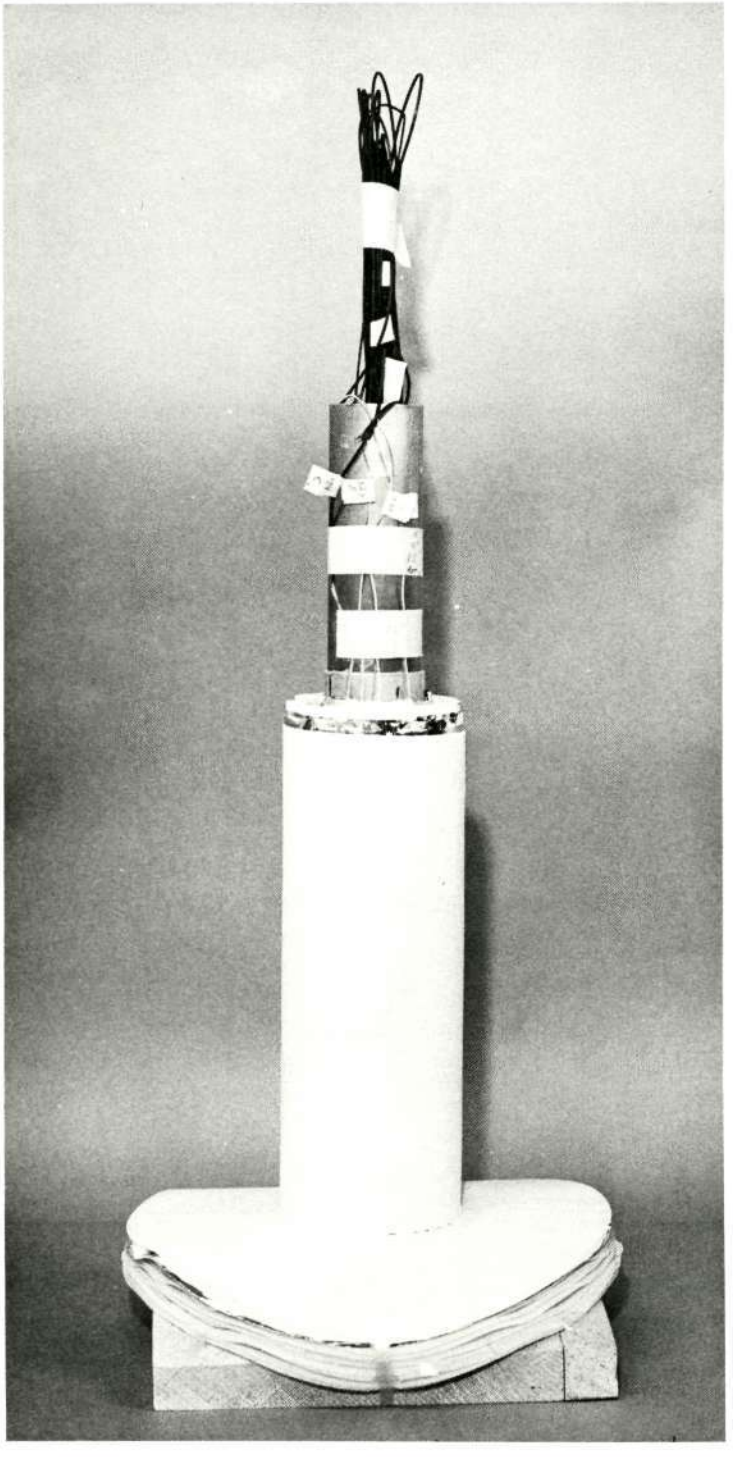

Figure 85. - Typical foam spacer layer during layup of penetration insulation sleeve.

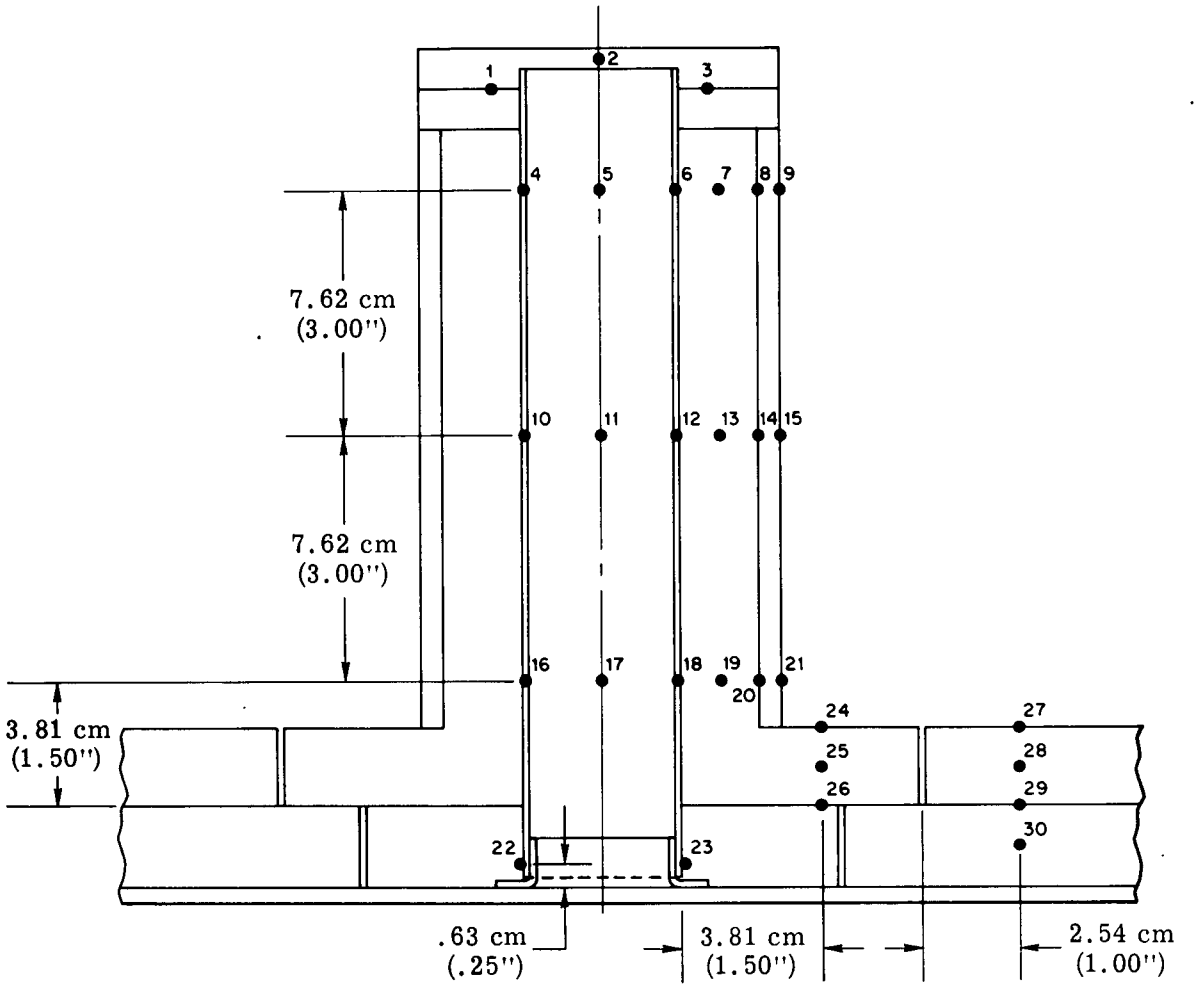

Figure 86. - Thermocouple locations on penetration insulation on the cylindrical calorimeter.

Figure 87. This provides an isotropic "buffer" material shielding the edge of the inner panel from extraneous heat sources and sinks.

The GAC-9 insulation flanged sleeve was installed over the penetration tube and secured by Vycron cord lacing between eyelets in the GAC-9 insulation panel edgebands and eyelets in the penetration insulation. A disc of glass wool is installed between the exposed edges of the penetration insulation and the aluminum disc heat sink on the end of the penetration tube as shown in Figure 88.

The outer wrap of multilayer insulation was added to the cylinder section to complete the penetration insulation as shown in Figure 89.

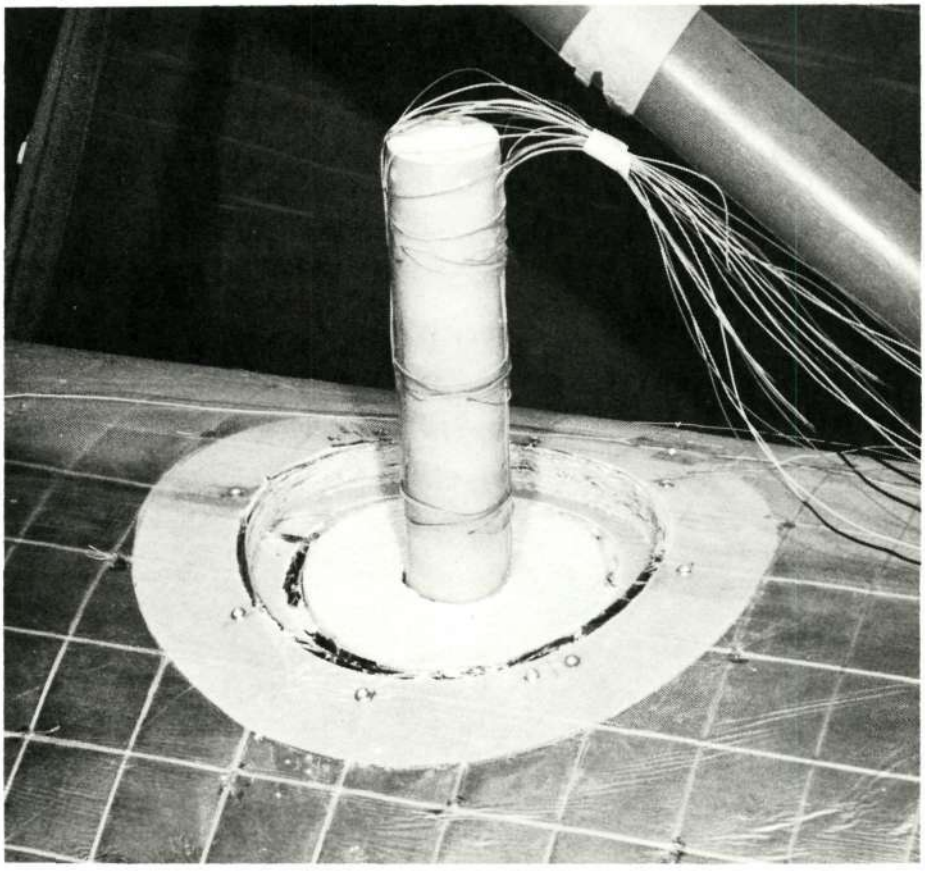

Figure 87. - Fiberglass penetration tube and glass wool buffer material installed on the cylindrical calorimeter.

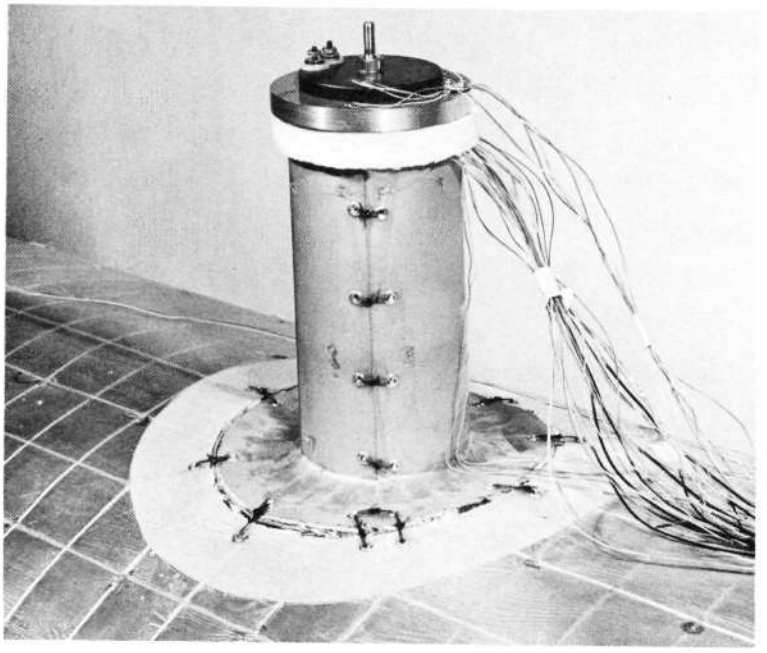

Figure 88. - GAC-9 insulation and aluminum heat sink attached to penetration on the cylindrical calorimeter.

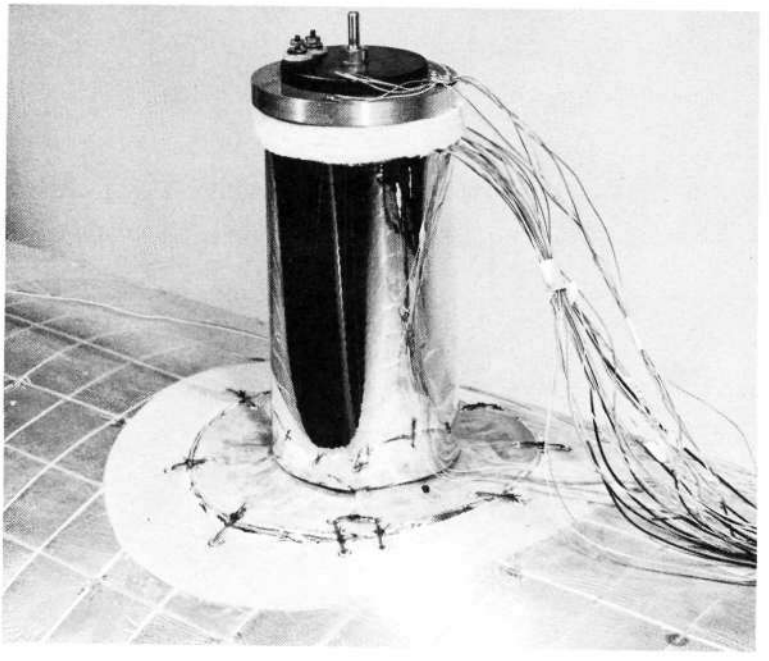

Figure 89. - Completed penetration and insulation on the cylindrical calorimeter.

C. PURGE SYSTEM TEST

1. Test Apparatus and Test Plan

The GAC-9 insulation purge system on the cylindrical calorimeter was tested under simulated ground-hold and space environments in the GAC Wingfoot Lake LH_2 test facility. The test facility, shown in Figure 90, consists of a vacuum chamber, liquid hydrogen transfer system, vent and metering systems, liquid-level sensors, pressure transducers, electronic pressure meter, vacuum gages, and thermocouple instrumentation.

A schematic of the plumbing system for the calorimeter is shown in Figure 91. This system was used for ground-hold and space-simulation tests and therefore is designed to measure high or low boil-off gas rates. Orifice-type flow transmitters were used to measure high flow rates, and wet test meters were employed to measure low flow rates. Back-pressure control of the measuring and lower guard vessels during space-hold testing was obtained by bubbling the vent gases through the mercury bubbler described in section III of this report.

Pressure in the upper guard vessel was maintained at approximately 0.5 psi higher than the measuring vessel pressure by throttling the flow in the vent line. Bubbling the boil-off gas from the upper guard is not practical because of the high flow rate and the necessity of frequent refilling or "topping off" to a required liquid level.

The GAC-9 insulated cylindrical calorimeter was attached to the lid of the vacuum chamber with purge jacket folded, as shown in Figure 92, and with purge jacket deployed, as shown in Figure 93.

The test procedures used to evaluate the thermal performance of the GAC-9 insulation system on the cylindrical calorimeter were in accordance with accepted standards for boil-off calorimetry. These procedures were successfully employed in previous programs, using the facilities described above to test high performance multilayer insulation systems.

The test plan outlined in Table X describes the test specimens and the test objectives using the test apparatus and procedures discussed above.

TABLE X. - 76-CM (30-IN.) DIAMETER CYLINDRICAL CALORIMETER TESTS

Test No.	Description of test specimen	Test description	Test objectives
1.	Existing GAC-9 insulation panels on 76-cm (30-inch) diameter cylindrical calorimeter with purge system per Figure 67 and pressure sensing instrumentation. Purge jacket folded away from insulation.	Space test No. 1. 1. Evacuate chamber and insulation for minimum of 1.73×10^5s (48 hours). Obtain data on chamber pressure and temperature, and insulation pressures and temperature before LH_2 filling. 2. Fill calorimeter with LH_2 and perform simulated space test. Obtain test data to include: a. Boil-off b. Insulation temperature and pressure c. Chamber temperature and pressure d. Barometric pressure e. Ambient temperature Continue test for approximately 1.73×10^5s (48 hours) after GAC-9 insulation has achieved thermal equilibrium or until bulk temperature of insulation is decreasing at a rate of less than $0.55^{\circ}K$ ($0.5^{\circ}F$) per 3600 s (1 hour). 3. At conclusion of test, empty calorimeter of LH_2 and purge with gaseous helium. Warm up calorimeter and insulation in vacuum.	1. Obtain space condition thermal performance after installation of purge system and pressure sensing instrumentation. 2. Compare test results with space test performance from previous program.
2.	Same as test No. 1 with purge jacket deployed and closed.	Ground hold test, followed by ascent pressure decay and space test. 1. Purge insulation and jacket with gaseous helium using flow-through purge system. Purge 7200 s (2 hours) at helium flow	1. Check operation of purge and vent system. 2. Obtain ground hold thermal performance. 3. Compare space test 2 with test No. 1 to determine efficiency of purge and vent system.

TABLE X. - 76-CM (30-IN.) DIAMETER CYLINDRICAL CALORIMETER TESTS - Continued

Test No.	Description of test specimen	Test description	Test objectives
		rate of 4.0×10^{-4} m^3/s (1.0 cubic foot/minute). Monitor helium purity at helium outlet. 2. Fill calorimeter with LH_2 and perform ground hold test for minimum of 7200s (2 hours). Obtain test data to include: a. Boil-off b. Insulation temperature and pressure c. Chamber temperature and pressure d. Barometric pressure e. Ambient temperature 3. Perform vacuum chamber pump-down to simulate ascent. Monitor purge jacket zipper release and opening. Obtain test data during ascent pressure decay to include: a. Insulation temperature and pressure b. Chamber pressure c. Boil-off 4. Perform space test No. 2. Same as test No. 1, step 2 and subsequent.	4. Obtain data on interstitial gas pressure during simulated ground hold, launch, and space conditions to the limit of pressure sensing equipment.
3.	Same as test No. 1	Ground hold test, followed by ascent pressure decay without purge jacket. 1. Same as test No. 1. 2. Backfill chamber and insulation with gaseous helium. 3. Same as test No. 2, step 2. 4. Perform vacuum chamber pump down to simulate	1. Obtain ground hold thermal performance with ideal helium purge - no purge jacket. 2. Obtain data on interstitial gas pressure during simulated ground hold and launch, pressure decay without purge jacket.

TABLE X. - 76-CM (30-IN.) DIAMETER CYLINDRICAL CALORIMETER TESTS - Continued

Test No.	Description of test specimen	Test description	Test objectives
		ascent. Obtain test data to include: a. Insulation temperature and pressure b. Chamber pressure c. Boil-off 4. Same as test No. 1, step 3.	
4.	Same as test No. 2.	Ground hold test, followed by ascent pressure decay and space test of limited duration. 1. Same as test No. 2. 2. Same as test No. 2. 3. Same as test No. 2. 4. Perform limited duration space test for 2.16×10^4s (6 hours).	1. Check operation of purge and vent system. 2. Obtain ground hold thermal performance - compare with test No. 2 and test No. 3. 3. Obtain data on interstitial gas pressure during simulated ground hold and launch pressure decay with purge jacket. Compare with test No. 2 and test No. 3.
5.	Same as test No. 1 with penetration and penetration insulation added to sidewall of calorimeter measuring vessel. Purge jacket deployed but not closed.	Ground hold test, followed by ascent pressure decay and space test of limited duration. 1. Evacuate chamber and insulation for a minimum of 1.73×10^5s (48 hours). Obtain data on chamber pressure and temperature and insulation pressures and temperature before LH_2 filling. 2. Backfill chamber and insulation with gaseous helium. 3. Same as test No. 2, step 2. 4. Same as test No. 2, step 3. 5. Same as test No. 1, step 3.	1. Obtain ground hold, ascent and space conditions thermal performance. 2. Compare test No. 1 with space test portion of test No. 4 to determine the performance of the penetration insulation.

Figure 90. - LH_2 test facility for cylindrical calorimeter.

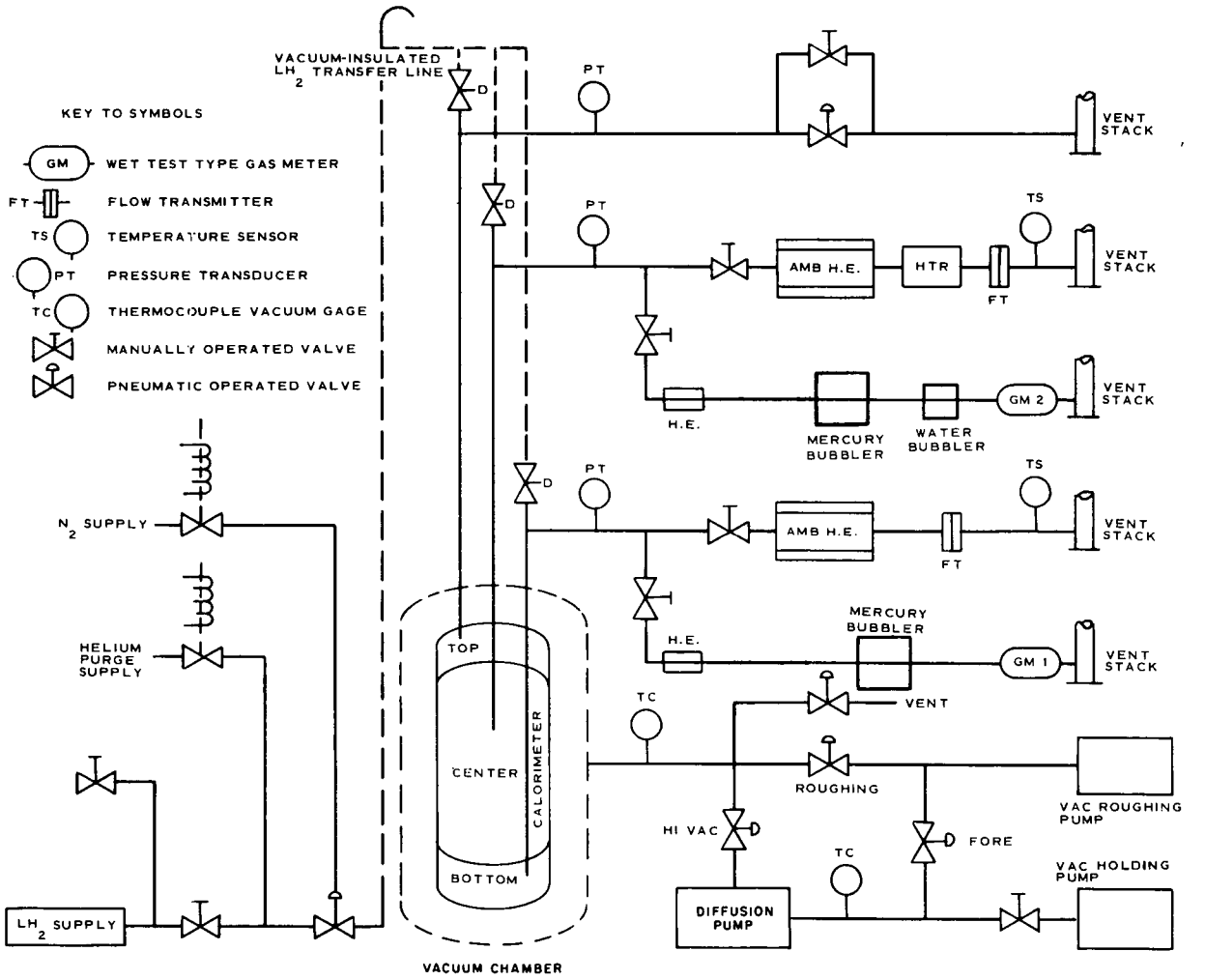

Figure 91. - Plumbing for cylindrical calorimeter

Figure 92. - GAC-9 insulated cylindrical calorimeter with purge jacket bundled into neck region.

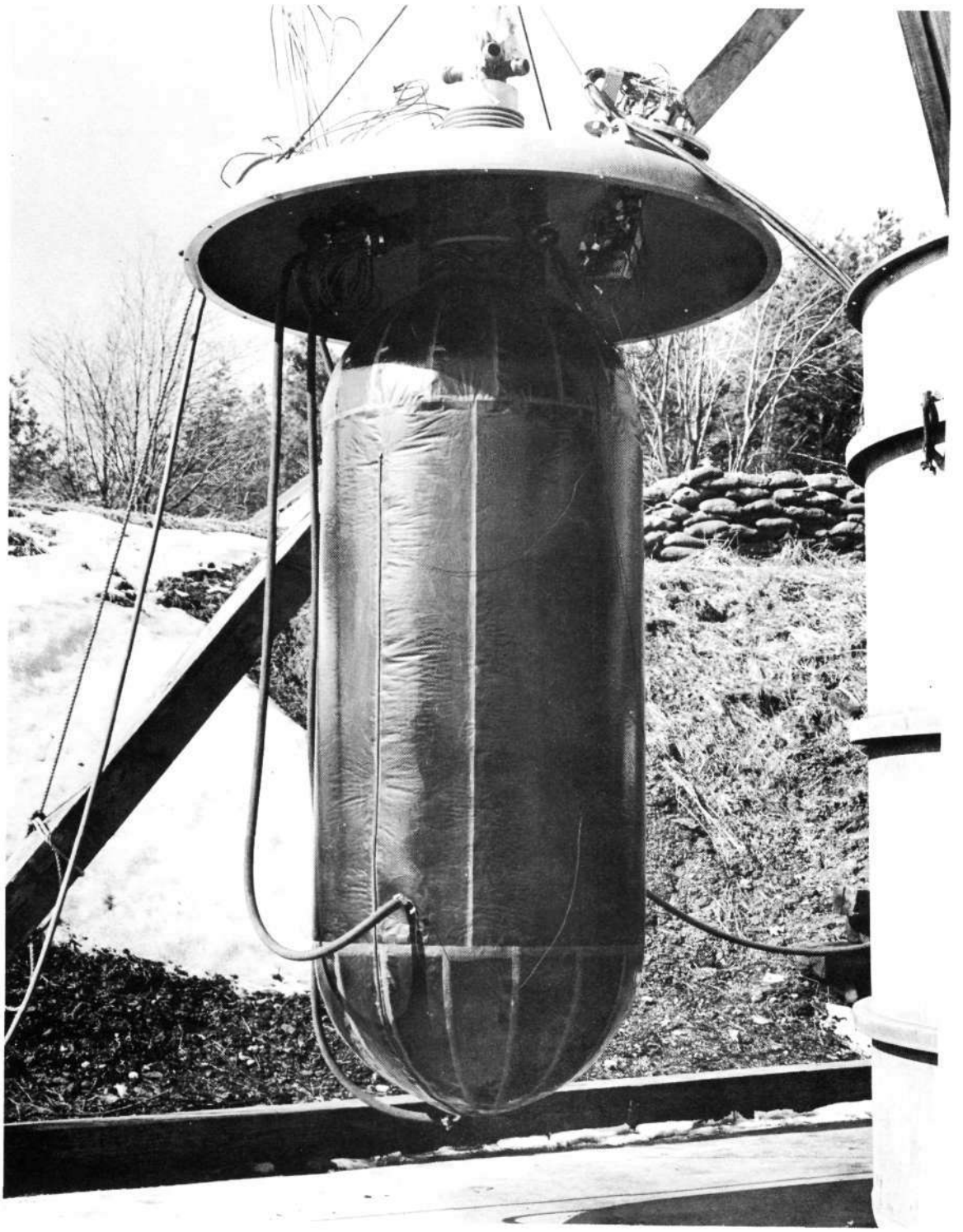

Figure 93. - Purge jacketed cylindrical calorimeter attached to vacuum chamber lid.

2. Testing and Analysis of Test Results

a. Test No. 1. A space test of the GAC-9 insulation system incorporating pressure sensing probes was conducted for approximately seven days using the cylindrical calorimeter. To evaluate the performance of the insulation, it is necessary to measure the boil-off, correct the boil-off for pressure and temperature at the measuring strument, and then correct this total for non-equilibrium conditions, edge effects, heat leak attributable to pressure probes, and variations in ullage pressure. In addition the pressure at a probe within the insulation system is reported as a function of test time.

(1) Boil-Off. The LH_2 boil-off was recorded throughout the time period of testing and is shown in Figure 94 as a function of elapsed time. The high boil-off experienced during the first few days of testing was the initial cooling of the insulation. A gradual decrease in the boil-off rate occurred during the last three days of testing. During this final cool-down period the fill line was removed and the bubbler installed to dampen any variations in the barometric pressure. The total boil-off, measured over 5.04×10^4 s (14 hours) of testing, was 3.23×10^{-5} m^3/s (4.10 cubic feet/hour) at a meter temperature of 299°K (538°R) and a meter pressure of 94.55×10^3 N/m^2 (28.0 inches mercury). Correcting to standard conditions, the boil-off becomes:

$$\dot{W}_{corr} = \dot{W}_{measured} \times \frac{T_{standard}}{T_{reading}} \times \frac{P_{test}}{P_{standard}}$$

$$= .116 \times \frac{293}{299} \times \frac{94.55 \times 10^3}{100.96 \times 10^3}$$

$$= 2.95 \times 10^{-5} \text{ m}^3/\text{s} \text{ (3.76 cubic feet/hour) (standard conditions).}$$

The corresponding total heat transfer to the measuring vessel is given by:

$$Q = \frac{m^3}{s} \times \frac{kg}{m^3} \times \frac{J}{kg}$$

$$= 2.95 \times 10^{-5} \times 0.0839 \times 4.53 \times 10^5$$

$$= 1.12 \text{ W (3.84 Btu/hr)}$$

There are two time periods when data was not presented in Figure 94: one when the mercury bubbler was installed necessitating a gradual build up of pressure, and the second period when a hose connection was accidentally loosened and erratic data was obtained for several hours before the cause was determined.

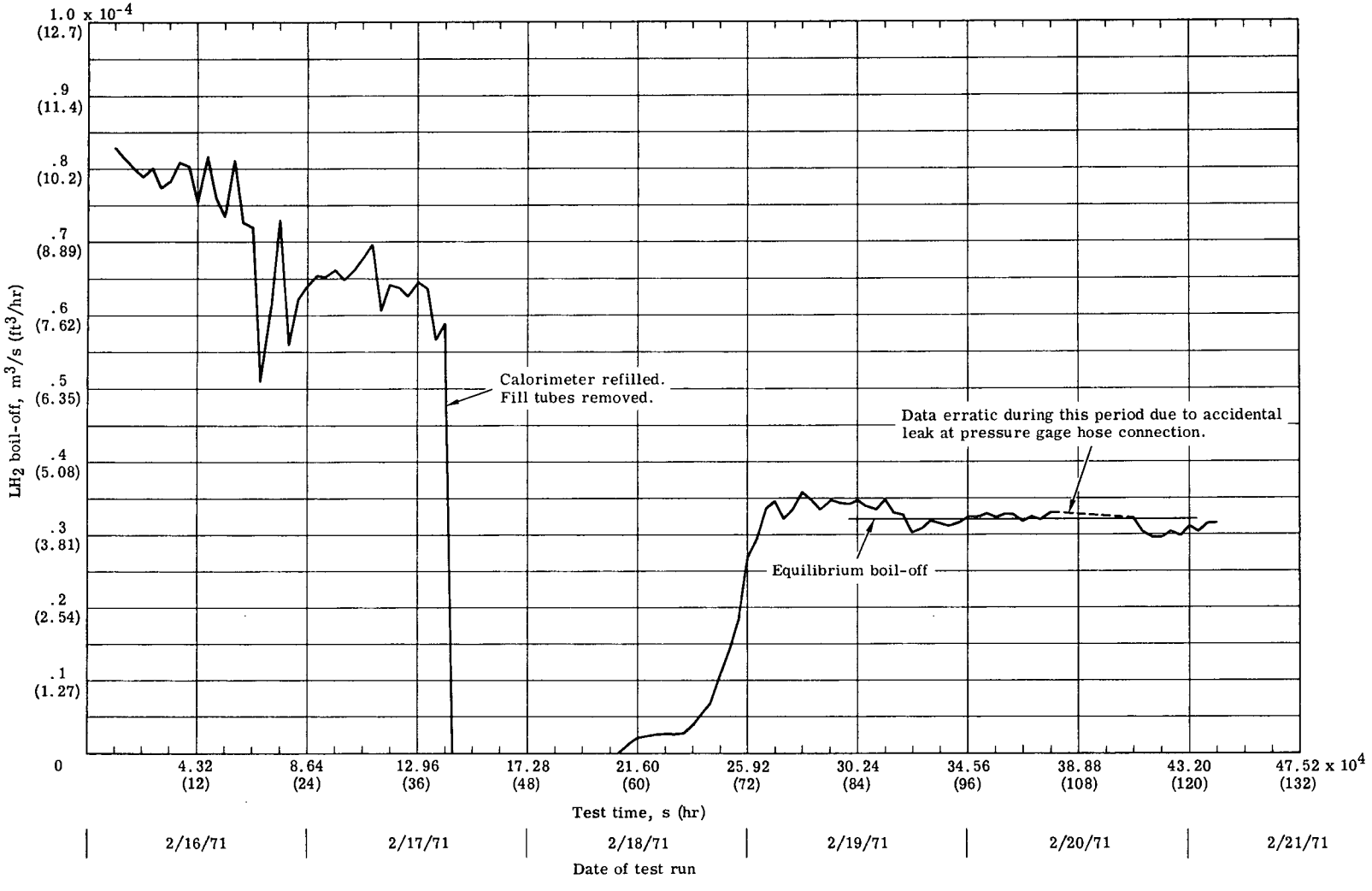

Figure 94. - LH_2 boil-off versus time for GAC-9 insulation system - test No. 1.

(2) Equilibrium Condition. To determine the cooling rate of the insulation, the mid-layer insulation temperature, computed by averaging the readings at thermocouples 3B and 10B, was used as a representative indicator. Thermocouples 3B and 10B are located at the center of the calorimeter measuring vessel at the middle of the insulation panel, and between the inner and outer insulation panels. During the 5.04×10^4s (14 hour) time period over which the equilibrium boil-off was measured, the mid-layer insulation temperature dropped approximately three degrees. In Figure 95, both the mid-layer temperature and the surface temperature of the insulation have been plotted versus the time period of testing. The surface temperature was computed by averaging the four thermocouples (3D, 10D, 14D, and 17D) on the insulation surface. Thermocouple locations on the GAC-9 insulation are illustrated on Figure 96.

As an additional check of the equilibrium condition, the bulk temperature of the insulation was calculated from the following summation:

$$T_b = \frac{1}{4N}\left[\sum_{i=1}^{N}\left(T_{A_i} + T_{B_i} + T_{C_i} + \frac{T_{D_i} + T_{LH_2}}{2}\right)\right]$$

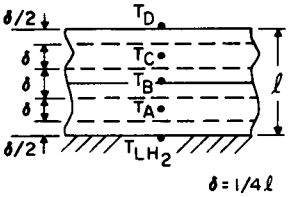

where T_b = the test specimen bulk temperature

T = the insulation temperature

T_{LH_2} = the liquid hydrogen temperature

N = the number of thermocouples around the calorimeter

A, B, C, D refer to the location of the thermocouple within the insulation blanket.

As illustrated in Figure 95, the insulation bulk temperature dropped two degrees from 186°K to 185°K (-125°F to -127°F) during the 5.04×10^4s (14 hour) time period over which the equilibrium boil-off was measured.

The heat flow into the measuring vessel coming from the insulation material that was still cooling or otherwise identified as the nonequilibrium heat leak correction was obtained from:

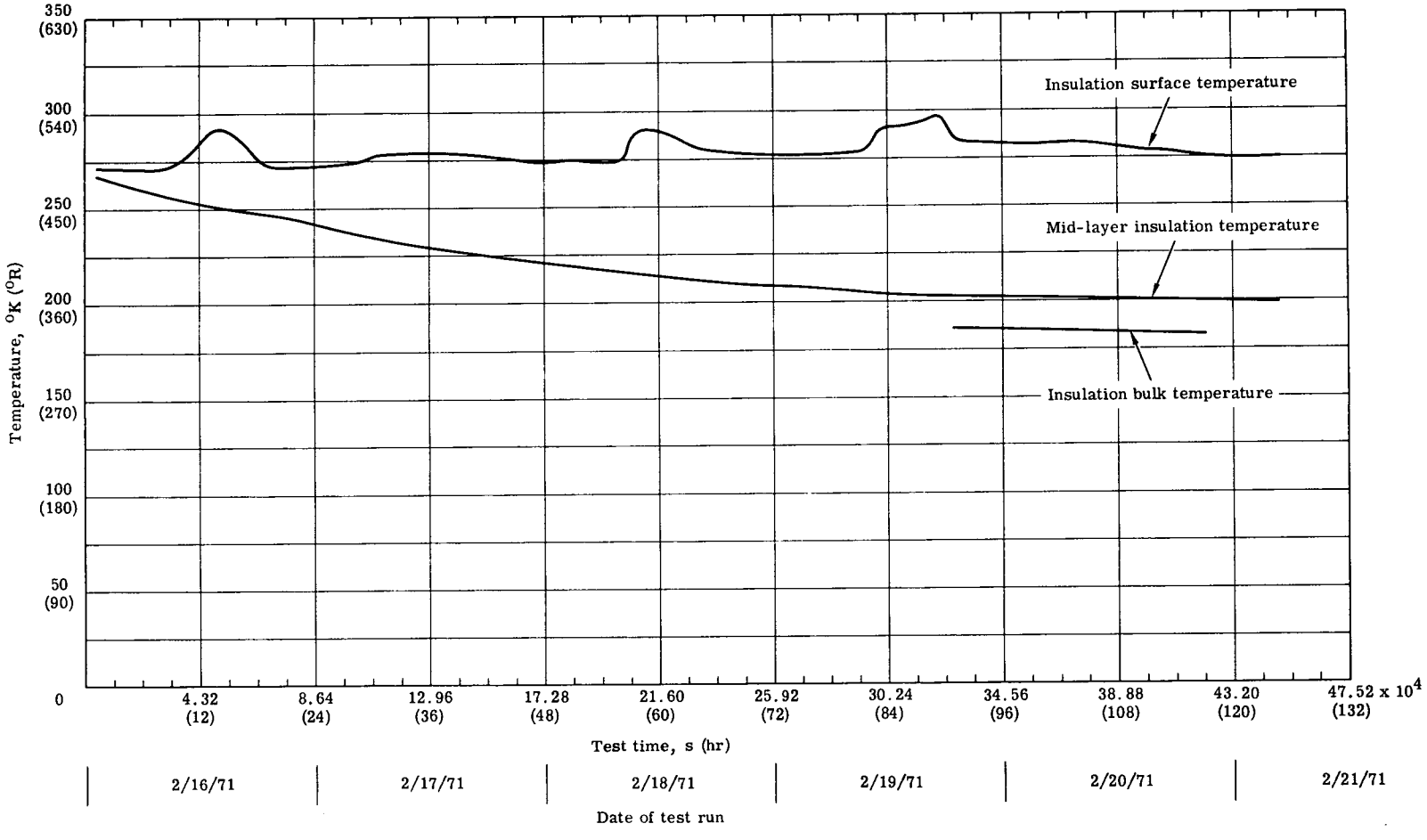

Figure 95. - Insulation temperature versus time - test No. 1.

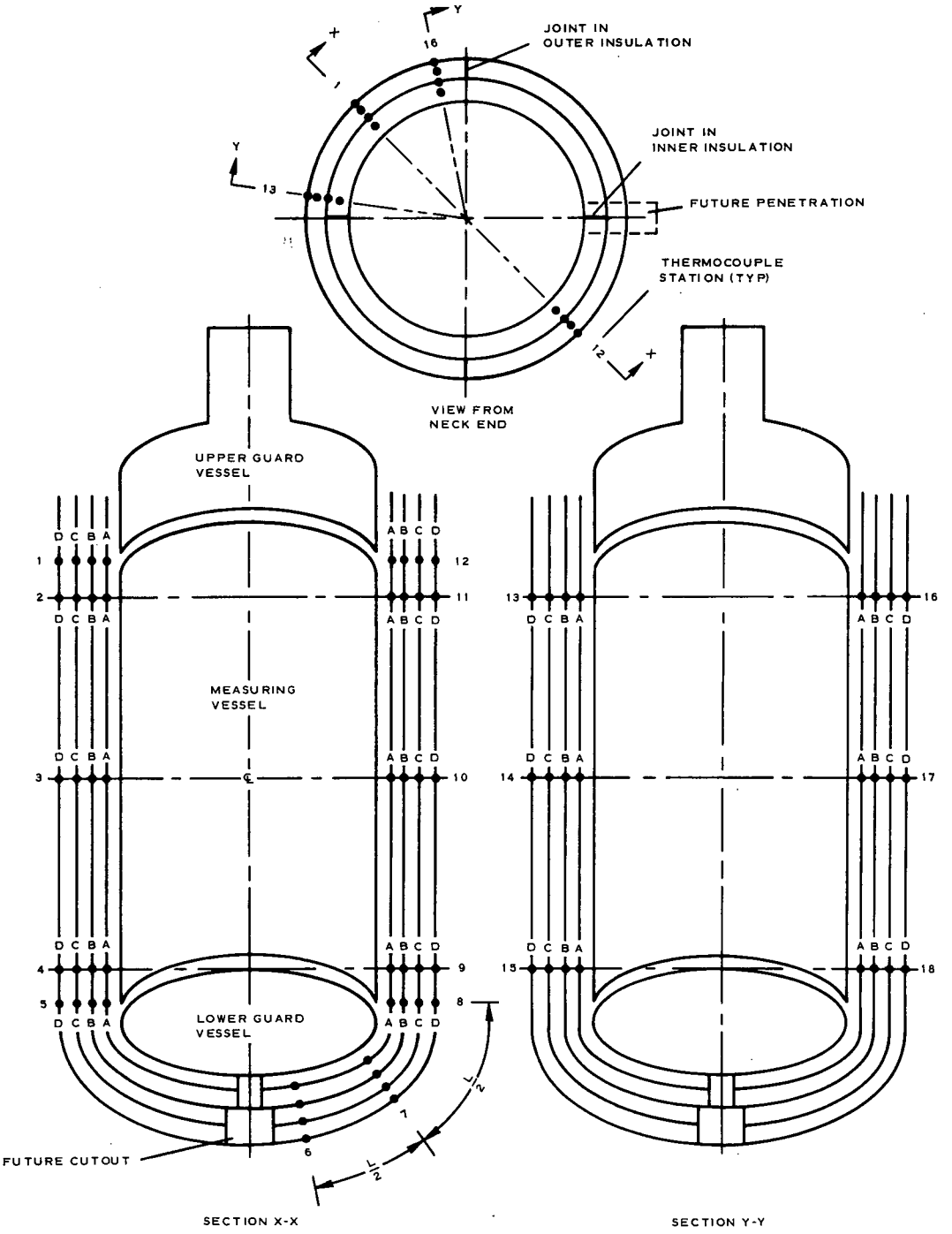

Figure 96. - Thermocouple locations on the cylindrical calorimeter GAC-9 insulation.

$$Q_{insulation} = W C_p \left(\frac{\Delta T}{\Delta t}\right)$$

$$= 5570 \times .460 \times \frac{1.111}{5.04 \times 10^4}$$

$$= .059 W (.20 Btu/hr)$$

where W = the weight of the insulation panels in grams

C_p = the specific heat of the insulation J/g^oK

ΔT = the change in bulk temperature ^oK

Δt = the time increment of temperature change in s

(3) Variation in Ullage Pressure. No corrections were required for changes in the saturation condition or heat storage of the test cryogen. The ullage pressure was relatively constant over the time period of measurement. The largest variation in ullage pressure was .2 percent of the average absolute ullage pressure of 106,790 N/m^2 (801 torr).

(4) Edge Effects. Certain modifications were made to the neck and polar cap regions of the GAC-9 insulation system that was installed on the cylindrical calorimeter during the previous program, Contract NAS 8-30140. In the neck region, the multilayer insulation close-out collars between the insulation panels and the calorimeter neck were replaced with an inlet purge plenum that was filled with PF 105-500 fiberglass mat 9.6 kg/m^3 (0.6 lb/ft^3). The purge plenum filler should minimize the edge effects that in multilayer insulation can be detected in the lateral direction for distances as great as 50 times the panel thickness. In the polar cap region two step-jointed multilayer insulation plugs were installed where the seams of the inner and outer insulation panels had previously terminated at a common point.

The results of the above modifications to the insulation system of the cylindrical calorimeter are shown in Figure 97, which shows the bulk temperature of the insulation along the calorimeter profile. The increased effectiveness of the system design is verified by the much lower insulation bulk temperatures at all points along the calorimeter profile.

The temperature gradient in the polar cap region is particularly flatter in the current program test than in the 1969 test. The gradients at each "knuckle" or transition region where the cylindrical section meets the elliptical head are also lower. The effect of the neck modification has been to prevent heat from traveling laterally along the full length of the calorimeter. As indicated at thermocouple locations 8-9 and 11-12, heat enters the measuring vessel from both ends of the calorimeter,whereas previously heat entered the measuring section from the

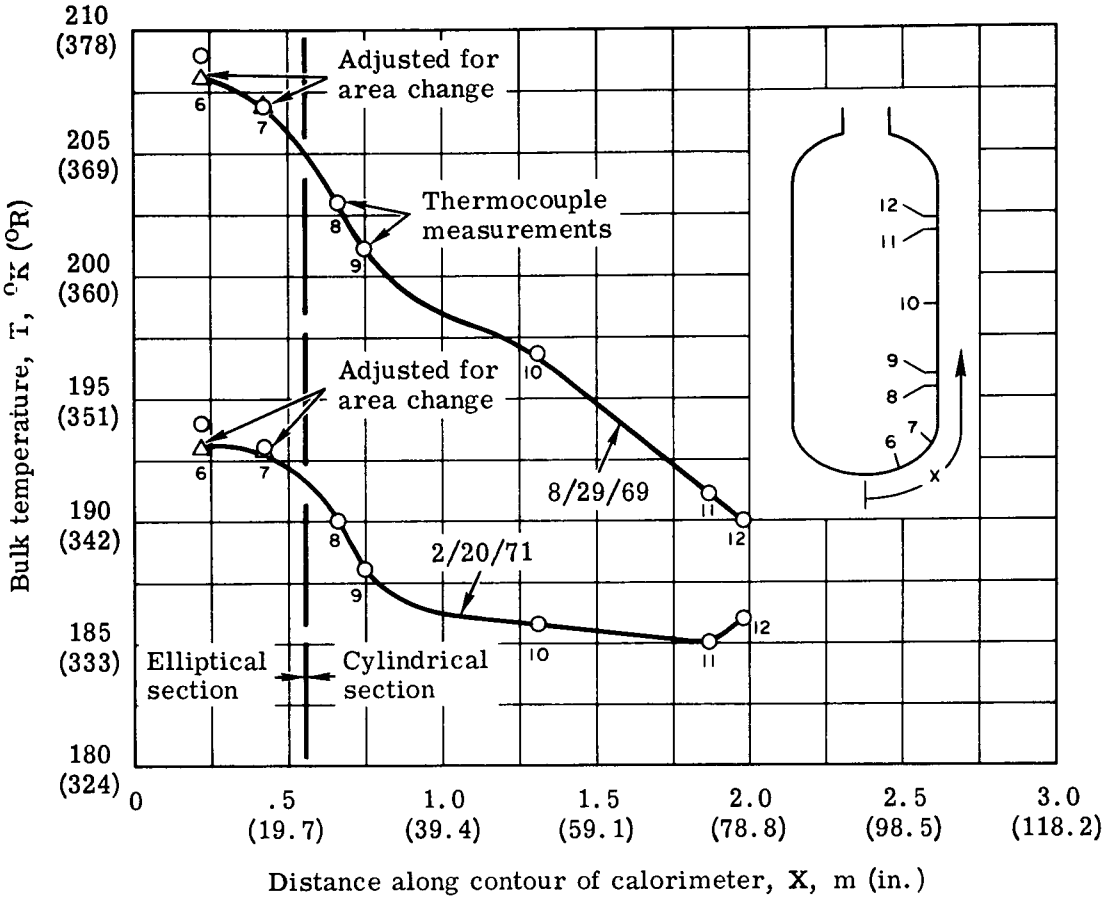

Figure 97. - Bulk insulation temperature along contour of cylindrical calorimeter - test No. 1.

bottom dome and left the measuring section at the upper dome. The heat leak attributed to edge effects is calculated by:

$$Q_{lat} = K_{lat} \times A_{lat} \times (\Delta T/\Delta x)$$

where K_{lat} = lateral thermal conductivity (based on 500A° aluminum film thickness on each Mylar shield)

A_{lat} = lateral flow area of aluminum film

$(\Delta T/\Delta x)$ = temperature gradient at measuring vessel boundary

The lateral heat leak has been calculated to be 0.0469 W (.16 Btu/hr.)

(5) Pressure Probes. The fiberglass extensions of the pressure sensing tubes contribute a source of heat to the measuring section. The heat leak attributed to the 12 probes is calculated to be 0.155 W (0.53 Btu/hr).

(6) Thermal Conductivity. As a result of the above test data evaluation, the corrected heat flow into the measuring section is 0.864 W (2.95 Btu/hr). The thermal conductivity for the panelized GAC-9 insulation system is derived from the equation:

$$K = \frac{Q_{corr} X}{A \Delta T}$$

$$= \frac{0.864 \times .0508}{3.066 \times 262} \times 3.6 \times 10^{9}$$

$$= 1.96 \frac{J}{m - s - {}^{o}K} \left(3.15 \times 10^{-5} \frac{BTU}{hr\text{-}ft\text{-}{}^{o}F} \right)$$

where Q_{corr} = corrected heat flow in watts

X = insulation thickness in meters

A = insulation area in meters^2

ΔT = temperature differential ^{o}K

(7) Insulation Pressures. During the vacuum chamber evacuation prior to test No. 1 pressure differentials were monitored continuously at tap 10 and intermittently at the other taps. In Figure 98 the differential pressure at tap 10 is shown versus the time of chamber evacuation. A calibration curve for the matched 0.46-cm (0.18-inch) bore tubing used in sensing pressures within the GAC-9 insulation system is shown in Figure 99, where P_R is the reference pressure side of the instrument and P_X is the pressure being measured. The measured pressure differentials were signficantly larger than the calibrated differentials, and therefore no corrections of the measured pressure data were necessary. The pressures at the other taps within the insulation were not significantly different from those measured at tap 10 and therefore have not been reported.

(8) Conclusions. The 76-cm (30-inch) diameter calorimeter thermal conductivity test value of 1.96×10^{4} J/m-s-^{o}K (3.15×10^{-5} Btu/ft-hr-^{o}F) agrees very well with the 1.87 J/m-s-^{o}K (3.0×10^{-5} Btu/ft-hr-^{o}F) value obtained on the first space test conducted on GAC-9 insulation under Contract NAS 8-30140. The five percent difference in test values is considered to be within the accuracy of test data acquisition and data reduction calculation.

The outer GAC-9 insulation panels were removed from the cylindrical calorimeter and subjected to considerable handling and reinstalled on the calorimeter during the installation of

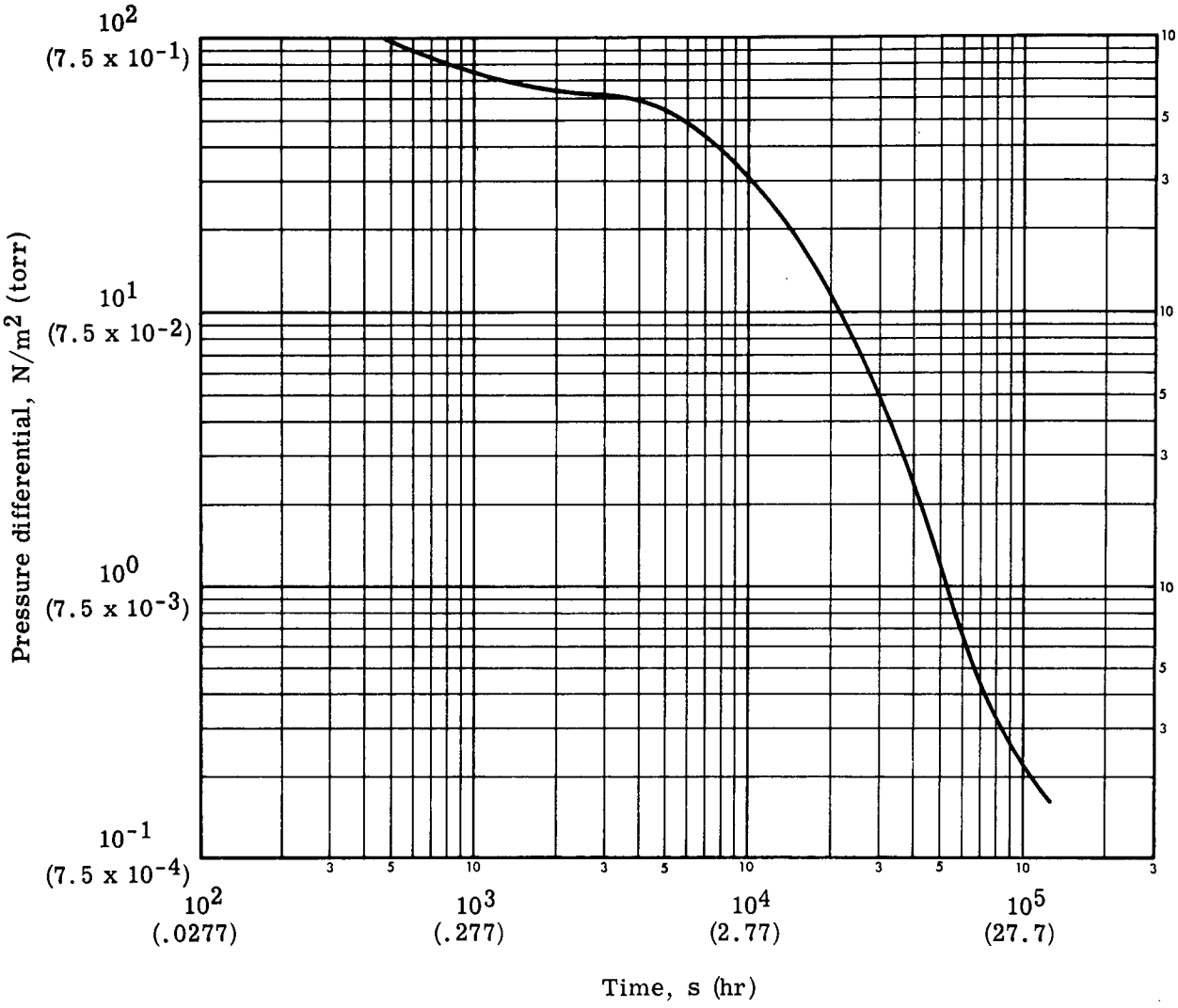

Figure 98. - Insulation pressure differential versus time at pressure tap 10 - test No. 1.

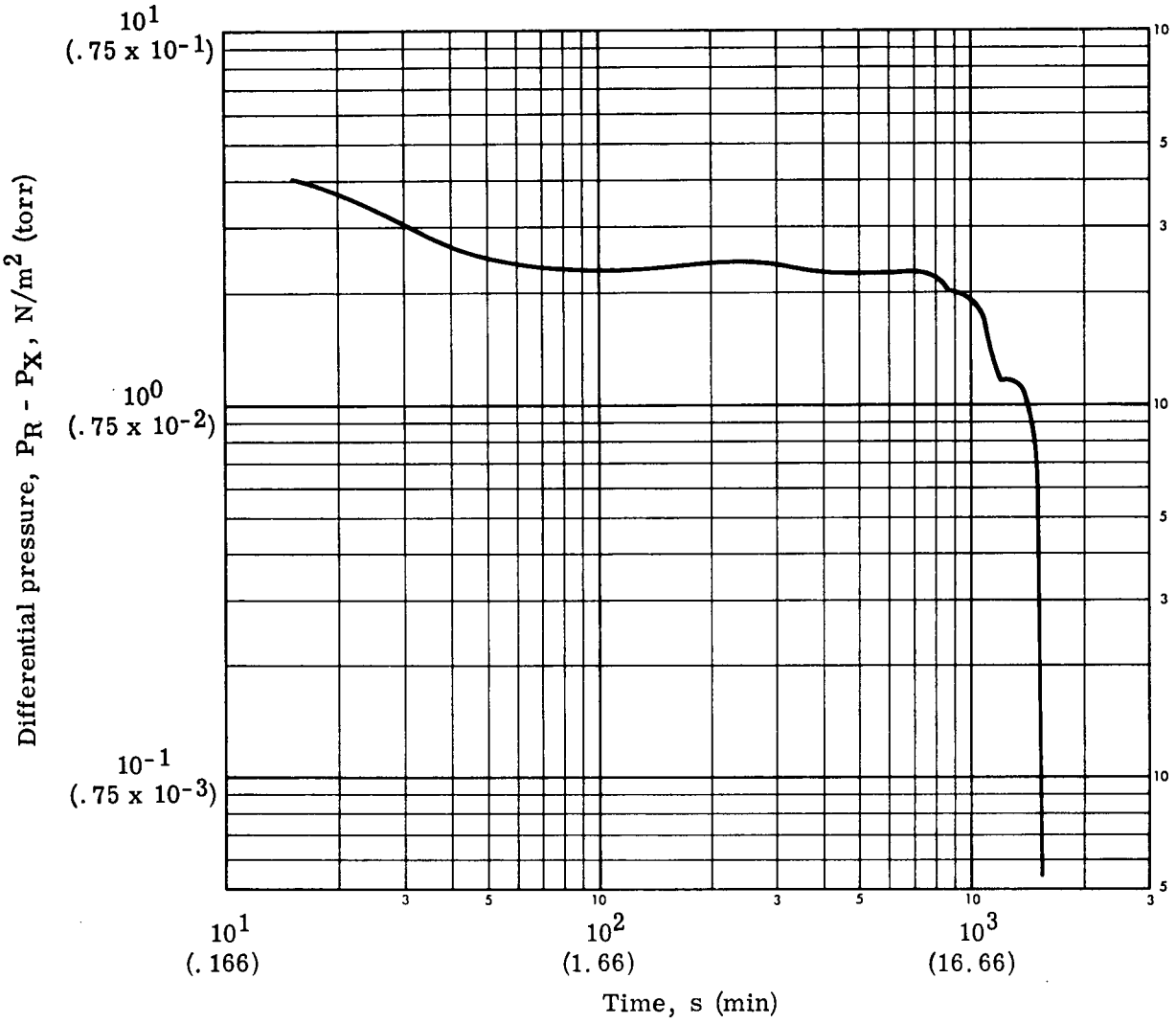

Figure 99. - Calibration curve for matched 0.46-cm (0.18-in.) tubing used in cylindrical calorimeter tests.

pressure sensing probes and rework of the polar cap and neck plenum regions. It may be concluded that this handling did not noticeably degrade the GAC-9 insulation space thermal performance.

b. Test No. 2. The first ground hold test was conducted with the purge jacket surrounding the calorimeter. A ground hold thermal conductivity of 0.079 J/m-s-^{o}K (0.0456 Btu/ft-hr-^{o}F) was obtained for a boil-off of 1.09 x 10^{-3} kg/s (15.66 lbs/hr). During the test period, difficulty was encountered with the calorimeter reaching space conditions. The boil-off rate

F

was decreasing at a much slower rate than usual and the test was stopped prior to reaching space conditions. A pressure comparison was obtained, however, between the insulation and test chamber during the ascent period. A plot of the insulation to chamber pressure differential and chamber pressure is shown in Figure 100. A maximum differential of approximately 6.0 N/m^2 (0.045 torr) was obtained during the early part of the test and leveled off to approximately .60 N/m^2 (0.0045 torr) during the later part of the test.

The thermal conductivity for the ground hold condition was normal as shown in Figure 101 where the comparison of all ground tests conducted in the program can be made and compared to the thermal conductivity of helium gas.

The 0.60 N/m^2 (0.0045 torr) pressure differential verifies the boil-off rate not reaching space condition performance. A post-test visual examination of the test setup showed the purge bag did not open and restricted the venting of the insulation. The ground hold test results are unaffected by the purge jacket malfunction and are, therefore, considered acceptable. The ascent and space test results are not valid or presented.

c. Test No. 3. Test No. 3 was a ground hold, ascent test with the purge jacket folded away from the insulation. A boil-off rate of 2.17×10^{-3} kg/s (17.30 lbs/hr) was obtained for this test giving a thermal conductivity value of 0.0715 J/m-s-^{o}K (0.0413 BTU/hr-ft-^{o}F). The results obtained for this test agree very well with the values obtained for previous ground hold tests conducted on GAC-9 and GAC-4 insulation as shown in Figure 101.

A plot of the ascent period chamber pressure and pressure differential between the insulation and chamber is shown in Figure 102. A maximum pressure differential of 66 N/m^2 (0.30 torr) was measured during the chamber pump down. The minimum pressure differential was 0.13 N/m^2 (0.0012 torr) at a chamber pressure of 4.0×10^{-2} N/m^2 (3.0×10^{-4} torr). After 10^4s (2.8 hours) of chamber pumping, the chamber pressure did not drop below this value;therefore some leakage in the test setup was suspected. Chamber pumping was continued for an additional 2.99×10^4s (8.3 hours) with no apparent drop in chamber pressure and the test was concluded.

Sufficient LH_2 remained in the calorimeter to conduct an additional ground hold test. This test gave a thermal conductivity of 0.075 J/m-s-^{o}K (0.0430 Btu/hr-ft-^{o}F) and a boil-off rate of 2.26×10^{-3} kg/s (18.03 lbs/hr) which is comparable to the previous ground hold test discussed above.

Further investigations were made to remedy the chamber leakage problem prior to conducting additional planned boil-off tests.

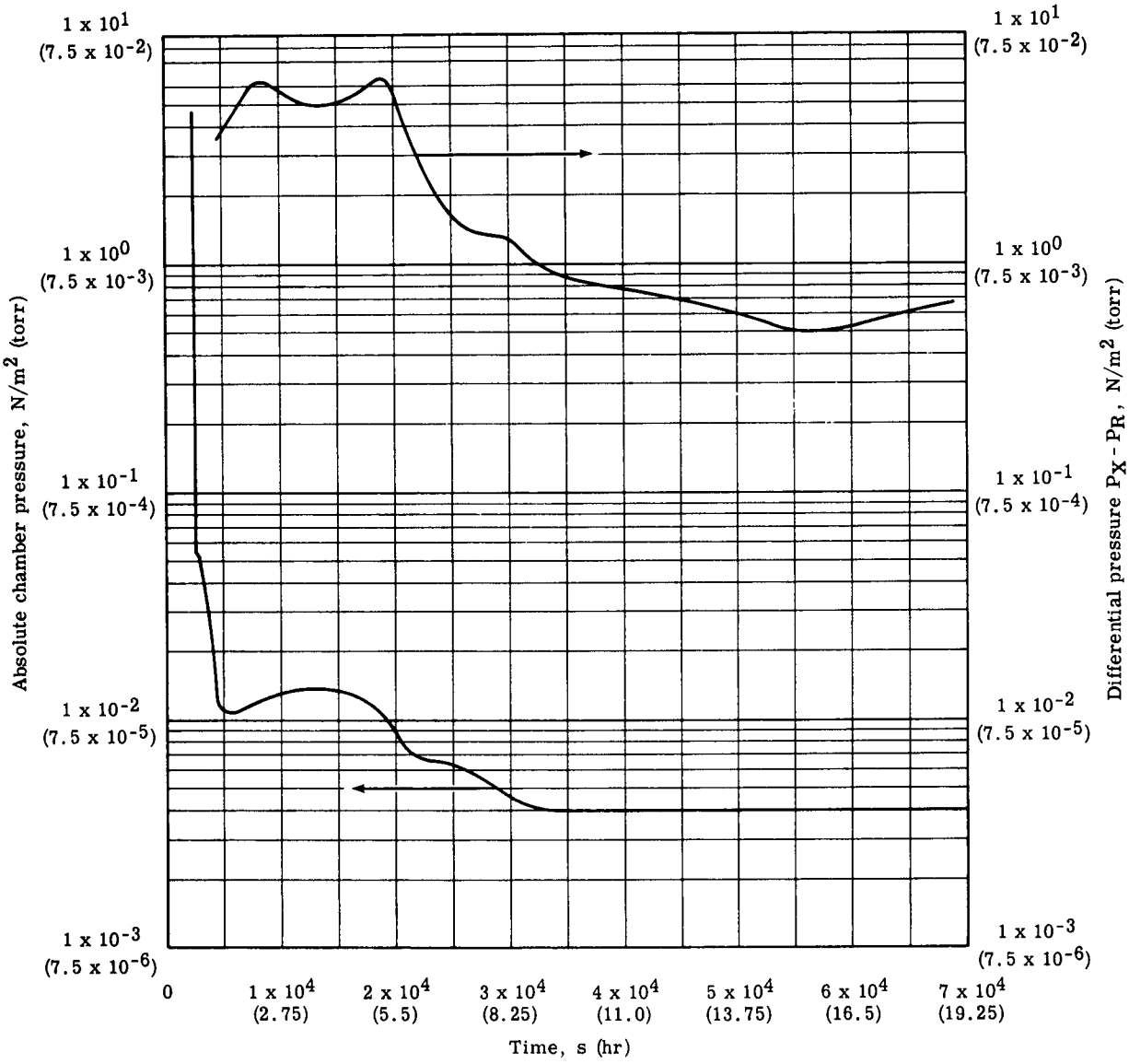

Figure 100. - Chamber pressure and insulation to chamber pressure differential pressure - test No. 2.

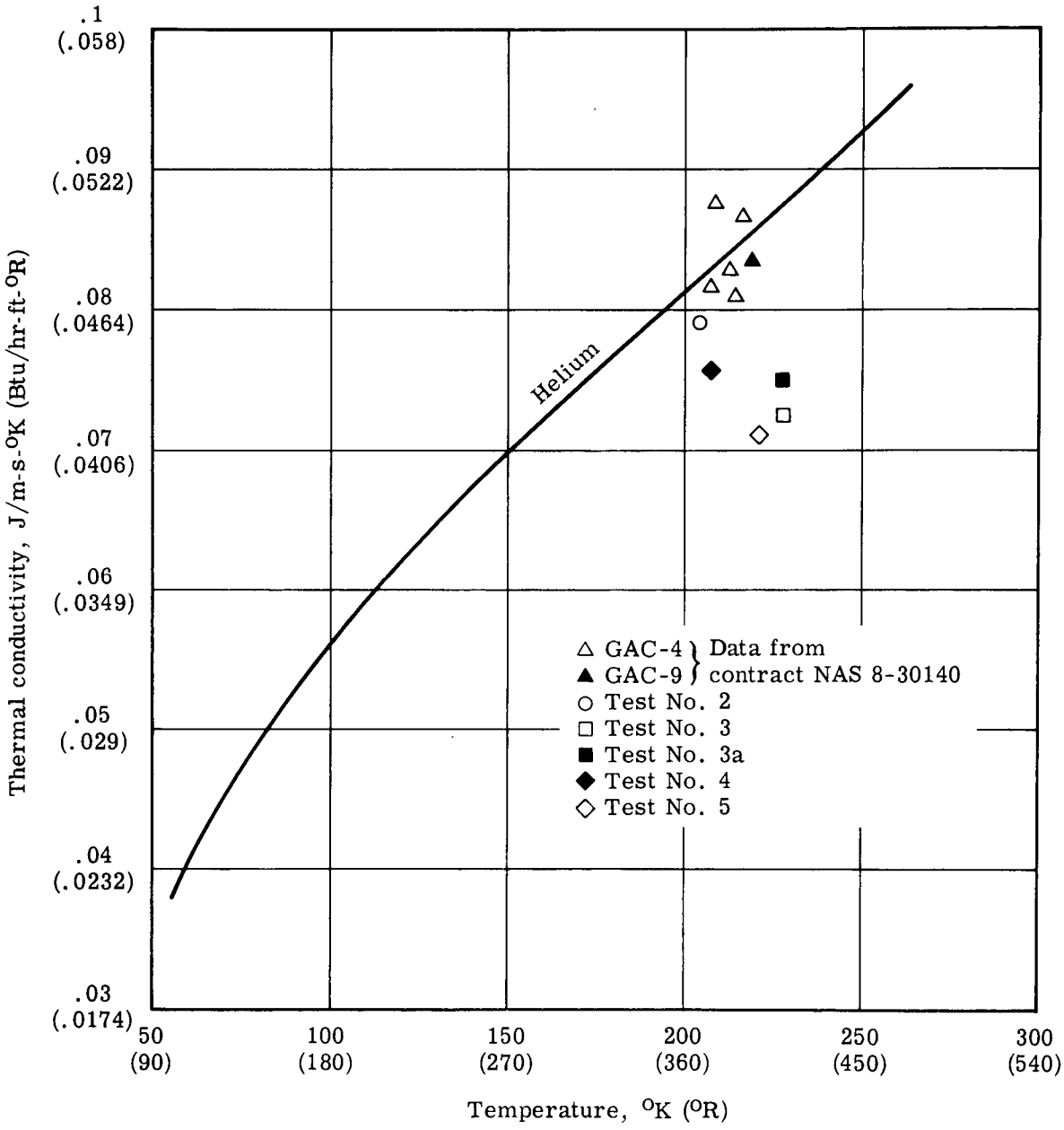

Figure 101. - Insulation system ground hold thermal performance.

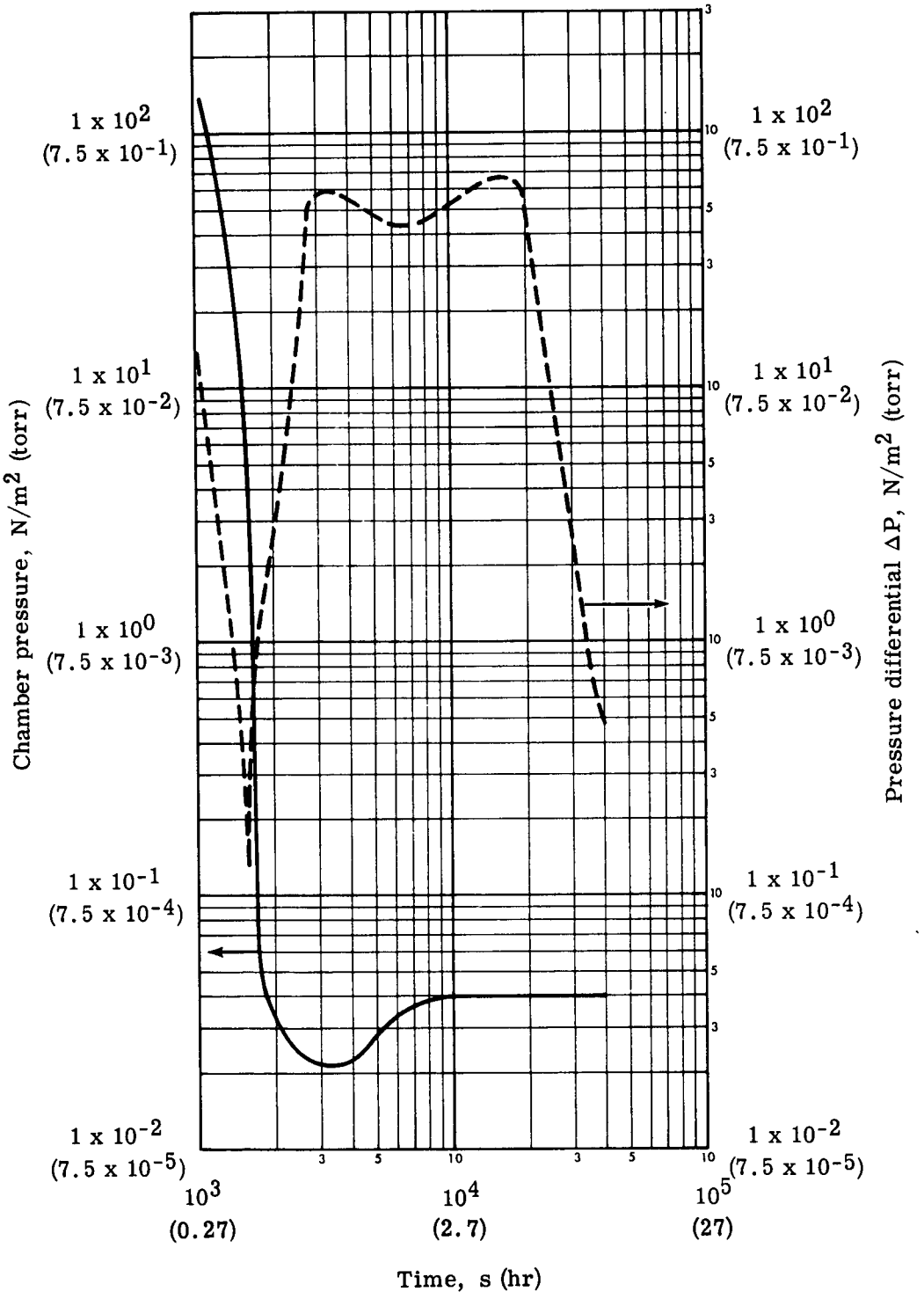

Figure 102. - Chamber pressure and insulation to chamber pressure differential pressure - test No. 3.

d. Purge Jacket Opening Test. During the cylindrical calorimeter test No. 2 (reference Table X), the purge jacket did not open to vent purge gas. A post-test examination of the jacket and zipper release device revealed no defects or damage which would prevent the zipper from opening at an internal pressure of 3.14×10^3 N/m^2 (0.5 lbf/in.^{2}). The previous zipper opening tests conducted prior to calorimeter test No. 2 demonstrated reliable opening at the desired internal pressure load level as discussed in section IV, B. 1 of this report. These tests were not conducted in a vacuum chamber; therefore, the zipper opening differential pressure loads were induced by raising the jacket internal pressure rather than reducing the external pressure as would be the case in a vacuum chamber test. It was concluded that during the vacuum chamber pump down (simulated ascent pressure decay) in calorimeter test No. 2, the small leaks at the purge jacket to calorimeter attachments permitted sufficient pump out of the jacket interior gas to prevent build up of the pressure differential required for activating the zipper opening device.

Prior to cylindrical calorimeter test No. 3, zipper opening tests were performed at ambient temperature in the vacuum chamber to determine the test procedural steps to insure operation of the zipper opening device during chamber pump down. The jacket opening tests were conducted as follows:

(1) A jacket pressurization test was performed to determine the helium purge gas flow rate required to maintain 2.07×10^3 N/m^2 (0.30 lbf/in.^{2}) internal pressure in the purge jacket. A helium inlet flow of 1×10^{-3} m^3/s (2.15 ft^3/min) was required to maintain the desired jacket pressure.

(2) A simulated ground hold and ascent pressure decay test was performed to open the purge jacket. Helium gas was introduced into the insulation and purge jacket through the inlet plenum chamber at the ground-hold purge flow rate of 4.7×10^{-4} m^3/s (1.0 ft^3/min). Just prior to initiation of vacuum chamber pump-down, the helium gas flow was increased to the rate predetermined in step 1. Five seconds after start of chamber pump-down, the zipper retainer clip snapped off and the purge jacket opened in a normal manner.

A post-test examination of the purge jacket revealed the jacket zipper had opened to a greater length than experienced on previous jacket opening tests conducted outside the vacuum chamber. The additional opening may be attributed to the elastic cords provided to hold the jacket open. The open jacket is shown in Figure 75.

Based on the jacket opening tests, the procedures for calorimeter test No. 4 were revised to include the added step of increasing the purge jacket internal gas pressure to 2.07×10^3 N/m^2 (0.3 lbf/in.^{2}) prior to the start of the vacuum chamber pump-down.

e. Test No. 4. Test No. 4 was a ground hold and ascent thermal performance test which incorporated a flow-through helium purge system and a purge jacket around the insulated calorimeter. A ground hold thermal conductivity value of 0.0750 J/m-s-^{o}K (0.0435 Btu/hr-ft-^{o}F) was obtained for the insulation with a boil-off rate of 1.74×10^{-3} kg/s (13.83 lbs/hr).

In Figure 101 a comparison of this thermal conductivity value with data of previous ground hold tests show that the results obtained from test No. 4 are representative of GAC-9 insulation and are in the expected band of performance values. Since previous ground hold tests have been conducted under conditions of ideal helium purge, that is, with vacuum chamber evacuation and helium backfill to purge the insulation, it is concluded that the flow-through helium purge system was effective when judged on the basis of comparable ground hold thermal performance.

The ascent test was conducted with the purge bag split at one end to permit evacuation of the GAC-9 insulation during vacuum chamber pump-down. Figure 103 shows the chamber pressure and pressure differential between the insulation and test chamber as a function of elapsed test time. The chamber pressure reached space conditions $p_c < 10^{-2}$ N/m^2 ($< 0.75 \times 10^{-3}$ torr) approximately 3600s (one hour) after the start of the chamber pump down. The insulation to chamber pressure differential showed a negative value after 1500s (25 minutes) which indicates that the insulation pressure is lower than the pressure differential across the matched tube sensing vacuum chamber pressure. A maximum differential pressure of -3.0 N/m^2 (2.25×10^{-2} torr) is recorded at approximately 2200s (37 minutes) and increases towards zero with increased test time. This pressure differential is a relatively small value and can be attributed to the difference in volumes between both matched tubing pressure sensing lines. The volume difference is in the electronic pressure meter which is constructed such that the total line volume on the reference side of the pair of sensing tubes is 32.8 cm^3 (2.0 inches^3) larger which creates a slower response time for a pressure variation in the vacuum chamber. If this effect is neglected for practical considerations, it may be concluded that the insulation pressure followed the chamber pressure very closely or excellent evacuation was accomplished.

The rate of venting helium purge gas from the insulation depends on the function of the purge jacket zipper release device. During the ascent phase of this test the zipper release device did not function as planned. However, the zipper did separate to a small opening approximately 60 cm (24 inches) long and 0.47 cm (0.187 inch) wide in the top dome region of

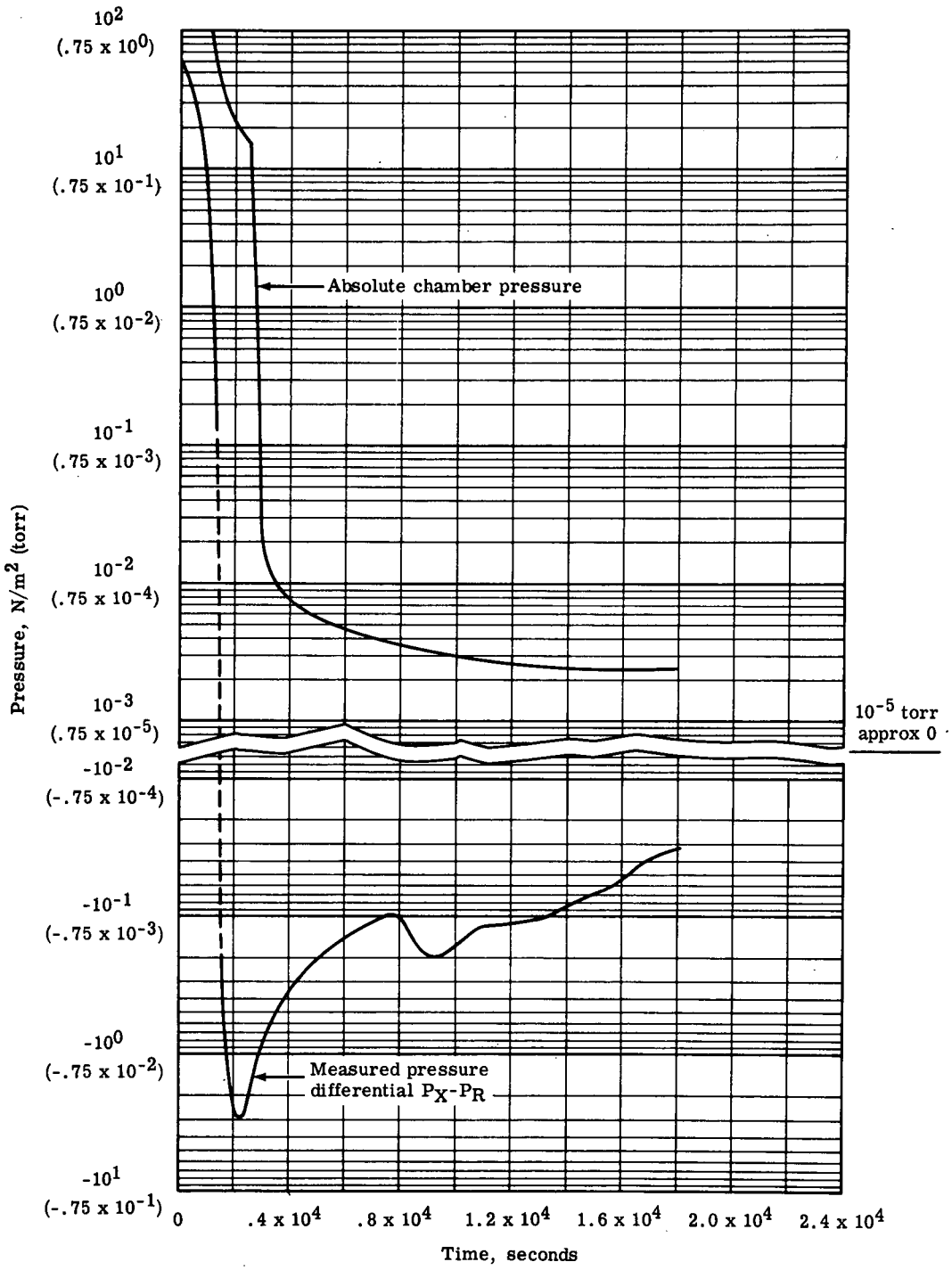

Figure 103. - Chamber pressure and insulation to chamber pressure differential pressure - test No. 4.

the jacket, as shown in Figure 104. A post-test examination of the zipper showed the probable cause for zipper opening in this region was incomplete closure resulting from inconspicuous damage from previous tests. This opening had a vent area of 27.74 cm^2 (4.3 $inches^2$) which is much less than the normal vent area in excess of 1290 cm^2 (200 $inches^2$) provided by the zipper release and retracting devices discussed in sections IV.B.1 and IV.C.2.d of this report. The limited opening did not impede evacuation of helium purge gas because the rate of vacuum chamber pressure decay was comparable to previous ascent tests without a purge jacket surrounding the insulated calorimeter. It may be concluded that the jacket zipper opening, as designed, was very redundant and that a purge jacket vent area that is 2 percent or more of the insulation outer surface area would be adequate for venting 5.08 cm (2 inch) thick GAC-9 insulation.

The boil-off rate of the calorimeter is influenced by the rapid change in pressure of the gas in the insulation. This gas pressure is affected by both the change in pressure of the vacuum chamber and the ability of the insulation to vent the purge gas. A plot of the boil-off rate and the vacuum chamber pressure history in the regime of interest is shown in Figure 105. The chamber has limited pumping capacity and approximately 2.7×10^3s (45 minutes) of pumping elapsed before the high vacuum diffusion pump could be turned on. This delay in turning on the high vacuum pump effects the apparent venting characteristics of the insulation. Approximately 7.2×10^3 (2 hours) of high vacuum pumping was required before the chamber pressure reached 3.0×10^{-3} N/m^2 (2.25×10^{-5} torr) and the boil-off rate began to level off. It may be concluded that with the pumping capacity of the test facility, the GAC-9 insulation will vent down to an acceptable internal gas pressure in less than 7.2 to 9.0×10^3s (2 to 2.5 hours) as an outside limit. With greater pumping capacity, approaching ascent conditions, the insulation venting time should be reduced. Because of limited duration of the test, the liquid hydrogen fill lines were not removed which accounts for the boil-off value at the end of test being higher than the equilibrium flow rate experienced in previous tests with fill lines removed. The decrease in boil-off rate associated with removal of the fill lines is approximately 0.05×10^{-3} m^3/s (6 ft^3/hr). Deducting this value, the measured boil-off at the end of test is corrected to approach the normal equilibrium boil-off of 0.03×10^{-3} m^3/s (4 ft^3/hr), which is shown by the dashed curve.

A compilation of the GAC-9 insulation temperature gradients as a function of time for a typical pressure environment encountered in a simulated space flight is shown in Figure 106. Curve (1) shows the temperature gradient after a ground hold condition where a small gradient is noted. After a vacuum chamber pump down of 3600s (one hour) to simulated ascent, the

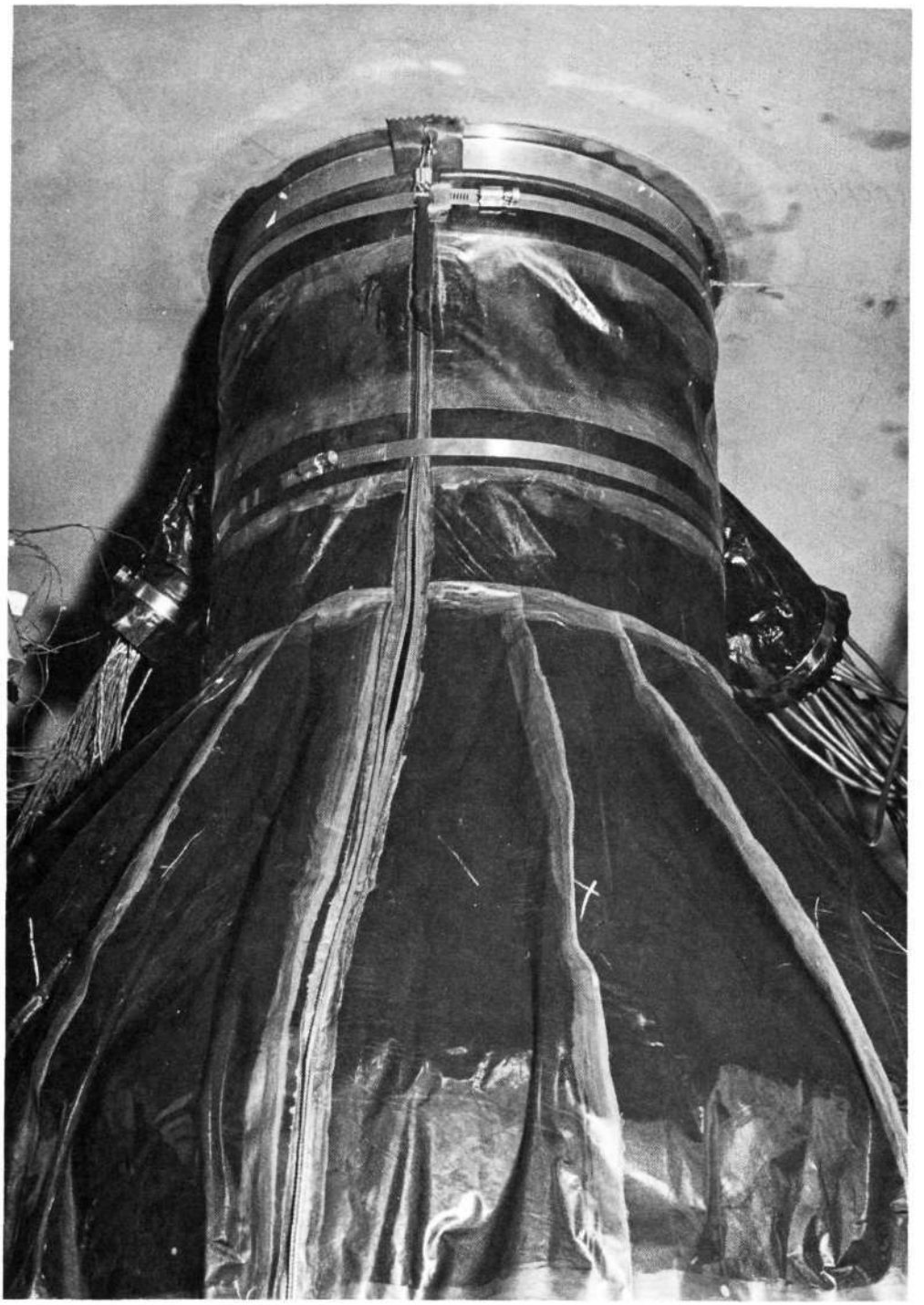

Figure 104. - Purge jacket zipper opening in cylindrical calorimeter - test No. 4.

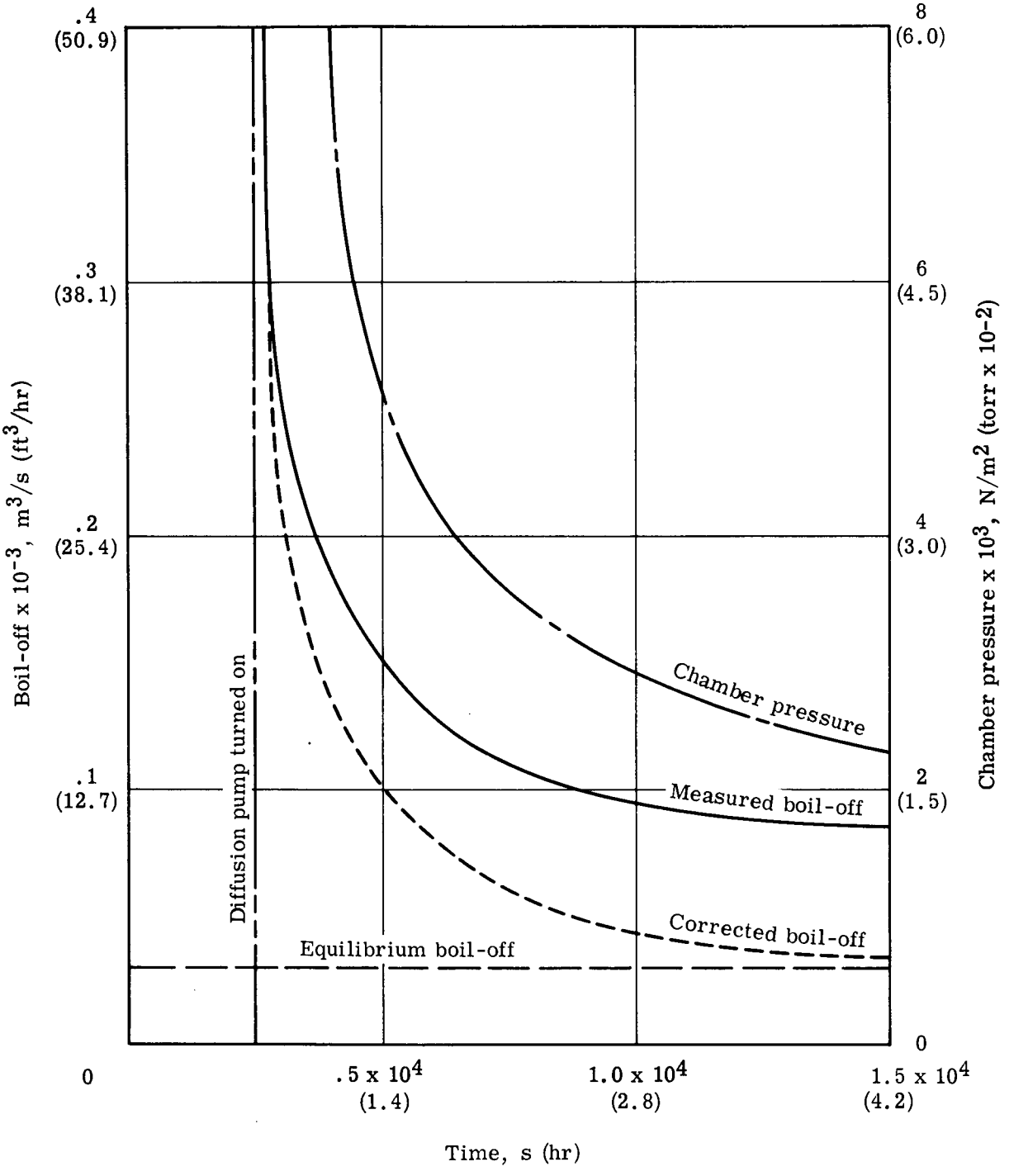

Figure 105. - LH_2 boil-off versus time - GAC-9 insulation system test No. 4.

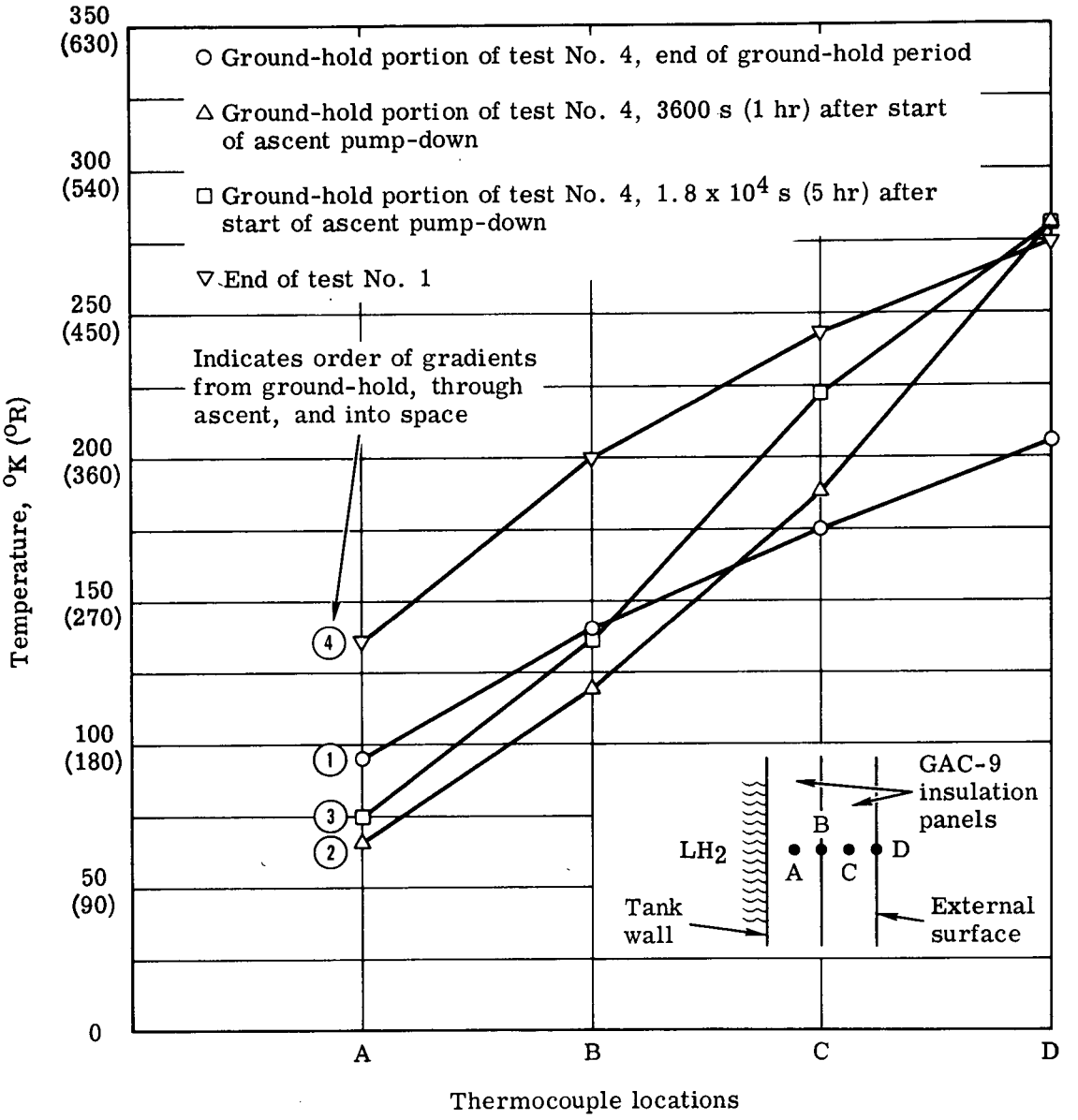

Figure 106. - GAC-9 insulation temperature gradients during simulated ground hold, ascent, and space tests.

temperature gradient increases,with the inner temperature decreasing and the external temperature increasing as shown on curves (2) and (3). This temperature gradient decreases with increasing time,and after a space test the gradient approaches the value of curve (4).

A hypothesis of what transpires in the insulation during this pressure change is as follows: After the initial pumping is started, the cold gases leaving the insulation intercept the incoming heat and early evacuation of the outer layers results in insulation near the outer surface allowing the insulation near the tank surface to decrease in temperature. As the pressure decreases and time is increased, the gases will leave the insulation and the bulk temperature will gradually rise by external heat penetration and eventually reach the gradient shown as curve (4). A parabolic curve is normal at space conditions where two modes of heat transfer are prevalent (conduction and radiation). If conduction is the major mode of heat transfer such as ground hold curve (1), a nearly straight line is the normal temperature gradient profile.

Test No. 4 was considered to be an excellent test to show the purge and vent characteristics and thermal performance of GAC-9 insulation with a flow-through purge system configured to the 30-inch cylindrical calorimeter. The insulation purged well as shown by a comparison of ground hold thermal performance data from test No. 3 and test No. 4. During ascent the insulation evacuated rapidly to reach space performance conditions. The corresponding insulation temperatures and boil-off rates showed effective changes to signify the change in insulation performance.

f. Test No. 5. A ground hold and limited space test of the GAC-9 insulation system incorporating a 5.0-cm (2-inch) diameter pipe penetration was conducted using the 76-cm (30.0-inch) diameter calorimeter. To evaluate the effects of the penetration on space condition performance, test No. 5 will be compared to test No. 1 which had the same insulation except for the penetration and did not have the purge bag surrounding the calorimeter during the testing period. For all practical purposes, the variation in performance of the insulation between the two tests can be attributed to the addition of the penetration. The ground hold performance of test No. 5 is compared to the ground hold portion of test No. 4.

(1) Ground Hold Test Data. The corrected ground hold boil-off was 7.05 kg/hr (15.5 lbs/hr) giving a heat loss of 875 W (2984 Btu/hr) and a thermal conductivity value of 0.0718 J/m-s-^{o}K (0.0415 Btu/hr-ft-^{o}F). The ground hold portion of test No. 4 which also has a purge jacket surrounding the insulation gave a heat loss of 852 W (2910 Btu/hr) and a thermal conductivity value of 0.0753 J/m-s-^{o}K (0.0435 Btu/hr-ft-^{o}F). The effect of the penetration on the heat leakage rate during the ground hold condition should be negligible as

the leakage rate will be nearly the ratio of the increased insulation area which is approximately 4 percent. It can be concluded from these two tests that the penetration will have little effect on the heat leak under ground hold conditions.

(2) Space Test Data. As mentioned previously, the results of the penetration test can best be evaluated by comparison to the results of test No. 1. The construction of the calorimeter is identical for both tests with the exception of the penetration. Another slight difference, however, is that the penetration test had a purge bag surrounding the calorimeter, while test No. 1 had the bag folded away from the insulation and secured near the top of the chamber. This should have little effect on the test results as the surface temperatures of the insulations are comparable for both tests.

(a) Boil-Off. The LH_2 boil-off recorded throughout the test period is shown in Figure 107 as a function of elapsed time.

The boil-off curve had a cyclic trend. However, a leveling off would result if the test time were extended. Due to the limited time available, the test was concluded before equilibrium was achieved. The boil-off data was analyzed and an estimated end point of 33.98×10^{-4} m^3/s (7.20 ft^3/hr) was selected. Correcting the measured flow rate to standard conditions, the boil-off becomes:

$$W_{corr} = W_{measured} \times \frac{T_{standard}}{T_{measured}} \times \frac{P_{test}}{P_{standard}}$$

$$= 33.98 \times \frac{293}{299} \times \frac{9.71 \times 10^4}{10.1 \times 10^4}$$

$$= 32.1 \times 10^{-4} \text{ m}^3/\text{s} \text{ (6.80 ft}^3/\text{hr) (standard conditions)}$$

The corresponding total heat transfer to the measuring vessel is:

$$Q = \frac{m^3}{s} \times \frac{kg}{m^3} \times \frac{J}{kg}$$

$$= 32.1 \times 10^{-4} \times 0.08384 \times 4.53 \times 10^5$$

$$= 2.04\text{W (6.96 Btu/hr)}$$

The corrected heat flow into the calorimeter was made by using the values obtained from test No. 1. From test No. 1 a corrected value of 0.864 W (2.95 Btu/hr) compared to 1.124 W (3.84 Btu/hr) measured boil-off gave a correction of 0.26 W (0.89 Btu/hr). Using this value to correct the penetration boil-off:

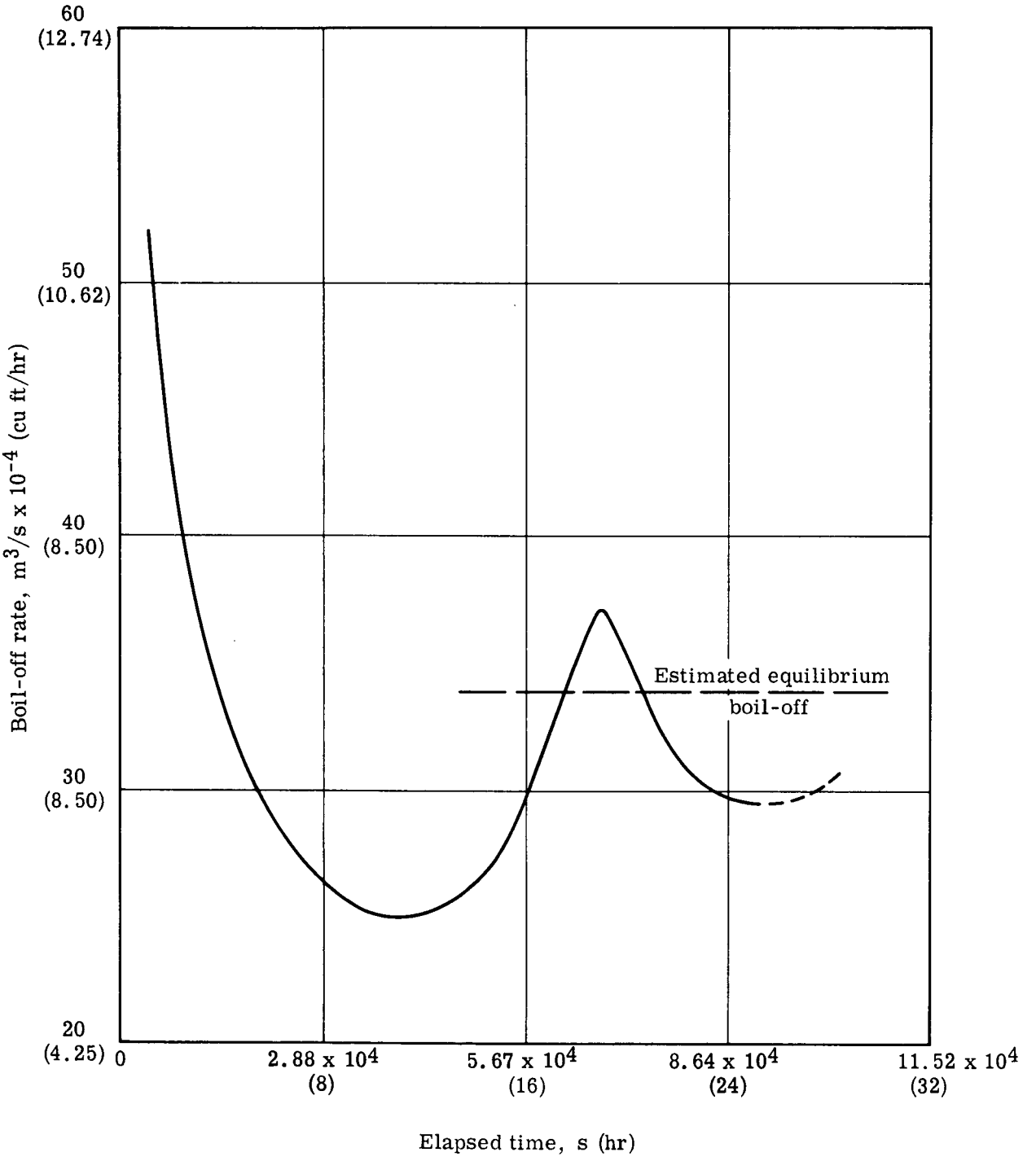

Figure 107. - LH_2 boil-off versus time - test No. 5.

$$Q_{corrected} = 2.04 - 0.26$$

$$= 1.78 \text{ W } (6.07 \text{ Btu/hr})$$

The heat leak attributed to the penetration is

$$Q_{penetration} = 1.78 - 0.86$$

$$= 0.91 \text{ W } (3.12 \text{ Btu/hr})$$

(b) Temperatures. The temperatures of the penetration and its insulation were monitored during the test. The temperature readings taken at the conclusion of the test are shown in Table XI for thermocouple locations shown in Figure 86.

Heat flow calculations based on these temperatures show the direction and magnitude of four paths of heat energy entering the calorimeter:

Path	Value	
	Watts	(Btu/hr)
(1) Along the penetration tube	0.043	(0.146)
(2) Through the glass wool fill in the tube interior	0.044	(0.150)
(3) Across the inner glass wool washer	0.662	(2.260)
(4) Along the penetration GAC-9 insulation flanged sleeve	0.154	(0.525)
Total heat leak	0.903	(3.086)

A major portion of the total heat leak occurs across the inner washer of glass wool which has a relatively high thermal conductivity compared to multilayer insulation. An appropriate reduction in the washer outside diameter (and area) would reduce the magnitude of this heat leak.

The remaining heat energy entering the calorimeter from the penetration insulation was derived by using the temperature differences noted at thermocouples 24 through 25 and the lateral thermal conductance KA/x of this insulation.

The total heat value of 0.903 W (3.086 Btu/hr) is in close agreement with the heat leak determined from the boil-off, 0.91 W (3.12 Btu/hr). Based on this close agreement between the computed heat losses from both the boil-off and the temperature profiles, it can be concluded that the assumed paths of heat leak are verified.

TABLE XI. - PENETRATION TEMPERATURES - TEST NO. 5

T.C. No.	^{o}K	(^{o}F)	T.C. No.	^{o}K	(^{o}F)	T.C. No.	^{o}K	(^{o}F)
1	322	(+121)	11	238	(- 31)	21	300	(+ 80)
2	325	(+126)	12	242	(- 24)	22	31	(-404)
3	322	(+121)	13	273	(+ 31)	23	32	(-402)
4	285	(+ 54)	14	294	(+ 67)	24	302	(+ 84)
5	285	(+ 54)	15	301	(+ 82)	25	252	(- 5)
6	285	(+ 54)	16	172	(-150)	26	140	(-207)
7	285	(+ 54)	17	172	(-150)	27	303	(+ 86)
8	293	(+ 68)	18	172	(-150)	28	233	(- 40)
9	302	(+ 85)	19	255	(- 1)	29	164	(-164)
10	241	(- 26)	20	299	(79)	30	101	(-278)

To efficiently design the penetration insulation, every effort must be made to reduce the amount of heat energy entering laterally along the insulation. To accomplish this, the exposed edges of the insulation should have a low-emittance cap of aluminized Mylar. In addition, the width of the glass wool buffer material should be reduced from two to one insulation thickness.

SECTION V

CONCLUSIONS AND RECOMMENDATIONS

A. CONCLUSIONS

Conclusions drawn from the work accomplished during the program are summarized in the following paragraphs.

Flow coefficient measurements obtained from laboratory tests of helium purge gas flow parallel to the layers of GAC-9 insulation compared favorably with flow coefficients obtained theoretically. In contrast, the measured gas flow perpendicular or broadside to the layers of insulation did not agree with predictions in that no measurable flow was found in laboratory tests. Broadside flow characteristics will be difficult to predict with reasonable accuracy due to variables in radiation shield perforations for drop threads.

For large scale GAC-9 insulation panels, the capability of venting purge gas broadside as well as parallel to layers (via joints) will be beneficial to the rapid reduction of insulation internal pressure to attain space performance.

Broadside flow improvements suggest the use of perforated radiation shields. Flat plate calorimeter tests of GAC-9 insulation specimen using radiation shields perforated to 2.38 percent open area showed an insulation K value of 3.9×10^{-5} J/m-s-^{o}K (2.26×10^{-5} Btu/hr-ft-^{o}F) which is 52 percent higher than the conductivity of GAC-9 insulation with unperforated radiation shields. To avoid this magnitude of thermal performance degradation, the use of perforated radiation shields with a smaller percentage of open area should be considered and investigated.

Subscale tank tests for ground-hold and space conditions verified the ability of GAC-9 insulation to be purged with gaseous helium during ground hold and vented during ascent and space conditions. The purging and venting was accomplished by means of a flow-through purge system configured to the 76-cm (30-inch) diameter cylindrical calorimeter.

With an exception of a minor zipper release malfunction, the purge and insulation systems performed their function with no evidence of deterioration or change from the as-fabricated and installed condition. The thermal performance value for ground hold correlated closely with helium purge gas conductivity. Performance under space conditions was in good agreement with space performance data obtained from previous GAC-9 insulation tests.

The feasibility of mechanizing the installation of drop threads in GAC-9 insulation was demonstrated with a mattress tufter machine. The machine manufacturer, United Mattress Machinery Company, has indicated that the machine design may be altered to be satisfactory for laminated insulation tying. The basic principle of operation would be retained with the components made lighter to handle the desired thread size. The adjustment for controlling compression and length of tie would be refined to meet the desired drop thread bearing pressure in the insulation panels.

B. RECOMMENDATIONS

Recommendations as to the scope and technical nature of work to be given consideration for continued investigation are presented in the following paragraphs.

Conduct study of purge gas flow across insulation panel joints that lie transverse to the flow direction. Determine the effect of these joints on purging capability and evaluate joint modifications or purge system changes to maintain adequate purging across these joints.

Continue the evaluation of perforated radiation shields. Obtain thermal performance and gas flow characteristics of insulation specimens containing a spectrum of shield perforation sizes and percent of open area. Determine optimum radiation shield perforations for improved venting of large scale insulation panels.

Investigate insulation panel outer face sheet designs containing pressure release devices that will remain closed to prevent loss of purge gas during purging and open during ascent to permit rapid escape of purge gas by broadside venting.

Conduct study to determine the maximum size GAC-9 insulation panel that will vent adequately by parallel flow to the panel edges. This study would determine the basis for selecting insulation panel venting by either parallel flow or broadside flow or combination of both modes as a function of panel size.

APPENDIX

MICROMETEOROID IMPACT TEST PROGRAM

To limit testing to a minimum, two test conditions were chosen that represented the extreme positions of the bumper wall location with respect to the multilayer insulation. The first condition, designated "7.62-cm (3-in.) void condition," had the 0.040-cm (0.016-in.) aluminum bumper wall spaced 7.62 cm (three in.) in front of the multilayer test specimen. The second condition, designated "no-void condition," had the 0.040-cm (0.016-in.) aluminum bumper wall placed against the front of the multilayer insulation test specimen. In both conditions, the multilayer insulation consisted of two 2.54-cm (one-in.) thick specimens placed together to simulate 5.08 cm (two in.) of insulation. A 0.406-cm (0.160-in.) aluminum back-up (witness) plate was placed against the back face of the test specimen.

The target configurations and test data are summarized in Table XII. Figure 108 shows the damage to the test specimens and the unmarked back-up plates for the 7.62 cm (3-in.) void test condition and the damage to the test specimens and the back-up plates for the no-void test condition. The following conclusions were reached from the test results:

(1) A 7.62-cm (3-in.) spacing between the 0.040-cm (0.016-in.) aluminum bumper and the 5.08-cm (two-in.) multilayer panel will prevent complete penetration of the multilayer panel.

(2) The 0.040-cm (0.016-in.) aluminum bumper placed against the 5.08-cm (two-in.) multilayer panel will not prevent penetration completely through the multilayer panel. Noticeable marking or pitting occurred on the back-up plate.

(3) The perforations in GAC-9 insulation radiation shield have no significant effect on the hypervelocity impact resistance of this insulation.

TABLE XII. - SUMMARY OF HYPERVELOCITY IMPACT TESTS

Test No.	Specimen No.	Void	Velocity	Target Configuration	Impact Data and Comments
352	GAC-9A	7.62 cm (3 in.)	6.96 km/s (22,800 ft/sec)	0.040-cm (0.016-in.) bumper wall 5052-H36 aluminum 7.62-cm (3.00-in.) void 5.08-cm (2.00-in.) GAC-9 insulation with perforated shields 0.406-cm (0.160-in.) back-up plate 6061-T6 aluminum	All layers were penetrated by tungsten particles. Aluminum pellet damage stopped at fiberglass grid face sheet next to the back-up plate. Back-up plate pitted by tungsten particles but no damage from aluminum projectile.
353	GAC-9B	None	6.49 km/s (21,300 ft/sec)	0.040-cm (0.016-in.) bumper wall 5052-H36 aluminum 5.08-cm (2.00-in.) GAC-9 insulation with perforated shields 0.406-cm (0.160-in.) back-up plate 6061-T6 aluminum	All layers damaged. Slight damage on back-up plate.

NOTES: 1. All projectiles were 0.317-cm (0.125-in.) aluminum 7075-T6 spheres weighing 0.0454 gr.
2. Target materials are listed in sequence from bumper and back-up plate.
3. Multilayer test panels were made in accordance with Figure 55.

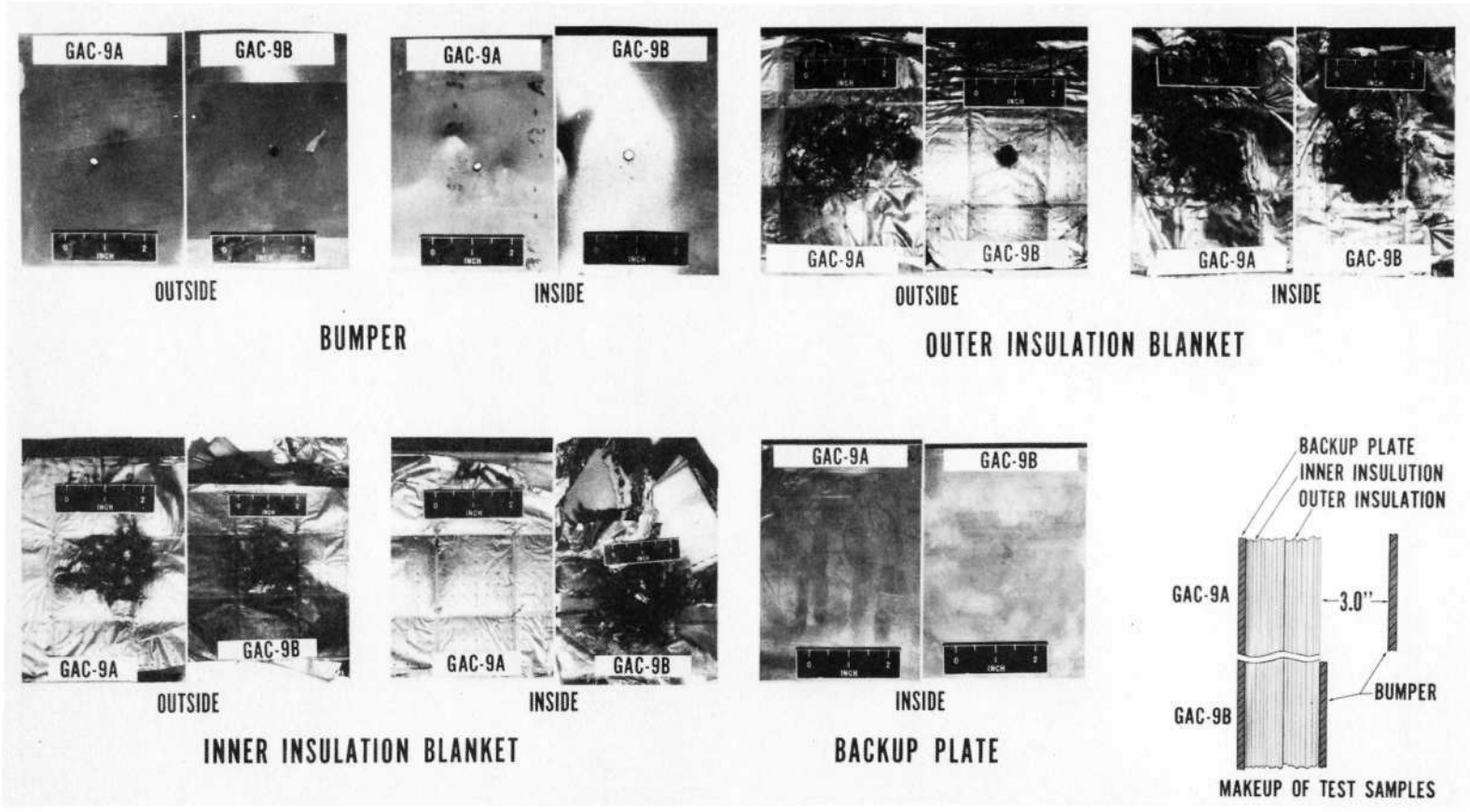

Figure 108. - Hypervelocity impact tests on GAC-9 insulation - progressive damage from bumper wall to backup plate.

REFERENCES

1. Shriver, C. B.; Apisa, J. N.; and Kariotis, A. H.: Development of Materials and Materials Application Concepts for Joint Use as Cryogenic Insulation and Micrometeoroid Bumpers. GER-14071 S/11, Goodyear Aerospace Corporation, 30 November 1969.

2. High-Performance Thermal Protection Systems. LMSC-A964947, Vol 1, Lockheed Missiles and Space Company, 31 December 1969.

3. Kneisel, K. M.; and Benett, F. O.: Prediction of Interstitial Gas Pressure in a Multilayer Insulation During Rapid Evacuation. AIAA Paper 69-608, 4th Thermophysics Conference, American Institute of Aeronautics and Astronautics, June 1969.

4. Coston, R. M.: Experimental Evaluation of Equations and Parameters Governing Flow Through Multilayer Insulations During Evacuation. Lockheed Missiles and Space Company, Sunnyvale, California.

5. Nast, T. C.; and Coston, R. M.: Investigation of Gas Flow Within Multilayer Insulations and Its Effect on Cryogenic Space Vehicle Design. Chem. Eng. Prog. Symp. Series, Volume 62, Number 61, 1966.

6. Instruction Manual for United Lace Tufter, United Mattress Machinery Company, Quincy, Massachusetts.

7. Instruction Manual and Parts Catalog: United Automatic Tufting Machine, United Mattress Machinery Company, Quincy, Massachusetts.